

The back-calculation procedures used to obtain the residual strength are not simple—many assumptions and approximations are involved. Combined with the variability of the SPT and the difficulty in selecting a single SPT value to represent each case history, these residual strengths must be considered approximate, as suggested by the wide band in Figure 9.57. As more data become available and as back-calculation procedures improve, this uncertainty is likely to decrease.

Example 9.9

In the 1971 San Fernando earthquake, soil within the upstream slope of Lower San Fernando Dam liquefied and produced a flow slide that nearly breached the dam (Figure 1.7). Subsurface investigations indicated that the hydraulically placed silty sand in the upstream slope contained about 25% fines and had an average measured $(N_1)_{60}$ of about 11.5. Estimate the residual strength of the silty sand.

Solution For a sand with 25% fines, $N_{\text{corr}} = 2$, so

$$(N_1)_{60-cs} = 11.5 + 2 = 13.5$$

Referring to Figure 9.57, the estimated residual strength should be between about 300 lb/ft² and 750 lb/ft² (the values given by the upper and lower curves). Considering that the data from actual case histories of earthquake-induced liquefaction fall in the lower portion of this range, the residual strength appears most likely to be on the order of 300 to 500 lb/ft².

Normalized Strength Approach: Residual Strength Ratio. The concept of *normalized strength* is widely accepted in geotechnical engineering practice for cohesive soils (Ladd and Foott, 1974). The general concept can also be applied to the residual strength of liquefied soils. The significant advantage of this approach is that it allows estimation of residual strength from initial effective stresses, which are much easier to determine accurately than initial void ratios.

If the consolidation curve and steady-state line of a liquefiable soil are parallel, the steady state strength should be proportional to the consolidation stress (i.e., $S_{su}/\sigma'_{1c} = \text{constant}$). Application of this concept is complicated by the fact that sandy soils do not exhibit unique consolidation curves; hence the ratio S_{su}/σ'_{1c} is not unique for a given soil. However, if laboratory specimens are prepared with the same void ratio and soil fabric that exist in the field at comparable initial effective stresses, measured *residual strength ratios* can be representative of field conditions (Vasquez-Herrera et al., 1990; Baziar et al., 1992; Ishihara, 1993). Vasquez-Herrera et al. (1990) found that $S_r/\sigma'_{v0} \approx 0.12$ for reconstituted specimens of silty sand from Lower San Fernando Dam. Byrne et al. (1993) used specimens obtained by freezing and coring at Duncan Dam to measure $S_r/\sigma'_{v0} \approx 0.21$. The normalized strength approach has also been used with residual strength measured in field vane shear tests. Castro and Troncoso (1989) used vane shear tests to measure S_r/σ'_{v0} values of 0.07, 0.11, and 0.08 in very loose slimes (PI = 20 to 22) at three different tailings dams in Chile. For a clayey silt in the foundation of Sardis Dam (Finn et al., 1991), vane shear tests indicated that $S_r/\sigma'_{v0} \approx 0.075$. The limited available data indicate that the normalized strength approach has promise as a practical tool for estimation of the residual strength of liquefied soils. The data also clearly indicate that residual strength ratios can vary over a considerable range and that their evaluation requires careful, site-specific investigation and testing.

The basic normalized strength approach requires site-specific measurement of the residual strength ratio. It is logical to expect that different soils would have different residual

strength ratios; for example, the residual strength ratio of a well-graded angular sand should be greater than that of a uniform rounded sand. Assuming that the factors that influence the residual strength ratio also influence in situ test results, it should be possible to relate the residual strength ratio to in situ test parameters. Stark and Mesri (1992) used back-calculated and laboratory-measured residual strengths from field case histories to correlate values of residual strength ratio to SPT resistance, that is,

$$\frac{S_r}{\sigma'_{v0}} = 0.0055(N_1)_{60-cs} \quad (9.23)$$

where $(N_1)_{60-cs}$ is computed using the values of N_{corr} given in Table 9-5. Although this procedure has the important advantage of allowing the residual strength ratio to be estimated from SPT resistance, equation (9.23) must be recognized as a reasonably conservative approximation to a set of scattered empirical data.

Example 9.10

According to Stark and Mesri (1992), the effective overburden pressure at the center of the liquefied portion of the upstream slope of Lower San Fernando Dam (see Example 9.9) was 3930 lb/ft². Estimate the residual strength of these soils using the Stark–Mesri approach.

Solution According to the Stark–Mesri approach, a silty sand with 25% fines would indicate (from Table 9-6) $N_{corr} = 6$, so

$$(N_1)_{60-cs} = 11.5 + 6 = 17.5$$

Then, using equation (9.23), the residual strength can be estimated as

$$S_r = 0.0055(N_1)_{60-cs} \sigma'_{v0} = (0.0055)(17.5)(3930 \text{ lb/ft}^2) = 378 \text{ lb/ft}^2$$

This value is consistent with the range of values obtained in Example 9.9.

Discussion. Evaluation of the residual strength of a liquefied sand is one of the most difficult problems in contemporary geotechnical earthquake engineering practice. Steady-state concepts are very useful for understanding the behavior of liquefiable soil, but steady-state strengths can be stress path dependent. In the field, failure generally involves different stress paths, and consequently different steady-state strengths, on different parts of the failure surface. Furthermore, some drainage may occur during failure. Given these factors, it is not surprising that residual strengths are difficult to determine.

The laboratory testing approach is rational and based on tests in which the shear stresses are accurately known, but the sensitivity of its results to uncertain input parameters introduces considerable uncertainty into steady-state strength estimates. The in situ testing approach is also rational, but the variability of soil and stress conditions in the case histories on which it is based introduces considerable uncertainty into residual strength estimates. Upon reviewing the application of these approaches to the Lower San Fernando Dam case history, Marcuson et al. (1990) preferred the in situ approach but suggested that both be used where hazards are high. The normalized strength approach offers some advantages over the other approaches, but available data suggest that residual strength ratios vary considerably for different soils.

9.6.4.2 Flow Failures

Liquefaction-induced flow failures occur when the shear stresses required to maintain static equilibrium are greater than the shear strength of a liquefied soil. This situation can arise

in several different ways; the National Research Council (1985) identified four different mechanisms of flow failure. Estimation of the deformations produced by liquefaction-induced flow failures is extremely difficult; available procedures are described in Section 10.6.2.1.

Flow Liquefaction Failures (NRC Mechanism A). Flow liquefaction represents an important flow failure mechanism. Flow liquefaction occurs under totally undrained conditions—no redistribution of pore water (or change in void ratio) is involved. As described in Section 9.5.2.1, flow liquefaction is initiated when sufficient pore pressure is generated to move the effective stress path of an element of soil from its initial position to the flow liquefaction surface. When that occurs, the element becomes unstable and flow liquefaction failure begins in that element of soil. In other words, a flow liquefaction failure occurs at the locations where liquefaction is initiated by earthquake shaking. These characteristics can be used to distinguish between flow liquefaction failures and other types of flow failures. Flow liquefaction failures often occur very quickly and produce large soil movements (Figure 9.58).

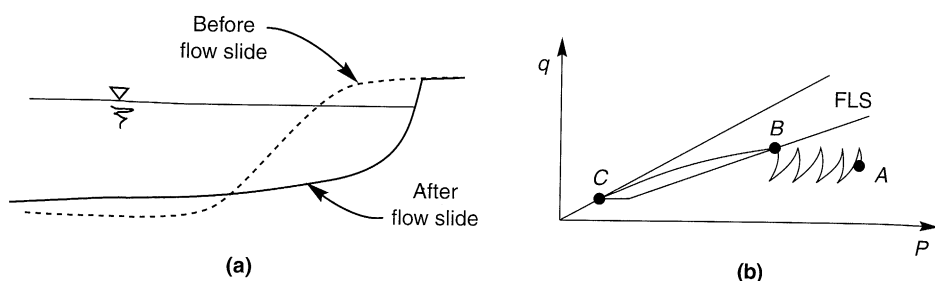


Figure 9.58 (a) Typical cross section through a flow slide showing how liquefied materials can travel large distances and come to rest on very flat surfaces; (b) stress conditions at typical element of soil within failed mass. Prior to earthquake, element is in equilibrium at point A under static shear stress greater than steady state (or residual) strength. Cyclic loading brings stress path to FLS (point B) after which strain softening reduces shearing resistance to steady-state (or residual) strength (point C).

Flow liquefaction failures can develop progressively (i.e., the initiation of flow liquefaction in a small volume of soil may spread to produce a large flow failure). When flow liquefaction is initiated at a particular location, the shearing resistance drops to the steady-state strength. The static shear stresses that were resisted at that location must then be transferred to the surrounding soil, where they may initiate further flow liquefaction. As the redistribution of stresses proceeds, the zone of liquefaction grows. Eventually, a massive flow slide may develop.

Local Loosening Flow Failure (NRC Mechanism B). Since the steady-state strength is very sensitive to the density of many soils, a small amount of loosening can reduce the steady-state strength substantially. In some cases, loosening may reduce the steady-state strength to a value smaller than the shear stress required for equilibrium, thereby producing a flow failure.

If a sand layer is overlain by a less permeable material that does not permit drainage during the earthquake itself, the total volume of the sand will remain constant. If a condition

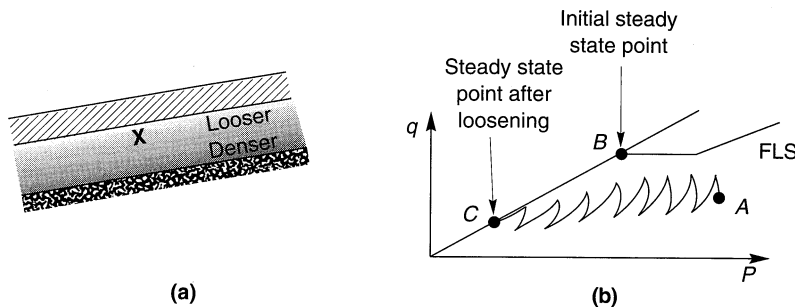


Figure 9.59 Flow failure due to loosening: (a) redistribution of grains in sand layer causes local volume change even though total volume remains constant; (b) stress conditions at point marked with \times . Prior to earthquake, soil is in equilibrium at point A with steady-state strength (point B) that is greater than static shear stress. As effective stresses are reduced during earthquake, loosening of soil reduces steady-state strength to lower value (point C), thereby allowing flow failure to occur.

of initial liquefaction (zero effective stress) is reached, however, the sand particles may rearrange under the action of gravity so that the lower part of the layer becomes denser and the upper part looser. If the upper part loosens sufficiently to reduce the steady-state strength to a value smaller than the static shear stress, a *local loosening flow failure* can occur, as illustrated in Figure 9.59. In extreme cases a water interlayer may form beneath the less permeable material. Since the water interlayer would have zero shear strength, a flow failure could easily be produced.

Global Loosening Flow Failure (NRC Mechanism C). High excess pore pressures generated at depth will cause porewater to flow toward drainage boundaries during and after an earthquake. As illustrated in Figure 9.60a, most of the flow is usually directed toward the ground surface. Shallow soils may be loosened by this flow to the extent that their steady-state strength drops below the shear stress required to maintain equilibrium. In contrast with the local loosening case, this loosening is not compensated for by densification at a different location. The process is illustrated schematically in Figure 9.60b. Since the steady-state strength is not reduced until water flows into the shallower soil, failure may not occur until well after the earthquake. Cracking of the surficial soils may also contribute to the failure.

Interface Flow Failure (NRC Mechanism D). Flow-type failures can also occur when the shear strength of the interface between a liquefiable soil and a structure becomes smaller than the shear stress required for equilibrium. Plunging failure of friction piles (DeAlba, 1983) is an example of an interface flow failure. If the interface is smooth, as with steel or precast concrete piles, interface flow failure does not require volume change of the soil and therefore can occur in contractive or dilative sands.

9.6.4.3 Deformation Failures

Not all liquefaction-related failures involve flow and large displacements. Cyclic mobility can produce small, incremental, permanent deformations that, by the end of an earthquake, may be sufficient to produce extensive damage. Lateral spreading is an example of deformation failure. As illustrated in Figure 9.61, lateral spreading causes surficial

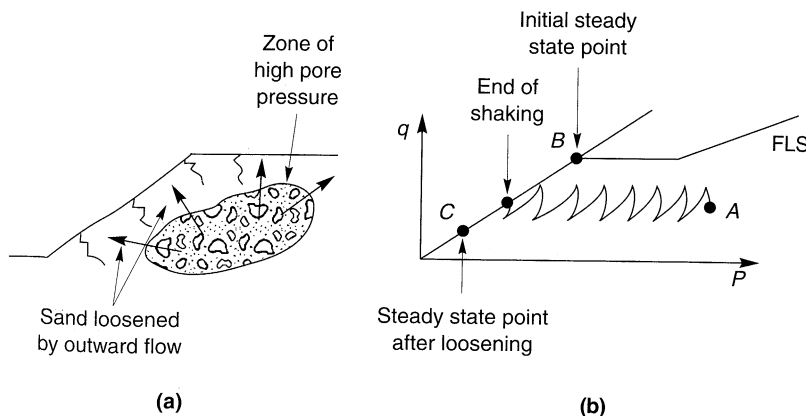


Figure 9.60 (a) Example of global loosening flow failure (after National Research Council, 1985) where earthquake-induced pore pressure at depth causes flow that loosens surficial soils; (b) possible effective stress path for element of surficial soil. Prior to earthquake, static shear stress (point A) is less than steady-state strength (point B). Loosening due to outward flow of porewater reduces steady-state strength (from point B to point C), allowing flow failure to occur.

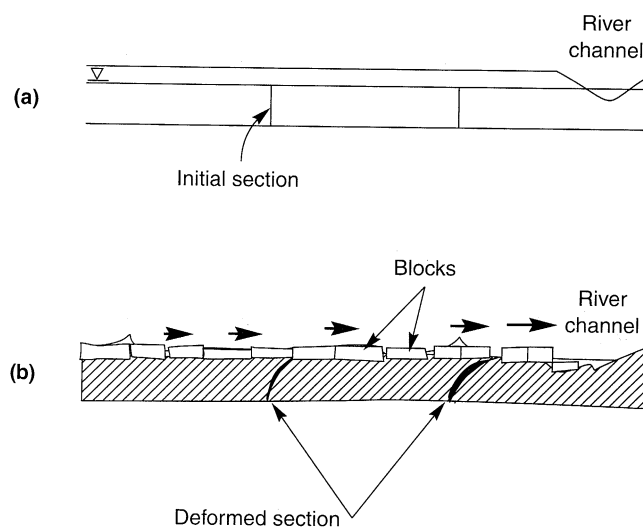


Figure 9.61 Lateral spreading adjacent to a river channel (a) before and (b) after earthquake. Lateral movement of liquefied soil (shaded zone) breaks surface layer into blocks separated by fissures. Blocks may tilt and settle differentially, and sand boils may erupt at fissures. (After Youd, 1984b.)

layers to break into blocks that progressively move downslope or toward a free face (Figure 9.2) during earthquake shaking. The ground surface may exhibit fissures and scarps at the head of the lateral spread, shear zones along its lateral margins, and compressed or buckled

soil at the toe. The surficial blocks usually move irregularly in both horizontal and vertical directions; buildings and pipelines extending across or through the head of a lateral spread may be pulled apart, pipelines crossing the lateral margins may be sheared, and bridges or pipelines near the toe may be buckled (Figure 1.8). Lateral displacements usually range from a few centimeters to a meter or two, but may be larger if shaking is particularly strong or of long duration. Procedures for estimating lateral spreading deformations are described in Section 10.6.2.2.

9.7 SUMMARY

1. The term *liquefaction* has been used to describe a number of related but different phenomena observed in loose, saturated soils. For engineering purposes, these phenomena can be divided into three main groups: flow liquefaction, cyclic mobility, and level-ground liquefaction.
2. Flow liquefaction can occur when the static shear stress in a liquefiable soil deposit is greater than the steady-state strength of the soil. It can produce devastating flow slide failures during or after earthquake shaking. Flow liquefaction can occur only in loose soils.
3. Cyclic mobility can occur when the static shear stress is less than the steady-state strength and the cyclic shear stress is large enough that the steady-state strength is exceeded momentarily. Deformations produced by cyclic mobility develop incrementally but can become substantial by the end of a strong and/or long-duration earthquake. Cyclic mobility can occur in both loose and dense soils but deformation decreases markedly with increased density.
4. Level-ground liquefaction can occur when cyclic loading is sufficient to produce high excess pore pressures, even when static driving stresses are absent. Its occurrence is generally manifested by ground oscillation, postearthquake settlement, and/or the development of sand boils. Permanent lateral displacements due to level-ground liquefaction are usually small. Level-ground liquefaction can occur in loose and dense soils.
5. Liquefaction hazard evaluation requires that questions of liquefaction susceptibility, initiation, and effects be addressed. For a site to be considered free from liquefaction hazards, the soils must be nonsusceptible to liquefaction, the anticipated loading must be insufficient to initiate liquefaction, or the effects of liquefaction must be tolerable.
6. Liquefaction susceptibility can be judged on the basis of historical, geologic, compositional, and state considerations. Geologic, compositional, and state criteria must be met for a soil to be susceptible to liquefaction; if any of these criteria are not met, the soil is nonsusceptible to liquefaction.
7. Liquefaction susceptibility is different for different liquefaction phenomena. A soil that is susceptible to cyclic mobility or level-ground liquefaction may not be susceptible to flow liquefaction. Susceptibility to various liquefaction phenomena depends primarily on the state (stress and density conditions) of the soil at the time of the earthquake.

8. Under given loading conditions, any sand will reach a unique combination of effective confining pressure, shear strength, and density at large strains. The combination can be described graphically by a steady-state line. The position of the steady-state line is most strongly influenced by grain size and grain shape characteristics. The behavior of a sand is strongly related to its position relative to the steady-state line.
9. Flow liquefaction is initiated when the principal effective stress ratio reaches a critical value under undrained, stress-controlled conditions. The stress state at the initiation of flow liquefaction can be described graphically in stress path space by the flow liquefaction surface. Once the effective stress path of an element of soil reaches the flow liquefaction surface, additional straining will induce additional excess pore pressure and the available shearing resistance will drop to the steady-state strength.
10. Because the state of a loose sand in equilibrium under high initial shear stress is closer to the flow liquefaction surface than that of a similar soil subjected to lower initial shear stress, less excess pore pressure is required to initiate flow liquefaction. Flow liquefaction can be triggered by small undrained disturbances in soils subjected to high initial shear stresses. Such soils may represent a high liquefaction hazard.
11. Cyclic mobility can produce high excess pore pressures and low effective stresses, but unidirectional movement will cause the soil to dilate. The increased shearing resistance produced by dilation will arrest soil movement so that flow slides cannot develop.
12. The existence of sand boils is often taken as evidence of level-ground liquefaction. Sand boil formation, however, depends on factors such as the depth, thickness, and void volume of the liquefied layer and on the characteristics of overlying soils. Since level-ground liquefaction of a thin and/or silty layer at depth may not be expressed at the ground surface, the absence of sand boils does not necessarily indicate that level-ground liquefaction has not occurred.
13. The cyclic stress approach to evaluation of liquefaction potential characterizes both earthquake loading and soil liquefaction resistance in terms of cyclic stresses. A transient earthquake motion is converted to an equivalent series of uniform cycles of shear stress. The number of equivalent cycles, a function of the duration of the motion, is correlated with the magnitude of the earthquake. Liquefaction resistance is obtained from laboratory or in situ tests. Cyclic triaxial and cyclic simple shear tests are usually used in the laboratory; liquefaction resistance is expressed in terms of the number of cycles required to produce failure of a soil of given density subjected to a particular level of cyclic shear stress. The cyclic stress-based liquefaction resistance, however, is influenced by factors such as soil fabric, stress and strain history, and age that may be destroyed by sampling and are difficult to replicate in the laboratory. In situ test-based procedures characterize liquefaction resistance in terms of in situ test parameters associated with soils that have liquefied in past earthquakes; the SPT resistance is most commonly used, but other insitu parameters, including CPT resistance and shear wave velocity, are gaining acceptance. The cyclic stress approach allows estimation of a factor of safety against liquefaction.
14. In the cyclic strain approach, earthquake loading and liquefaction resistance are characterized by cyclic strains. Since the factors that influence the cyclic shear stresses

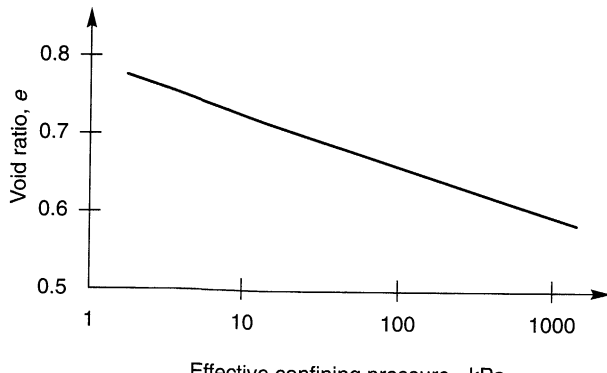
required to initiate liquefaction have a similar effect on the shear modulus, the cyclic strain (the ratio of cyclic shear stress to shear modulus) is less sensitive to them. The shear modulus is an important liquefaction resistance parameter in the cyclic strain approach. Liquefaction is expected at locations where the cyclic strain amplitude induced for a particular number of cycles by an earthquake is greater than the cyclic strain amplitude required to initiate liquefaction in the same number of cycles. The cyclic strain approach does not produce a factor of safety against liquefaction.

15. Other approaches to the evaluation of liquefaction potential have been developed. Dissipated energy has been used as a measure of liquefaction resistance; its comparison with the energy content of a ground motion allows liquefaction potential to be evaluated. Effective stress ground response analyses, with cyclic stress-strain and pore pressure models or advanced constitutive models, can be used to predict the generation of excess pore pressure and its redistribution both during and after earthquake shaking. Probabilistic approaches, based both on laboratory tests results and on field performance observations, allow estimation of the likelihood of liquefaction.
16. The effects of liquefaction are different for different liquefaction phenomena. Although flow liquefaction is capable of producing the most spectacular effects, cyclic mobility and level-ground liquefaction can also produce extensive damage.
17. Liquefaction can dramatically alter the amplitude and frequency content of ground surface motions. As the buildup of excess pore pressure causes a layer of liquefiable soil to soften, ground surface displacements may increase even when ground surface accelerations decrease. Ground oscillation may produce chaotic permanent movement of fractured blocks of surficial soil.
18. Ground surface settlement can develop during and/or after earthquakes due to densification of dry or saturated sands. Settlement of dry sand occurs almost immediately, but settlement of saturated sands may not develop until well after earthquake shaking has ended. The magnitude of postearthquake settlement depends on the density of the sand, and on the amplitude and duration of shaking.
19. When earthquake-induced shear stresses exceed the shear strength of a liquefied soil, instability failures can occur. The shear strength of liquefied soil may be evaluated by careful undisturbed sampling and laboratory testing or by comparison with in situ test parameters and back-calculated strengths from liquefaction case histories. All available approaches produce strength estimates with considerable uncertainty.
20. Liquefaction flow failures occur when static shear stresses exceed the shear strength of a liquefied soil. This situation can arise during and/or after an earthquake. The effects of soil loosening due to porewater flow on shear strength must be recognized and accounted for in an evaluation of possible flow failure.
21. Deformation failures, such as lateral spreading, develop incrementally during the period of earthquake shaking. For strong levels and/or long durations of shaking, deformation failures can produce large displacements and cause significant damage. Procedures have been developed to estimate displacements caused by deformation failures.

HOMEWORK PROBLEMS

- 9.1** A rounded sand subjected to a series of monotonic triaxial compression tests exhibits the steady-state line (SSL) shown below. Assuming that the sand can mobilize a friction angle of 33° in the steady state, estimate the steady-state strength that would be mobilized by the following test specimens:

| Specimen | Initial Void Ratio | Initial σ'_{3c} | Test Condition |
|----------|--------------------|------------------------|----------------|
| A | 0.75 | 100 kPa | Drained |
| B | 0.75 | 100 kPa | Undrained |
| C | 0.60 | 50 kPa | Drained |
| D | 0.60 | 50 kPa | Undrained |



Effective confining pressure - kPa

Figure P9.1

- 9.2** Consider an anisotropically consolidated direct simple shear test specimen with the initial conditions shown below. Show graphically how the pore pressure ratio at the initiation of liquefaction, $r_{u,t}$, varies with the amplitude of the cyclic shear stress.

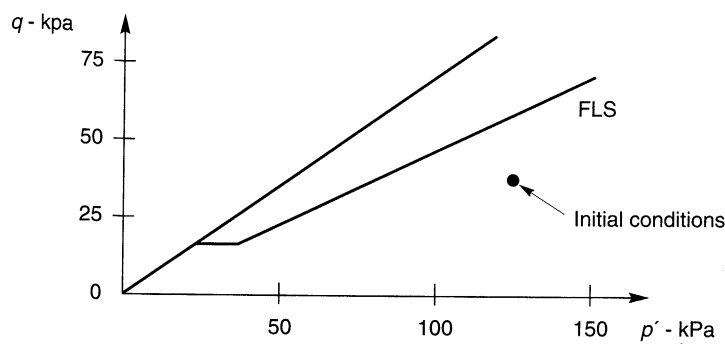


Figure P9.2

- 9.3** A 10 m thick deposit of loose sand is saturated below a depth of 3 m. The soil below the water table is highly susceptible to liquefaction. Estimate the ground surface acceleration that would be required to produce sand boils in a $M = 7.7$ earthquake.
- 9.4** Estimate the variation of uniform cyclic shear stress amplitude with depth for the upper 50 ft of soil (assume $\gamma = 120$ pcf) at the Gilroy No. 2 (soil) station in the Loma Prieta earthquake (see Figure 3.1). Estimate the number of equivalent uniform stress cycles.
- 9.5** A level deposit of saturated clean sand has an average $(N_1)_{60}$ -value of 18 and an average dry unit weight of 105 pcf. Plot the variation of cyclic shear stress required to produce liquefaction in $M = 5.5, 6.5, 7.5$, and 8.5 earthquakes.
- 9.6** Repeat Problem 9.5 assuming that the sand has 15% fines.
- 9.7** The surface of a thick deposit of silty sand (30% fines) slopes at an angle of 10° . Standard penetration tests indicate an average $(N_1)_{60}$ -value of 12; density tests indicate an average density of 1.80 Mg/m^3 . Compute and plot the cyclic shear stress required to produce liquefaction in the upper 30 ft of the silty sand in a $M = 7.5$ earthquake.
- 9.8** A level deposit of clean sand with an average void ratio of 0.70 has an uncorrected CPT tip resistance of 80 tsf at a depth of 20 ft. The mean grain size of the sand is 0.40 mm and the groundwater table is at a depth of 4 ft. Compute the cyclic shear stress required to produce liquefaction at a depth of 20 ft in a $M = 6.5$ earthquake.
- 9.9** Prior to the 1989 Loma Prieta earthquake, a site investigation at the Hunters Point Navy Base in San Francisco showed 13 to 15 m of clean, hydraulically filled sand with $D_{50} = 0.29$ mm. The water table was at a depth of about 2.5 m. CPT tests produced the following average tip resistances:

| Depth Interval (m) | Average q_c (MPa) |
|--------------------|---------------------|
| 3–4 | 6.5 |
| 4–5 | 5.7 |
| 5–6 | 5.2 |
| 6–7 | 4.9 |
| 7–8 | 5.1 |
| 8–9 | 6.3 |
| 9–10 | 6.9 |
| 10–11 | 7.6 |

The Loma Prieta earthquake produced peak ground accelerations on the order of $0.15g$ to $0.20g$ at similar sites in the Bay Area. Assuming that the sand has an average dry density of 1.60 Mg/m^3 , compute and plot the factor of safety against liquefaction that would have been expected in the Loma Prieta earthquake.

- 9.10** Plot the estimated porewater pressure distribution at the end of the Loma Prieta earthquake at the Hunters Point site described in Problem 9.9.
- 9.11** Repeat Problem 9.9 for a $M = 7.6$ earthquake that produces a peak ground acceleration of $0.30g$.
- 9.12** Using the energy-based criterion of Law et al. (1990) [(equation (9.16))], plot the limiting hypocentral distance beyond which liquefaction would not be expected in $N_1 = 10$ soils as a function of earthquake magnitude. Compare the result with Figure 9.4 and comment on the differences.

- 9.13** Estimate the vertical settlement that would have been expected at Hunters Point (see Problem 9.9) following the 1989 Loma Prieta earthquake.
- 9.14** Estimate and plot the variation of the post-liquefaction residual strength of the sand at the site described in Example 9.4 using (a) the Seed-Harder approach, and (b) the Stark-Mesri approach.

10

Seismic Slope Stability

10.1 INTRODUCTION

Landslides occur on a regular basis throughout the world as part of the ongoing evolution of landscapes. Many landslides occur in natural slopes, but slides also occur in man-made slopes from time to time. At any point in time, then, slopes exist in states ranging from very stable to marginally stable. When an earthquake occurs, the effects of earthquake-induced ground shaking is often sufficient to cause failure of slopes that were marginally to moderately stable before the earthquake. The resulting damage can range from insignificant to catastrophic depending on the geometric and material characteristics of the slope.

Earthquake-induced landslides, which have been documented from as early as 1789 B.C. (Li, 1990), have caused tremendous amounts of damage throughout history. In many earthquakes, landslides have been responsible for as much or more damage than all other seismic hazards combined. In the 1964 Alaska earthquake, for example, an estimated 56% of the total cost of damage was caused by earthquake-induced landslides (Youd, 1978; Wilson and Keefer, 1985). Kobayashi (1981) found that more than half of all deaths in large ($M > 6.9$) earthquakes in Japan between 1964 and 1980 were caused by landslides. The 1920 Haiyuan earthquake ($M = 8.5$) in the Ningxia Province of China produced hundreds of large landslides that caused more than 100,000 deaths (Close and McCormick, 1922). Evaluation of seismic slope stability is one of the most important activities of the geotechnical earthquake engineer.

This chapter we describes different types of earthquake-induced landslides and the conditions under which they occur. It also reviews the basic principles of slope stability evaluation, including static stability analysis, and then presents several methods for seismic slope stability analysis.

10.2 TYPES OF EARTHQUAKE-INDUCED LANDSLIDES

Many factors, including geologic and hydrologic conditions, topography, climate, weathering, and land use, influence the stability of slopes and the characteristics of landslides. A number of procedures for classification of landslides have been proposed; that of Varnes (1978) is perhaps most widely used in the United States. Similar principles and terminology can be used to classify earthquake-induced landslides (Table 10-1) on the basis of material type (soil

Table 10-1 Types and Characteristics of Earthquake-Induced Landslides

| Name | Type of Movement | Internal Disruption ^a | Water content ^b | | | | Velocity ^c | Depth ^d | |
|-----------------------------------|--|----------------------------------|----------------------------|---|----|---|-------------------------------|--------------------|--|
| | | | D | U | PS | S | | | |
| <i>Disrupted Slides and Falls</i> | | | | | | | | | |
| Rock falls | Bounding, rolling, free fall | High or very high | × | × | × | × | Extremely rapid | Shallow | |
| Rock slides | Translational sliding on basal shear surface | High | × | × | × | × | Rapid to extremely rapid | Shallow | |
| Rock avalanches | Complex, involving sliding and/or flow, as stream of rock fragments | Very high | × | × | × | × | Extremely rapid | Deep | |
| Soil falls | Bounding, rolling, free fall | High or very high | × | × | × | × | Extremely rapid | Shallow | |
| Disrupted soil | Translational sliding on basal shear surface or zone of weakened, sensitive clay | High | × | × | × | × | Moderate to rapid | Shallow | |
| Soil avalanches | Translational sliding with subsidiary flow | Very high | × | × | × | × | Very rapid to extremely rapid | Shallow | |
| <i>Coherent Slides</i> | | | | | | | | | |
| Rock slumps | Sliding on basal shear surface with component of headward rotation | Slight or moderate | ? | × | × | × | Slow to rapid | Deep | |

Table 10-1 Types and Characteristics of Earthquake-Induced Landslides (*continued*)

| Name | Type of Movement | Internal Disruption ^a | Water content ^b | | | | Velocity ^c | Depth ^d | |
|----------------------------------|---|--|----------------------------|---|----|---|---|--------------------------------------|--|
| | | | D | U | PS | S | | | |
| Rock block slides | Translational sliding on basal shear surface | Slight or moderate | ? | × | × | × | Slow to rapid | Deep | |
| Soil slumps | Sliding on basal shear surface with component of headward rotation | Slight or moderate | ? | × | × | × | Slow to rapid | Deep | |
| Soil block slides | Translational sliding on basal shear surface | Slight or moderate | ? | ? | × | × | Slow to rapid | Deep | |
| Slow earth flows | Translational sliding on basal shear surface with minor internal flow | Slight | | | × | × | Very slow to moderate with very rapid surges | Generally shallow, occasionally deep | |
| <i>Lateral Spreads and Flows</i> | | | | | | | | | |
| Soil lateral spreads | Translation on basal zone of liquefied sand, or silt or weakened, sensitive clay | Generally moderate, occasionally slight, occasionally high | | | × | × | Very rapid | Variable | |
| Rapid soil flows | Flow | Very high | ? | ? | ? | × | Very rapid to extremely rapid | Shallow | |
| Subaqueous landslides | Complex, generally involving lateral spreading, and/or flow; occasionally involving slumping and/or block sliding | Generally high or very high, occasionally moderate or slight | | | × | × | Generally rapid to extremely rapid, occasionally slow to moderate | Variable | |

Source: Keefer (1984).

^aInternal disruption: "slight" signifies landslide consists of one or a few coherent blocks; "moderate" signifies several coherent blocks; "high" signifies numerous small blocks and individual soil grains and rock fragments; "very high" signifies nearly complete disaggregation into individual soil grains or small rock fragments.

^bWater content: D, dry; U, moist, but unsaturated; PS, partly saturated; S, saturated.

^cVelocity:

| 0.6 m/yr | 1.5 m/yr | 1.5 m/month | 1.5 m/day | 0.3 m/min | 3 m/sec |
|----------------|-----------|-------------|-----------|-----------|------------|
| extremely slow | very slow | slow | moderate | rapid | very rapid |

^dDepth: "shallow" signifies thickness generally < 3 m; "deep" generally > 3 m.

or rock), character of movement (disrupted or coherent), and other attributes, such as velocity, depth, and water content. Earthquake-induced landslides can be divided into three main categories: disrupted slides and falls, coherent slides, and lateral spreads and flows.

Disrupted slides and falls include rock falls, rock slides, rock avalanches, soil falls, disrupted soil slides, and soil avalanches. The earth materials involved in such failures are sheared, broken, and disturbed into a nearly random order. These types of failures, usually found in steep terrain, can produce extremely rapid movements and devastating damage; rock avalanches and rock falls have historically been among the leading causes of death from earthquake-induced landslides.

Coherent slides, such as rock and soil slumps, rock and soil block slides, and slow earth flows, generally consist of a few coherent blocks that translate or rotate on somewhat deeper failure surfaces in moderate to steeply sloping terrain. Most coherent slides occur at lower velocities than disrupted slides and falls.

Lateral spreads and flows generally involve liquefiable soils, although sensitive clays can produce landslides with very similar characteristics. Due to the low residual strength of these materials, sliding can occur on remarkably flat slopes and produce very high velocities. Liquefaction-induced spreads and flow slides were discussed in detail in Chapter 9.

The different types of earthquake-induced landslides occur with different frequencies. Rock falls, disrupted soil slides, and rock slides appear to be the most common types of landslides observed in historical earthquakes (Table 10-2). Subaqueous landslides, slow earth flows, rock block slides, and rock avalanches are least common, although the difficulty of observing subaqueous slides may contribute to their apparent rarity.

Table 10-2 Relative Abundance of Earthquake-Induced Landslides from Study of 40 Historical Earthquakes Ranging from $M_s = 5.2$ to $M_w = 9.5$

| Abundance | Description |
|---|---|
| Very abundant (> 100,000 in the 40 earthquakes) | Rock falls, disrupted soil slides, rock slides |
| Abundant (10,000 to 100,000 in the 40 earthquakes) | Soil lateral spreads, soil slumps, soil block slides, soil avalanches |
| Moderately common (1000 to 10,000 in the 40 earthquakes) | Soil falls, rapid soil flows, rock slumps |
| Uncommon | Subaqueous landslides, slow earth flows, rock block slides, rock avalanches |

Source: Keefer (1984).

10.3 EARTHQUAKE-INDUCED LANDSLIDE ACTIVITY

For preliminary stability evaluations, knowledge of the conditions under which earthquake-induced landslides have occurred in past earthquakes is useful. It is logical to expect that the extent of earthquake-induced landslide activity should increase with increasing earthquake magnitude and that there could be a minimum magnitude below which earthquake-induced

landsliding would rarely occur. It is equally logical to expect that the extent of earthquake-induced landslide activity should decrease with increasing source-to-site distance and that there could be a distance beyond which landslides would not be expected in earthquakes of a given size.

A study of 300 U.S. earthquakes between 1958 and 1977 showed that the smallest earthquakes noted to have produced landslides had local magnitudes of about 4.0 (Keefer, 1984). Minimum magnitudes for different types of landslides were estimated as shown in Table 10-3. Where magnitudes were not available, minimum Modified Mercalli Intensity (MMI) values of IV and V have been observed for disrupted slides or falls and other types of slides, respectively. Although these empirically based limits are useful, their approximate nature must be recognized; failure of slopes that are near the brink of failure under static conditions could be produced by quite weak earthquake shaking.

Table 10-3 Estimates of the Smallest Earthquakes Likely to Cause Landslides

| M_L | Description |
|-------|---|
| 4.0 | Rock falls, rock slides, soil falls, disrupted soil slides |
| 4.5 | Soil slumps, soil block slides |
| 5.0 | Rock slumps, rock block slides, slow earth flows, soil lateral spreads, rapid soil flows, and subaqueous landslides |
| 6.0 | Rock avalanches |
| 6.5 | Soil avalanches |

Source: After Keefer (1984).

The maximum source-to-site distance at which landslides have been produced in historical earthquakes are different for different types of landslides (Figure 10.1). Disrupted slides or falls, for example, have rarely been found beyond epicentral distances of about 15 km for $M = 5$ events but have been observed as far as about 200 km (124 mi.) in $M = 7$ earthquakes. Note that the curve for lateral spreads and flows correlates reasonably well with the magnitude-distance curve for liquefaction shown in Figure 9.5. Similarly, the area over which earthquake-induced landsliding can be expected also increases with increasing earthquake magnitude (Figure 10.2). Regional differences in attenuation behavior have little apparent influence on the area of earthquake-induced landsliding.

Example 10.1

Estimate the maximum distances at which rock avalanches, soil slumps, and soil lateral spreads would be expected in a $M = 6.5$ earthquake.

Solution Rock avalanches, soil slumps, and soil lateral spreads fall under the headings of disrupted falls and slides, coherent slides, and lateral spreads and flows, respectively. From Figure 10.1, the maximum distances of these types of slides from the fault rupture zone would be

| | |
|----------------------|-------|
| Rock avalanche | 61 km |
| Soil slumps | 22 km |
| Soil lateral spreads | 20 km |

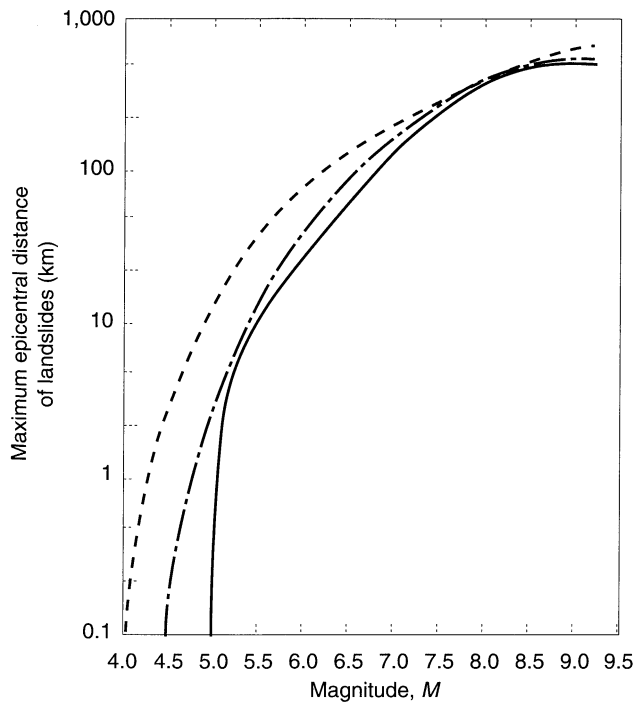


Figure 10.1 Maximum epicentral distance for different types of landslides. Dashed line is for disrupted falls and slides, dash-dot line is for coherent slides, and solid line is for lateral spreads and flows. (After Keefer, 1984. Used by permission of the Geological Society of America.)

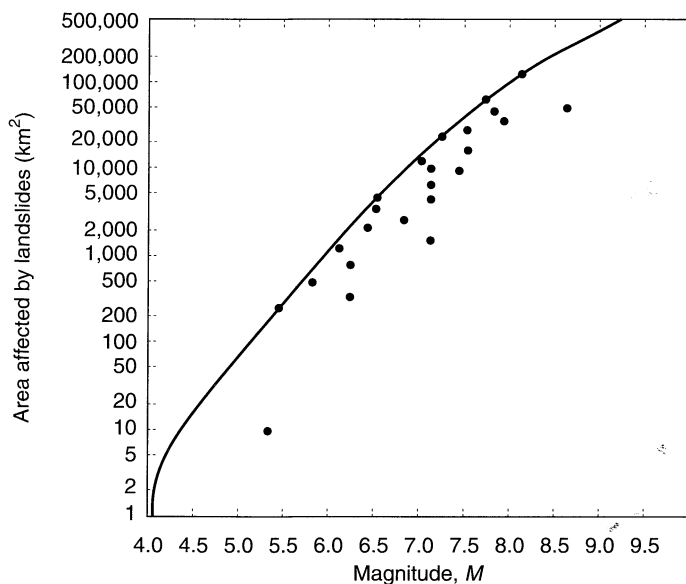


Figure 10.2 Area affected by landslides for earthquakes of different magnitude. (After Keefer, 1984. Used by permission of the Geological Society of America.)

10.4 EVALUATION OF SLOPE STABILITY

The stability of slopes is influenced by many factors, and a complete slope stability evaluation must consider the effects of each. Geological, hydrological, topographical, geometrical, and material characteristics all influence the stability of a particular slope. Information on these characteristics is needed to reliably perform and interpret the results of both static and seismic slope stability analyses. Review of available documents, field reconnaissance, field monitoring, subsurface investigation, and material testing can all be used to obtain this information.

For many sites, considerable useful information can be obtained from previously published documents such as geologic maps, soil survey and/or agricultural maps, topographic maps, natural hazard maps, and geologic and geotechnical engineering reports. Additional information may be obtained from aerial photographs (particularly stereo-paired aerial photographs) and other forms of remote sensing.

Field reconnaissance involves careful observation and detailed mapping of a variety of site characteristics associated with existing or potential slope instability. Features such as scarps; tension cracks; bulges; hummocky terrain; displaced ditches, channels, and fences; cracked foundations, walls, or pavements; and leaning trees or poles can be identified and mapped as evidence of instability. The locations of streams, springs, seeps, ponds, and moist areas, and differences in vegetative cover, can provide evidence of altered or disrupted water flow caused by slope instability.

If time permits, slope movement can be monitored. Surface monuments can be installed at points on and near the slope and surveyed periodically to identify the magnitude and direction of surface movement. Photogrammetric methods can be used to determine relative movements from sets of stereo-paired aerial photographs taken at different times. Inclinometers are very useful for monitoring lateral deformation patterns below the ground surface. In many cases, crack gauges, tiltmeters, and extensometers can also be used to observe the effects of slope movement. When, as is commonly the case, pore pressures are important, piezometers and/or observation wells can provide important information on pore pressures and their variation with time.

Subsurface investigation can include excavation and mapping of test pits and trenches, boring and sampling, in situ testing, and geophysical testing. Such investigations can reveal the depth, thickness, density, strength, and deformation characteristics of subsurface units, and the depth and variation of the groundwater table. In situ and geophysical tests are particularly useful for determining the location of an existing failure surface.

Laboratory tests are often used to quantify the physical characteristics of the various subsurface materials for input into a numerical slope stability analysis. Soil density, strength, and stress-strain behavior are of prime importance; other characteristics, such as grain size distribution, plasticity, permeability, and compressibility, are also useful.

Only after this information is obtained can a stability analysis be performed. Although in the remainder of this chapter we focus on methods of slope stability analysis, it is important to remember that the analysis itself is but a single part of a complete slope stability evaluation and that its accuracy will be reduced if careful attention is not given to the other aspects of the evaluation.

10.5 STATIC SLOPE STABILITY ANALYSIS

Slopes become unstable when the shear stresses required to maintain equilibrium reach or exceed the available shearing resistance on some potential failure surface. For slopes in which the shear stresses required to maintain equilibrium under static gravitational loading are high, the additional dynamic stresses needed to produce instability may be low. Hence the seismic stability of a slope is strongly influenced by its static stability. Because of this and the fact that the most commonly used methods of seismic stability analysis rely on static stability analyses, a brief summary of static slope stability analysis is presented.

The procedures for analysis of slope stability under static conditions are well established. An excellent, concise review of the state of the art for static analysis was presented by Duncan (1992). Detailed descriptions of specific methods of analysis can be found in standard references such as National Research Council (1976), Chowdhury (1978), and Huang (1983). Currently, the most commonly used methods of static slope stability analysis are *limit equilibrium analyses* and *stress-deformation analyses*.

10.5.1 Limit Equilibrium Analysis

Limit equilibrium analyses consider force and/or moment equilibrium of a mass of soil above a potential failure surface. The soil above the potential failure surface is assumed to be rigid (i.e., shearing can occur only on the potential failure surface). The available shear strength is assumed to be mobilized at the same rate at all points on the potential failure surface. As a result, the factor of safety is constant over the entire failure surface. Because the soil on the potential failure surface is assumed to be rigid–perfectly plastic (Figure 10.3), limit equilibrium analyses provide no information on slope deformations.

Slope stability is usually expressed in terms of an index, most commonly the *factor of safety*, which is usually defined as

$$FS = \frac{\text{available shear strength}}{\text{shear stress required to maintain equilibrium}} \quad (10.1)$$

Thus the factor of safety is a ratio of capacity (the shear strength of the soil) to demand (the shear stress induced on the potential failure surface). The factor of safety can also be viewed as the factor by which the strength of the soil would have to be divided to bring the slope to the brink of instability. In contrast to the assumptions of limit equilibrium analysis, the strength of the soil in actual slopes is not reached at the same time at all points on the failure surface (i.e., the local factor of safety is not constant).

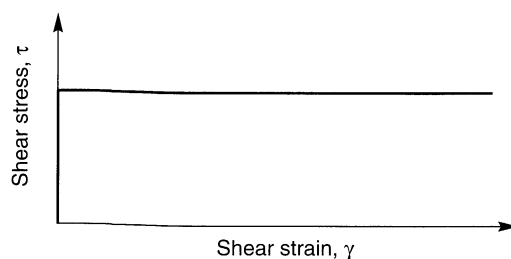


Figure 10.3 Stress-strain curve for a rigid–perfectly plastic material. No shear strain occurs until the strength of the material is reached, after which the material strains at constant shear stress.

A variety of limit equilibrium procedures have been developed to analyze the static stability of slopes. Slopes that fail by translation on a planar failure surface (Figure 10.4a) such as a bedding plane, rock joint, or seam of weak material can be analyzed quite easily by the Culmann method (Taylor, 1948). Slopes in which failure is likely to occur on two or three planes (Figure 10.4b) can be analyzed by wedge methods (e.g., Perloff and Baron, 1976; Lambe and Whitman, 1969). In homogeneous slopes, the critical failure surface usually has a circular (Figure 10.4c) or log-spiral shape. Since the minimum factors of safety for circular and log-spiral failure surfaces are very close, homogeneous slopes are usually analyzed by methods such as the ordinary method of slices (Fellenius, 1927) or Bishop's modified method (Bishop, 1955), which assume circular failure surfaces. When subsurface conditions are not homogeneous (e.g., when layers with significantly different strength, highly anisotropic strength, or discontinuities exist), failure surfaces are likely to be non-circular (Figure 10.4d). In such cases, methods like those of Morgenstern and Price (1965), Spencer (1967), and Janbu (1968) may be used. Nearly all limit equilibrium methods are susceptible to numerical problems under certain conditions. These conditions vary for different methods but are most commonly encountered where soils with high cohesive strength are present at the top of a slope and/or when failure surfaces emerge steeply at the base of slopes in soils with high frictional strength (Duncan, 1992).

In concept, any slope with a factor of safety above 1.0 should be stable. In practice, however, the level of stability is seldom considered acceptable unless the factor of safety is significantly greater than 1.0. Criteria for acceptable factors of safety recognize (1) uncertainty in the accuracy with which the slope stability analysis represents the actual mechanism of failure, (2) uncertainty in the accuracy with which the input parameters (shear strength, groundwater conditions, slope geometry, etc.) are known, (3) the likelihood and duration of exposure to various types of external loading, and (4) the potential consequences of slope failure. Typical minimum factors of safety used in slope design are about 1.5 for normal long-term loading conditions and about 1.3 for temporary slopes or end-of-construction conditions in permanent slopes (when dissipation of pore pressure increases stability with time).

When the minimum factor of safety of a slope reaches a value of 1.0, the available shear strength of the soil is fully mobilized on some potential failure surface and the slope

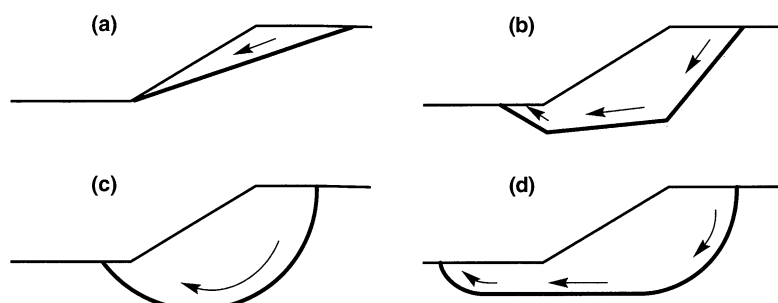


Figure 10.4 Common failure surface geometries: (a) planar; (b) multiplanar; (c) circular; (d) noncircular.

is at the point of incipient failure. Any additional loading will cause the slope to fail (i.e., to deform until it reaches a configuration in which the shear stresses required for equilibrium are less than or equal to the available shear strength of the soil). The limit equilibrium assumption of rigid–perfectly plastic behavior suggests that the required deformation will occur in a ductile manner. Many soils, however, exhibit brittle, strain-softening stress-strain behavior. In such cases the peak shear strength may not be mobilized simultaneously at all points on the failure surface. When the peak strength of a strain-softening soil is reached, such as point A in Figure 10.5a, the available shearing resistance will drop from the peak to the residual strength. As it does so, shear stresses related to the difference between the peak and residual strength of the soil at point A are transferred to the surrounding soil. These redistributed shear stresses may cause the peak strengths in the surrounding soil to be reached (Figure 10.5b) and exceeded, thereby reducing their available shearing resistances to residual values. As the stress redistribution process continues, the zone of failure may grow until the entire slope becomes unstable. Many instances of such *progressive failure* have been observed in strain-softening soils, even when the limit equilibrium factor of safety (based on peak strength) is well above 1.0. Within the constraints of limit equilibrium analysis, the stability of slopes with strain-softening materials can be analyzed reliably only by using residual shear strengths.

Limit equilibrium analyses must be formulated with great care. Since the available shearing resistance of the soil depends on porewater drainage conditions, those conditions must be considered carefully in the selection of shear strengths and pore pressure conditions for the analysis. Duncan (1992) provided guidelines for the selection of input parameters for limit equilibrium slope stability analyses.

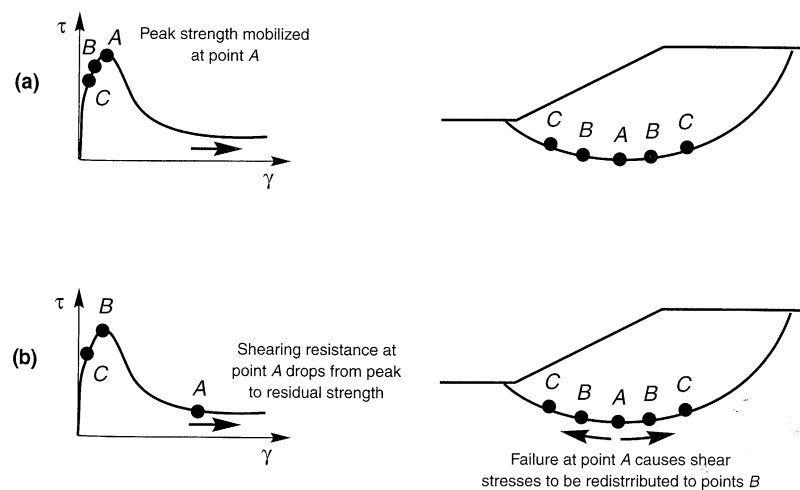


Figure 10.5 Development of progressive failure in slope comprised of strain-softening materials: (a) exceedance of peak strength at any point (A) reduces strength at that point to residual value; (b) redistribution of shear stresses from failure zone to surrounding area produces failure in surrounding zone (points B). Continued redistribution of stresses can eventually lead to failure of the entire slope (points C and beyond).

10.5.2 Stress-Deformation Analyses

Stress-deformation analyses allow consideration of the stress-strain behavior of soil and rock and are most commonly performed using the finite-element method. When applied to slopes, stress-deformation analyses can predict the magnitudes and patterns of stresses, movements, and pore pressures in slopes during and after construction/deposition. Non-linear stress-strain behavior, complex boundary conditions, irregular geometries, and a variety of construction operations can all be considered in modern finite-element analyses.

For static slope stability analysis, stress-deformation analyses offer the advantages of being able to identify the most likely mode of failure by predicting slope deformations up to (and in some cases beyond) the point of failure, of locating the most critically stressed zones within a slope, and of predicting the effects of slope failures. These advantages come at the cost of increased engineering time for problem formulation, characterization of material properties and interpretation of results, and increased computational effort.

The accuracy of stress-deformation analyses is strongly influenced by the accuracy with which the stress-strain model represents actual material behavior. Many different stress-strain models have been used for stress-deformation analysis of slopes; each has advantages and limitations. The accuracy of simple models is usually limited to certain ranges of strain and/or certain stress paths. Models that can be applied to more general stress and strain conditions are often quite complex and may require a large number of input parameters whose values can be difficult to determine. For many problems, the hyperbolic model (Kondner, 1963; Kondner and Zelasko, 1963; Duncan and Chang, 1970; Duncan et al., 1980) offers an appropriate compromise between simplicity and accuracy.

10.6 SEISMIC SLOPE STABILITY ANALYSIS

The previously described procedures for static slope stability analysis have been used for many years and calibrated against many actual slope failures. The database against which seismic slope stability analyses can be calibrated is much smaller. Analysis of the seismic stability of slopes is further complicated by the need to consider the effects of (1) dynamic stresses induced by earthquake shaking, and (2) the effects of those stresses on the strength and stress-strain behavior of the slope materials.

Seismic slope instabilities may be grouped into two categories on the basis of which of these effects is predominant in a given slope. In *inertial instabilities*, the shear strength of the soil remains relatively constant, but slope deformations are produced by temporary exceedances of the strength by dynamic earthquake stresses. *Weakening instabilities* are those in which the earthquake serves to weaken the soil sufficiently that it cannot remain stable under earthquake-induced stresses. Flow liquefaction and cyclic mobility (Chapter 9) are the most common causes of weakening instability. A number of analytical techniques, based on both limit equilibrium and stress-deformation analyses, are available for both categories of seismic instability.

10.6.1 Analysis of Inertial Instability

Earthquake motions can induce significant horizontal and vertical dynamic stresses in slopes. These stresses produce dynamic normal and shear stresses along potential failure surfaces within a slope. When superimposed upon the previously existing static shear

stresses, the dynamic shear stresses may exceed the available shear strength of the soil and produce inertial instability of the slope. A number of techniques for the analysis of inertial instability have been proposed. These techniques differ primarily in the accuracy with which the earthquake motion and the dynamic response of the slope are represented. The following sections describe several common approaches to the analysis of inertial instability. The first, pseudostatic analysis, produces a factor of safety against seismic slope failure in much the same way that static limit equilibrium analyses produce factors of safety against static slope failure. All the other approaches attempt to evaluate permanent slope displacements produced by earthquake shaking.

10.6.1.1 Pseudostatic Analysis

Beginning in the 1920s, the seismic stability of earth structures has been analyzed by a *pseudostatic* approach in which the effects of an earthquake are represented by constant horizontal and/or vertical accelerations. The first explicit application of the pseudostatic approach to the analysis of seismic slope stability has been attributed to Terzaghi (1950).

In their most common form, pseudostatic analyses represent the effects of earthquake shaking by pseudostatic accelerations that produce inertial forces, F_h and F_v , which act through the centroid of the failure mass (Figure 10.6). The magnitudes of the pseudostatic forces are

$$F_h = \frac{a_h W}{g} = k_h W \quad (10.2a)$$

$$F_v = \frac{a_v W}{g} = k_v W \quad (10.2b)$$

where a_h and a_v are horizontal and vertical pseudostatic accelerations, k_h and k_v are dimensionless horizontal and vertical pseudostatic coefficients, and W is the weight of the failure mass. The magnitudes of the pseudostatic accelerations should be related to the severity of the anticipated ground motion; selection of pseudostatic accelerations for design is, as discussed in the next section, not a simple matter. Resolving the forces on the potential failure mass in a direction parallel to the failure surface,

$$FS = \frac{\text{resisting force}}{\text{driving force}} = \frac{cl_{ab} + [(W - F_v) \cos\beta - F_h \sin\beta] \tan\phi}{(W - F_v) \sin\beta + F_h \cos\beta} \quad (10.3)$$

where c and ϕ are the Mohr–Coulomb strength parameters that describe the shear strength on the failure plane and l_{ab} is the length of the failure plane. The horizontal pseudostatic

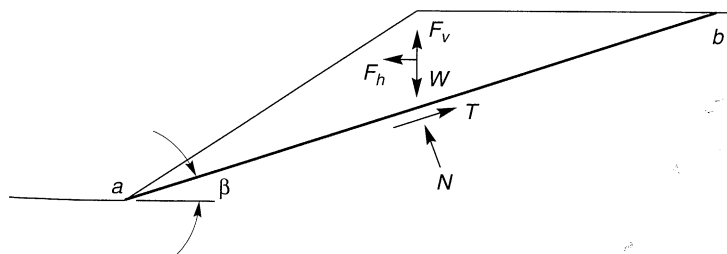


Figure 10.6 Forces acting on triangular wedge of soil above planar failure surface in pseudostatic slope stability analysis.

force clearly decreases the factor of safety—it reduces the resisting force (for $\phi > 0$) and increases the driving force. The vertical pseudostatic force typically has less influence on the factor of safety since it reduces (or increases, depending on its direction) both the driving force and the resisting force—as a result, the effects of vertical accelerations are frequently neglected in pseudostatic analyses. The pseudostatic approach can be used to evaluate pseudostatic factors of safety for planar, circular, and noncircular failure surfaces. Many commercially available computer programs for limit equilibrium slope stability analysis have the option of performing pseudostatic analyses.

Example 10.2

Assuming $k_h = 0.1$ and $k_v = 0.0$, compute the static and pseudostatic factors of safety for the 30-ft-high 2:1 (H:V) slope shown in Figure E10.2.

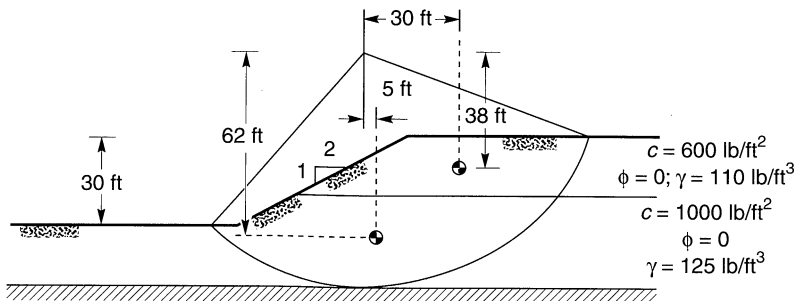


Figure E10.2

Solution Using a simple moment equilibrium analysis, the factor of safety can be defined as the ratio of the moment that resists rotation of a potential failure mass about the center of a circular potential failure surface to the moment that is driving the rotation. The critical failure surface, defined as that which has the lowest factor of safety, is identified by analyzing a number of potential failure surfaces. Shown below are the factor-of-safety calculations for one potential failure surface which may or may not be the critical failure surface.

Computation of the factor of safety requires evaluation of the overturning and resisting moments for both static and pseudostatic conditions. The overturning moment for static conditions results from the weight of the soil above the potential failure surface. The overturning moment for pseudostatic conditions is equal to the sum of the overturning moment for static conditions and the overturning moment produced by the pseudostatic forces. The horizontal pseudostatic forces are assumed to act in directions that produce positive (clockwise, in this case) driving moments. In the calculations shown in tabular form below, the soil above the potential failure mass is divided into two sections.

Overturning moments:

| Section | Area (ft ²) | γ (lb/ft ³) | W (kips/ft) | Static | | | Pseudostatic | | | Total Moment (kip-ft/ft) |
|---------|----------------------------|--------------------------------|-------------|--------------------|-----------------------|----------------------|--------------------|-----------------------|--------|--------------------------------|
| | | | | Moment Arm (ft) | Moment (kip-ft/ft) | $k_h W$ (kips/ft) | Moment Arm (ft) | Moment (kip-ft/ft) | | |
| A | 1360 | 110 | 149.6 | 30 | 4488.1 | 15.0 | 38 | 570.0 | 5058.0 | |
| B | 2300 | 125 | 287.5 | 5 | 1437.5 | 28.8 | 62 | 1785.6 | 3223.1 | 8281.1 |

Resisting moment:

| Section | Length (ft) | c (lb/ft 2) | Force (kips) | Moment Arm (ft) | Moment (kip-ft/ft) |
|---------|-------------|-------------------|--------------|-----------------|--------------------|
| A | 11.5 | 600 | 6.9 | 78 | 538.2 |
| B | 129.3 | 1000 | 129.3 | 78 | <u>10,085.4</u> |
| | | | | | 10,623.6 |

Factor of safety:

$$\text{Static FS} = \frac{\text{resisting moment}}{\text{static overturning moment}} = \frac{10,623.6}{5925.5} = 1.79$$

$$\begin{aligned}\text{Pseudostatic FS} &= \frac{\text{resisting moment}}{\text{static + pseudostatic overturning moments}} \\ &= \frac{10,623.6}{8281.1} = 1.28\end{aligned}$$

Selection of Pseudostatic Coefficient. The results of pseudostatic analyses are critically dependent on the value of the seismic coefficient, k_h . Selection of an appropriate pseudostatic coefficient is the most important, and most difficult, aspect of a pseudostatic stability analysis. The seismic coefficient controls the pseudostatic force on the failure mass, so its value should be related to some measure of the amplitude of the inertial force induced in the potentially unstable material. If the slope material was rigid, the inertial force induced on a potential slide would be equal to the product of the actual horizontal acceleration and the mass of the unstable material. This inertial force would reach its maximum value when the horizontal acceleration reached its maximum value. In recognition of the fact that actual slopes are not rigid and that the peak acceleration exists for only a very short time, the pseudostatic coefficients used in practice generally correspond to acceleration values well below a_{\max} . Terzaghi (1950) originally suggested the use of $k_h = 0.1$ for “severe” earthquakes (Rossi-Forel IX), $k_h = 0.2$ for “violent, destructive” earthquakes (Rossi-Forel X), and $k_h = 0.5$ for “catastrophic” earthquakes. Seed (1979) listed pseudostatic design criteria for 14 dams in 10 seismically active countries; 12 required minimum factors of safety of 1.0 to 1.5 with pseudostatic coefficients of 0.10 to 0.12. Marcuson (1981) suggested that appropriate pseudostatic coefficients for dams should correspond to one-third to one-half of the maximum acceleration, including amplification or deamplification effects, to which the dam is subjected. Using shear beam models, Seed and Martin (1966) and Dakoulas and Gazetas (1986) showed that the inertial force on a potentially unstable slope in an earth dam depends on the response of the dam and that the average seismic coefficient for a deep failure surface is substantially smaller than that of a failure surface that does not extend far below the crest. Seed (1979) also indicated that deformations of earth dams constructed of ductile soils (defined as those that do not generate high pore pressures or show more than 15% strength loss upon cyclic loading) with crest accelerations less than $0.75g$ would be acceptably small for pseudostatic factors of safety of at least 1.15 with $k_h = 0.10$ ($M = 6.5$) to $k_h = 0.15$ ($M = 8.25$). This criteria would allow the use of pseudostatic accelerations as small as 13 to 20% of the peak crest acceleration. Hynes-Griffin and Franklin (1984) applied the Newmark sliding block analysis described in the following section to over 350 accelerograms and concluded that earth dams with pseudostatic factors of safety greater than 1.0 using $k_h = 0.5a_{\max}/g$ would not develop “dangerously large” deformations.

As the preceding discussion indicates, there are no hard and fast rules for selection of a pseudostatic coefficient for design. It seems clear, however, that the pseudostatic coefficient should be based on the actual anticipated level of acceleration in the failure mass (including any amplification or deamplification effects) and that it should correspond to some fraction of the anticipated peak acceleration. Although engineering judgment is required for all cases, the criteria of Hynes-Griffin and Franklin (1984) should be appropriate for most slopes.

Limitations of the Pseudostatic Approach. Representation of the complex, transient, dynamic effects of earthquake shaking by a single constant unidirectional pseudostatic acceleration is obviously quite crude. Even in its infancy, the limitations of the pseudostatic approach were clearly recognized. Terzaghi (1950) stated that "the concept it conveys of earthquake effects on slopes is very inaccurate, to say the least," and that a slope could be unstable even if the computed pseudostatic factor of safety was greater than 1. Detailed analyses of historical and recent earthquake-induced landslides (e.g., Seed et al., 1969, 1975; Marcuson et al., 1979) have illustrated significant shortcomings of the pseudostatic approach. Experience has clearly shown, for example, that pseudostatic analyses can be unreliable for soils that build up large pore pressures or show more than about 15% degradation of strength due to earthquake shaking. As illustrated in Table 10-4, pseudostatic analyses produced factors of safety well above 1 for a number of dams that later failed during earthquakes. These cases illustrate the inability of the pseudostatic method to reliably evaluate the stability of slopes susceptible to weakening instability. Nevertheless, the pseudostatic approach can provide at least a crude index of relative, if not absolute, stability.

Discussion. The pseudostatic approach has a number of attractive features. The analysis is relatively simple and straightforward; indeed, its similarity to the static limit equilibrium analyses routinely conducted by geotechnical engineers makes its computations easy to understand and perform. It produces a scalar index of stability (the factor of safety) that is analogous to that produced by static stability analyses. It must always be recognized, however, that the accuracy of the pseudostatic approach is governed by the accuracy with which the simple pseudostatic inertial forces represent the complex dynamic inertial forces that actually exist in an earthquake. Difficulty in the assignment of appropriate pseudostatic coefficients and in interpretation of pseudostatic factors of safety, coupled with the development of more realistic methods of analysis, have reduced the use of the pseudostatic approach for seismic slope stability analyses. Methods based on evaluation of permanent slope deformation, such as those described in the following sections, are being used increasingly for seismic slope stability analysis.

Table 10-4 Results of Pseudostatic Analyses of Earth Dams That Failed during Earthquakes

| Dam | k_h | FS | Effect of Earthquake |
|------------------------|-------|--------|--|
| Sheffield Dam | 0.10 | 1.2 | Complete failure |
| Lower San Fernando Dam | 0.15 | 1.3 | Upstream slope failure |
| Upper San Fernando Dam | 0.15 | ~2–2.5 | Downstream shell, including crest slipped about 6 ft downstream |
| Tailings dam (Japan) | 0.20 | ~1.3 | Failure of dam with release of tailings |

Source: After Seed (1979).

10.6.1.2 Newmark Sliding Block Analysis

The pseudostatic method of analysis, like all limit equilibrium methods, provides an index of stability (the factor of safety) but no information on deformations associated with slope failure. Since the serviceability of a slope after an earthquake is controlled by deformations, analyses that predict slope displacements provide a more useful indication of seismic slope stability. Since earthquake-induced accelerations vary with time, the pseudostatic factor of safety will vary throughout an earthquake. If the inertial forces acting on a potential failure mass become large enough that the total (static plus dynamic) driving forces exceed the available resisting forces, the factor of safety will drop below 1.0. Newmark (1965) considered the behavior of a slope under such conditions. When the factor of safety is less than 1.0, the potential failure mass is no longer in equilibrium; consequently, it will be accelerated by the unbalanced force. The situation is analogous to that of a block resting on an inclined plane (Figure 10.7). Newmark used this analogy to develop a method for prediction of the permanent displacement of a slope subjected to any ground motion.

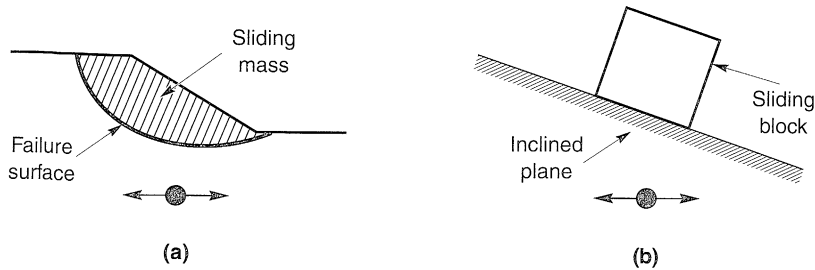


Figure 10.7 Analogy between (a) potential landslide and (b) block resting on inclined plane.

Consider the block in stable, static equilibrium on the inclined plane of Figure 10.7b. Under static conditions, equilibrium of the block (in the direction parallel to the plane) requires that the available static resisting force, R_s , exceed the static driving force, D_s (Figure 10.8a). Assuming that the block's resistance to sliding is purely frictional ($c = 0$)

$$FS = \frac{\text{available resisting force}}{\text{static driving force}} = \frac{R_s}{D_s} = \frac{W \cos \beta \tan \phi}{W \sin \beta} = \frac{\tan \phi}{\tan \beta} \quad (10.4)$$

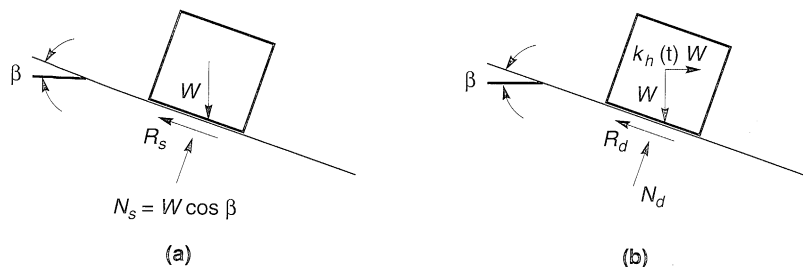


Figure 10.8 Forces acting on a block resting on an inclined plane: (a) static conditions; (b) dynamic conditions.

where ϕ is the angle of friction between the block and the plane. Now consider the effect of inertial forces transmitted to the block by horizontal vibration of the inclined plane with acceleration, $a_h(t) = k_h(t)g$ (the effects of vertical accelerations will be neglected for simplicity). At a particular instant of time, horizontal acceleration of the block will induce a horizontal inertial force, k_hW (Figure 10.8b). When the inertial force acts in the downslope direction, resolving forces perpendicular to the inclined plane gives

$$FS_d(t) = \frac{\text{available resisting force}}{\text{pseudostatic driving force}} = \frac{R_d(t)}{D_d(t)} = \frac{[\cos\beta - k_h(t)\sin\beta]\tan\phi}{\sin\beta + k_h(t)\cos\beta} \quad (10.5)$$

Obviously, the dynamic factor of safety decreases as k_h increases and there will be (for a statically stable block) some positive value of k_h that will produce a factor of safety of 1.0 (Figure 10.9). This coefficient, termed the *yield coefficient*, k_y , corresponds to the *yield acceleration*, $a_y = k_yg$. The yield acceleration is the minimum pseudostatic acceleration required to produce instability of the block. For the block of Figure 10.8,

$$k_y = \tan(\phi - \beta) \quad (10.6)$$

for sliding in the downslope direction. For sliding in the uphill direction (which can occur when β and ϕ are small),

$$k_y = \frac{\tan\phi + \tan\beta}{1 + \tan\phi\tan\beta} \quad (10.7)$$

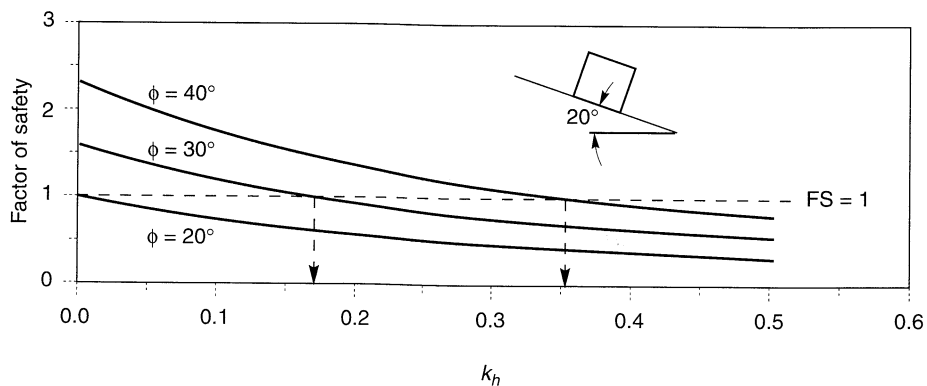


Figure 10.9 Variation of pseudostatic factor of safety with horizontal pseudostatic coefficient for block on plane inclined at 20° . For $\phi = 20^\circ$, block is at the point of failure (FS = 1) under static conditions, so the yield coefficient is zero. For $\phi = 30^\circ$ and $\phi = 40^\circ$, yield coefficients are 0.17 and 0.36, respectively.

Example 10.3

Compute the yield acceleration for the slope described in Example 10.2.

Solution The yield acceleration can be computed by trial and error, or computed directly for relatively simple slopes. Reviewing Example 10.2, it is apparent that the total moment is equal to

$$\begin{aligned} M_t &= 4488 \text{ k-ft/ft} + k_h(5685 \text{ k-ft/ft}) + 1438 \text{ k-ft/ft} + k_h(17825 \text{ k-ft/ft}) \\ &= 5926 \text{ k-ft/ft} + k_h(23510 \text{ k-ft/ft}) \end{aligned}$$

The yield coefficient is the value of k_h that produces a pseudostatic factor of safety of 1. Because the resisting moment is equal to the overturning moment when FS = 1,

$$5926 \text{ k-ft/ft} + k_h(23510 \text{ k-ft/ft}) = 10624 \text{ k-ft/ft}$$

or

$$k_h = \frac{10624 \text{ k-ft/ft} - 5926 \text{ k-ft/ft}}{23510 \text{ k-ft/ft}} = 0.20$$

Therefore, the yield acceleration is $0.20g$.

When a block on an inclined plane is subjected to a pulse of acceleration that exceeds the yield acceleration, the block will move relative to the plane. To illustrate the procedure by which the resulting permanent displacements can be calculated, consider the case in which an inclined plane is subjected to a single rectangular acceleration pulse of amplitude A and duration Δt . If the yield acceleration, a_y , is less than A (Figure 10.10a), the acceleration of the block relative to the plane during the period from t_0 to $t_0 + \Delta t$ is

$$a_{\text{rel}}(t) = a_b(t) - a_y = A - a_y \quad t_0 \leq t \leq t_0 + \Delta t \quad (10.8a)$$

where $a_b(t)$ is the acceleration of the inclined plane. The relative movement of the block during this period can be obtained by integrating the relative acceleration twice, that is,

$$v_{\text{rel}}(t) = \int_{t_0}^t a_{\text{rel}}(t) dt = [A - a_y](t - t_0) \quad t_0 \leq t \leq t_0 + \Delta t \quad (10.8b)$$

$$d_{\text{rel}}(t) = \int_{t_0}^t v_{\text{rel}}(t) dt = \frac{1}{2}[A - a_y](t - t_0)^2 \quad t_0 \leq t \leq t_0 + \Delta t \quad (10.8c)$$

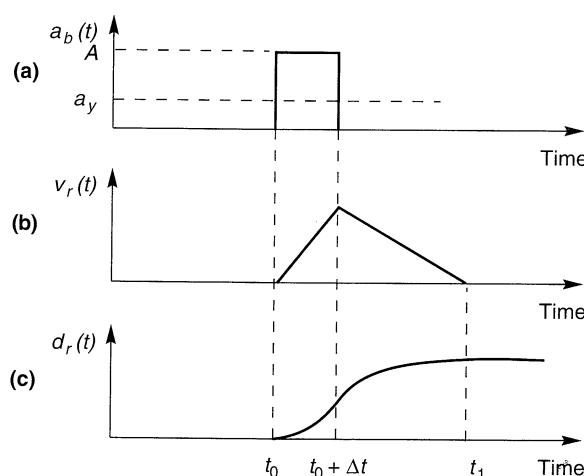


Figure 10.10 Variation of relative velocity and relative displacement between sliding block and plane due to rectangular pulse that exceeds yield acceleration between $t = t_0$ and $t = t_0 + \Delta t$.

At $t = t_0 + \Delta t$, the relative velocity reaches its maximum value. At that time

$$v_{\text{rel}}(t_0 + \Delta t) = [A - a_y]\Delta t \quad (10.9a)$$

$$d_{\text{rel}}(t_0 + \Delta t) = \frac{1}{2}[A - a_y]\Delta t^2 \quad (10.9b)$$

After the base acceleration drops to zero (at $t = t_0 + \Delta t$), the sliding block is decelerated by the friction force acting on its base. The block will continue to slide on the plane, but at a decreasing velocity which eventually reaches zero. The acceleration during this time is given by

$$a_{\text{rel}}(t) = a_b(t) - a_y = 0 - a_y = -a_y \quad t_0 + \Delta t \leq t \leq t_1 \quad (10.10a)$$

where t_1 is the time at which the relative velocity becomes zero (note that the block undergoes negative acceleration, or deceleration, during this period). Between $t_0 + \Delta t$ and t_1 , the relative velocity will decrease with time according to

$$v_{\text{rel}}(t) = v_{\text{rel}}(t_0 + \Delta t) + \int_{t_0 + \Delta t}^t a_{\text{rel}} dt = A \Delta t - a_y(t - t_0) \quad t_0 + \Delta t \leq t \leq t_1 \quad (10.10b)$$

Setting the relative velocity equal to zero at $t = t_1$ gives

$$t_1 = t_0 + \frac{A}{a_y} \Delta t$$

Then

$$d_{\text{rel}}(t) = \int_{t_0 + \Delta t}^t v_{\text{rel}}(t) dt = A \Delta t (t - t_0 - \Delta t) - \frac{1}{2} [t^2 - (t_0 + \Delta t)^2] \quad t_0 + \Delta t \leq t \leq t_1 \quad (10.10c)$$

After time t_1 , the block and inclined plane move together. During the total period of time between $t = t_0$ and $t = t_1$, the relative movement of the block is as shown in Figure 10.10. Between t_0 and $t_0 + \Delta t$, the relative velocity increases linearly and the relative displacement quadratically. At $t_0 + \Delta t$, the relative velocity has reached its maximum value, after which it decreases linearly. The relative displacement continues to increase (but at a decreasing rate) until $t = t_1$. Note that the total relative displacement

$$d_{\text{rel}}(t_1) = \frac{1}{2} (A - a_y) \Delta t^2 \frac{A}{a_y} \quad (10.11)$$

depends strongly on both the amount by which and the length of time during which the yield acceleration is exceeded. This suggests that the relative displacement caused by a single pulse of strong ground motion should be related to both the amplitude and frequency content of that pulse. An earthquake motion, however, can exceed the yield acceleration a number of times and produce a number of increments of displacement (Figure 10.11). Thus the total displacement will be influenced by strong-motion duration as well as amplitude and frequency content. Indeed, application of this approach to a variety of simple waveforms (e.g., Sarma, 1975; Yegian et al., 1991) have shown that the permanent displacement of a sliding block subjected to rectangular, sinusoidal, and triangular periodic base motions is proportional to the *square* of the period of the base motion.

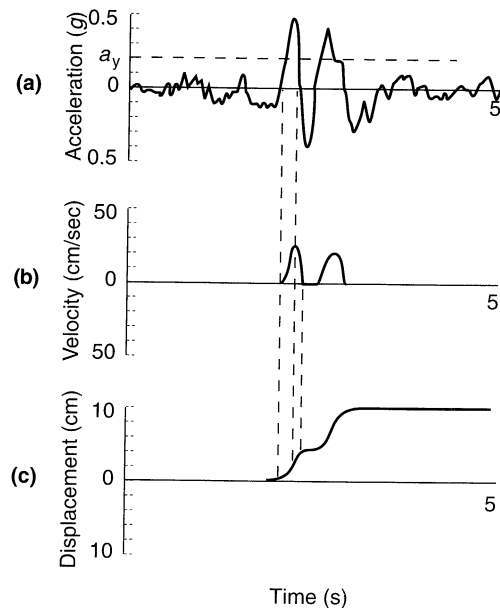


Figure 10.11 Development of permanent slope displacements for actual earthquake ground motion. (After Wilson and Keefer, 1985.)

Influence of Yield Acceleration on Slope Displacements. Obviously, the sliding block model will predict zero permanent slope displacement if earthquake-induced accelerations never exceed the yield acceleration ($a_y/a_{\max} \geq 1.0$) as illustrated in Figure 10.12a. Since the permanent displacement is obtained by double integration of the excess acceleration, the computed displacements for a slope with a relatively low yield acceleration (small a_y/a_{\max}) will be greater than that of a slope with a higher yield acceleration (Figure 10.12b, c). The relationship between slope displacement and a_y/a_{\max} has been investigated by a number of researchers.

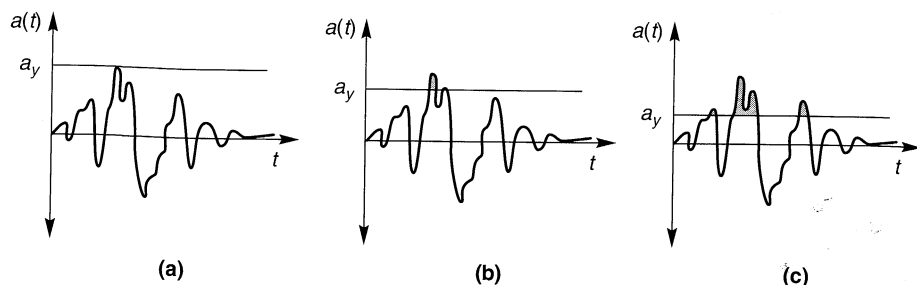


Figure 10.12 Permanent slope displacements depend on the relationship between the yield acceleration and the maximum acceleration. (a) If the yield acceleration of a slope is greater than the maximum acceleration of a particular ground motion, no displacement will occur. As yield accelerations decrease, as in (b) and (c), slope displacements increase quickly.

Using the rectangular pulse solution developed in Section 10.6.1.1, Newmark (1965) related single-pulse slope displacement to peak base velocity, v_{\max} , by

$$d_{\text{rel}} = \frac{v_{\max}^2}{2a_y} \left(\frac{1 - a_y}{A} \right) \quad (10.12)$$

[note that equation (10.12) is equivalent to equation (10.11) with $v_{\max} = A \Delta t$]. Analysis of several earthquake motions normalized to peak accelerations of $0.5g$ and peak velocities of 30 in./sec (76 cm/sec) suggested that the effective number of pulses in an earthquake motion could be approximated by A/a_y . Newmark found that a reasonable upper bound to the permanent displacements produced by these earthquake motions was given by

$$d_{\max} = \frac{v_{\max}^2}{2a_y} \frac{a_{\max}}{a_y} \quad (10.13)$$

where $a_y/a_{\max} \geq 0.17$. Sarma (1975) and Yegian et al. (1988) derived closed-form solutions for the permanent displacements produced by simple periodic (triangular, sinusoidal, and rectangular) input motions (Figure 10.13). Studies of permanent displacements predicted by the sliding block method for actual earthquake motions (e.g., Sarma, 1975; Franklin and Chang, 1977; Makdisi and Seed, 1978; Ambraseys and Menu, 1988) show shapes that are similar to those of the sinusoidal and triangular waves at a_y/a_{\max} values greater than about 0.5. Ambraseys and Menu (1988) found that the shape at smaller a_y/a_{\max} values was influenced by whether or not upslope movements were considered; for the case in which they were not, permanent displacements (in centimeters) caused by actual ground motions were given by

$$\log u = 0.90 + \log \left[\left(1 - \frac{a_y}{a_{\max}} \right)^{2.53} \left(\frac{a_y}{a_{\max}} \right)^{-1.09} \right] \quad \sigma_{\log u} = 0.30 \quad (10.14)$$

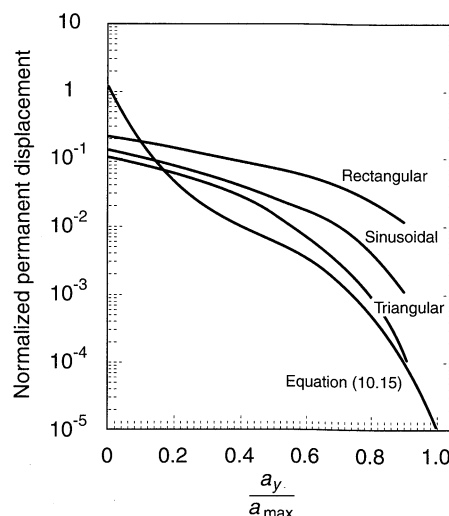


Figure 10.13 Variation of normalized permanent displacement with ratio of yield acceleration to maximum acceleration for simple waveforms. The normalized permanent displacement is defined in equation (10.15). (After Yegian et al., 1991.)

for $0.1 \leq a_y/a_{\max} \leq 0.9$, $6.6 \leq M_s \leq 7.3$, and a_y computed using residual soil strength. To allow measures of frequency content and duration to be considered explicitly, Yegian et al. (1991) used the database of Franklin and Chang (1977) to develop the following expression for the median permanent normalized displacement:

$$\log u^* = \log \left(\frac{u}{a_{\max} N_{\text{eq}} T^2} \right) = 0.22 - 10.12 \frac{a_y}{a_{\max}} + 16.38 \left(\frac{a_y}{a_{\max}} \right)^2 - 11.48 \left(\frac{a_y}{a_{\max}} \right)^3 \quad (10.15)$$

$$\sigma_{\log u^*} = 0.45$$

where N_{eq} is an equivalent number of cycles and T is the predominant period of the input motion. Considering only this source of uncertainty (i.e., neglecting uncertainty in a_{\max} , a_y , N_{eq} , and T), probabilities of exceeding various displacements can be determined (Figure 10.14). Alternative approaches to the probabilistic analysis of slope displacements have been presented by Constantinou and Gazetas (1984) and Lin and Whitman (1986).

Recognition of the limitations of peak acceleration as a sole descriptor of strong ground motion has led to the use of other ground motion parameters in slope-displacement prediction. Sliding block displacements have been correlated with Arias intensity:

$$\log u = 1.460 \log I_a - 6.642 a_y + 1.546 \quad \sigma_{\log u} = 0.409 \quad (10.16)$$

where u is in cm, I_a is in m/sec, and a_y is in g's (Jibson, 1994) and used to predict areal limits of earthquake-induced landsliding (Wilson and Keefer, 1985).

Two aspects of seismic slope stability are clearly illustrated by the studies described in the preceding paragraphs. First, earthquake-induced slope displacements are very sensitive to the value of the yield acceleration. Consequently, small differences in yield acceleration can produce large variations in predicted slope displacement. Second, the great variability in distributions of acceleration pulse amplitudes between different ground motions produces great variability in predicted slope displacements. Even ground motions with similar amplitudes, frequency contents, and durations can produce significantly different predicted slope

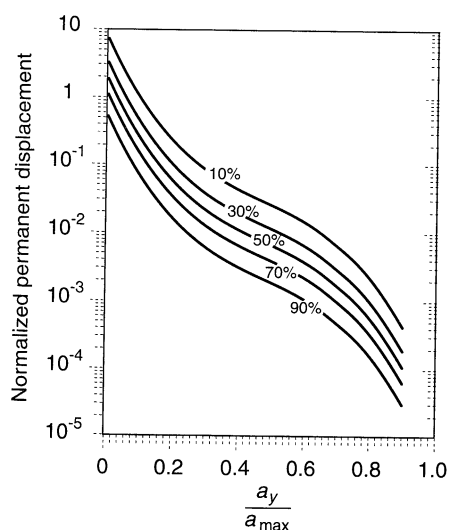


Figure 10.14 Contours of equal probability of exceedance of normalized permanent displacement. (After Yegian et al., 1991.)

displacements. This uncertainty must be recognized in the prediction of earthquake-induced slope deformations.

Example 10.4

Estimate the expected permanent displacement of the slope described in Example 10.3 if subjected to a ground motion equivalent to the Gilroy No. 1 (rock) earthquake motion. Use the procedures of Newmark (Equation 10.13) and Jibson (Equation 10.16).

Solution From Example 3.1, the peak acceleration and velocity of the Gilroy No. 1 (rock) motion are

$$\begin{aligned}a_{\max} &= 0.442 \\v_{\max} &= 33.7 \text{ cm/sec}\end{aligned}$$

The yield acceleration was computed as $0.20g$ in Example 10.3. Then, using the Newmark procedure (Equation 10.13), an upper bound estimate of the permanent displacement would be

$$d_{\max} = \frac{(33.7 \text{ cm/sec})^2}{2(0.20g)(981 \text{ cm/sec}^2/g)} \frac{0.442g}{0.200g} = 6.4 \text{ cm}$$

The Arias Intensity of the Gilroy No. 1 (rock) motion was computed as $I_a = 167.7 \text{ cm/sec}$ in Example 3.6. Using the Jibson procedure (Equation 10.16), the average permanent displacement would be given by

$$\log u = 1.460 \log(1.677) - 6.642(0.20) + 1.546 = 0.545$$

so

$$u = 10^{0.545} = 3.5 \text{ cm}$$

Input Motions. The accuracy of a sliding block analysis depends on the accuracy of the input motion applied to the inclined plane. As originally proposed, the sliding block method assumes the potential failure mass to be rigid, in which case the appropriate input motion would be the ground motion at the level of the failure surface. Actual slopes, however, are compliant—they deform during earthquake shaking. Their dynamic response depends on their geometry and stiffness and on the amplitude and frequency content of the motion of the underlying ground. For slopes composed of very stiff soils and/or slopes subjected to low-frequency motion (a combination that produces long wavelengths), lateral displacements throughout the potential failure mass will be nearly in phase (Figure 10.15a) and the rigid block assumption will be at least approximately satisfied. Lateral displacements in

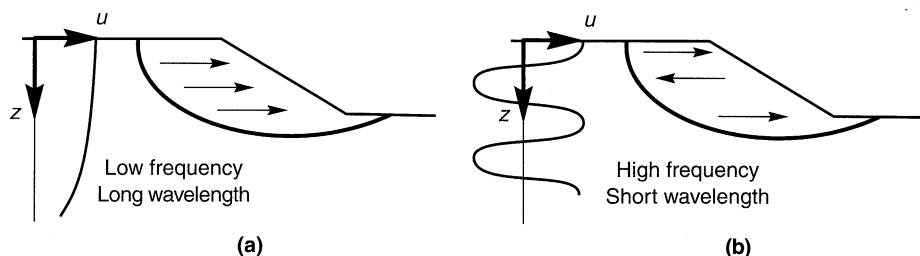


Figure 10.15 Influence of frequency on motions induced in slopes. Long wavelength associated with low-frequency motion (a) causes soil above failure surface to move essentially in phase. For higher-frequency motion (b), portions of soil above failure surface may be moving in opposite directions.

potential failure masses of slopes in softer soils (and/or slopes subjected to higher-frequency motion), however, may be out of phase (Figure 10.15b). When this occurs, the inertial forces at different points within the potential failure mass may be acting in opposite directions and the resultant inertial force may be significantly smaller than that implied by the rigid-block assumption.

The effects of slope response on the inertial force acting on a potential failure mass can be computed using dynamic stress-deformation analyses (Chopra, 1966). Using a dynamic finite-element analysis (Figure 10.16a), the horizontal components of the dynamic stresses acting on a potential failure surface (Figure 10.16b) are integrated over the failure surface to produce the time-varying resultant force that acts on the potential failure surface. This resultant force can then be divided by the mass of the soil above the potential failure surface to produce the average acceleration of the potential failure mass. Although the procedure was developed originally for dams, the basic concept can be applied to any type of slope. The average acceleration time history, which may be of greater or smaller amplitude than the base acceleration time history (depending on the input motions and the amplification characteristics of the slope), provides the most realistic input motion for a sliding block analysis of the potential failure mass.

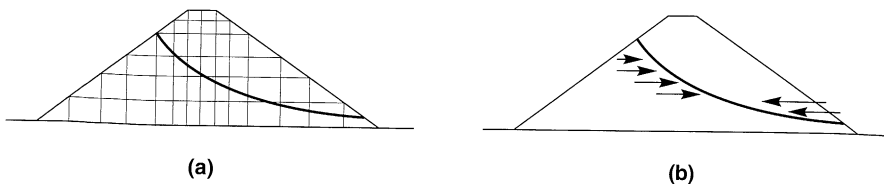


Figure 10.16 Evaluation of average acceleration for slope in embankment. Finite-element analysis predicts variation of shear and normal stresses on potential failure plane with time. Integration of horizontal components of stresses over potential failure surface gives resultant horizontal force acting on potentially unstable soil. Time history of average acceleration is obtained by dividing resultant force by mass of potentially unstable soil.

Other Factors Influencing Slope Displacement. The standard sliding block analysis is based on the assumption of rigid-perfectly plastic stress-strain behavior on a planar failure surface. Conditions for actual slopes may vary from these assumptions in a number of ways.

The shear strength of some soils is rate dependent. Since earthquake-induced shear stresses are applied at different rates, the shear strength (and hence the yield acceleration) can vary with time throughout an earthquake (e.g., Hungr and Morgenstern, 1984; Lemos et al., 1985). Consideration of rate-dependent strength in a sliding block analysis is complicated by differences between strain rates in the field and in the laboratory tests used to measure the strength. Lemos and Coelho (1991) and Tika-Vassilicos et al. (1993) suggested procedures for incorporating rate-dependent field strengths into numerical sliding block analyses.

In the field, soils rarely behave as perfectly plastic materials. Instead, they usually exhibit strain-hardening or strain-softening stress-strain behavior (Figure 10.17) after yielding. The yield accelerations of slopes comprised of strain-hardening or strain-softening soils will vary with slope displacement. Consequently, the permanent displacement of

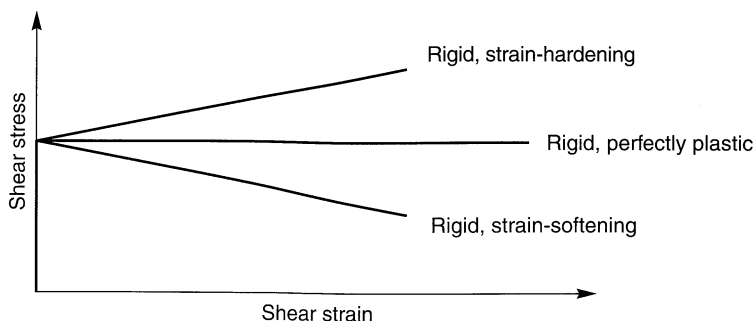


Figure 10.17 Stress-strain behavior of rigid-perfectly plastic, rigid-strain hardening, and rigid-strain softening materials.

a slope in strain-hardening materials will be smaller than predicted by a conventional sliding block analysis; the reverse will be true for strain-softening soils. Modification of sliding block analyses for consideration of displacement-dependent strength is fairly straightforward.

Many slopes fail by mechanisms that differ from the planar failure mechanism assumed in sliding block analyses (see Figure 10.4). Neglecting the effects of rate- and displacement-dependent strength, the stability of a block on a plane will be the same both before and after a pulse of displacement—because the geometry of the block relative to the plane is unchanged. Movement of a slope on a nonplanar failure surface, however, tends to flatten the slope, thereby reducing the driving forces. As a result, the yield acceleration should increase due to changes in the geometry of the unstable soil. For most slopes, however, this effect does not become significant until large displacements have occurred.

10.6.1.3 Makdisi-Seed Analysis

Makdisi and Seed (1978) used average accelerations computed by the procedure of Chopra (1966) and sliding block analyses to compute earthquake-induced permanent deformations of earth dams and embankments. By making simplifying assumptions about the results of dynamic finite element and shear beam analyses of such structures, a simplified procedure for prediction of permanent displacements was developed.

In the simplified procedure, the yield acceleration for a particular potential failure surface is computed using the dynamic yield strength [80% of the undrained strength (Section 6.5.2)] of the soil. The dynamic response of the dam/embankment is accounted for by an acceleration ratio that varies with the depth of the potential failure surface relative to the height of the dam/embankment (Figure 10.18).

By subjecting several real and hypothetical dams to several actual and synthetic ground motions scaled to represent different earthquake magnitudes, Makdisi and Seed computed the variation of permanent displacement with a_y/a_{\max} and magnitude. Scatter in the predicted displacements was reduced by normalizing the displacement with respect to the peak base acceleration and the fundamental period of the dam/embankment (note that the normalized displacement has units of seconds). Prediction of permanent displacements by the Makdisi-Seed procedure is accomplished with the charts shown in Figure 10.19.

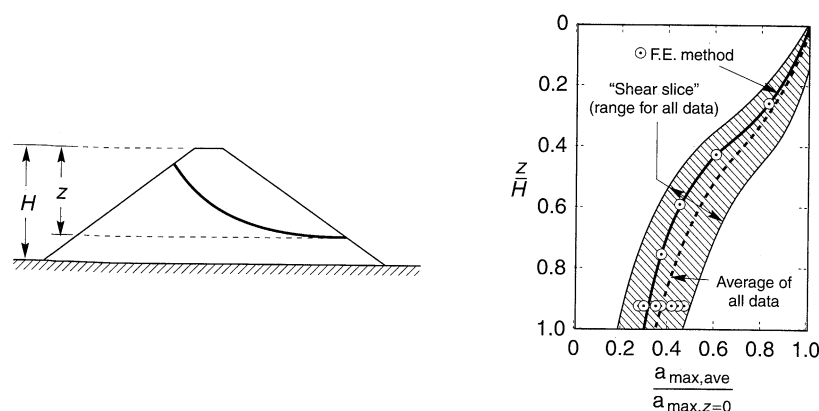


Figure 10.18 Variation of average maximum acceleration with depth of potential failure surface for dams and embankments. (After Makdisi and Seed (1978). Simplified procedure for estimating dam and embankment earthquake-induced deformations, Journal of the Geotechnical Engineering Division, Vol. 104, No. GT7. Reprinted by permission of ASCE.)

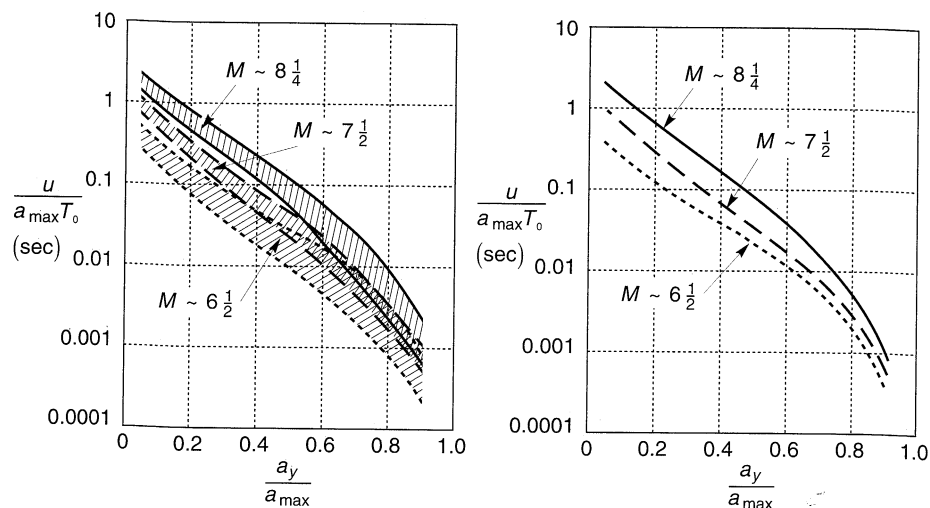


Figure 10.19 Variation of normalized permanent displacement with yield acceleration for earthquakes of different magnitudes: (a) summary for several earthquakes and dams/embankments; (b) average values. (After Makdisi and Seed (1978). Simplified procedure for estimating dam and embankment earthquake-induced deformations, Journal of the Geotechnical Engineering Division, Vol. 104, No. GT7. Reprinted by permission of ASCE.)

Example 10.5

Assume that a failure surface that extends over the upper two-thirds of the earth dam shown in Example 7.6 has a yield acceleration of $0.24g$. Estimate the permanent displacement that would occur if the base of the dam was subjected to the Gilroy No. 1 (rock) motion.

Solution The Gilroy No. 1 motion was recorded in the 1989 Loma Prieta earthquake which had a magnitude of 7.1. The peak acceleration was $0.442g$. From Example 7.6, the fundamental period of the dam is

$$T_o = \frac{2\pi}{19.2 \text{ rad/sec}} = 0.33 \text{ sec}$$

Using Figure 10.19b with $a_y/a_{\max} = 0.24g/0.442g = 0.54$ and $M = 7.1$, the average normalized displacement is about 0.04. Therefore,

$$u = 0.04 a_{\max} T_o = 0.04(0.442g)(32.2 \text{ ft/sec}^2/g)(0.33 \text{ sec}) = 0.19 \text{ ft} = 2.3 \text{ in}$$

The Makdisi–Seed simplified procedure is widely used for estimation of permanent displacements in dams and embankments. Because the procedure is based on the dynamic response characteristics of dams and embankments, its results must be interpreted with caution when applied to other types of slopes.

10.6.1.4 Stress–Deformation Analysis

Just as stress–deformation analyses of static slope stability are usually performed using static finite-element analyses, stress–deformation analyses of seismic slope stability are usually performed using dynamic finite-element analyses (Section 7.3.1). In such analyses the seismically induced permanent strains in each element of the finite-element mesh are integrated to obtain the permanent deformation of the slope. Permanent strains within individual elements can be estimated in different ways. The strain potential and stiffness reduction approaches estimate permanent strains using laboratory test results to determine the “stiffness” of soils subjected to earthquake loading. Nonlinear analysis approaches use the nonlinear inelastic stress–strain behavior of the soil to compute the development of permanent strains throughout an earthquake.

Strain Potential Approach. In their landmark investigation of the slides that occurred in the Upper and Lower San Fernando dams during the 1971 San Fernando earthquake, Seed et al. (1973) developed a procedure for estimating earthquake-induced slope deformation from the results of linear or equivalent linear analyses. In this procedure the cyclic shear stresses are computed in each element of a dynamic finite-element analysis. Using the results of cyclic laboratory tests, the computed cyclic shear stresses are used to predict the *strain potential*, expressed as a shear strain, for each element. Deformations are then estimated as the product of the average strain potential along a vertical section through the slope and the height of that section. The method implicitly assumes that the strains that develop in the field will be the same as those that develop in a similarly loaded laboratory test specimen and that the maximum shear stress acts in the horizontal direction in all elements. Consequently, the strain potential approach estimates only horizontal displacements. Analyses based on the strain potential approach are clearly very approximate, and their results should always be interpreted with that fact in mind.

Stiffness Reduction Approach. Another method for estimation of permanent slope displacement was developed by Lee (1974) and Serff et al. (1976). In this approach, computed strain potentials are used to reduce the stiffness of the soil as illustrated in Figure 10.20. Earthquake-induced slope displacements are then taken as the difference between the nodal point displacements from two static finite-element analyses: one using the initial shear moduli and the other using the reduced shear moduli. The technique can be used with linear or nonlinear models. Unlike the strain potential approach, the stiffness reduction approach can estimate vertical as well as horizontal movements. It is a very approximate procedure, however, and is subject to many of the limitations of the strain potential approach. Work-energy principles can be used to provide a more fundamental procedure for stiffness reduction (Byrne, 1991; Byrne et al., 1992).

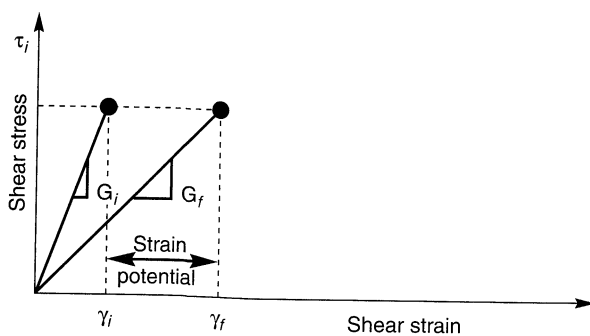


Figure 10.20 Procedure used to reduce stiffness from initial value, G_i , to final value, G_f , in stiffness reduction approach to estimation of permanent slope deformation. (After Serff et al., 1976.)

Nonlinear Analysis Approach. Permanent slope deformations can also be computed by finite-element analyses that employ nonlinear inelastic soil models. The basic procedures of nonlinear finite-element analysis of earth structures were introduced in Section 7.2.3. The seismic performance of slopes has been analyzed with two- and three-dimensional finite-element analyses using both cyclic stress-strain models (e.g., Finn et al., 1986) and advanced constitutive models (e.g., Prevost, 1981; Mizuno and Chen, 1982; Kawai, 1985; Daddazio et al., 1987). The most common application of these techniques, to date, has been the analysis of earth dams. Examples of such analyses can be found in Prevost et al. (1985), Griffiths and Prevost (1988), Finn (1990), Elgamal et al. (1990), and Sucarieh et al. (1991). As discussed in Chapter 7, the accuracy of nonlinear finite-element analyses depends primarily on the accuracy of the stress-strain or constitutive models on which they are based.

10.6.2 Analysis of Weakening Instability

Through a process of pore pressure generation and/or structural disturbance, earthquake-induced stresses and strains can reduce the shear strength of a soil. Weakening instabilities can occur when the reduced strength drops below the static and dynamic shear stresses induced in the slope. Weakening instabilities are usually associated with liquefaction

phenomena and can be divided into two main categories, *flow failures* (Section 9.6.3.2) and *deformation failures* (Section 9.6.3.3). Flow failures occur when the available shear strength becomes smaller than the static shear stress required to maintain equilibrium of a slope. Flow failures, therefore, are actually driven by static stresses. They can produce very large deformations that occur quickly and without warning. Deformation failures occur when the shear strength of a soil is reduced to the point where it is temporarily exceeded by earthquake-induced shear stresses. Much like inertial failures, deformation failures occur as a series of “pulses” of permanent displacement that cease at the end of earthquake shaking. Different procedures are available for the analysis of flow failures and deformation failures.

10.6.2.1 Flow Failure Analysis

Because they usually involve significant reduction in soil strength, flow failures usually produce large deformations and severe damage. The first step in their analysis is generally to determine whether or not one will occur. To estimate the extent of the damage produced by flow failures, procedures for estimation of flow failure deformations have also been developed.

Analysis of Stability. Potential flow slide instability is most commonly evaluated by conventional static slope stability analyses using soil strengths based on end-of-earthquake conditions (Marcuson et al., 1990). In a typical analysis, the factors of safety against liquefaction at all points on a potential failure surface is first computed. Residual strengths are then assigned to those portions of the failure surface on which the factor of safety against liquefaction is less than 1. At locations where the factor of safety against liquefaction is greater than 1, strength values are based on the effective stresses at the end of the earthquake (i.e., considering pore pressures generated during the earthquake). With these strengths, conventional limit equilibrium slope stability analyses are used to calculate an overall factor of safety against flow sliding. If the overall factor of safety is less than 1, flow sliding is expected. The possibility of progressive failure (Section 10.5.1) must be considered in stability evaluations of this type—the redistribution of stresses involved in progressive failure are not accounted for directly in limit equilibrium analyses.

Analysis of Deformations. If stability analyses indicate that flow failure is likely, the extent of the zone influenced by the failure can be determined from an analysis of flow failure deformations. By neglecting the small deformations that precede the triggering of flow sliding, rough estimates of flow sliding deformations can be obtained from procedures based on limit equilibrium, fluid mechanics, and stress-deformation analyses.

Simple plane strain, limit equilibrium procedures can be used to estimate the distance a liquefied soil would flow over a gentle (< 3 to 4°) slope (Lucia et al., 1981). By assuming that the liquefied soil would eventually come to rest with a linear surface, a postfailure geometry that satisfies equilibrium and volumetric constraints can be identified. With reference to the notation of Figure 10.21, the procedure can be implemented in the following steps:

1. Using Figure 10.22a, compute values of the height of the slope at the end of flow (when the static factor of safety reaches 1.0) based on strength considerations using

$$H_{T,s} = N_o \frac{S_r}{\gamma} \quad (10.17)$$

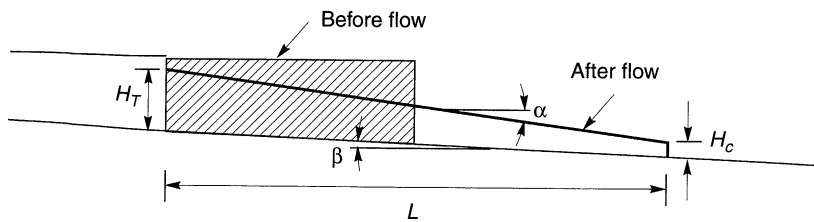


Figure 10.21 Geometric notation for estimation of flow failure distance by procedure of Lucia et al. (1981).

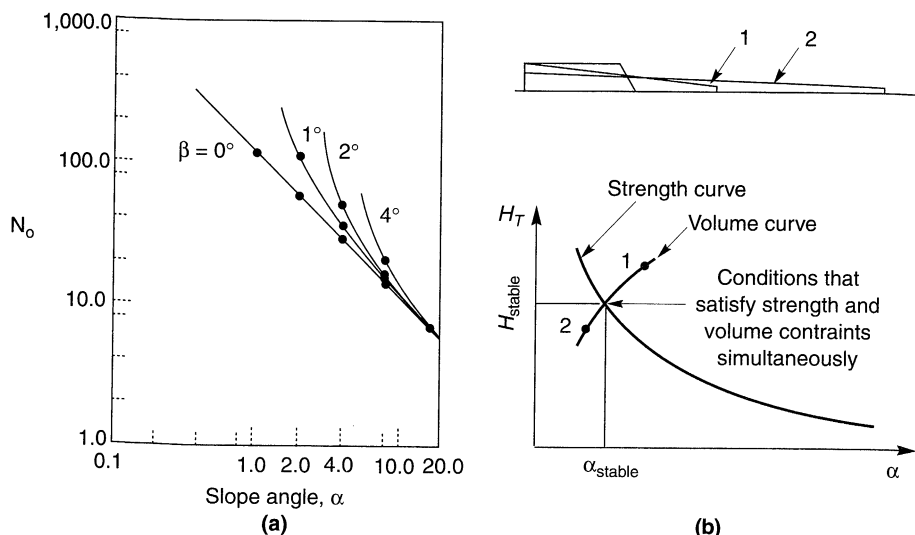


Figure 10.22 Charts for estimation of flow failure distance: (a) stability number charts for computing strength curve; (b) determination of H_T and α values that simultaneously satisfy strength and volume constraints. After Lucia et al. (1981).

for various assumed values of the slope angle, α . Plot the data in the form of a “strength curve” as in Figure 10.22b.

2. For various assumed values of α , calculate the height of the slope after flow based on constant-volume conditions using

$$H_{T,V} = \sqrt{A_1^2 H_c^2 + A_2 V_f} - A_3 H_c \quad (10.18)$$

where

$$\begin{aligned} A_1 &= \frac{\tan \alpha}{\tan \alpha - \tan \beta} & A_2 &= \frac{2 \tan^2 \alpha}{\tan \alpha - \tan \beta} \\ A_3 &= \frac{\tan \beta}{\tan \alpha - \tan \beta} & H_c &= \frac{4 S_r}{\gamma} \end{aligned}$$

and V_f is the estimated volume of soil involved in the flow slide. Plot the resulting data in the form of a “volume curve” as in Figure 10.22b.

3. The strength and volume curves intersect where $H_{T,S} = H_{T,V}$. The resulting H_{stable} and α_{stable} values satisfy both strength and volume requirements with a factor of safety equal to 1. The horizontal distance covered by the flow slide can then be computed as

$$L = \frac{H_{\text{stable}} - H_c}{\tan \alpha_{\text{stable}}} \quad (10.19)$$

Although the procedure involves several simplifying assumptions and requires an estimate of the strength of the liquefied soil (Section 9.6.4.1), it can provide at least a crude estimate of the deformations involved in certain flow slides.

The fluidlike behavior of liquefied soils has motivated fluid mechanics approaches to the modeling of flow slide behavior. Most of this work has been directed toward debris flows (e.g., Johnson, 1970; Iverson and Denlinger, 1987) and tailings dam failures (e.g., Jeyapalan et al., 1981). Rheological modeling of liquefied soils is quite difficult. The Bingham model (strength = $\tau_y + \eta_p \dot{\gamma}$, where τ_y and η_p are the Bingham yield strength and plastic viscosity, respectively, and $\dot{\gamma}$ is the shear strain rate) is most commonly used (Johnson, 1970; Jeyapalan, 1980; O’Brien and Julien, 1988; Phillips and Davies, 1991), although its ability to represent the frictional nature of liquefied soil is limited (Iverson and LaHusen, 1993).

The development of advanced nonlinear dynamic analyses have made an alternative approach possible. The finite-element program TARA-3FL (Finn and Yogendrakumar, 1989), for example, can reduce the strength of any element in the slope to the residual strength at the time liquefaction of the element is initiated. The program periodically updates the finite-element mesh at each time step to allow computation of large deformations (Figure 10.23). Finn (1990) described its application to Sardis Dam in Mississippi, where liquefaction of the core and a thin seam of clayey silt was expected (Figure 10.23). Analyses of this type not only indicate whether flow sliding will occur but also provide an estimate of the distribution and magnitude of any resulting deformations.

10.6.2.2 Deformation Failure Analysis

Although deformation failures generally involve smaller deformations than flow failures, they are capable of causing considerable damage. Lateral spreading is the most common type of deformation failure. In recent years a number of investigators have developed methods to estimate permanent displacements produced by deformation failures. Because the mechanisms that produce deformation failures are so complicated, procedures for prediction of the resulting displacements are largely empirical in nature.

Hamada et al. Approach. Hamada et al. (1986) considered the effects of geotechnical and topographic conditions on permanent ground displacements observed in uniform sands of medium grain size in the 1964 Niigata ($M = 7.5$), 1971 San Fernando ($M = 7.1$), and 1983 Nihonkai-Chubu ($M = 7.7$) earthquakes. Permanent displacements were found to be most strongly influenced by the thickness of the liquefied layer and the slopes of the ground surface and lower boundary of the liquefied zone. Permanent horizontal ground displacement, D , was found to vary according to the empirical relationship

$$D(m) = 0.75H^{1/2}\theta^{1/3} \quad (10.20)$$

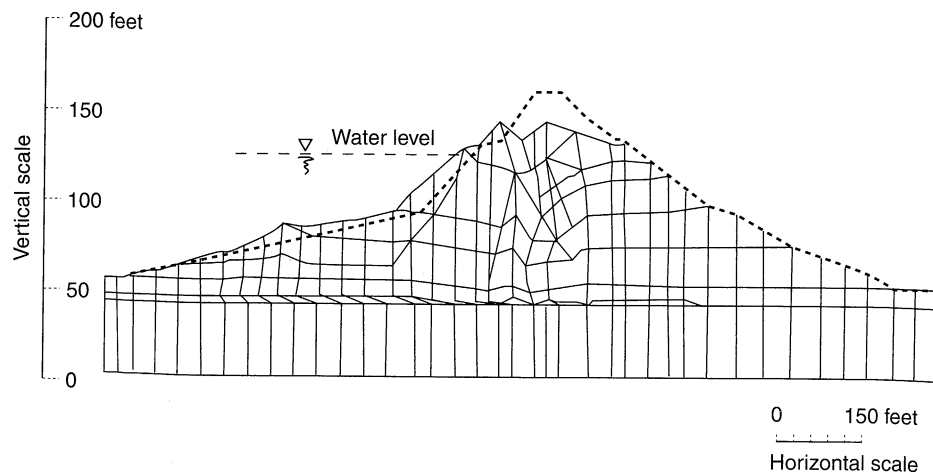


Figure 10.23 Initial (dashed) and postliquefaction (solid) configurations of Sardis Dam in Mississippi from TARA-3FL analyses. Note the large strains due to liquefaction in core and thin seam below the upstream shell. (After Finn, 1990.) Liquefaction hazards were reduced by driving compaction piles into the upstream embankment (see Figure 12.8).

where H is the thickness of the liquefied layer in meters and θ is the larger of the ground surface slope or the slope of the lower boundary of the liquefied zone in percent. For case histories from the three listed earthquakes, 80% of the observed displacements were within a factor of 2 of those predicted by equation (10.20). Note that equation (10.20) does not account for the strength of the liquefied soil; like all such empirical approaches, it must be applied cautiously when conditions vary from those on which it is based.

Youd and Perkins (Liquefaction Severity Index) Approach. Based on observed lateral displacements from a number of case histories in the western United States, Youd and Perkins (1987) defined the *liquefaction severity index* (LSI) as “the general maximum d -value (in inches) for lateral spreads generated on wide active flood plains, deltas, or other areas of gently-sloping Late Holocene fluvial deposits.” As defined, the LSI represents a conservative estimate of ground displacement in a given area; failures with smaller displacements would also be expected in the area. An analysis of the case history database indicated that LSI could be predicted by

$$\log(\text{LSI}) = -3.49 - 1.85 \log R + 0.98 M_w \leq 100 \quad (10.21)$$

where R is the horizontal distance from the seismic energy source in kilometers. The variation of LSI with M and R is shown in Figure 10.24. Qualitative descriptions of the nature of deformation failures for different LSI values are presented in Table 10-5. The dependence of LSI on magnitude and distance lends itself to incorporation into a probabilistic seismic hazard analysis. Youd and Perkins (1987) used this approach to produce probabilistic LSI maps for southern California.

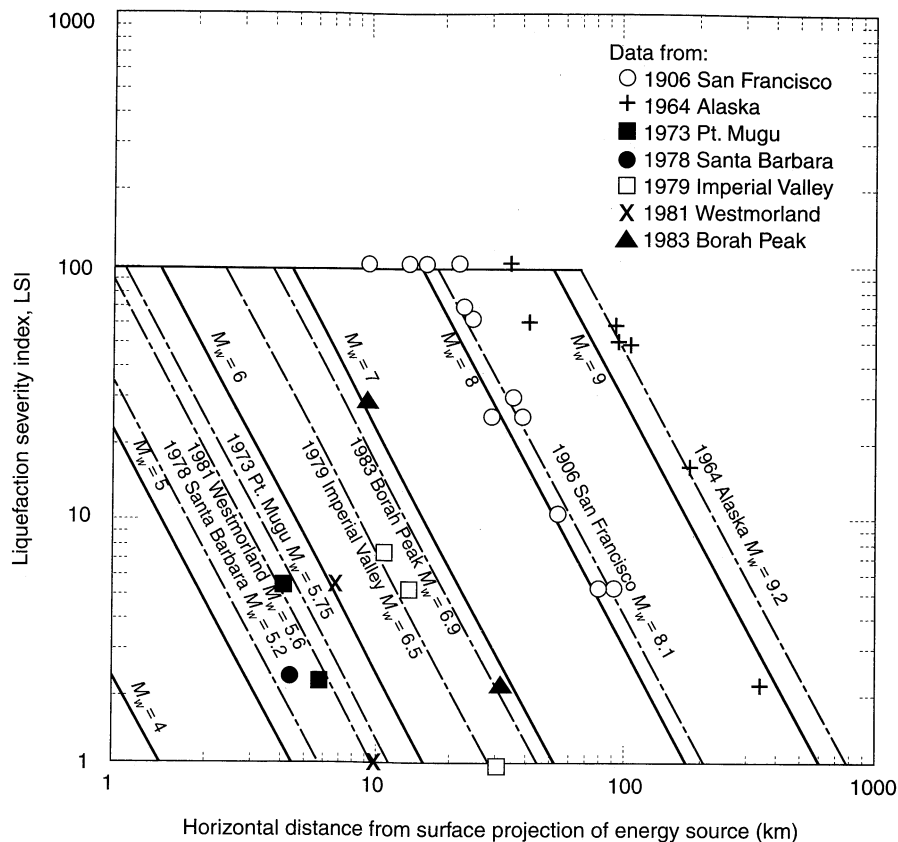


Figure 10.24 Variation of LSI with distance and earthquake magnitude. (After Youd and Perkins, 1986. Mapping of liquefaction severity index, Journal of Geotechnical Engineering, Vol. 103, No. 11. Reprinted by permission of ASCE.)

Byrne Approach. Modeling a slope as a crust of intact soil resting on a layer of liquefied soil (Figure 10.25), Byrne (1991) used work-energy principles with an elastic–perfectly plastic model of liquefied soil to develop expressions for estimation of permanent slope displacement. In this approach, the permanent displacement, D , is obtained from

$$\frac{D^3 S_r}{3(\gamma_{\text{lim}} T_L)^2} - D \tau_{st} - \frac{1}{2} m v_0^2 = 0 \quad D < \gamma_{\text{lim}} T_L \quad (10.22a)$$

$$D = \frac{3m v_0^2 + 4S_r \gamma_{\text{lim}} T_L}{6(S_r - \tau_{st})} \quad D \geq \gamma_{\text{lim}} T_L \quad (10.22b)$$

where S_r is the residual strength of the liquefied soil (Figure 9.56), γ_{lim} the limiting shear strain, T_L the thickness of the liquefied layer, τ_{st} the average shear stress required for static equilibrium (on a failure surface passing through the middepth of the liquefied layer), m the mass of the soil above the failure surface, and v_0 the velocity of the mass at the instant of liquefaction. Typical

Table 10-5 Abundance and General Character of Liquefaction Effects for Different LSI Values in Areas with Widespread Liquefiable Deposits

| LSI | Description |
|-----|--|
| 5 | Very sparsely distributed minor ground effects include sand boils with sand aprons up to 0.5 m (1.5 ft) in diameter, minor ground fissures with openings up to 0.1 m (0.3 ft) wide, ground settlements of up to 25 mm (1 in.). Effects lie primarily in areas of recent deposition and shallow groundwater table such as exposed streambeds, active floodplains, mudflats, shorelines, etc. |
| 10 | Sparingly distributed ground effects include sand boils with aprons up to 1 m (3 ft) in diameter, ground fissures with openings up to 0.3 m (1 ft) wide, ground settlements of a few inches over loose deposits such as trenches or channels filled with loose sand. Slumps with up to a few tenths of a meter displacement along steep banks. Effects lie primarily in areas of recent deposition with a groundwater table less than 3 m (10 ft) deep. |
| 30 | Generally sparse but locally abundant ground effects include sand boils with aprons up to 2 m (6 ft) diameter, ground fissures up to several tenths of a meter wide, some fences and roadways noticeably offset, sporadic ground settlements of as much as 0.3 m (1 ft), slumps with 0.3 m (1 ft) of displacements common along steep stream banks. Larger effects lie primarily in areas of recent deposition with a groundwater table less than 3 m (10 ft) deep. |
| 50 | Abundant effects include sand boils with aprons up to 3 m (10 ft) in diameter that commonly coalesce into bands along fissures, fissures with widths up to 1.5 m (4.5 ft), fissures generally parallel or curve toward streams or depressions and commonly break in multiple strands, fences and roadways are offset or pulled apart as much as 1.5 m (4.5 ft) in some places, ground settlements of more than 1 ft (0.3 m) occur locally, slumps with a meter of displacement are common in steep stream banks. |
| 70 | Abundant effects include many large sand boils [some with aprons exceeding 6 m (20 ft) in diameter that commonly coalesce along fissures], long fissures parallel to rivers or shorelines, usually in multiple strands with many openings as wide as 2 m (6 ft), many large slumps along streams and other steep banks, some intact masses of ground between fissures displaced 1 to 2 m (3 to 6 ft) down gentle slopes, frequent ground settlements of more than 0.3 m (1 ft). |
| 90 | Very abundant ground effects include numerous sand boils with large aprons, 30% or more of some areas covered with freshly deposited sand, many long fissures with multiple parallel streams and shorelines with openings as wide as 2 m or more, some intact masses of ground between fissures are horizontally displaced a couple of meters down gentle slopes, large slumps are common in stream and other steep banks, ground settlements of more than 0.3 m (1 ft) are common. |

Source: After Youd and Perkins (1987).

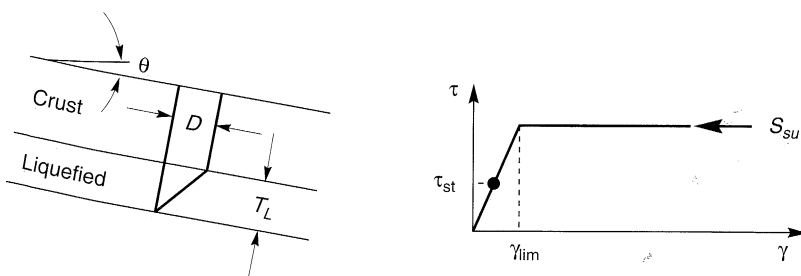


Figure 10.25 Stress, strain, and geometric notation for deformation estimation model of Byrne (1991). Elastic perfectly plastic approximation to stress-strain behavior assumes that residual strength is mobilized at limiting shear strain.

values of γ_{lim} are presented in Table 10-6. Displacements predicted by equations (10.22) agree well with those of equation (10.20) for slopes flatter than about 3% and $(N_1)_{60} = 4$. For higher $(N_1)_{60}$ values, equations (10.22) predict considerably smaller displacements.

Table 10-6 Average Values of Limiting Shear Strain for Clean Sand

| $(N_1)_{60}$ | γ_{lim} |
|--------------|----------------|
| 4 | 1.00 |
| 6 | 0.80 |
| 8 | 0.63 |
| 10 | 0.50 |
| 12 | 0.40 |
| 16 | 0.25 |
| 20 | 0.16 |
| 30 | 0.05 |
| 40 | 0.015 |
| 50 | 0 |

Source: Seed et al. (1985).

Byrne et al. (1992) extended this approach to determine factors by which the initial stiffness of a soil should be reduced for finite-element analysis of deformation failures. Deformations predicted by this approach were in good agreement with those observed in the 1971 failure of Upper San Fernando Dam (Figure 10.26).

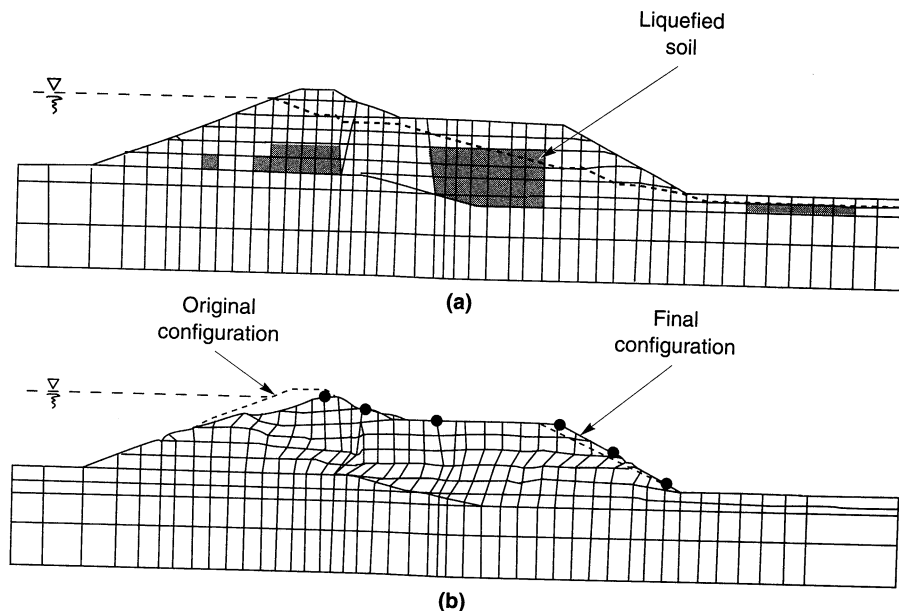


Figure 10.26 (a) Finite-element mesh for analysis of Upper San Fernando Dam with elements determined to have liquefied by Serff et al. (1976) shaded; (b) positions of original and final meshes (displacements exaggerated by factor of 2) by procedure of Byrne et al. (1992). Note large shear strains in liquefied zones.

Example 10.6

The gently sloping site shown below consists of a 2 m thick layer of silty clay overlying a 4 m thick layer of loose, saturated sand. The sand has an average fines content of about 3% and an average $D_{50} = 0.22$ mm. Subsurface investigations indicate that the corrected SPT resistance of the sand is quite consistent with an average value of 11. Estimate the permanent displacement of the slope when subjected to earthquake shaking sufficient to cause liquefaction of the sand.

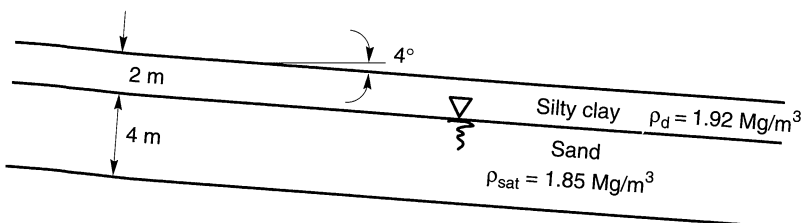


Figure E10.6

Solution The static shear stress at the center of the liquefiable layer is

$$\tau_{st} = \sigma_v \sin \alpha = \left[(2 \text{ m}) \left(1.92 \frac{\text{Mg}}{\text{m}^3} \right) \left(9.81 \frac{\text{m}}{\text{sec}^2} \right) + (2 \text{ m}) \left(1.85 \frac{\text{Mg}}{\text{m}^3} \right) \left(9.81 \frac{\text{m}}{\text{sec}^2} \right) \right] \\ = 5.2 \text{ kPa}$$

From Table 10.6, $\gamma_{lim} = 0.45$ and from Figure 9.57, $S_{su} \approx 300 \text{ psf} = 14.4 \text{ kPa}$. Assuming that the slope has no initial velocity ($v_0 = 0$), the direct solution of Equation 10.22b gives

$$D = \frac{0 + 4(14.4 \text{ kPa})(0.45)(4 \text{ m})}{6(14.4 \text{ kPa} - 5.2 \text{ kPa})} = 1.88 \text{ m}$$

Because this displacement is less than $\gamma_{lim} T_L$, the permanent displacement must be determined using the cubic equation of Equation 10.22a

$$\frac{D^3(14.4 \text{ kPa})}{3[(0.45)(4 \text{ m})]} - D(5.2 \text{ kPa}) - 0 = 0$$

from which

$$D = 1.87 \text{ m}$$

Thus, the estimated permanent displacement would be about 1.9 m. Note that this estimate is based on an average value of the residual strength of the liquefied soil; considering the range of uncertainty of that strength (Figure 9.58), the actual permanent displacement could be considerably smaller or larger.

Baziar et al. Approach. Using a sliding block analysis to describe fundamental aspects of seismic slope stability, Baziar et al. (1992) developed a general expression for permanent lateral displacement

$$d = N \frac{v_{\max}^2}{a_{\max}} f\left(\frac{a_y}{a_{\max}}\right) \quad (10.23)$$

where N is the equivalent number of cycles of harmonic loading, v_{\max} is the peak horizontal velocity, a_{\max} is the peak horizontal acceleration, and a_y is the yield acceleration. The function $f(a_y/a_{\max})$ was obtained by assuming harmonic accelerations (Figure 10.27). Calibration

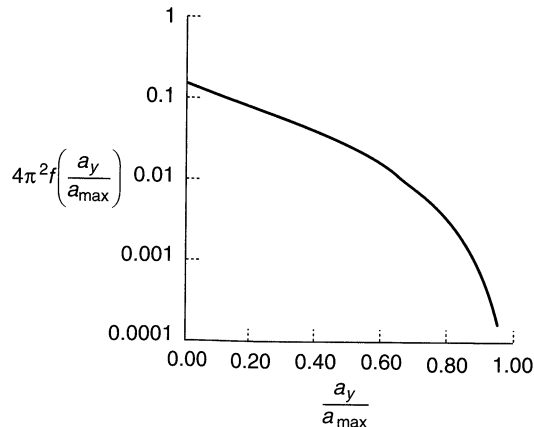


Figure 10.27 Variation of $f(a_y/a_{\max})$ with a_y/a_{\max} . (After Baziar et al., 1992.)

against case histories from the western United States suggested the use of $N = 2$ for $5.0 \leq M_w \leq 7.7$. By assuming a yield acceleration representative of those associated with the case history database of Youd and Perkins (1987), Baziar et al. (1992) were able to compare displacements predicted by equation (10.23) with the corresponding LSI values. As shown in Figure 10.28, the two approaches are quite consistent at longer site distances, but less so at shorter distances. Until additional near-source data becomes available, the physical basis of equation (10.23) appears to provide a stronger basis than LSI for estimation of displacements.

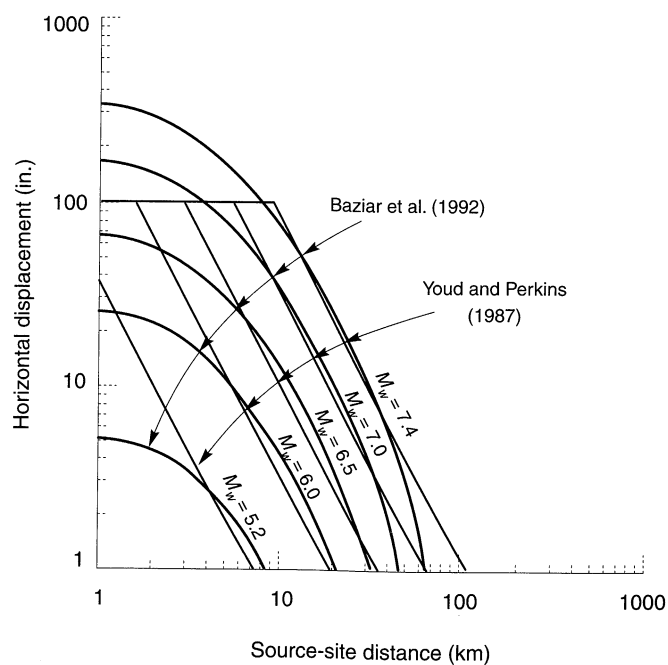


Figure 10.28 Comparison of permanent displacements with LSI. (After Baziar et al., 1992.)

Bartlett and Youd Approach. Bartlett and Youd (1992) used a large database of lateral spreading case histories to develop empirical expressions relating lateral ground displacement to a number of source and site parameters. The database included sites from the western United States and Japan at source–site distances up to 90 km subjected to earthquakes ranging from $M_w = 6.4$ to $M_w = 9.2$. Regression analyses were used to identify the factors that most strongly influenced lateral ground displacements, so that the empirical model could be based on those factors.

Two empirical models were developed: a *free-face model* for sites near steep banks and a ground-slope model for gently sloping sites. For free-face sites, displacements can be obtained from

$$\begin{aligned} \log D_H = & -16.3658 + 1.1782M_w - 0.9275\log R - 0.0133R + 0.6572\log W \\ & + 0.3483\log T_{15} + 4.5720\log(100 - F_{15}) - 0.9224(D_{50})_{15} \end{aligned} \quad (10.24)$$

where D_H is the estimated lateral ground displacement in meters, M_w the moment magnitude, R the horizontal distance from the seismic energy source in kilometers, W the ratio of the height of the free face to the horizontal distance between the base of the free face and the point of interest (Figure 10.29), T_{15} the cumulative thickness of saturated granular layers with $(N_{10})_{60} < 15$ in meters, F_{15} the average fines content for the granular layers comprising T_{15} in percent, and $(D_{50})_{15}$ the average mean grain size for the granular layers comprising T_{15} in millimeters. For gently sloping sites, the *ground-slope model* predicts

$$\begin{aligned} \log D_H = & -16.3658 + 1.1782M_w - 0.9275\log R - 0.0133R + 0.4293\log S \\ & + 0.3483\log T_{15} + 4.5720\log(100 - F_{15}) - 0.9224(D_{50})_{15} \end{aligned} \quad (10.25)$$

where S is the ground slope in percent (Figure 10.29). Application of these equations to the case history database showed that 90% of the observed displacements were within a factor

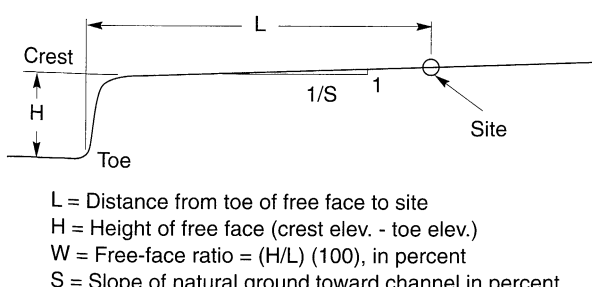


Figure 10.29 Parameters describing slope geometry for free-face and ground-slope deformation models. L , distance from toe of free face to site under consideration; H , height of free face (crest elev. - toe elev.); W , free-face ratio = $(H/L)(100)$, n percent; S , slope of natural ground toward channel = $1/X \cdot 100$, in percent. (After Bartlett and Youd, 1992.)

of 2 of the values predicted. The ranges of input parameters for which predicted results are verified by case history observations are shown in Table 10-7.

Table 10-7 Range of Parameter Values for Which Equations (10.24) and (10.25) Can Be Applied

| Input Parameter | Range of Values |
|----------------------------|--|
| Magnitude | $6.0 < M_w < 8.0$ |
| Free-face ratio | $1.0\% < W < 20\%$ |
| Thickness of loose layer | $0.3 \text{ m} < T_{15} < 12 \text{ m}$ |
| Fines content | $0\% < F_{15} < 50\%$ |
| Mean grain size | $0.1 \text{ mm} < (D_{50})_{15} < 1.0 \text{ mm}$ |
| Ground slope | $0.1\% < S < 6\%$ |
| Depth to bottom of section | Depth to bottom of liquefied zone $< 15 \text{ m}$ |

Source: After Bartlett and Youd (1992).

Example 10.7

Estimate the permanent displacement of the slope described in Example 10.6 due to $M_w = 6.5$ and $M_w = 7.5$ earthquakes occurring at a (horizontal source-site) distance of 30 km.

Solution From the description in Example 10.6, the ground-slope model of Bartlett and Youd is most appropriate. The relevant parameters are

$$\begin{aligned} S &= 4 \\ T_{15} &= 4 \\ F_{15} &= 3 \\ (D_{50})_{15} &= 0.22 \end{aligned}$$

Then, the permanent displacement due to the $M_w = 6.5$ earthquake can be estimated from equation 10.25 as

$$\begin{aligned} \log D &= -16.3658 + (1.1782)(6.5) - 0.9275 \log(30) - 0.0133(30) + 0.4293 \log(4) \\ &\quad + 0.3483 \log(4) + 4.5270 \log(100 - 3) - 0.9224(0.22) = -1.217 \end{aligned}$$

so

$$D = 10^{-1.217} = 0.061 \text{ m} = 6.1 \text{ cm}$$

For the $M_w = 7.5$ earthquake,

$$\begin{aligned} \log D &= -16.3658 + (1.1782)(7.5) - 0.9275 \log(30) - 0.0133(30) + 0.4293 \log(4) \\ &\quad + 0.3483 \log(4) + 4.5270 \log(100 - 3) - 0.9224(0.22) = -0.039 \end{aligned}$$

so

$$D = 10^{-0.039} = 0.91 \text{ m} = 91 \text{ cm}$$

Discussion. The preceding sections presented a variety of methods for estimation of the permanent displacements produced by deformation failures. Most of these methods are highly empirical, and all produce only approximate estimates of permanent

displacements. The applicability of each method to a particular site depends on the similarity between the conditions at that site and those corresponding to the databases from which the method was developed.

10.7 SUMMARY

1. Historically, earthquake-induced landslides have been among the most damaging of all seismic hazards. Their characteristics are influenced by geologic, hydrologic, topographic, climatic, weathering, and land-use conditions. Slides can be classified on the basis of material type, type of movement, degree of internal disruption, water content, velocity, and depth. Earthquake-induced landslides are usually divided into three main categories: disrupted slides and falls, coherent slides, and lateral spreads and flows.
2. Analysis of historical data allows estimation of the minimum earthquake magnitude required to produce different types of landslides and of the maximum distance to which landslides can be expected in earthquakes of different magnitudes.
3. A slope stability analysis is only one part of a comprehensive evaluation of slope stability. Prior to the analysis, detailed information on geologic, hydrologic, topographic, geometric, and material characteristics must be obtained. The accuracy of the analysis will be only as good as the accuracy of this information.
4. The dynamic shear stresses produced by earthquake shaking represent a source of loading and may also influence the strength and stress-strain behavior of the slope materials. Seismic slope instabilities may be grouped into two categories on the basis of which of these effects is predominant in a given slope. Inertial instabilities are those in which the shear strength of the soil remains essentially constant and slope deformations are caused by its temporary exceedance by dynamic earthquake stresses. Weakening instabilities occur when the earthquake serves to weaken the soil sufficiently that it cannot remain stable under earthquake-induced stresses.
5. Inertial instabilities are most commonly analyzed by pseudostatic, sliding block, or stress-deformation analyses. The Makdisi-Seed approach, based on the results of sliding block analyses, is also used frequently.
6. Pseudostatic analyses represent the effects of an earthquake by applying static horizontal and/or vertical accelerations to a potentially unstable mass of soil. The inertial forces induced by these pseudostatic accelerations increase the driving forces and may decrease the resisting forces acting on the soil. Pseudostatic analyses are not appropriate for soils that build up large pore pressures or show more than about 15% degradation of strength due to earthquake shaking. Stability is expressed in terms of a pseudostatic factor of safety calculated by limit equilibrium procedures. Selection of an appropriate pseudostatic acceleration requires great care; values considerably smaller than the peak acceleration of the sliding mass are usually used.
7. The pseudostatic acceleration required to bring a slope to the point of incipient failure is known as the yield acceleration. If earthquake-induced accelerations in a slope

momentarily exceed the yield acceleration, the unstable soil will momentarily accelerate relative to the material beneath it. Sliding block analyses can be used to calculate the amount of displacement that occurs. The total displacement depends on the amount by which the yield acceleration is exceeded (a function of the ground motion amplitude), the time over which the yield acceleration is exceeded (a function of the frequency content of the ground motion), and the number of times the yield acceleration is exceeded (a function of ground motion duration). Given the highly variable nature of ground motion characteristics, computed displacements can be quite variable.

8. The Makdisi–Seed procedure is based on sliding block analyses of earth dams and embankments. Knowing the fundamental period of vibration of the dam/embankment and the yield acceleration of the slope, simple charts can be used to estimate earthquake-induced permanent displacements.
9. Stress–deformation analyses have been used to estimate permanent deformations caused by inertial instabilities. Strain potential and stiffness reduction approaches allow estimation of permanent deformations from relatively simple analyses; their estimates are highly approximate. Although the computational effort is dramatically increased, permanent deformations can be analyzed more rigorously using nonlinear finite-element techniques. As the accuracy of constitutive models for soils improve, the use of nonlinear finite-element analyses is likely to increase.
10. Weakening instabilities occur when earthquake-induced stresses and strains reduce the shear strength of the soil within a slope. Depending on whether the reduced strength is greater than or less than the stresses required to maintain static equilibrium, weakening instabilities may be classified as flow failures or deformation failures.
11. Flow failure instability is usually evaluated by limit equilibrium analysis. Residual strengths are applied to those portions of the failure surface that pass through liquefied soil. A factor of safety less than 1 suggests that flow failure is likely. Simple limit equilibrium analyses combined with constant-volume constraints can be used to estimate the distance over which materials travel in flow failures. Fluid mechanics models have also been used to estimate flow failure deformations. Nonlinear dynamic analyses that allow weakening of liquefied elements and large strains have also been developed.
12. The effects of deformation failures are usually expressed in terms of slope deformations. A number of approaches, ranging from purely empirical to sliding block model based, have been developed to estimate the displacements produced by deformation failures.

HOMEWORK PROBLEMS

- 10.1 The slope shown below is intersected by two 6-inch-thick seams of clayey material. The intact slope materials can be characterized by the parameters, $c = 2500$ psf, $\phi = 0$, $\gamma = 130$ pcf. The clayey seams exhibit $c = 750$ psf, $\phi = 0$, and $\gamma = 120$ psf. Compute the minimum static factor of safety for the slope.

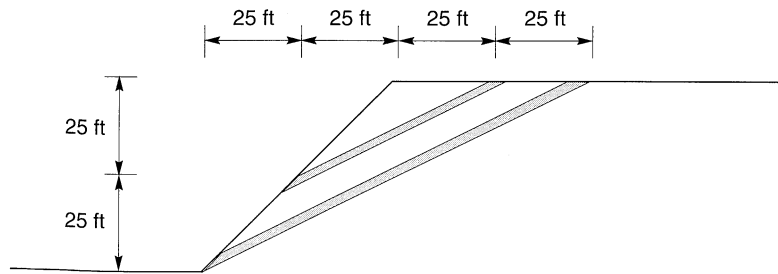


Figure P10.1

- 10.2** Compute the minimum pseudostatic factor of safety for the slope of Problem 10.1 assuming a pseudostatic coefficient of 0.1g.
- 10.3** Compute the yield acceleration for the slope of Problem 10.1.
- 10.4** Using hand calculations, slope stability charts, or a slope stability analysis computer program, locate the critical circular failure surface for the slope shown below. Considering only this failure surface, compute the yield acceleration for the slope.

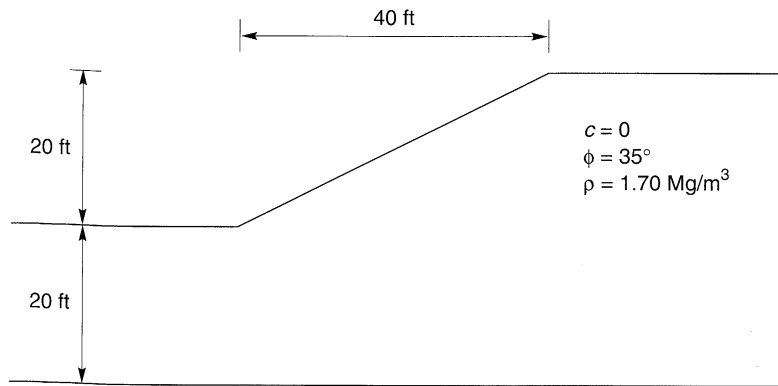


Figure P10.4

- 10.5** The slope shown in Problem 10.4 is subjected to the time history of crest acceleration shown below. Compute the permanent displacement of the slope.

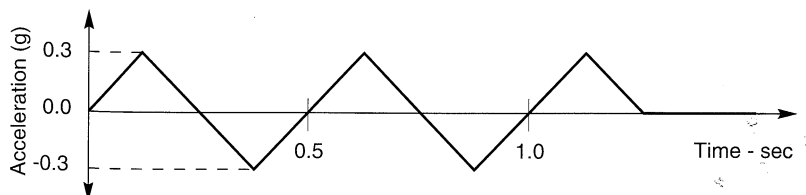


Figure P10.5

- 10.6** An existing embankment is determined to have a yield acceleration of 0.2g. Using the relationships of Ambraseys and Menu (equation 10.14), estimate the probability that an earthquake

that produces a peak acceleration of $0.3g$ would cause a permanent slope displacement greater than 2.5 cm.

- 10.7** A slope in cohesive soil is determined to have a yield acceleration of $0.17g$. Assuming $N_{eq} = 10$ and using the relationship of Yegian et al. (equation 10.15), compute the expected value of permanent slope displacement if the slope was subjected to (a) the Gilroy No. 1 (rock) motion, and (b) the Gilroy No. 2 (soil) motion. (Note: Peak accelerations and predominant periods of these motions were computed in the example problems in Chapter 3.)
- 10.8** Using the relationship of Jibson (equation 10.16), repeat Problem 10.7. Then compute the permanent slope displacement that would have a 5 percent probability of being exceeded for each ground motion.
- 10.9** The fundamental frequency of the earth dam in Example 7.6 was computed as 3.1 Hz. Pseudo-static slope stability analyses indicate a yield acceleration of $0.21g$. Use the Makdisi-Seed procedure to estimate the permanent displacement of the dam in a $M = 7$ earthquake that produces a peak acceleration of $0.28g$.
- 10.10** The slope shown below consists of 5 m of loose, clean sand overlying very dense clayey gravel with a groundwater table 2 m below the ground surface. Using the Byrne approach, estimate the permanent displacements that would occur if the slope was subjected to earthquake shaking strong enough to initiate liquefaction of the loose sand.

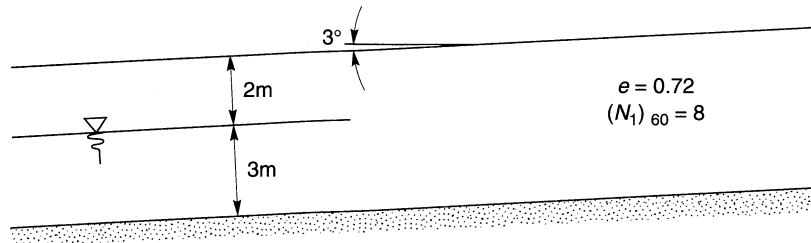


Figure P10.10

- 10.11** Using the approach of Baziar et al., estimate the permanent displacements that would have occurred in identical slopes with yield accelerations of $0.26g$ if subjected to (a) the Gilroy No. 1 (rock) motion, and (b) the Gilroy No. 2 (soil) motion. Comment on the usefulness of peak acceleration as a sole indicator of potential slope deformations.
- 10.12** The slope shown below consists of a loose silty sand overlying stiff clay. Estimate the lateral spreading displacement that would develop if a $M_w = 7.3$ earthquake occurred at a distance (to seismic source) of 40 km.

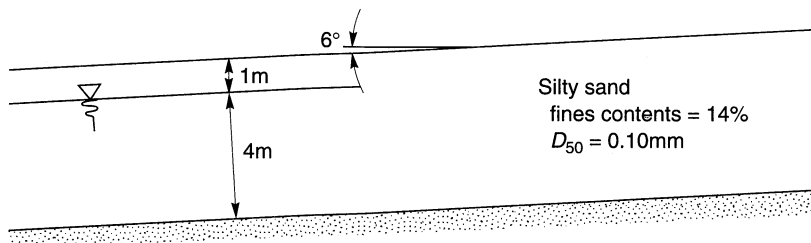


Figure P10.12



11

Seismic Design of Retaining Walls

11.1 INTRODUCTION

Earth retaining structures, such as retaining walls, bridge abutments, quay walls, anchored bulkheads, braced excavations, and mechanically stabilized walls, are used throughout seismically active areas. They frequently represent key elements of ports and harbors, transportation systems, lifelines, and other constructed facilities. Earthquakes have caused permanent deformation of retaining structures in many historical earthquakes. In some cases, these deformations were negligibly small; in others they caused significant damage. In some cases, retaining structures have collapsed during earthquakes, with disastrous physical and economic consequences. This chapter discusses the behavior of retaining walls during earthquakes and presents several of the most common approaches to the seismic design of different types of retaining walls.

11.2 TYPES OF RETAINING WALLS

The problem of retaining soil is one of the oldest in geotechnical engineering; some of the earliest and most fundamental principles of soil mechanics were developed to allow rational design of retaining walls. Many different approaches to soil retention have been developed and used successfully. In recent years, the development of metallic, polymer, and geotextile reinforcement has led to the development of many innovative types of mechanically stabilized earth retention systems.

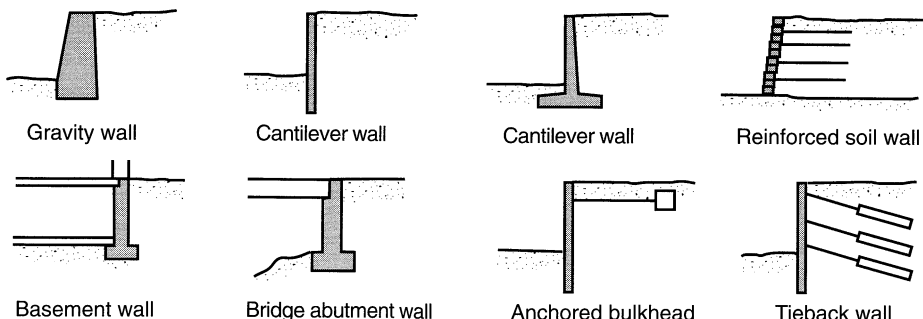


Figure 11.1 Common types of earth retaining structures.

Retaining walls are often classified in terms of their relative mass, flexibility, and anchorage conditions. *Gravity walls* (Figure 11.1) are the oldest and simplest type of retaining wall. Gravity walls are thick and stiff enough that they do not bend; their movement occurs essentially by rigid-body translation and/or rotation. Certain types of composite wall systems, such as crib walls and mechanically stabilized walls, are thick enough that they bend very little and consequently are often designed as gravity walls (with appropriate consideration of internal stability). *Cantilever walls*, which bend as well as translate and rotate, rely on their flexural strength to resist lateral earth pressures. The actual distribution of lateral earth pressure on a cantilever wall is influenced by the relative stiffness and deformation of both the wall and the soil. *Braced walls* are constrained against certain types of movement by the presence of external bracing elements. In the cases of basement walls and bridge abutment walls, lateral movements of the tops of the walls may be restrained by the structures they support. Tieback walls and anchored bulkheads are restrained against lateral movement by anchors embedded in the soil behind the walls. The provision of lateral support at different locations along a braced wall may keep bending moments so low that relatively flexible structural sections can be used.

11.3 TYPES OF RETAINING WALL FAILURES

To design retaining walls, it is necessary to define “failure” and to know how walls can fail. Under static conditions, retaining walls are acted upon by body forces related to the mass of the wall, by soil pressures, and by external forces such as those transmitted by braces. A properly designed retaining wall will achieve equilibrium of these forces without inducing shear stresses that approach the shear strength of the soil. During an earthquake, however, inertial forces and changes in soil strength may violate equilibrium and cause permanent deformation of the wall. Failure, whether by sliding, tilting, bending, or some other mechanism, occurs when these permanent deformations become excessive. The question of what level of deformation is excessive depends on many factors and is best addressed on a site-specific basis.

Gravity walls usually fail by rigid-body mechanisms such as sliding and/or overturning or by gross instability (Figure 11.2). Sliding occurs when horizontal force equilibrium is not maintained (i.e., when the lateral pressures on the back of the wall produce a thrust

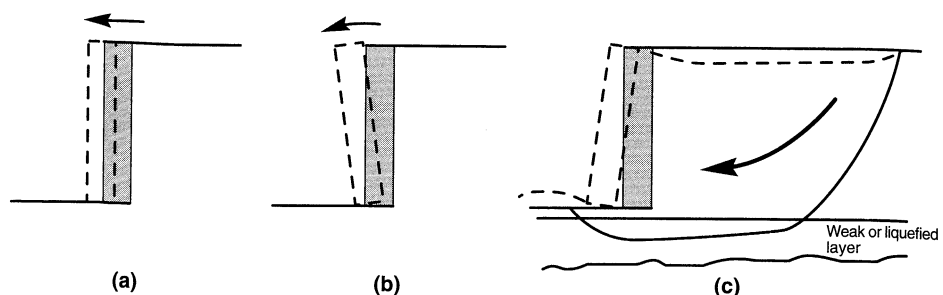


Figure 11.2 Typical failure mechanisms for a gravity retaining wall: (a) sliding (translational) failure; (b) overturning (rotational) failure; (c) gross instability failure.

that exceeds the available sliding resistance on the base of the wall). Overturning failures occur when moment equilibrium is not satisfied; bearing failures at the base of the wall are often involved. Gravity walls may also be damaged by gross instability of the soils behind and beneath them. Such failures may be treated as slope stability failures that encompass the wall. Composite wall systems, such as crib walls, bin walls, and mechanically stabilized walls, can fail in the same ways or by a number of internal mechanisms that may involve shearing, pullout, or tensile failure of various wall elements.

Cantilever walls are subject to the same failure mechanisms as gravity walls, and also to flexural failure mechanisms. Soil pressures and bending moments in cantilever walls depend on the geometry, stiffness, and strength of the wall-soil system (Figure 11.3a,b; pressure and moment diagrams for typical wall). If the bending moments required for equilibrium exceed the flexural strength of the wall, flexural failure may occur (Figure 11.3c). The structural ductility of the wall itself may influence the level of deformation produced by flexural failure.

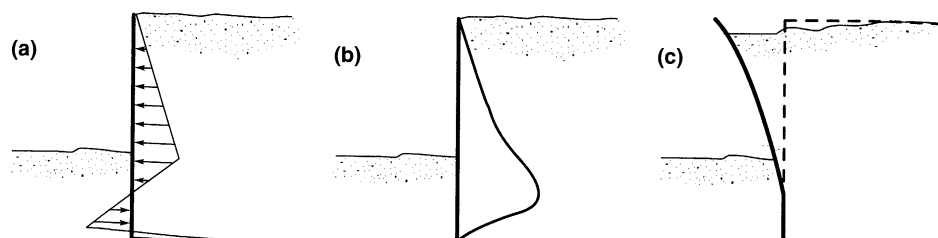


Figure 11.3 (a) Soil pressures, (b) bending moments, and (c) flexural failure mechanism for cantilever retaining wall.

Braced walls usually fail by gross instability, tilting, flexural failure, and/or failure of bracing elements. Tilting of braced walls typically involves rotation about the point at which the brace acts on the wall, often the top of the wall as in the cases of basement and bridge abutment walls (Figure 11.4a). Anchored walls with inadequate penetration may tilt by “kicking out” at their toes (Figure 11.4b). As in the case of cantilever walls, anchored walls may fail in flexure, although the point of failure (maximum bending moment) is likely to be different. Failure of bracing elements can include anchor pullout, tierod failure, or

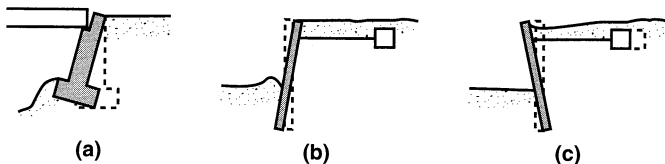


Figure 11.4 Potential modes of failure for braced walls: (a) rotation of bridge abutment about top; (b) rotation of anchored bulkhead due to lack of passive resistance (“kick-out”) at the toe; (c) lack of adequate anchor capacity.

bridge buckling. Backfill settlements can also impose additional axial and transverse loading on bracing elements such as tierods and tiebacks.

11.4 STATIC PRESSURES ON RETAINING WALLS

The seismic behavior of retaining walls depends on the total lateral earth pressures that develop during earthquake shaking. These total pressures include both the static gravitational pressures that exist before an earthquake occurs, and the transient dynamic pressures induced by the earthquake. Since the response of a wall is influenced by both, a brief review of static earth pressures is presented.

Static earth pressures on retaining structures are strongly influenced by wall and soil movements. *Active earth pressures* develop as a retaining wall moves away from the soil behind it, inducing extensional lateral strain in the soil. When the wall movement is sufficient to fully mobilize the strength of the soil behind the wall, *minimum active earth pressures* act on the wall. Because very little wall movement is required to develop minimum active earth pressures (for the usual case of cohesionless backfill materials), free-standing retaining walls are usually designed on the basis of minimum active earth pressures. Where lateral wall movements are restrained, such as in the cases of tieback walls, anchored bulkheads, basement walls, and bridge abutments, static earth pressures may be greater than minimum active. *Passive earth pressures* develop as a retaining wall moves toward the soil, thereby producing compressive lateral strain in the soil. When the strength of the soil is fully mobilized, *maximum passive earth pressures* act on the wall. The stability of many free-standing retaining walls depends on the balance between active pressures acting predominantly on one side of the wall and passive pressures acting on the other.

Even under static conditions, prediction of actual retaining walls forces and deformations is a complicated soil–structure interaction problem. Deformations are rarely considered explicitly in design—the typical approach is to estimate the forces acting on a wall and then to design the wall to resist those forces with a factor of safety high enough to produce acceptably small deformations. A number of simplified approaches are available to evaluate static loads on retaining walls. The most commonly used are described in the following sections.

11.4.1 Rankine Theory

Rankine (1857) developed the simplest procedure for computing minimum active and maximum passive earth pressures. By making assumptions about the stress conditions and

strength envelope of the soil behind a retaining wall (the *backfill soil*), Rankine was able to render the lateral earth pressure problem determinate and directly compute the static pressures acting on retaining walls.

For minimum active conditions, Rankine expressed the pressure at a point on the back of a retaining wall as

$$p_A = K_A \sigma'_v - 2c\sqrt{K_A} \quad (11.1)$$

where K_A is the *coefficient of minimum active earth pressure*, σ'_v is the vertical effective stress at the point of interest, and c is the cohesive strength of the soil. When the principal stress planes are vertical and horizontal (as in the case of a smooth vertical wall retaining a horizontal backfill), the coefficient of minimum active earth pressure is given by

$$K_A = \frac{1 - \sin \phi}{1 + \sin \phi} = \tan^2\left(45 - \frac{\phi}{2}\right) \quad (11.2)$$

For the case of a cohesionless backfill inclined at an angle β with the horizontal, infinite slope solutions can be used (Terzaghi, 1943; Taylor, 1948) to compute K_A as

$$K_A = \cos \beta \frac{\cos \beta - \sqrt{\cos^2 \beta - \cos^2 \phi}}{\cos \beta + \sqrt{\cos^2 \beta - \cos^2 \phi}} \quad (11.3)$$

for $\beta \leq \phi$ [equation (11.3) is equivalent to equation (11.2) when $\beta = 0$]. The pressure distribution on the back of the wall, as indicated by equations (11.1), depends on the relative magnitudes of the frictional and cohesive components of the backfill soil strength (Figure 11.5). Although the presence of cohesion indicates that tensile stresses will develop between the upper portion of the wall and the backfill, tensile stresses do not actually develop in the field. The creep, stress relaxation, and low-permeability characteristics of cohesive soils render them undesirable as backfill material for retaining structures, and their use in that capacity is generally avoided whenever possible. For dry homogeneous cohesionless backfill, Rankine theory predicts a triangular active pressure distribution oriented parallel to the backfill surface. The active earth pressure resultant, P_A , acts at a point located $H/3$ above the base of a wall of height, H (Figure 11.5a) with magnitude

$$P_A = \frac{1}{2} K_A \gamma H^2 \quad (11.4)$$

Under maximum passive conditions, Rankine theory predicts wall pressures given by

$$p_P = K_p \sigma'_v + 2c\sqrt{K_p} \quad (11.5)$$

where K_p is the *coefficient of maximum passive earth pressure*. For smooth, vertical walls retaining horizontal backfills,

$$K_p = \frac{1 + \sin \phi}{1 - \sin \phi} = \tan^2\left(45 + \frac{\phi}{2}\right) \quad (11.6)$$

and

$$K_p = \cos \beta \frac{\cos \beta + \sqrt{\cos^2 \beta - \cos^2 \phi}}{\cos \beta - \sqrt{\cos^2 \beta - \cos^2 \phi}} \quad (11.7)$$

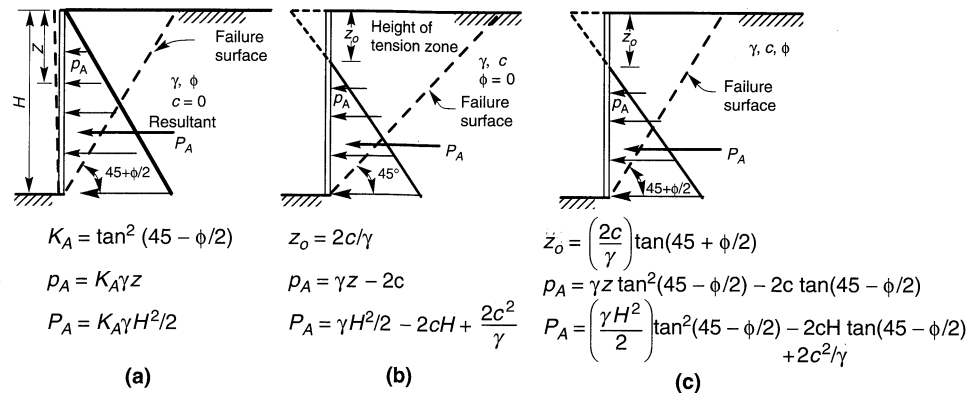


Figure 11.5 Minimum Rankine active earth pressure distributions for backfills with various combinations of frictional and cohesive strength: (a) frictional resistance, no cohesion; (b) cohesive soil, no frictional resistance; (c) combined cohesion and friction. (After NAVFAC, 1982.)

for backfills inclined at β to the horizontal. Passive pressure distributions for various backfill strength characteristics are shown in Figure 11.6. For a dry homogeneous backfill, Rankine theory predicts a triangular passive pressure distribution oriented parallel to the backfill surface. The passive earth pressure resultant, or *passive thrust*, P_P , acts at a point located $H/3$ above the base of a wall of height H (Figure 11.6a) with magnitude

$$P_P = \frac{1}{2} K_P \gamma H^2 \quad (11.8)$$

The presence of water in the backfill behind a retaining wall influences the effective stresses and hence the lateral earth pressure that acts on the wall. For wall design the hydrostatic

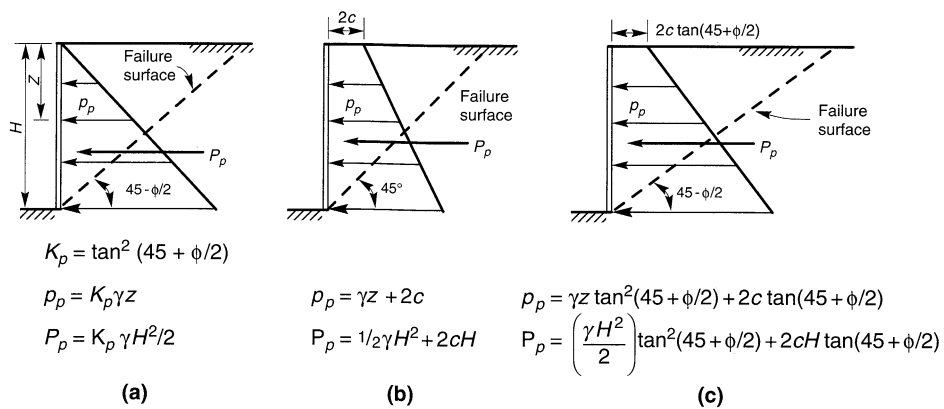


Figure 11.6 Maximum Rankine passive earth pressure distributions for backfills with various combinations of frictional and cohesive strength: (a) frictional resistance, no cohesion; (b) cohesive soil, no frictional resistance; (c) combined cohesion and friction. (After NAVFAC, 1982.)

pressure due to the water must be added to the lateral earth pressure. Because the total lateral thrust on a wall retaining a saturated backfill is considerably greater than that on a wall retaining dry backfill, the provision of backfill drainage is an important part of retaining wall design.

11.4.2 Coulomb Theory

Coulomb (1776) was the first to study the problem of lateral earth pressures on retaining structures. By assuming that the force acting on the back of a retaining wall resulted from the weight of a wedge of soil above a planar failure surface, Coulomb used force equilibrium to determine the magnitude of the soil thrust acting on the wall for both minimum active and maximum passive conditions. Since the problem is indeterminate, a number of potential failure surfaces must be analyzed to identify the critical failure surface (i.e., the surface that produces the greatest active thrust or the smallest passive thrust).

Under minimum active earth pressure conditions, the active thrust on a wall with the geometry shown in Figure 11.7a is obtained from force equilibrium (Figure 11.7b). For the critical failure surface, the active thrust on a wall retaining a cohesionless soil can be expressed as

$$P_A = \frac{1}{2} K_A \gamma H^2 \quad (11.9)$$

where

$$K_A = \frac{\cos^2(\phi - \theta)}{\cos^2\theta \cos(\delta + \theta) \left[1 + \sqrt{\frac{\sin(\delta + \phi)\sin(\phi - \beta)}{\cos(\delta + \theta)\cos(\beta - \theta)}} \right]^2} \quad (11.10)$$

δ is the angle of interface friction between the wall and the soil (Table 11-1), and β and θ are as shown in Figure 11.7a. The critical failure surface is inclined at an angle

$$\alpha_A = \phi + \tan^{-1} \left[\frac{\tan(\phi - \beta) + C_1}{C_2} \right] \quad (11.11)$$

to the horizontal where

$$C_1 = \sqrt{\tan(\phi - \beta) [\tan(\phi - \beta) + \cot(\phi - \theta)] [1 + \tan(\delta + \theta)\cot(\phi - \theta)]}$$

$$C_2 = 1 + \{ \tan(\delta + \theta) [\tan(\phi - \beta) + \cot(\phi - \theta)] \}$$

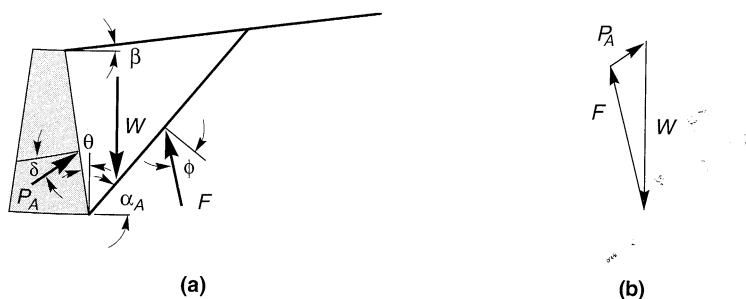


Figure 11.7 (a) Triangular active wedge bounded by planar backfill surface, failure surface, and wall; (b) force polygon for active Coulomb wedge. The critical failure surface is that which gives the largest value of P_A .

Table 11-1 Typical Interface Friction Angles

| | Interface Materials | Interface Friction Angle δ |
|----------------------------|---|--|
| Mass concrete against: | clean sound rock clean gravel, gravel-sand mixtures, coarse sand clean fine to medium sand, silty medium to coarse sand, silty or clayey gravel clean fine sand, silty or clayey fine to medium sand fine sandy silt, nonplastic silt | 25 29-31 24-29 19-24 17-19 |
| Formed concrete against: | medium-stiff and stiff clay and silty clay clean gravel, gravel-sand mixture, well-graded rock fill with spalls clean sand, silty sand-gravel mixture, single-size hard rock fill | 17-19 22-26 17-22 |
| Steel sheet piles against: | silty sand, gravel, or sand mixed with silt or clay fine sandy silt, nonplastic silt clean gravel, gravel-sand mixture, well-graded rock fill with spalls clean sand, silty sand-gravel mixture, single-size hard rock fill silty sand, gravel, or sand mixed with silt or clay fine sandy silt, nonplastic silt | 17 14 22 17 14 11 |

Source: After NAVFAC (1982).

Coulomb theory does not explicitly predict the distribution of active pressure, but it can be shown to be triangular for linear backfill surfaces with no surface loads. In such cases, P_A acts at a point located $H/3$ above the height of a wall of height H .

For maximum passive conditions in cohesionless backfills (Figure 11.8), Coulomb theory predicts a passive thrust

$$P_P = \frac{1}{2}K_P\gamma H^2 \quad (11.12)$$

where

$$K_P = \frac{\cos^2(\phi + \theta)}{\cos^2\theta \cos(\delta - \theta) \left[1 + \sqrt{\frac{\sin(\delta + \phi)\sin(\phi + \beta)}{\cos(\delta - \theta)\cos(\beta - \theta)}} \right]^2} \quad (11.13)$$

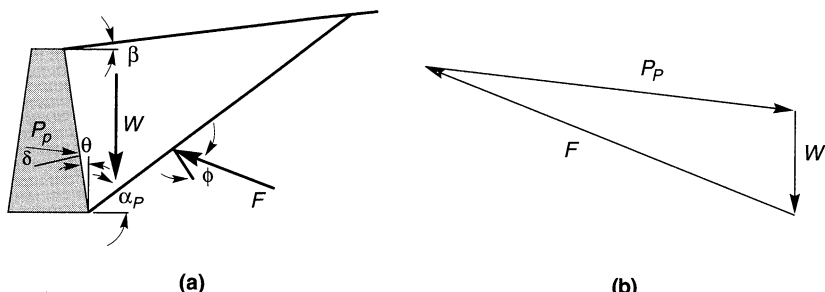


Figure 11.8 (a) Triangular passive wedge bounded by planar backfill surface, failure surface, and wall; (b) force polygon for passive Coulomb wedge. The critical failure surface is that which gives the largest value of P_p .

The critical failure surface for maximum passive earth pressure conditions is inclined to the horizontal at

$$\alpha_P = -\phi + \tan^{-1} \left[\frac{\tan(\phi + \beta) + C_3}{C_4} \right] \quad (11.14)$$

where

$$C_3 = \sqrt{\tan(\phi + \beta) [\tan(\phi + \beta) + \cot(\phi + \theta)] [1 + \tan(\delta - \theta) \cot(\phi + \theta)]}$$

$$C_4 = 1 + \{ \tan(\delta - \theta) [\tan(\phi + \beta) + \cot(\phi + \theta)] \}$$

In contrast to Rankine theory, Coulomb theory can be used to predict soil thrusts on walls with irregular backfill slopes, concentrated loads on the backfill surface, and seepage forces. By considering the soil above a potential failure plane as a free body and including forces due to concentrated loads, boundary water pressures, and so on, the magnitude of the resultant thrust (P_A or P_P) can easily be computed.

11.4.3 Logarithmic Spiral Method

Although the major principal stress axis may be nearly perpendicular to the backfill surface at some distance behind a rough ($\delta > 0$) wall, the presence of shear stresses on the wall-soil interface can shift its position near the back of the wall. If the inclination of the principal stress axes varies within the backfill, the inclination of the failure surface must also vary. In other words, the failure surface must be curved. A logarithmic spiral function has been used to describe such curved failure surfaces for active and passive earth pressure conditions.

For active earth pressure conditions, the critical failure surface consists of a curved portion near the back of the wall and a linear portion that extends up to the ground surface (Figure 11.9a). The active earth pressure distribution is triangular (Figure 11.9b) for walls retaining planar, cohesionless backfills. Thus the active soil thrust can be expressed in the same form as equation (11.4), where the log spiral coefficients of minimum active earth pressure for various wall and backfill inclinations are given in Table 11-2. The active earth pressure coefficients given by the log spiral approach are generally considered to be slightly more accurate than those given by Rankine or Coulomb theory, but the difference is so small that the more convenient Coulomb approach is usually used.

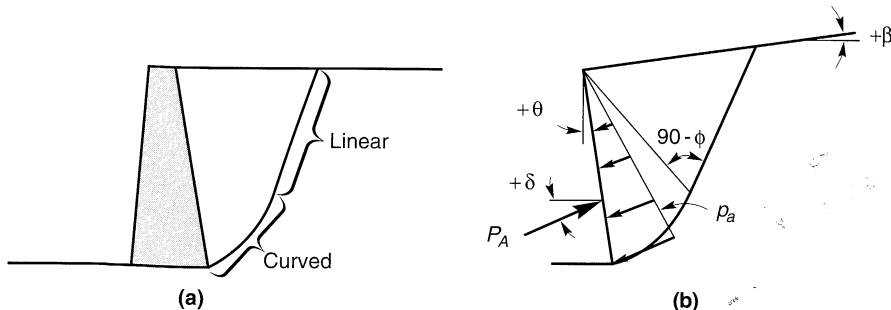


Figure 11.9 (a) Logarithmic spiral representation of the critical failure surface for minimum active earth pressure conditions; (b) orientation of critical failure surface for nonvertical wall with inclined backfill surface.

Table 11-2 Values for K_A for Log-Spiral Failure Surface

| δ | β | θ | ϕ | | | | | |
|----------|---------|----------|--------|------|------|------|------|------|
| | | | 20° | 25° | 30° | 35° | 40° | 45° |
| 0° | -15° | -10° | 0.37 | 0.30 | 0.24 | 0.19 | 0.14 | 0.11 |
| | | 0° | 0.42 | 0.35 | 0.29 | 0.24 | 0.19 | 0.16 |
| | | 10° | 0.45 | 0.39 | 0.34 | 0.29 | 0.24 | 0.21 |
| 0° | 0° | -10° | 0.42 | 0.34 | 0.27 | 0.21 | 0.16 | 0.12 |
| | | 0° | 0.49 | 0.41 | 0.33 | 0.27 | 0.22 | 0.17 |
| | | 10° | 0.55 | 0.47 | 0.40 | 0.34 | 0.28 | 0.24 |
| 0° | 15° | -10° | 0.55 | 0.41 | 0.32 | 0.23 | 0.17 | 0.13 |
| | | 0° | 0.65 | 0.51 | 0.41 | 0.32 | 0.25 | 0.20 |
| | | 10° | 0.75 | 0.60 | 0.49 | 0.41 | 0.34 | 0.28 |
| ϕ | -15° | -10° | 0.31 | 0.26 | 0.21 | 0.17 | 0.14 | 0.11 |
| | | 0° | 0.37 | 0.31 | 0.26 | 0.23 | 0.19 | 0.17 |
| | | 10° | 0.41 | 0.36 | 0.31 | 0.27 | 0.25 | 0.23 |
| ϕ | 0° | -10° | 0.37 | 0.30 | 0.24 | 0.19 | 0.15 | 0.12 |
| | | 0° | 0.44 | 0.37 | 0.30 | 0.26 | 0.22 | 0.19 |
| | | 10° | 0.50 | 0.43 | 0.38 | 0.33 | 0.30 | 0.26 |
| ϕ | 15° | -10° | 0.50 | 0.37 | 0.29 | 0.22 | 0.17 | 0.14 |
| | | 0° | 0.61 | 0.48 | 0.37 | 0.32 | 0.25 | 0.21 |
| | | 10° | 0.72 | 0.58 | 0.46 | 0.42 | 0.35 | 0.31 |

Source: After Caquot and Kerisel (1948).

The effect of wall friction on the shape of the critical failure surface is more noticeable for passive earth pressure conditions. The passive failure surface also has curved and linear portions (Figure 11.10a), but the curved portion is much more pronounced than for active conditions. For planar cohesionless backfills, the passive earth pressure distribution is triangular (Figure 11.10b), so the passive thrust can be expressed in the form of equation (11.8), where the log spiral coefficients of maximum passive earth pressure are as given in Table 11-3. The passive earth pressure coefficients given by the log spiral method are

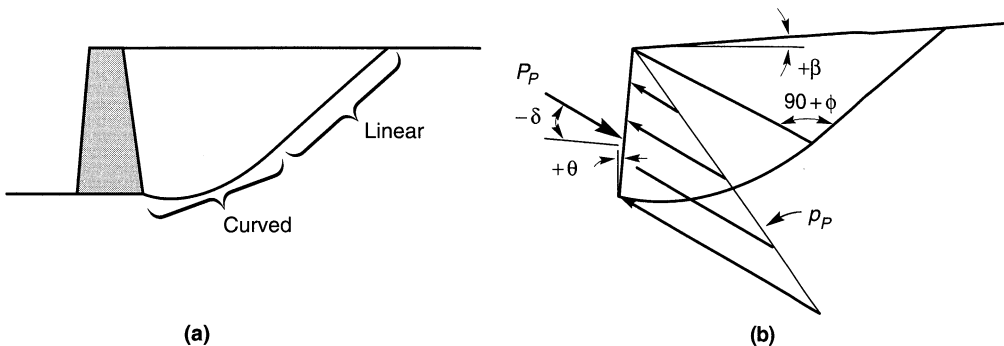


Figure 11.10 (a) Logarithmic spiral representation of the critical failure surface for maximum passive earth pressure conditions; (b) orientation of critical failure surface for nonvertical wall with inclined backfill surface.

Table 11-3 Values for K_p for Log-Spiral Failure Surface

| δ | β | θ | ϕ | | | | | |
|----------|---------|----------|--------|------|------|------|------|------|
| | | | 20° | 25° | 30° | 35° | 40° | 45° |
| 0° | -15° | -10° | 1.32 | 1.66 | 2.05 | 2.52 | 3.09 | 3.95 |
| | | 0° | 1.09 | 1.33 | 1.56 | 1.82 | 2.09 | 2.48 |
| | | 10° | 0.87 | 1.03 | 1.17 | 1.30 | 1.33 | 1.54 |
| 0° | 0° | -10° | 2.33 | 2.96 | 3.82 | 5.00 | 6.68 | 9.20 |
| | | 0° | 2.04 | 2.46 | 3.00 | 3.69 | 4.59 | 5.83 |
| | | 10° | 1.74 | 1.89 | 2.33 | 2.70 | 3.14 | 3.69 |
| 0° | 15° | -10° | 3.36 | 4.56 | 6.30 | 8.98 | 12.2 | 20.0 |
| | | 0° | 2.99 | 3.86 | 5.04 | 6.72 | 10.4 | 12.8 |
| | | 10° | 2.63 | 3.23 | 3.97 | 4.98 | 6.37 | 8.20 |
| ϕ | -15° | -10° | 1.95 | 2.90 | 4.39 | 6.97 | 11.8 | 22.7 |
| | | 0° | 1.62 | 2.31 | 3.35 | 5.04 | 7.99 | 14.3 |
| | | 10° | 1.29 | 1.79 | 2.50 | 3.58 | 5.09 | 8.86 |
| ϕ | 0° | -10° | 3.45 | 5.17 | 8.17 | 13.8 | 25.5 | 52.9 |
| | | 0° | 3.01 | 4.29 | 6.42 | 10.2 | 17.5 | 33.5 |
| | | 10° | 2.57 | 3.50 | 4.98 | 7.47 | 12.0 | 21.2 |
| ϕ | 15° | -10° | 4.95 | 7.95 | 13.5 | 24.8 | 50.4 | 115 |
| | | 0° | 4.42 | 6.72 | 10.8 | 18.6 | 39.6 | 73.6 |
| | | 10° | 3.88 | 5.62 | 8.51 | 13.8 | 24.3 | 46.9 |

Source: After Caquot and Kerisel (1948).

considerably more accurate than those given by Rankine or Coulomb theory; the Rankine and Coulomb coefficient tend to underpredict and overpredict the maximum passive earth pressure, respectively. Rankine theory greatly underpredicts actual passive earth pressures and is rarely used for that purpose. Coulomb theory overpredicts passive pressures (an unconservative error) by about 11% for $\delta = \phi/2$ and by 100% or more for $\delta = \phi$. For that reason, Coulomb theory is rarely used to evaluate passive earth pressures when $\delta > \phi/2$.

11.4.4 Stress–Deformation Analysis

Since the actual pressures that act on retaining walls depend on interaction between the wall and the surrounding soil, it seems logical to expect that they could be estimated by stress–deformation techniques such as the finite-element method. Finite-element analyses are, in fact, very useful for estimating retaining wall pressures and movements (Clough and Duncan, 1971; Duncan et al., 1990). In addition, they can help explain unexpected or anomalous field measurements of actual wall behavior (Clough and Duncan, 1971; Duncan and Clough, 1971).

The accuracy of stress–deformation analyses, however, depends on how well they are able to model the actual field conditions. A useful method of analysis should be able to describe the stress–strain behavior of the soil (which is nonlinear) and wall (usually assumed to remain linear), the stress–displacement behavior of the soil–wall interface, and the sequence of wall construction and backfill placement. Without careful attention to each of these factors, the results of a finite-element analysis may have limited applicability.

11.5 DYNAMIC RESPONSE OF RETAINING WALLS

The dynamic response of even the simplest type of retaining wall is quite complex. Wall movements and pressures depend on the response of the soil underlying the wall, the response of the backfill, the inertial and flexural response of the wall itself, and the nature of the input motions. Since few well-documented case histories involving field measurements of wall response are available, most of the current understanding of the dynamic response of retaining walls has come from model tests and numerical analyses. These tests and analyses, the majority of which have involved gravity walls, indicate that:

1. Walls can move by translation and/or rotation. The relative amounts of translation and rotation depend on the design of the wall; one or the other may predominate for some walls (Nadim and Whitman, 1984), and both may occur for others (Siddharthan et al., 1992).
2. The magnitude and distribution of dynamic wall pressures are influenced by the mode of wall movement (e.g., translation, rotation about the base, or rotation about the top) (Sherif et al., 1982; Sherif and Fang, 1984a,b).
3. The maximum soil thrust acting on a wall generally occurs when the wall has translated or rotated *toward* the backfill (i.e., when the inertial force on the wall is directed toward the backfill). The minimum soil thrust occurs when the wall has translated or rotated *away* from the backfill.
4. The shape of the earth pressure distribution on the back of the wall changes as the wall moves. The point of application of the soil thrust therefore moves up and down along the back of the wall. The position of the soil thrust is highest when the wall has moved toward the soil and lowest when the wall moves outward.
5. Dynamic wall pressures are influenced by the dynamic response of the wall and backfill and can increase significantly near the natural frequency of the wall–backfill system (Steedman and Zeng, 1990). Permanent wall displacements also increase at frequencies near the natural frequency of the wall–backfill system (Nadim, 1982). Dynamic response effects can also cause deflections of different parts of the wall to be out of phase. This effect can be particularly significant for walls that penetrate into the foundation soils when the backfill soils move out of phase with the foundation soils.
6. Increased residual pressures may remain on the wall after an episode of strong shaking has ended (Whitman, 1990).

Given these complex, interacting phenomena and the inherent variability and uncertainty of soil properties, it is not currently possible to analyze all aspects of the seismic response of retaining walls accurately. As a result, simplified models that make various assumptions about the soil, structure, and input motion are most commonly used for seismic design of retaining walls.

11.6 SEISMIC PRESSURES ON RETAINING WALLS

One common approach to the seismic design of retaining walls involves estimating the loads imposed on the wall during earthquake shaking and then ensuring that the wall can

resist those loads. Because the actual loading on retaining walls during earthquakes is extremely complicated, seismic pressures on retaining walls are usually estimated using simplified methods.

11.6.1 Yielding Walls

Retaining walls that can move sufficiently to develop minimum active and/or maximum passive earth pressures are referred to as *yielding walls*. The dynamic pressures acting on yielding walls are usually estimated by pseudostatic procedures that share many features of those described for seismic slope stability analysis in Section 10.6.1.1. More recently, a pseudodynamic procedure that accounts, in an approximate manner, for the dynamic response of the backfill has been developed.

11.6.1.1 Mononobe-Okabe Method

Okabe (1926) and Mononobe and Matsuo (1929) developed the basis of a pseudostatic analysis of seismic earth pressures on retaining structures that has become popularly known as the Mononobe-Okabe (M-O) method. The M-O method is a direct extension of the static Coulomb theory to pseudostatic conditions. In a M-O analysis, pseudostatic accelerations are applied to a Coulomb active (or passive) wedge. The pseudostatic soil thrust is then obtained from force equilibrium of the wedge.

Active Earth Pressure Conditions. The forces acting on an active wedge in a dry, cohesionless backfill are shown in Figure 11.11a. In addition to the forces that exist under static conditions (Figure 11.7), the wedge is also acted upon by horizontal and vertical pseudostatic forces whose magnitudes are related to the mass of the wedge by the pseudostatic accelerations $a_h = k_h g$ and $a_v = k_v g$. The total active thrust can be expressed in a form similar to that developed for static conditions, that is,

$$P_{AE} = \frac{1}{2} K_{AE} \gamma H^2 (1 - k_v) \quad (11.15)$$

where the dynamic active earth pressure coefficient, K_{AE} , is given by

$$K_{AE} = \frac{\cos^2(\phi - \theta - \psi)}{\cos \psi \cos^2 \theta \cos(\delta + \theta + \psi) \left[1 + \sqrt{\frac{\sin(\delta + \phi) \sin(\phi - \beta - \psi)}{\cos(\delta + \theta + \psi) \cos(\beta - \theta)}} \right]^2} \quad (11.16)$$

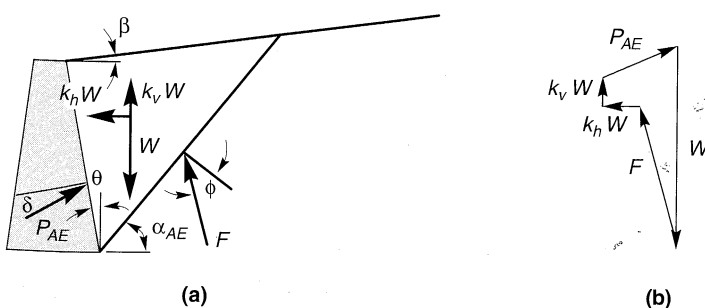


Figure 11.11 (a) Forces acting on active wedge in Mononobe-Okabe analysis, (b) force polygon illustrating equilibrium of forces acting on active wedge.

where $\phi - \beta \geq \psi$, $\gamma = \gamma_d$, and $\psi = \tan^{-1}[k_h/(1 - k_v)]$. The critical failure surface, which is flatter than the critical failure surface for static conditions, is inclined (Zarrabi-Kashani, 1979) at an angle

$$\alpha_{AE} = \phi - \psi + \tan^{-1} \left[\frac{-\tan(\phi - \psi - \beta) + C_{1E}}{C_{2E}} \right] \quad (11.17)$$

where

$$C_{1E} =$$

$$\sqrt{\tan(\phi - \psi - \beta) [\tan(\phi - \psi - \beta) + \cot(\phi - \psi - \theta)] [1 + \tan(\delta + \psi + \theta) \cot(\phi - \psi - \theta)]}$$

$$C_{2E} = 1 + \{ \tan(\delta + \psi + \theta) [\tan(\phi - \psi - \beta) + \cot(\phi - \psi - \theta)] \}$$

Although the M-O analysis implies that the total active thrust should act at a point $H/3$ above the base of a wall of height, H , experimental results suggest that it actually acts at a higher point under dynamic loading conditions. The total active thrust, P_{AE} [equation (11.15)], can be divided into a static component, P_A [equation (11.9)], and a dynamic component, ΔP_{AE} :

$$P_{AE} = P_A + \Delta P_{AE} \quad (11.18)$$

The static component is known to act at $H/3$ above the base of the wall. Seed and Whitman (1970) recommended that the dynamic component be taken to act at approximately $0.6H$. On this basis, the total active thrust will act at a height

$$h = \frac{P_A H/3 + \Delta P_{AE}(0.6H)}{P_{AE}} \quad (11.19)$$

above the base of the wall. The value of h depends on the relative magnitudes of P_A and P_{AE} —it often ends up near the midheight of the wall. M-O analyses show that k_v , when taken as one-half to two-thirds the value of k_h , affects P_{AE} by less than 10%. Seed and Whitman (1970) concluded that vertical accelerations can be ignored when the M-O method is used to estimate P_{AE} for typical wall designs.

Example 11.1

Compute the overturning moment about the base of the wall shown below for $k_h = 0.15$ and $k_v = 0.075$.

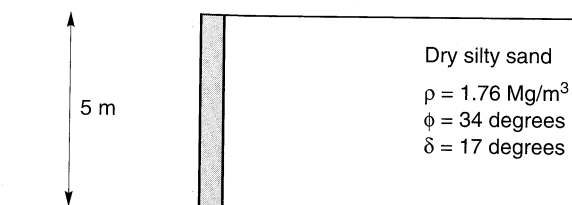


Figure E11.1

Solution First, estimate the static active thrust on the wall. Because the wall is not smooth ($\delta > 0$), Coulomb theory should be used. From equations (11.9) and (11.10),

$$K_A = \frac{\cos^2(34^\circ - 0^\circ)}{\cos^2(0^\circ)\cos(17^\circ + 0^\circ) \left[1 + \sqrt{\frac{\sin(17^\circ + 34^\circ)\sin(34^\circ - 0^\circ)}{\cos(17^\circ + 0^\circ)\cos(0^\circ - 0^\circ)}} \right]^2} = 0.256$$

and

$$P_A = \frac{1}{2} K_A \gamma H^2 = \frac{1}{2} (0.256) (1.76 \text{ Mg/m}^3) (9.81 \text{ m/sec}^2) (5 \text{ m})^2 = 55.3 \text{ kN/m}$$

Now, the total active thrust can be computed from equations (11.15) and (11.16). The angle, ψ , is given by

$$\psi = \tan^{-1} \left(\frac{k_h}{1 - k_v} \right) = \tan^{-1} \left(\frac{0.15}{1 - 0.075} \right) = 9.2^\circ$$

and

$$K_{AE} = \frac{\cos^2(34^\circ - 0^\circ - 9.2^\circ)}{\cos(9.2^\circ) \cos^2(0^\circ) \cos(17^\circ + 0^\circ + 9.2^\circ) \left[1 + \sqrt{\frac{\sin(17^\circ + 34^\circ) \sin(34^\circ + 0^\circ - 9.2^\circ)}{\cos(17^\circ + 0^\circ + 9.2^\circ) \cos(0^\circ - 0^\circ)}} \right]^2} \\ = 0.362$$

and

$$P_{AE} = \frac{1}{2} K_{AE} \gamma H^2 (1 - k_v) = \frac{1}{2} (0.362) (1.76 \text{ Mg/m}^3) (9.81 \text{ m/sec}^2) (5 \text{ m})^2 (1 - 0.075) \\ = 72.3 \text{ kN/m}$$

The dynamic component of the total thrust is

$$\Delta P_{AE} = P_{AE} - P_A = 72.3 \text{ kN/m} - 55.3 \text{ kN/m} = 17 \text{ kN/m}$$

From equation (11.19), the total thrust acts at a point

$$h = \frac{P_A \frac{H}{3} + \Delta P_{AE}(0.6H)}{P_{AE}} = \frac{55.3 \text{ kN/m} \frac{5 \text{ m}}{3} + 17 \text{ kN/m}(0.6)(5 \text{ m})}{72.3 \text{ kN/m}} = 1.98 \text{ m}$$

above the base of the wall. Because only the horizontal component of the total active thrust contributes to the overturning moment about the base, the overturning moment is given by

$$M_o = (P_{AE})_h h = (72.3 \text{ kN/m}) \cos(17^\circ) (1.98 \text{ m}) = 137 \frac{\text{kN}\cdot\text{m}}{\text{m}}$$

Passive Earth Pressure Conditions. The total passive thrust on a wall retaining a dry, cohesionless backfill (Figure 11.12) is given by

$$P_{PE} = \frac{1}{2} K_{PE} \gamma H^2 (1 - k_v) \quad (11.20)$$

where the dynamic passive earth pressure coefficient, K_{PE} , is given by

$$K_{PE} = \frac{\cos^2(\phi + \theta - \psi)}{\cos \psi \cos^2 \theta \cos(\delta - \theta + \psi) \left[1 - \sqrt{\frac{\sin(\delta + \phi) \sin(\phi + \beta - \psi)}{\cos(\delta - \theta + \psi) \cos(\beta - \theta)}} \right]^2} \quad (11.21)$$

The critical failure surface for M-O passive conditions is inclined from horizontal by an angle

$$\alpha_{PE} = \psi - \phi + \tan^{-1} \left[\frac{\tan(\phi + \psi + \beta) + C_{3E}}{C_{4E}} \right] \quad (11.22)$$

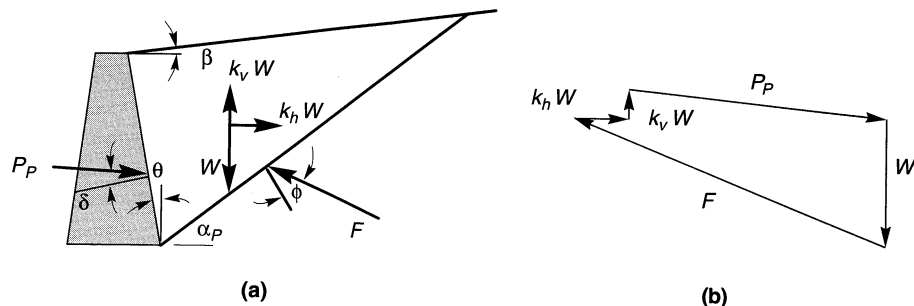


Figure 11.12 (a) Forces acting on passive wedge in Mononobe-Okabe analysis; (b) force polygon illustrating equilibrium of forces acting on passive wedge.

where

$$C_{3E} =$$

$$\sqrt{\tan(\phi + \beta - \psi) [\tan(\phi + \beta - \psi) + \cot(\phi + \theta - \psi)] [1 + \tan(\delta + \psi - \theta) \cot(\phi + \theta - \psi)]}$$

$$C_{4E} = 1 + \{ \tan(\delta + \psi - \theta) [\tan(\phi + \beta - \psi) + \cot(\phi + \theta - \psi)] \}$$

The total passive thrust can also be divided (Towhata and Islam, 1987) into static and dynamic components:

$$P_{PE} = P_P + \Delta P_{PE} \quad (11.23)$$

where P_{PE} and P_P are computed from equations (11.20) and (11.12), respectively. Note that the dynamic component acts in the opposite direction of the static component, thus reducing the available passive resistance.

Discussion. Although conceptually quite simple, the M-O analysis provides a useful means of estimating earthquake-induced loads on retaining walls. A positive horizontal acceleration coefficient causes the total active thrust to exceed the static active thrust and the total passive thrust to be less than the static passive thrust. Since the stability of a particular wall is generally reduced by an increase in active thrust and/or a decrease in passive thrust, the M-O method produces seismic loads that are more critical than the static loads that act prior to an earthquake. The effects of distributed and discrete surface loads and irregular backfill surfaces are easily considered by modifying the free-body diagram of the active or passive wedge. In such cases, equations (11.16) and (11.21) no longer apply—the total thrusts must be obtained from the analysis of a number of potential failure planes.

As a pseudostatic extension of the Coulomb analysis, however, the M-O analysis is subject to all of the limitations of pseudostatic analyses as well as the limitations of Coulomb theory. As in the case of pseudostatic slope stability analyses (Section 10.6.1.1), determination of the appropriate pseudostatic coefficient is difficult and the analysis is not appropriate for soils that experience significant loss of strength during earthquakes (e.g., liquefiable soils). Just as Coulomb theory does under static conditions, the M-O analysis will overpredict the actual total passive thrust, particularly for $\delta > \phi/2$. For these reasons the M-O method should be used and interpreted carefully.

11.6.1.2 Steedman-Zeng Method

As a pseudostatic analysis, the M-O method accounts for the dynamic nature of earthquake loading in a very approximate way. It is possible, however, to account for certain dynamic response characteristics in a relatively simple manner. To account for phase difference and amplification effects within the backfill behind a retaining wall can be considered using a simple pseudodynamic analysis of seismic earth pressures (Steedman and Zeng, 1990).

Consider the fixed-base cantilever wall shown in Figure 11.13. If the base is subjected to harmonic horizontal acceleration of amplitude a_h , the acceleration at a depth z , below the top of the wall can be expressed as

$$a(z, t) = a_h \sin \left[\omega \left(t - \frac{H-z}{v_s} \right) \right] \quad (11.24)$$

If the seismic wall pressures are assumed to result from the soil within a triangular wedge inclined at α to the horizontal, the mass of a thin element of the wedge at depth z is

$$m(z) = \frac{\gamma H - z}{g \tan \alpha} dz \quad (11.25)$$

where γ is the unit weight of the backfill. The total inertial force acting on the wall can therefore be expressed as

$$Q_h(t) = \int_0^H m(z) a(z, t) dz = \frac{\lambda \gamma a_h}{4\pi^2 g \tan \alpha} [2\pi H \cos \omega \zeta + \lambda (\sin \omega \zeta - \sin \omega t)] \quad (11.26)$$

where $\lambda = 2\pi v_s / \omega$ is the wavelength of the vertically propagating shear wave and $\zeta = t - H/v_s$. The special case of a rigid wedge is given, in the limit, as

$$\lim_{v_s \rightarrow \infty} (Q_h)_{\max} = \frac{\gamma H^2 a_h}{2g \tan \alpha} = \frac{a_h}{g} W = k_h W \quad (11.27)$$

which is equivalent to the pseudostatic force assumed by the M-O method. The total (static plus dynamic) soil thrust can be obtained by resolving forces on the wedge, that is,

$$P_{AE}(t) = \frac{Q_h(t) \cos(\alpha - \phi) + W \sin(\alpha - \phi)}{\cos(\delta + \phi - \alpha)} \quad (11.28)$$

and the total earth pressure distribution by differentiating the total soil thrust

$$p_{AE}(t) = \frac{\partial P_{AE}(t)}{\partial z} = \frac{\gamma z}{\tan \alpha} \frac{\sin(\alpha - \phi)}{\cos(\delta + \phi - \alpha)} + \frac{k_h \gamma z}{\tan \alpha} \frac{\cos(\alpha - \phi)}{\cos(\delta + \phi - \alpha)} \sin \left[\omega \left(t - \frac{z}{v_s} \right) \right] \quad (11.29)$$

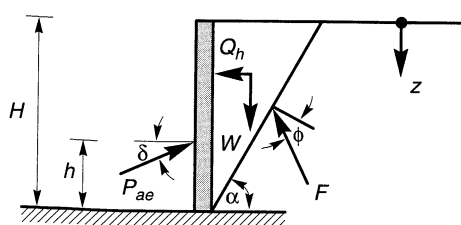


Figure 11.13 Wall geometry and notation for Steedman-Zeng method.

The first term in equation (11.29), which increases linearly with depth and does not vary with time, represents the static earth pressure acting on the wall. The resultant static thrust acts in accordance with static earth pressure theories at a point $h_s = H/3$ above the base of the wall. The second term represents the dynamic earth pressure. It increases as a nonlinear function of depth with a shape that depends on the ratio H/λ . A typical example of the nonlinear dynamic pressure is shown in Figure 11.14. Since the dynamic pressure increases nonlinearly with depth, the position of the dynamic thrust varies with time according to

$$h_d = H - \frac{2\pi^2 H^2 \cos \omega \zeta + 2\pi \lambda H \sin \omega \zeta - \lambda^2 (\cos \omega \zeta - \cos \omega t)}{2\pi H \cos \omega \zeta + \pi \lambda (\sin \omega \zeta - \sin \omega t)} \quad (11.30)$$

The point of application of the dynamic thrust for very low frequency motions (small H/λ , so the backfill moves essentially in phase) is at $h_d = H/3$. For higher-frequency motions, the point of application moves higher on the wall, as indicated in Figure 11.15.

Steedman and Zeng (1989) found that the soil thrusts for backfills of different stiffnesses were close to those obtained when the mean shear wave velocities of the backfill were used in the pseudodynamic analyses. Backfill amplification effects can also be considered by expressing a_h as a function of depth [rather than as a constant in equation (11.24)] and repeating the integration of equation (11.26). Note that backfill amplification will increase both the loads acting on the wall and the height of the resultant soil thrust. Assuming that $a_h(z, t)$ varied linearly from the input acceleration at the base of the wall to a value twice as large at the top, Steedman and Zeng (1990) showed good agreement with the results of centrifuge tests.

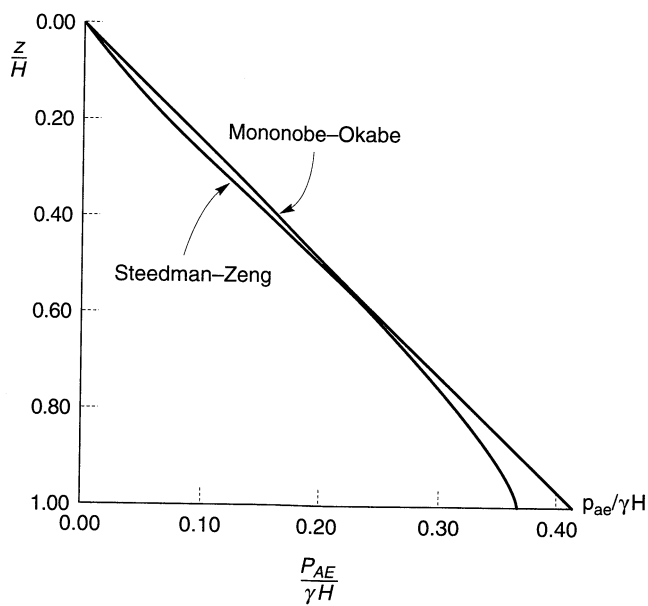


Figure 11.14 Comparison of normalized pressure distributions for M-O and Steedman-Zeng methods assuming that $k_h = 0.2$ and $H/\lambda = 0.3$. (After Steedman and Zeng, 1990.)

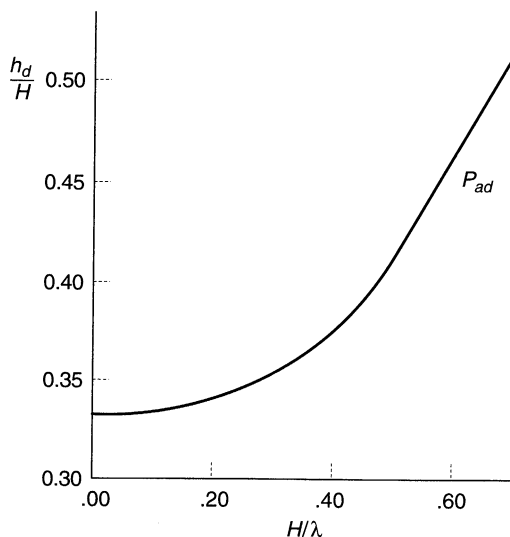


Figure 11.15 Location of dynamic thrust at instant of maximum overturning moment for $k_h = 0.2$. (After Steedman and Zeng, 1990.)

11.6.2 Nonyielding Walls

Some retaining structures, such as massive gravity walls founded on rock or basement walls braced at both top and bottom, do not move sufficiently to mobilize the shear strength of the backfill soil. As a result, the limiting conditions of minimum active or maximum passive earth pressures cannot be developed.

Wood (1973) analyzed the response of a homogeneous linear elastic soil trapped between two rigid walls connected to a rigid base (Figure 11.16). If the two walls are assumed to be spaced far apart, the pressures on one wall will not be strongly influenced by the presence of the other. Wood showed that dynamic amplification was negligible for low-frequency input motions [i.e., motions at less than half the fundamental frequency of the unrestrained backfill ($f_o = v_s/4H$)]. For this range of frequencies, in which many practical problems lie, wall pressures can be obtained from the elastic solution for the case of a uniform, constant, horizontal acceleration applied throughout the soil. For smooth rigid walls, Wood (1973) expressed the dynamic thrust and dynamic overturning moment (about the base of the wall) in the form

$$\Delta P_{eq} = \gamma H^2 \frac{a_h}{g} F_p \quad (11.31)$$

$$\Delta M_{eq} = \gamma H^3 \frac{a_h}{g} F_m \quad (11.32)$$

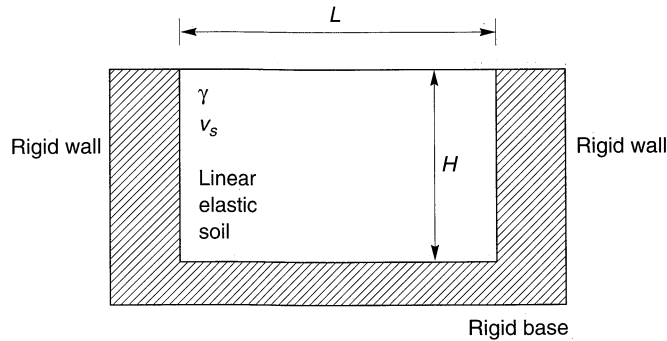


Figure 11.16 Wall geometry and notation for Wood (1973) analysis of pressures on nonyielding walls.

where a_h is the amplitude of the harmonic base acceleration and F_p and F_m are the dimensionless dynamic thrust and moment factors shown in Figures 11.17 and 11.18, respectively. The point of application of the dynamic thrust is at a height

$$h_{\text{eq}} = \frac{\Delta M_{\text{eq}}}{\Delta P_{\text{eq}}} \quad (11.33)$$

above the base of the wall; typically, $h_{\text{eq}} \approx 0.63H$.

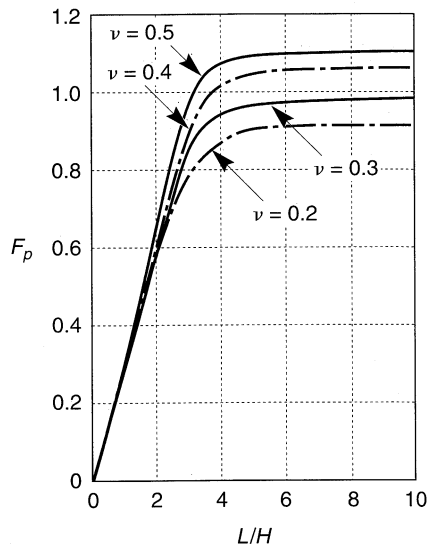


Figure 11.17 Dimensionless thrust factor for various geometries and soil Poisson's ratio values. After Wood (1973).

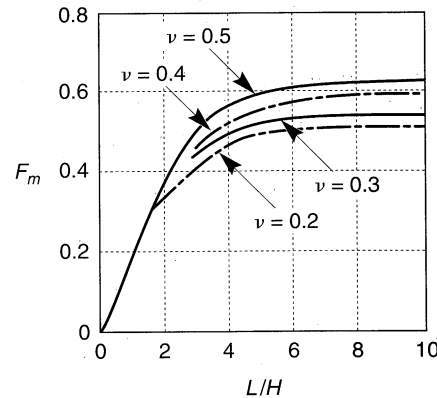
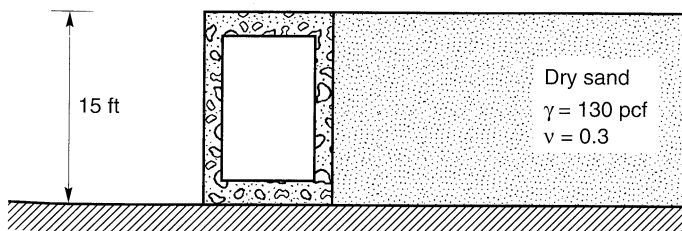


Figure 11.18 Dimensionless moment factor for various geometries and soil Poisson's ratio values. After Wood (1973).

Example 11.2

A reinforced concrete box culvert is used to provide an undercrossing through a railroad embankment as shown below. Estimate the dynamic thrust on a wall of the culvert when subjected to a ground motion with $k_h = 0.2$.

**Figure E11.2**

Solution Assuming they are properly reinforced and that the culvert cannot slide on its base, the culvert walls will not yield. Consequently, the dynamic thrust can be estimated using equation (11.31) and Figure 11.17

$$\Delta P_{eq} = \gamma H^2 \frac{a_h}{g} F_p = (130 \text{ pcf})(15 \text{ ft})^2 \frac{0.2}{g} (1.0) = 5850 \text{ lb/ft}$$

11.6.3 Effects of Water on Wall Pressures

The procedures for estimation of seismic loads on retaining walls described in the preceding sections have been limited to cases of dry backfills. Most retaining walls are designed with drains to prevent water from building up within the backfill. This is not possible, however, for retaining walls in waterfront areas, where most earthquake-induced wall failures have been observed.

The presence of water plays a strong role in determining the loads on waterfront retaining walls both during and after earthquakes. Water outboard of a retaining wall can exert dynamic pressures on the face of the wall. Water within a backfill can also affect the dynamic pressures that act on the back of the wall. Proper consideration of the effects of water is essential for the seismic design of retaining structures, particularly in waterfront areas. Since few waterfront retaining structures are completely impermeable, the water level in the backfill is usually at approximately the same level as the free water outboard of the wall. Backfill water levels generally lag behind changes in outboard water level—the difference in water level depends on the permeability of the wall and backfill and on the rate at which the outboard water level changes. The total water pressures that act on retaining walls in the absence of seepage within the backfill can be divided into two components: *hydrostatic pressure*, which increases linearly with depth and acts on the wall before, during, and after earthquake shaking, and *hydrodynamic pressure*, which results from the dynamic response of the water itself.

11.6.3.1 Water Outboard of Wall

Hydrodynamic water pressure results from the dynamic response of a body of water. For retaining walls, hydrodynamic pressures are usually estimated from Westergaard's

solution (Westergaard, 1931) for the case of a vertical, rigid dam retaining a semi-infinite reservoir of water that is excited by harmonic, horizontal motion of its rigid base. Westergaard showed that the hydrodynamic pressure amplitude increased with the square root of water depth when the motion is applied at a frequency lower than the fundamental frequency of the reservoir, $f_o = v_p/4H$, where v_p is the p-wave velocity of water (about 4700 ft/sec (1400 m/sec)) and H is the depth of water in the reservoir (the natural frequency of a 20-ft-deep (6.1 m) reservoir, for example, would be over 58 Hz, well above the frequencies of interest for earthquakes). Westergaard computed the amplitude of the hydrodynamic pressure as

$$p_w = \frac{7}{8} \frac{a_h}{g} \gamma_w \sqrt{z_w H} \quad (11.34)$$

The resultant hydrodynamic thrust is given by

$$P_w = \frac{7}{12} \frac{a_h}{g} \gamma_w H^2 \quad (11.35)$$

The total water pressure on the face of the wall is the sum of the hydrostatic and hydrodynamic water pressures. Similarly, the total lateral thrust due to the water is equal to the sum of the hydrostatic and hydrodynamic thrusts.

Another important consideration in the design of a waterfront retaining wall is the potential for rapid drawdown of the water outboard of the wall. Earthquakes occurring near large bodies of water often induce long-period motion of the water, such as tsunamis or seiches (Section 1.4.7), that cause the water surface to move up and down. While the upward movement of water outboard of a retaining wall will generally tend to stabilize the wall (assuming that it does not rise above the level of the top of the wall), downward movement can create a destabilizing rapid drawdown condition. When liquefiable soils exist under relatively high levels of initial shear stress, failures can be triggered by very small changes in water level. Such failures can originate in the soils adjacent to or beneath the retaining structure rather than in the backfill.

11.6.3.2 Water in Backfill

The presence of water in the backfill behind a retaining wall can influence the seismic loads that act on the wall in three ways: (1) by altering the inertial forces within the backfill, (2) by developing hydrodynamic pressures within the backfill, and (3) by allowing excess porewater pressure generation due to cyclic straining of the backfill soils.

The inertial forces in saturated soils depend on the relative movement between the backfill soil particles and the porewater that surrounds them. If, as is usually the case, the permeability of the soil is small enough (typically $k \leq 10^{-3}$ cm/sec (33×10^{-5} ft/sec) or so) that the porewater moves with the soil during earthquake shaking (no relative movement of soil and water, or *restrained porewater conditions*), the inertial forces will be proportional to the *total* unit weight of the soil. If the permeability of the backfill soil is very high, however, the porewater may remain essentially stationary while the soil skeleton moves back and forth (the soil particles move through the porewater in *free porewater conditions*). In such cases, inertial forces will be proportional to the *buoyant* (or submerged) unit weight of the soil. Hydrodynamic water pressures (Section 11.5.3.1) can also develop under free

pore-water conditions and must be added to the computed soil and hydrostatic pressures to obtain the total loading on the wall.

For restrained porewater conditions, the M-O method can be modified to account for the presence of porewater within the backfill (Matsuzawa et al., 1985). Representing the excess porewater pressure in the backfill by the pore pressure ratio, r_u (Section 9.5.1.1), the active soil thrust acting on a yielding wall can be computed from equation (11.15) using

$$\gamma = \gamma_b(1 - r_u) \quad (11.36)$$

$$\psi = \tan^{-1} \left[\frac{\gamma_{\text{sat}} k_h}{\gamma_b(1 - r_u)(1 - k_v)} \right] \quad (11.37)$$

An equivalent hydrostatic thrust based on a fluid of unit weight $\gamma_{\text{eq}} = \gamma_w + r_u \gamma_b$ must be added to the soil thrust. Note that as r_u approaches 1 (as it could in a liquefiable backfill), the wall thrust approaches that imposed by a fluid of equivalent unit weight, $\gamma_{\text{eq}} = \gamma_{\text{sat}}$. As discussed in Chapter 9, subsequent unidirectional movement of a soil that develops high excess porewater pressures may, depending on its residual (or steady state) strength, cause dilation with accompanying porewater pressure reduction and strength gain.

Soil thrusts from partially submerged backfills may be computed using an average unit weight based on the relative volumes of soil within the active wedge that are above and below the phreatic surface (Figure 11.19):

$$\bar{\gamma} = \lambda^2 \gamma_{\text{sat}} + (1 - \lambda^2) \gamma_d \quad (11.38)$$

Again, the hydrostatic thrust (and hydrodynamic thrust, if present) must be added to the soil thrust.

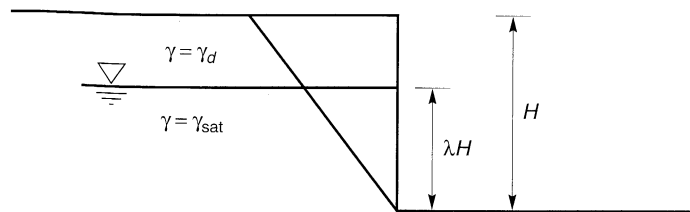


Figure 11.19 Geometry and notation for partially submerged backfill.

Example 11.3

Compute the total thrust that would be expected on the wall shown in Example 11.1 if the wall backfill was completely saturated. Assume that the pore pressure ratio, r_u , reaches a value of 0.5.

Solution The total active thrust can be computed from equation (11.15) using

$$\begin{aligned} \gamma &= \gamma_b(1 - r_u) = \rho_b g(1 - r_u) = \frac{G_s - 1}{G_s} \rho_d g(1 - r_u) \\ &= \frac{2.65 - 1}{2.65} (1.76 \text{ Mg/m}^3) (9.81 \text{ m/sec}^2) (1 - 0.5) = 5.44 \text{ kN/m}^3 \end{aligned}$$

$$\psi = \tan^{-1} \left[\frac{\gamma_{\text{sat}} k_h}{\gamma_b(1 - r_u)(1 - k_v)} \right] = \tan^{-1} \left[\frac{(10.9 \text{ kN/m}^3 + 9.8 \text{ kN/m}^3)(0.15)}{(10.9 \text{ kN/m}^3)(1 - 0.5)(1 - 0.075)} \right] = 31.6^\circ$$

Then

$$K_{AE} = \frac{\cos^2(34^\circ - 0^\circ - 31.6^\circ)}{\cos(31.6^\circ)\cos(0^\circ)\cos(17^\circ + 0^\circ + 31.6^\circ) \left[1 + \sqrt{\frac{\sin(17^\circ + 31.6^\circ)\sin(34^\circ - 0^\circ - 31.6^\circ)}{\cos(17^\circ + 0^\circ + 31.6^\circ)\cos(0^\circ - 0^\circ)}} \right]^2}$$

$$= 1.195$$

and

$$P_{AE} = \frac{1}{2} K_{AE} \gamma H^2 (1 - k_v) = \frac{1}{2} (1.195) (5.44 \text{ kN/m}^3) (5 \text{ m})^2 (1 - 0.075) = 75.2 \text{ kN/m}$$

The hydrostatic thrust is given by

$$P_w = \frac{1}{2} \gamma_{eq} H^2 = \frac{1}{2} (\gamma_w + r_u \gamma_b) H^2 = \frac{1}{2} [9.81 \text{ kN/m}^3 + (0.5)(10.9 \text{ kN/m}^3)] (5 \text{ m})^2$$

$$= 190.6 \text{ kN/m}$$

Therefore, the total thrust is

$$P_{tot} = P_{AE} + P_w = 75.2 \text{ kN/m} + 190.6 \text{ kN/m} = 265.8 \text{ kN/m}$$

11.6.4 Finite-Element Analysis

Earthquake-induced pressures on retaining walls can also be evaluated using dynamic response-analyses. A number of computer programs are available for such analyses (Section 7.3). Linear or equivalent linear analyses can be used to estimate wall pressures, although their inability to represent actual modes of failure can make their results difficult to interpret. Nonlinear analyses are capable of predicting permanent deformations (Section 11.6.3) as well as wall pressures.

11.7 SEISMIC DISPLACEMENTS OF RETAINING WALLS

Although the methods of analysis described in the preceding section provide useful information on the seismic loads that act on retaining walls, the postearthquake serviceability of such walls is more closely related to the permanent deformations that occur during earthquakes. While large permanent deformations may be acceptable for some walls, others may be considered to have failed at much smaller deformations. Analyses that predict permanent wall deformations may provide a more useful indication of retaining wall performance. Several methods have been proposed for predicting permanent deformations of yielding walls.

11.7.1 Richards-Elms Method

Richards and Elms (1979) proposed a method for the seismic design of gravity walls based on allowable permanent wall displacements. The method estimates permanent displacements in a manner analogous to the Newmark sliding block procedure (Section 10.6.1.2) developed originally for evaluation of seismic slope stability.

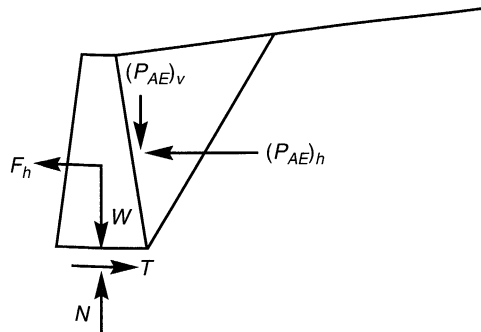


Figure 11.20 Gravity wall acted upon by gravity and pseudostatic accelerations.

Application of the Richards–Elms method requires evaluation of the yield acceleration for the wall–backfill system. Consider the gravity wall shown in Figure 11.20. When the active wedge is subjected to acceleration acting toward the backfill, the resulting inertial forces will act away from the backfill. The level of acceleration that is just large enough to cause the wall to slide on its base is the *yield acceleration*. When the acceleration is equal to the yield acceleration, horizontal and vertical equilibrium require that

$$\begin{aligned} T &= F_h + (P_{AE})_h \\ N &= W + (P_{AE})_v \end{aligned} \quad (11.39)$$

Substituting $T = N \tan \phi_b$, $F_h = a_y W/g$, $(P_{AE})_h = P_{AE} \cos(\delta + \theta)$, and $(P_{AE})_v = P_{AE} \sin(\delta + \theta)$, the yield acceleration can be computed as

$$a_y = \left[\tan \phi_b - \frac{P_{AE} \cos(\delta + \theta) - P_{AE} \sin(\delta + \theta)}{W} \right] g \quad (11.40)$$

Richards and Elms recommended that P_{AE} be calculated using the M-O method (since the M-O method requires that a_y be known, the solution of equation (11.40) must be obtained iteratively). Using the results of sliding block analyses in the same manner as Newmark (1965) and Franklin and Chang (1977), Richards and Elms proposed the following expression for permanent block displacement:

$$d_{\text{perm}} = 0.087 \frac{v_{\max}^2 a_{\max}^3}{a_y^4} \quad \frac{a_y}{a_{\max}} \geq 0.3 \quad (11.41)$$

where v_{\max} is the peak ground velocity, a_{\max} the peak ground acceleration, and a_y the yield acceleration for the wall–backfill system. Equation (11.41) provides displacement estimates that are close to the estimated maximum displacements [equation (10.13)] of Newmark (1965).

Example 11.4

Estimate the permanent displacement of the concrete gravity wall shown below that would be produced by the Gilroy No. 2 (soil) motion. Assume $k_v = 0$.

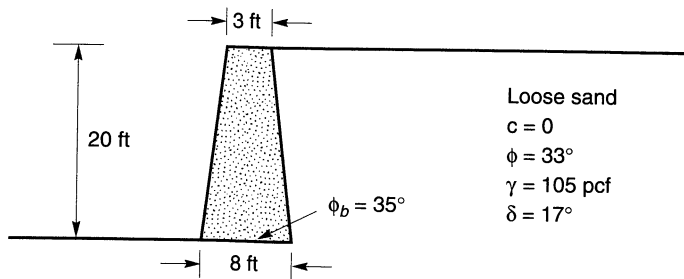


Figure E11.4

Solution The weight of the wall section is

$$W = (20 \text{ ft}) \left(\frac{8 \text{ ft} + 3 \text{ ft}}{2} \right) (150 \text{ lb/ft}^3) = 16500 \text{ lb/ft}$$

The total active thrust can be estimated by the Mononobe-Okabe approach. From equations (11.15) and (11.16). Assuming a trial pseudostatic acceleration of $0.10g$, $\psi = 5.7^\circ$ and

$$K_{AE} =$$

$$\frac{\cos^2(33^\circ - 7.1^\circ - 5.7^\circ)}{\cos(5.7^\circ)\cos^2(7.1^\circ)\cos(17^\circ + 7.1^\circ + 5.7^\circ) \left[1 + \sqrt{\frac{\sin(17^\circ + 33^\circ)\sin(33^\circ - 0^\circ - 5.7^\circ)}{\cos(17^\circ + 7.1^\circ + 5.7^\circ)\cos(0^\circ - 7.1^\circ)}} \right]^2} = 0.385$$

and

$$P_{AE} = \frac{1}{2}(0.385)(105 \text{ pcf})(20 \text{ ft})^2 = 8085 \text{ lb/ft}$$

Then, from equation (11.40),

$$a_y = \left[\tan(35^\circ) - \frac{(8085 \text{ lb/ft})\cos(17 + 7.1) - (8085 \text{ lb/ft})\sin(17 + 7.1)}{16500 \text{ lb/ft}} \right] g = 0.45g$$

Because the computed yield acceleration ($0.43g$) is inconsistent with the assumed pseudostatic acceleration ($0.10g$), another iteration is required. For the next iteration, assume that the pseudostatic acceleration is $0.30g$. Then ψ is 16.7° and

$$K_{AE} =$$

$$\frac{\cos^2(33^\circ - 7.1^\circ - 16.7^\circ)}{\cos(16.7^\circ)\cos^2(7.1^\circ)\cos(17^\circ + 7.1^\circ + 16.7^\circ) \left[1 + \sqrt{\frac{\sin(17^\circ + 33^\circ)\sin(33^\circ - 0^\circ - 16.7^\circ)}{\cos(17^\circ + 7.1^\circ + 16.7^\circ)\cos(0^\circ - 7.1^\circ)}} \right]^2} = 0.574$$

and

$$P_{AE} = \frac{1}{2}(0.574)(105 \text{ pcf})(20 \text{ ft})^2 = 12054 \text{ lb/ft}$$

Then, from equation (11.40),

$$a_y = \left[\tan(35^\circ) - \frac{(12054 \text{ lb/ft})\cos(17 + 7.1) - (12054 \text{ lb/ft})\sin(17 + 7.1)}{16500 \text{ lb/ft}} \right] g = 0.33g$$

Now, the computed yield acceleration is fairly close to the assumed pseudostatic acceleration. Using equation (11.41) with the results of Example 3.1

$$d_{\text{perm}} = 0.087 \frac{(39.2 \text{ cm/sec})^2 [(0.322g)(981 \text{ cm/sec}^2/g)]^3}{[(0.30g)(981 \text{ cm/sec}^2/g)]^4} = 6.5 \text{ cm}$$

11.7.2 Whitman-Liao Method

The Richards-Elms method offers a rational deterministic approach to the estimation of gravity wall displacements. Its simplicity comes, in part, from assumptions that neglect certain aspects of the dynamic earth pressure problem. Whitman and Liao (1985) identified several modeling errors that result from the simplifying assumptions of the Richards-Elms procedure. The most important of these are neglect of the dynamic response of the backfill, neglect of kinematic factors, neglect of tilting mechanisms, and neglect of vertical accelerations. Finite-element analyses of the effects of the dynamic response of the backfill on wall displacements (Nadim, 1982), for example, show that amplification occurs when input motions coincide with the natural period of the backfill and produce considerably greater permanent displacement than the rigid-block model used by Richards and Elms. Analyses in which the backfill wedge and wall were treated as separate blocks (Zarrabi-Kashani, 1979) show that the kinematic requirements of horizontal *and* vertical displacement of the backfill wedge cause systematically smaller displacements than the single-block model of Richards and Elms. Studies of combined tilting and sliding (Nadim, 1980; Siddharthan et al., 1992), indicate that tilting mechanisms generally increase wall displacements over those produced by sliding-only models such as that of Richards and Elms. Consideration of vertical accelerations produces slightly larger displacements than when they are neglected, at least for motions with high peak horizontal acceleration (a_{\max} greater than about 0.5g) and $a_y/a_{\max} \geq 0.4$ (Whitman and Liao, 1985). Whitman and Liao quantified and combined the effects of each of these sources of modeling error to describe the total modeling error by a lognormally distributed random variable with mean value, \bar{M} , and standard deviation, $\sigma_{\ln M}$.

Using the results of sliding block analyses of 14 ground motions by Wong (1982), Whitman and Liao found that the permanent displacements were lognormally distributed with mean value

$$\bar{d}_{\text{perm}} = \frac{37 v_{\max}^2}{a_{\max}} \exp\left(\frac{-9.4 a_y}{a_{\max}}\right) \quad (11.42)$$

Uncertainty due to statistical variability of ground motions was characterized by a lognormally distributed random variable, Q , with a mean value of \bar{Q} and standard deviation, $\sigma_{\ln Q}$.

The effects of uncertainty in soil properties, specifically the friction angles, on permanent displacement were also investigated. Using standard deviations of $\sigma_\phi = 2$ to 3° for soil friction angles and $\sigma_\delta = 5^\circ$ for wall-soil interface friction angles, the computed yield acceleration [the only term on the right side of equation (11.40) that is a function of ϕ and

$\delta]$ was defined as a random variable with mean value \bar{a}_y and standard deviation σ_{a_y} . The mean value \bar{a}_y is the yield acceleration computed using the mean values of ϕ and δ .

Combining all of these sources of uncertainty, the permanent displacement can be characterized as a lognormally distributed random variable with mean value

$$\bar{d} = \frac{37v_{\max}^2}{a_{\max}} \exp\left(\frac{-9.4\bar{a}_y}{a_{\max}}\right) \bar{Q} \bar{M} \quad (11.43)$$

and variance

$$\sigma_{\ln d}^2 = \left(\frac{9.4g}{a_{\max}}\right)^2 \sigma_{a_y}^2 + \sigma_{\ln M}^2 + \sigma_{\ln Q}^2 \quad (11.44)$$

Suggested values of the means and standard deviations of the ground motion, soil resistance, and model error factors are shown in Table 11-4.

Table 11-4 Mean and Standard Deviation Values for Gravity Wall Displacement Analysis

| Factor | Mean | Standard Deviation |
|-----------------|---|-----------------------------------|
| Model error | $\bar{M} = 3.5$ | $\sigma_{\ln M} = 0.84$ |
| Soil resistance | $\bar{a}_y = a_y(\bar{\phi}, \bar{\delta})$ | $\sigma_{a_y} = 0.04$ to 0.065 |
| Ground motion | $\bar{Q} = 1$ | $\sigma_{\ln Q} = 0.58$ to 1.05 |

Source: After Whitman and Liao (1985).

Using equations (11.43) and (11.44), along with the CDF for the standard normal variable (Table C-1), the probability of exceeding any particular value of d_{all} can easily be computed.

Example 11.5

Estimate the expected permanent displacement of the gravity wall shown in Example 11.4 using the Whitman–Liao approach.

Solution From equation (11.42), the mean or expected value of permanent displacement is given by

$$d_{\text{perm}} = 37 \frac{(39.2 \text{ cm/sec})^2}{[(0.322g)(981 \text{ cm/sec}^2/g)]} \exp [(-9.4)(0.30g)/0.322g] = 0.03 \text{ cm}$$

Note that the mean permanent displacement is considerably smaller than the displacement predicted by the Richards–Elms method in Example 11.4.

11.7.3 Finite-Element Analysis

Earthquake-induced deformations of retaining walls can be predicted by dynamic stress–deformation analyses. Obviously, prediction of permanent deformations requires the use of a nonlinear analysis (Section 7.2.3). A rigorous analysis should be capable of accounting for nonlinear, inelastic behavior of the soil and of the interfaces between the soil and wall elements. Among the relatively few examples of rigorous two-dimensional finite-element analyses that predict permanent deformations are those reported by Alampalli and Elgamal (1990), Finn et al. (1992), and Iai and Kameoka (1993).

11.8 SEISMIC DESIGN CONSIDERATIONS

The design of retaining walls for seismic conditions is similar, in many respects, to designing for static conditions. In both cases, potential modes of failure are identified and the wall designed to avoid initiating them. Although the response of retaining walls under seismic loading conditions is much more complex than under static conditions, conventional design procedures make use of simplifying assumptions that render the problem tractable. Several design approaches for different types of retaining walls are described in the following sections.

11.8.1 Gravity Walls

Gravity walls are the simplest type of retaining wall, and more attention has been paid to their design than to the design of other types of walls. Gravity wall design procedures, however, are commonly adapted as part of the design of cantilever walls and composite wall systems. Gravity walls are customarily designed by one of two approaches: a seismic pressure-based approach or a permanent displacement-based approach. Although the gravity wall design procedures are oriented toward prevention of sliding failure, the possibility of overturning due to bearing failure of the soil beneath the base of a wall must also be considered in design.

11.8.1.1 Design Based on Seismic Pressures

Gravity walls have traditionally been designed on the basis of seismic earth pressures. The M-O method is most commonly used along with an inertial force, using the same pseudostatic acceleration applied to the active wedge, applied to the wall itself. Pseudostatic accelerations are generally considerably smaller than anticipated peak accelerations. Values between $0.05g$ and $0.15g$, corresponding to one-third to one-half of the peak ground surface acceleration, are commonly used with factors of safety of 1.0 to 1.2 (Whitman, 1990).

Despite the considerable simplification of their complex actual behavior, gravity walls designed by the traditional approach have generally performed quite well in earthquakes. The reason, however, may have more to do with the conservatism commonly used in static wall design than with the accuracy of the M-O method. Design pressures that account for backfill amplification, such as those that can be obtained by the Steedman-Zeng method, should be considered for design of unusually tall or unusually displacement-sensitive walls.

11.8.1.2 Design Based on Allowable Displacements

Gravity walls are being designed on the basis of allowable displacements more and more frequently. This approach allows the designer to consider the consequences of permanent displacement for an individual wall when selecting an allowable displacement for design. Design procedures based on the Richards-Elms and Whitman-Liao procedures for estimation of permanent displacement are available.

The Richards-Elms design procedure involves calculation of the wall weight that would be required to ensure that permanent displacements are less than or equal to some allowable value. The procedure can be summarized as follows:

1. Select an allowable permanent displacement, d_{all} .
2. Calculate the yield acceleration required to produce the allowable permanent displacement from equation (11.41), rearranged in the form

$$a_y = \left(\frac{0.087 v_{\max}^2 a_{\max}^3}{d_{\text{all}}} \right)^{1/4} \quad (11.45)$$

3. Calculate P_{AE} using the M-O method with the yield acceleration from step 2 as the pseudostatic acceleration. This represents the soil thrust that would be expected to cause a maximum permanent displacement equal to d_{all} .
4. Calculate the wall weight required to limit the permanent displacement to the allowable permanent displacement using equation (11.40) rearranged in the form

$$W = \frac{P_{AE} \cos(\delta + \theta) - P_{AE} \sin(\delta + \theta) \tan \phi_b}{\tan \phi_b - a_y/g} \quad (11.46)$$

5. Apply a factor of safety to the weight of the wall. Richards and Elms originally suggested a factor of safety of 1.5, but subsequent research has shown that a wall weight factor of safety of 1.1 to 1.2 should be sufficient to reduce the probability of exceeding the allowable permanent displacement to 5% or less (Whitman and Liao, 1985).

Using the Whitman–Liao approach, gravity walls can be designed on the basis of allowable displacements that have defined probabilities of exceedance. The selection of an acceptable probability of exceedance is a complicated matter that may depend on the importance of the wall, the effects of failure, the cost of repair, and other technical and/or non-technical factors. The actual wall design is accomplished by using equation (11.43) to compute the yield acceleration as

$$a_y = \frac{a_{\max}}{9.4} \ln \frac{37 \bar{M} v_{\max}^2}{a_{\max} d_{\text{all}}} \quad (11.47)$$

and then using the M-O method to size the wall to meet or exceed the computed yield acceleration. Whitman and Liao suggest a conservative design (corresponding to a probability of exceedance of about 5%) can be obtained by assuming $d_{\text{all}} = 4 \bar{d}_{\text{perm}}$, where \bar{d}_{perm} is calculated from equation (11.42). A less conservative design (corresponding to about 10% probability of exceedance) is obtained by taking $d_{\text{all}} = 2.5 \bar{d}_{\text{perm}}$.

11.8.2 Cantilever Walls

Cantilever walls are designed in much the same way as gravity walls, except that bending failure must also be considered. Maximum bending moments are usually calculated using the M-O method to compute the maximum soil thrust, which is taken to act at the height given by equation (11.19). The maximum overturning moment is used for structural design of wall elements (to prevent flexural failure of the wall itself) and to determine the size of the wall footing required to prevent bearing failure of the supporting soils.

11.8.3 Braced Walls

Because their lateral displacements are constrained by bracing elements, braced walls do not develop minimum active (or maximum passive) earth pressures in the vicinity of the

bracing elements. The earth pressures that do develop depend on the stiffness of the brace and the relative stiffness of the wall and soil. Analysis of actual soil–wall–brace interaction is quite complicated, and simplified methods are generally adopted for design purposes.

11.8.3.1 Non-Yielding Braced Walls

Walls that are braced sufficiently that they do not move at all, such as braced walls founded on rock, are usually designed to resist the earth pressures predicted by Wood's (1973) analysis. To avoid cracking or yielding of such walls, design pressures are usually based on the peak acceleration (Whitman, 1991). This approach, however, can lead to very high design pressures and some data [e.g., Chang et al. (1990)], indicates that the pressures on braced walls that can move slightly are lower. Dynamic finite-element analyses of stiff, embedded basement walls suggest that the M-O method with the peak ground surface acceleration outside the structure produces reasonable design earth pressures (Whitman, 1990).

Specifications for design of bridge abutments (e.g., AASHTO, 1991) recommend that nonyielding abutments be designed to resist lateral thrust obtained from the M-O method with a pseudostatic horizontal acceleration 50% greater than the effective peak acceleration.

11.8.3.2 Flexible Braced Walls

The seismic response of flexible braced walls such as anchored bulkheads and tieback walls is particularly complicated. Again, these complexities require that simplified methods be used for design. Because these types of walls are very commonly used in waterfront areas, and because the great majority of earthquake-induced retaining wall failures occur in waterfront areas, special attention to their design is required. In the case of anchored bulkheads, the simplified design procedures can be supplemented by a useful empirical model of damage potential based on observations of actual wall performance.

Anchored Bulkheads. The design of anchored bulkheads in waterfront areas is strongly influenced by liquefaction hazards. If widespread liquefaction occurs, experience indicates that bulkhead failures are very likely. Consequently, steps should be taken prior to construction to ensure that such liquefaction will not occur. Permanent seaward movements of anchored bulkheads in the absence of widespread liquefaction, however, has also been observed. Conventional design procedures seek to minimize this type of damage using pseudostatically determined design pressures.

A recent design procedure uses the free earth support method and Rowe's moment reduction method, with earthquake effects represented by pseudostatic inertial forces. A brief summary of the procedure is presented below; a detailed description with a worked example may be found in Ebeling and Morrison (1993).

1. Design the anchored bulkhead for static loading conditions.
2. Select pseudostatic accelerations a_h and a_v .
3. Compute the active soil thrust on the back of the wall using the M-O method. The active wedge is assumed to originate at the bottom of the wall.
4. Compute the passive soil thrust acting on the front of the wall using the M-O method. The passive wedge is also assumed to originate at the bottom of the wall.
5. Compute the minimum required depth of wall penetration by summing moments about the wall–tierod connection. All water pressures (hydrostatic, hydrodynamic, and excess porewater, if present) must be included.

6. Compute the required anchor resistance by summing the horizontal forces acting on the wall. All water pressures (hydrostatic, hydrodynamic, and excess porewater, if present) must be included. The computed anchor resistance is termed the *free earth support anchor resistance*.
7. Compute the distribution of bending moments over the height of the wall. All water pressures (hydrostatic, hydrodynamic, and excess porewater, if present) must be included. The maximum bending moment is termed the *free earth support moment*.
8. Compute the design bending moment as the product of the free earth support moment and Rowe's moment reduction factor (Rowe, 1952).
9. Set the design tierod force at a level 30% greater than the free earth support anchor resistance.
10. Determine the required size of the anchor block to satisfy horizontal force equilibrium considering the active and passive pressures, as well as all water pressures, on both sides of the block. The effects of any water pressures on the bottom and top surfaces of the anchor block should also be considered.
11. Locate the anchor block at a sufficient distance behind the wall that the active wedge behind the wall does not intersect the passive wedge in front of the anchor block. Since the active and passive failure surfaces are flatter for seismic loading than for static loading, seismic design may require a considerably longer tierod than static design.
12. Check the effects of redistribution of any earthquake-induced excess porewater pressure after earthquake shaking has ended.

Case histories of anchored bulkhead performance (neglecting cases in which widespread liquefaction was observed) suggest that anchored bulkhead damage levels can be predicted approximately with the aid of two dimensionless indices: the *effective anchor index* and the *embedment participation index* (Gazetas et al., 1990). Referring to Figure 11.21a, the effective anchor index describes the relative magnitude of the available anchor capacity as

$$\text{EAI} = \frac{d}{H} \quad (11.48)$$

where d is the horizontal distance between the active wedge and the tierod-anchor connection and H is the height of the wall. The critical active failure plane is taken to originate at the effective *point of rotation* of the wall, which can be located using soil-structure interaction analyses or estimated as

$$f \approx \left(\frac{1 + k'_e}{2} - \frac{\Phi - 20^\circ}{50^\circ} \right) H \leq D \quad (11.49)$$

where

$$k'_e = \begin{cases} \frac{k_h}{1 - k_v} & \text{above the water table} \\ \frac{(a_h/g)_{\max}}{1 - 2(a_v/g)_{\max}/3} & \text{below the water table} \end{cases}$$

The inclination of the critical active failure plane can be approximated (Dennehy, 1985) as

$$\alpha_{AE} \approx 45^\circ + \frac{\phi}{2} - 135^\circ (k'_e)^{1.75} \quad (11.50)$$

for $0.10 \leq k'_e \leq 0.50$ and $25^\circ \leq \phi \leq 35^\circ$. Beyond these ranges, equation (11.17) can be used to estimate the inclination of the active wedge. The embedment participation index is defined as

$$EPI = \frac{F_{PE}}{F_{AE}} \left(1 + \frac{f}{f+H} \right) \quad (11.51)$$

where F_{AE} and F_{PE} are the potential active and passive thrusts, respectively. For uniform backfill and foundation soils,

$$EPI \approx \frac{K_{PE}}{K_{AE}} r^2 (1+r) \quad (11.52)$$

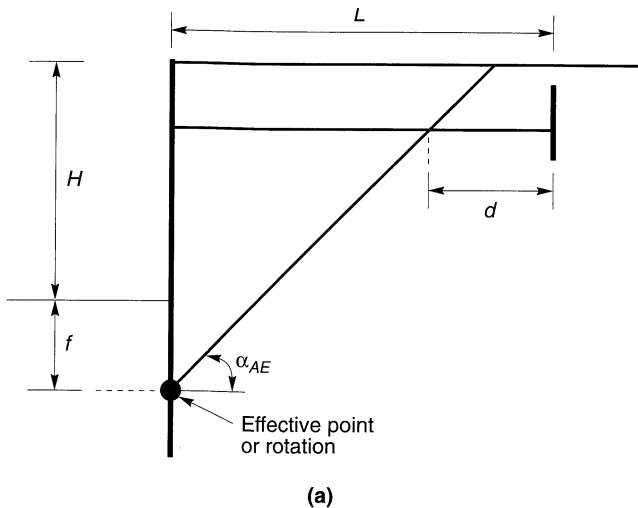
where $r = f/(f+H)$. Values of EAI and EPI have been computed for 75 anchored bulkheads for which degrees of damage in earthquake had been categorized as indicated in Table 11-5 (Gazetas et al., 1990). Comparison of degrees of damage with EAI and EPI showed significant trends in the characteristics of anchored bulkheads that performed well and those that performed poorly. As illustrated in Figure 11.21b, anchored bulkheads with high EAI and EPI values (zone I) generally suffered little or no damage. Anchored bulkheads with low EAI and EPI values (zone III) usually suffered severe damage. Moderate damage was generally associated with intermediate combinations of EAI and EPI (zone II). The chart of Figure 11.21b is a very useful tool for checking the design of anchored bulkheads in waterfront areas.

Table 11-5 Qualitative and Quantitative Descriptions of Reported Degrees of Damage to Anchored Bulkheads during Earthquakes

| Degree of Damage | Description of Damage | Permanent Horizontal Displacement at Top of Sheetpile (cm) |
|------------------|---|--|
| 0 | No damage | < 2 |
| 1 | Negligible damage to the wall itself; noticeable damage to related structures | 2–10 |
| 2 | Noticeable damage to the wall | 10–30 |
| 3 | General shape of anchored sheetpile preserved, but significantly damaged | 30–60 |
| 4 | Complete destruction | > 60 |

Source: After Kitajima and Uwabe (1979).

Tieback Walls. Because their use was originally restricted to temporary support of excavations, the seismic performance of tieback walls has received relatively little attention. As permanent tieback walls have become more common, however, recognition of the need to consider seismic loading in their design has increased. With respect to seismic performance, tieback walls are similar to anchored bulkheads—the primary differences are that tieback walls have multiple anchors and that the anchors are generally inclined. Although



(a)

Figure 11.21 (a) Geometry and notation for evaluation of anchored bulkhead design; (b) correlation between damage levels and dimensionless anchored bulkhead indices. After Gazetas et al. (1990). Empirical design method for waterfront anchored sheetpile walls, *Design and Performance of Earth Retaining Structures*. Reprinted by permission of ASCE.

formalized design procedures are not currently available, the results of a limited number of experimental and numerical investigations provide insight into special considerations for seismic design of tieback walls. Few observations of the seismic performance of tieback walls have been made, but those that are available generally indicate good performance (Ho et al., 1990).

Numerical analyses indicate that the stiffness and spacing of the anchors strongly influences the permanent displacements of a tieback wall (Siller and Frawley, 1992). In general, tieback walls with stiff anchors will develop smaller permanent displacements than walls with softer anchors. Tieback walls with smaller vertical spacing between anchors will experience smaller and more uniform permanent displacements than walls with greater anchor spacing. Earthquake-induced permanent displacements also appear sensitive to static design pressures—walls designed for higher static pressures suffer smaller permanent displacements during earthquakes than walls designed for lower static pressures. Tieback walls also tend to develop smaller permanent when higher rather than lower initial anchor preloads are used (Siller and Dolly, 1992).

Tieback walls can also be influenced by phase differences between the response of the soil behind the wall and the foundation soil (Fragaszy et al., 1987). Wall elements that extend into the foundation soils may be subjected to very high bending moments at the base of the wall. Further, inclined anchors that extend below the bottom of the excavation may experience very high tensile forces when the soil end moves one way and the wall end the other.

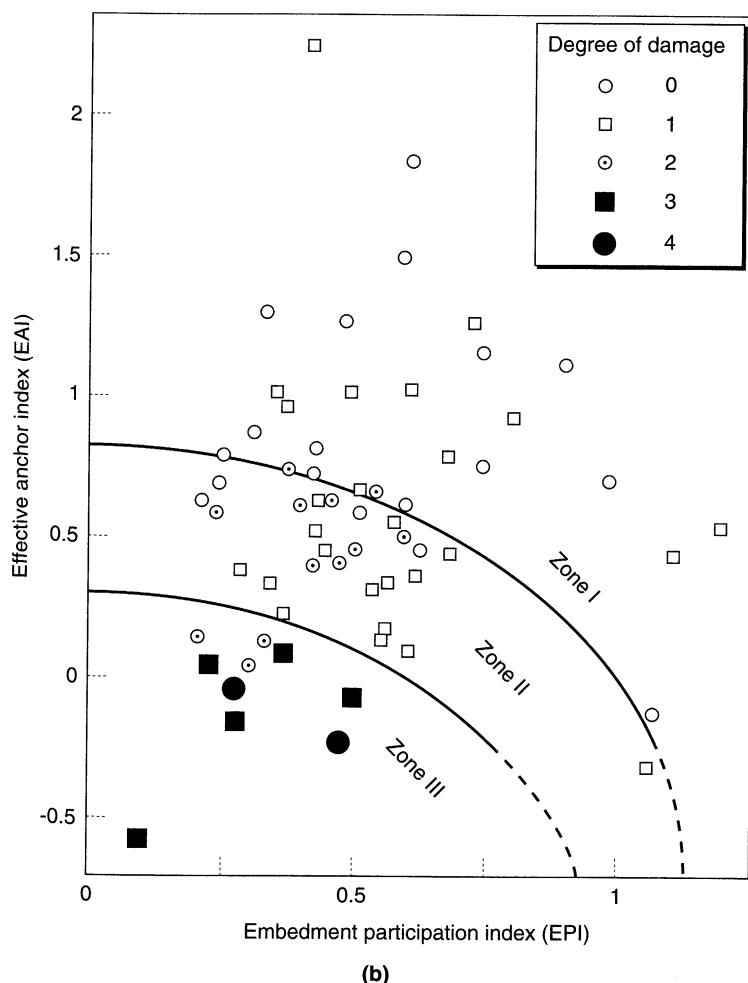


Figure 11.21 (continued)

11.8.4 Reinforced Soil Walls

Reinforced soil walls have become very popular in recent years. Although many different materials are used, reinforced soil walls consist of a zone of reinforced soil that retains unreinforced soil behind it. During an earthquake, a reinforced soil wall is subjected to a dynamic soil thrust at the back of the reinforced zone and to inertial forces within the reinforced zone in addition to static forces. The wall must be designed to avoid *external instability* (sliding or overturning failure of the reinforced zone) and *internal instability* (tensile or pullout failure of the reinforcement). Current design procedures, such as those described below (Christopher et al., 1990), use a pseudostatic approach, but displacement-based design procedures are likely to be developed in the future.

Reinforced soil walls use different materials and provide support by different mechanisms than do conventional retaining walls. Their design requires careful consideration of loading, time, and environmental factors that may not be significant for conventional retaining walls. The following sections are restricted to seismic aspects of reinforced soil wall design. Other aspects of design are discussed in detail by Mitchell and Villet (1987), Christopher et al. (1990), and Koerner (1994).

11.8.4.1 External Stability

For evaluation of external stability, a reinforced wall is treated much like a gravity wall. As illustrated in Figure 11.22, the reinforced zone is assumed to be acted on by its own weight, W , and the static soil thrust, P_A . Earthquake loading is represented pseudostatically by the dynamic soil thrust, ΔP_{AE} , and the inertial force on the reinforced zone, P_{IR} . The external stability of a particular wall design can be evaluated by the following procedure:

1. Determine the peak horizontal ground surface acceleration, a_{\max} .
2. Calculate the peak acceleration at the centroid of the reinforced zone from the equation

$$a_c = \left(1.45 - \frac{a_{\max}}{g} \right) a_{\max} \quad (11.53)$$

3. Calculate the dynamic soil thrust from

$$\Delta P_{AE} = 0.375 \frac{a_c \gamma^{(b)} H^2}{g} \quad (11.54)$$

where $\gamma^{(b)}$ is the unit weight of the backfill soil.

4. Calculate the inertial force acting on the reinforced zone from

$$P_{IR} = \frac{a_c \gamma^{(r)} H L}{g} \quad (11.55)$$

where $\gamma^{(r)}$ is the unit weight of the reinforced zone.

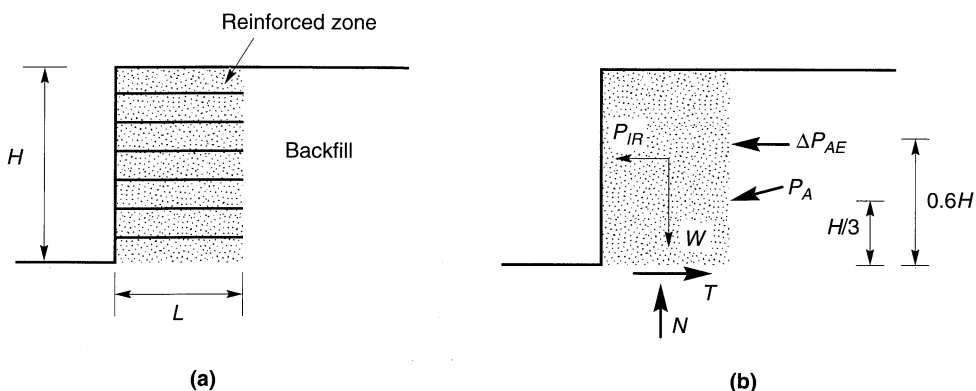


Figure 11.22 (a) Geometry and notation for reinforced soil walls; (b) static and pseudostatic forces acting on reinforced zone.

5. Add P_{AE} and 50% of P_{IR} to the static forces acting on the reinforced zone and check sliding and overturning stability (the reduced value of P_{IR} is allowed to account for the fact that the maximum values of ΔP_{AE} and P_{IR} are unlikely to occur at the same time). For seismic design, factors of safety against sliding and overturning should be greater than or equal to 75% of the minimum acceptable factors of safety for static loading.

11.8.4.2 Internal Stability

Internal stability evaluation depends on the nature of the reinforcement since the critical internal failure surface is different for inextensible and extensible reinforcement (Figure 11.23). Internal stability for seismic conditions can be evaluated in the following steps:

1. Determine the pseudostatic inertial force acting on the potentially unstable internal failure zone,

$$P_{IA} = \frac{a_c W_A}{g} \quad (11.56)$$

where W_A is the weight of the failure mass (the trapezoidal or triangular zones in Figure 11.23a and b for inextensible or extensible reinforcement, respectively).

2. Distribute P_{IA} to each reinforcement layer in proportion to its resistant area (the area of reinforcement that extends beyond the potential internal failure surface). This process produces a dynamic component of tensile force for each layer of reinforcement.
3. Add the dynamic components of tensile force to the static components of tensile force to obtain the total tensile force for each layer of reinforcement.
4. Check to see that the allowable tensile strength of the reinforcement is at least 75% of the total tensile force in each layer of reinforcement.
5. Check to see that each layer of reinforcement extends far enough beyond the potential internal failure surface to avoid pullout failure with a factor of safety not less than 75% of the minimum static factor of safety when the total tensile force is applied.

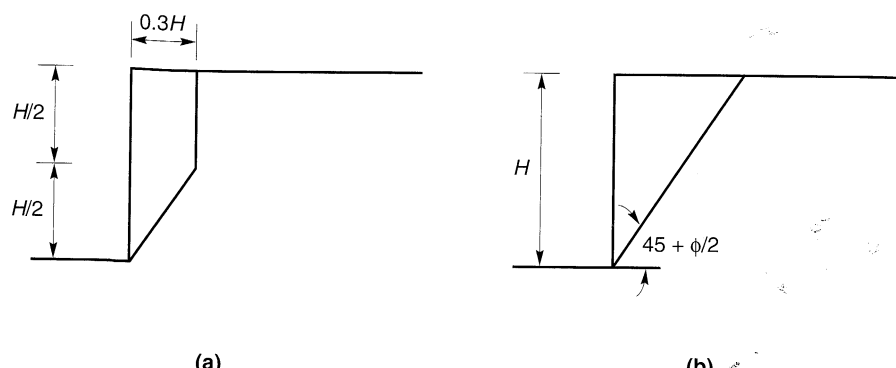


Figure 11.23 Critical potential failure surfaces for evaluation of internal seismic stability of reinforced soil walls: (a) inextensible reinforcement; (b) extensible reinforcement.

11.9 SUMMARY

1. A variety of different systems are used to retain soil; many innovative systems have been developed and used in the last 20 years. For seismic design purposes, most retaining systems fall into three general categories: gravity walls, cantilever walls, and braced walls. Each of these types of walls resists the lateral pressures of the retained soil differently.
2. Retaining walls can fail in many different ways. Gravity walls fail by sliding, overturning, or gross instability. Cantilever walls can fail in the same ways as gravity walls, but can also fail in bending. Braced walls can fail in the same ways as cantilever walls, but also by bracing element failure or rotation about the brace connection.
3. The seismic performance of a retaining wall depends on the total pressures (i.e., static plus dynamic pressures) that act on it during an earthquake. Consequently, the level of dynamic pressures required to damage the wall depends on the level of static pressures that exist before the earthquake. Analysis of the seismic behavior of a retaining wall, therefore, requires an initial analysis of the behavior under static conditions.
4. The seismic response of retaining walls is a complex example of soil–structure interaction. Because of this complexity, design procedures are usually based on a number of simplifying assumptions. Although the simplified procedures do not represent all aspects of wall–soil behavior accurately, they have been shown to provide a reasonable basis for design.
5. The soil pressure on a retaining wall depends on whether the wall is able to move relative to the soil. The dynamic pressures acting on a yielding wall are usually estimated by the pseudostatic Mononobe–Okabe analysis. The dynamic pressures on nonyielding walls are usually estimated by an elastic analysis.
6. The presence of water on either side of a retaining wall strongly influences the seismic behavior of the wall. Water on the outboard side of the wall can exert dynamic, in addition to hydrostatic, pressures on the face of the wall. Water within the backfill can influence the inertial forces acting on the wall and can develop hydrodynamic or excess porewater pressures.
7. Earthquake-induced displacements of retaining walls can be estimated by procedures analogous to the Newmark sliding block analysis for displacements of slopes. Refinements to this approach allow consideration of factors such as backfill amplification, wall tilting, kinematic constraints, and vertical acceleration. Procedures for estimation of probabilities of various displacement levels are also available.
8. Seismic design of retaining walls is generally based on seismic pressures or allowable displacements. In the former approach, pseudostatic or pseudodynamic analyses are used to estimate seismically induced wall pressures, and the wall is designed to resist those pressures without failing or causing failure of the surrounding soil. The latter approach involves designing the wall such that its seismically induced permanent displacement does not exceed a predetermined allowable displacement.
9. The majority of observed failures of retaining walls during earthquakes have occurred in waterfront areas; many have involved liquefaction of the backfill. Excessive permanent displacements of anchored bulkheads in waterfront areas have often been associated with inadequate wall embedment depths and/or insufficient anchor capacity.

HOMEWORK PROBLEMS

- 11.1** Compute the static thrust and overturning moment at the base of the concrete retaining wall shown below.

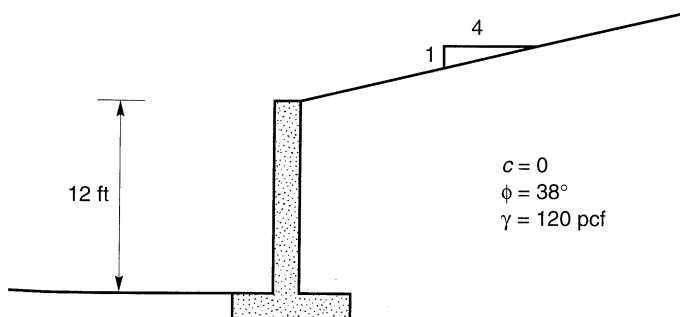


Figure P11.1

- 11.2** The wall shown in Problem 11.1 is subjected to earthquake shaking with a peak horizontal acceleration of $0.28g$. Assuming a pseudostatic coefficient, $k_h = 0.3 a_{\max}/g$, estimate (a) the total active thrust acting on the wall, (b) the height of the resultant of the total active thrust, and (c) the total overturning moment about the base of the wall.
- 11.3** Using the Steedman-Zeng approach, plot the distributions of maximum and minimum lateral pressure if the wall shown below is subjected to a $0.15g$ harmonic base motion at (a) a frequency of 0.5 Hz , and (b) a frequency of 5.0 Hz .

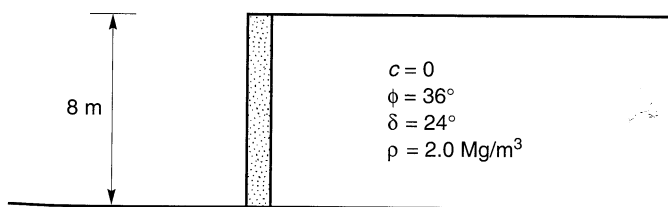


Figure P11.3

- 11.4** A 12 ft deep rigid basement wall is backfilled with dense gravelly sand: $c = 0$, $\phi = 45^\circ$, $\gamma = 140 \text{ pcf}$. Estimate the maximum dynamic thrust acting on the wall when subjected to a ground motion with $a_{\max} = 0.33g$.
- 11.5** Compute the yield acceleration for the concrete gravity wall shown below.

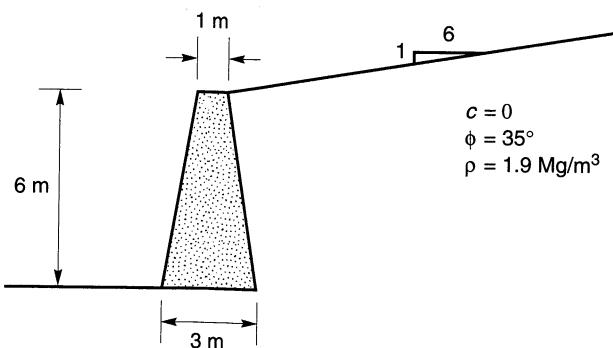


Figure P11.5

- 11.6** Using the Richards–Elms procedure, estimate the permanent displacement of the wall of Problem 11.5 when subjected to (a) the Gilroy No. 1 (rock) ground motion, and (b) the Gilroy No. 2 (soil) ground motion.
- 11.7** Using the Whitman–Liao procedure, estimate the permanent displacement of the wall of Problem 11.5 when subjected to (a) the Gilroy No. 1 (rock) ground motion, and (b) the Gilroy No. 2 (soil) ground motion.
- 11.8** Estimate the permanent displacement of the wall in Problem 11.5 that would have a 10% probability of exceedance if subjected to the Gilroy No. 2 (soil) motion.
- 11.9** A 15 ft tall gravity wall is to retain a level sand backfill ($c = 0$, $\phi = 35^\circ$, $\gamma = 115 \text{ pcf}$). The wall will be placed on a layer of dense sandy gravel ($c = 0$, $\phi = 44^\circ$, $\gamma = 140 \text{ pcf}$). Determine the wall weight that would be required to limit the permanent displacement of the wall to 1/4-inch if subjected to the Gilroy No. 2 (soil) ground motion.
- 11.10** The anchored bulkhead shown below is located in a seismically active area. Neglecting the effect of vertical motions, estimate the minimum peak acceleration levels that would be likely to produce (a) moderate damage, and (b) severe damage.

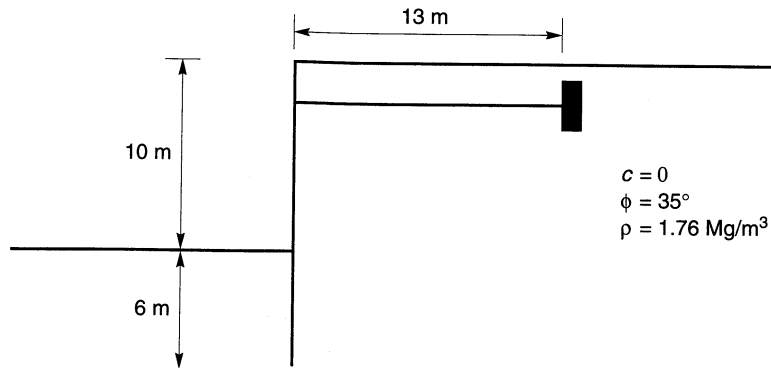


Figure P11.10

12

Soil Improvement for Mitigation of Seismic Hazards

12.1 INTRODUCTION

Soils have been modified to improve their engineering properties for hundreds of years. In the past 75 years, however, improved knowledge of soil behavior and geotechnical hazards has led to the development and verification of many innovative soil improvement techniques. Increased recognition of seismic hazards and improved understanding of the factors that control them have led these techniques to be applied to the mitigation of seismic hazards in the past 30 years.

In both seismically active and inactive areas, soil improvement techniques are commonly used at sites where the existing soil conditions are expected to lead to unsatisfactory performance. Unsatisfactory performance can take many forms, but usually involves unacceptably large soil movements. The movements may include horizontal or vertical (or both) components and may take place during and/or after earthquake shaking. In the absence of earthquake shaking, unacceptable movements usually result from insufficient soil strength and/or stiffness. Consequently, most soil improvement techniques were developed to increase the strength and stiffness of soil deposits. These techniques are described in detail in a number of useful references (e.g., Welsh, 1987; Van Impe, 1989; Hausmann, 1990;

Broms, 1991; Bell, 1993; Mosely, 1993); those which are not commonly used for mitigation of *seismic* hazards are not discussed in this chapter.

During earthquakes, other factors can contribute to unacceptable performance. In particular, the buildup of excess porewater pressure can lead to very large deformations. Consequently, commonly used techniques for mitigation of seismic hazards often involve reducing the tendency of the soil to generate positive excess porewater pressure during earthquake shaking as well as increasing the strength and stiffness of the soil.

The topic of soil improvement is somewhat different from topics presented in earlier chapters. Advances in soil improvement technology have generally resulted from the initiative and imagination of contractors. Research and explanatory "theories" have followed, rather than led, implementation; for some widely used techniques, proven theories have yet to be developed. In such cases, indirect or empirical evidence must be relied upon and the study of case histories is particularly important. This chapter does not attempt to describe all available soil improvement techniques in detail; instead, it presents an introduction to the soil improvement techniques that are most commonly used for mitigation of seismic hazards. References to more complete descriptions of the techniques are presented. Because soil improvement technology changes rapidly as new techniques are developed and existing techniques are tested by actual earthquakes, the relevant geotechnical engineering literature should be reviewed on a regular basis. Methods for verification of the effectiveness of soil improvement techniques are also described.

At present, a wide variety of soil improvement techniques are available for mitigation of seismic hazards. The costs of these methods vary widely, and the conditions under which they can be used are influenced by the nature and proximity of structures and constructed facilities. On the basis of the mechanisms by which they improve the engineering properties of the soil, the most common of these can be divided into four major categories: densification techniques, reinforcement techniques, grouting/mixing techniques, and drainage techniques. However, not all soil improvement techniques fall neatly into a single category.

12.2 DENSIFICATION TECHNIQUES

The particles that comprise a particular soil can be arranged in many different ways. However, the strength and stiffness of the soil is higher when the particles are packed in a dense configuration than when they are packed loosely. Also, the tendency to generate positive excess porewater pressure due to cyclic loading is lower when the soil is dense than when it is loose. As a result, *densification* is one of the most effective and commonly used means of improving soil characteristics for mitigation of seismic hazards. At the same time, it should be recognized that the increased stiffness of a densified soil deposit will cause it to respond differently to earthquake motion; displacement amplitudes are likely to decrease, but accelerations may be somewhat greater than they would have been had the soil not been improved.

Densification produces permanent volume changes that often result in settlement of the ground surface. Different densification techniques produce different amounts of

settlement; with some techniques additional soil is placed at or beneath the ground surface during the process of densification in order to minimize the settlement. Despite such efforts, some densification techniques are limited to sites without existing structures or facilities that could be damaged by ground settlement.

The most common approaches to densification include vibro techniques, dynamic compaction, blasting, and compaction grouting. Of these techniques, the first three make use of the tendency of granular soils to densify when subjected to vibrations. As such, their effectiveness is greatest for cohesionless soils such as clean sands and gravels. Just as fines tend to inhibit liquefaction during earthquakes, they tend to inhibit densification by vibration.

12.2.1 Vibro Techniques

Vibro techniques use probes that are vibrated through a soil deposit in a grid pattern to densify the soil over the entire thickness of the deposit. Vibro techniques can be divided into those based on horizontal vibration (*vibroflotation*) and those based on vertical vibration (*vibro rod systems*). Vibro techniques are among the most commonly used techniques for mitigation of seismic hazards.

12.2.1.1 Vibroflotation

In vibroflotation, a torpedolike probe (the *vibroflot*) suspended by a crane is used to densify a soil deposit. Vibroflots, usually 12 to 18 in. (30 to 46 cm) in diameter and about 10 to 16 ft (3.0 to 4.9 m) long, contain weights mounted eccentrically on a central shaft driven by electric or hydraulic power (Figure 12.1).

The vibroflot is initially lowered to the bottom of the deposit by a combination of vibration and water or air jetting through ports in its pointed nose cone. The vibroflot is then incrementally withdrawn in 2 to 3 ft (60 to 90 cm) intervals at an overall rate of about 1 ft/min (30 cm/min) while still vibrating. Water may be jetted through ports in the upper part of the vibroflot to loosen the soil above the vibroflot temporarily and aid in its withdrawal. The vibrations produce a localized zone of temporary liquefaction that causes the soil surrounding the vibroflot to densify. A conical depression usually forms at the ground surface above the probe. This depression can be filled with granular material (such as clean sand or gravel) as the vibroflot is withdrawn. Alternatively, vibroflots with bottom-feed systems can introduce granular material through the tip of the vibroflot. As the vibroflot is removed, it leaves behind a densified column of soil. When gravel or crushed stone is introduced into the soil, the resulting *stone column* provides benefits of reinforcement and drainage in addition to densification. The use of bottom-feed systems has increased rapidly in recent years. Air delivery systems have become quite common and tend to be preferred over water delivery systems at congested sites and in environmentally sensitive areas.

Vibroflotation is most effective in clean granular soils with fines contents less than 20% and clay contents below 3%. In such soils it typically produces high densities (relative densities of about 100%) within 12 to 18 in. (30 to 46 cm) of the vibroflot and lower densities at greater radial distances. To densify an entire site, vibroflotation is performed in a grid pattern with a spacing that depends on the soil conditions and the power of the vibroflot; spacings of 6 to 10 ft (2 to 3 m) are common. Vibroflotation has been used successfully

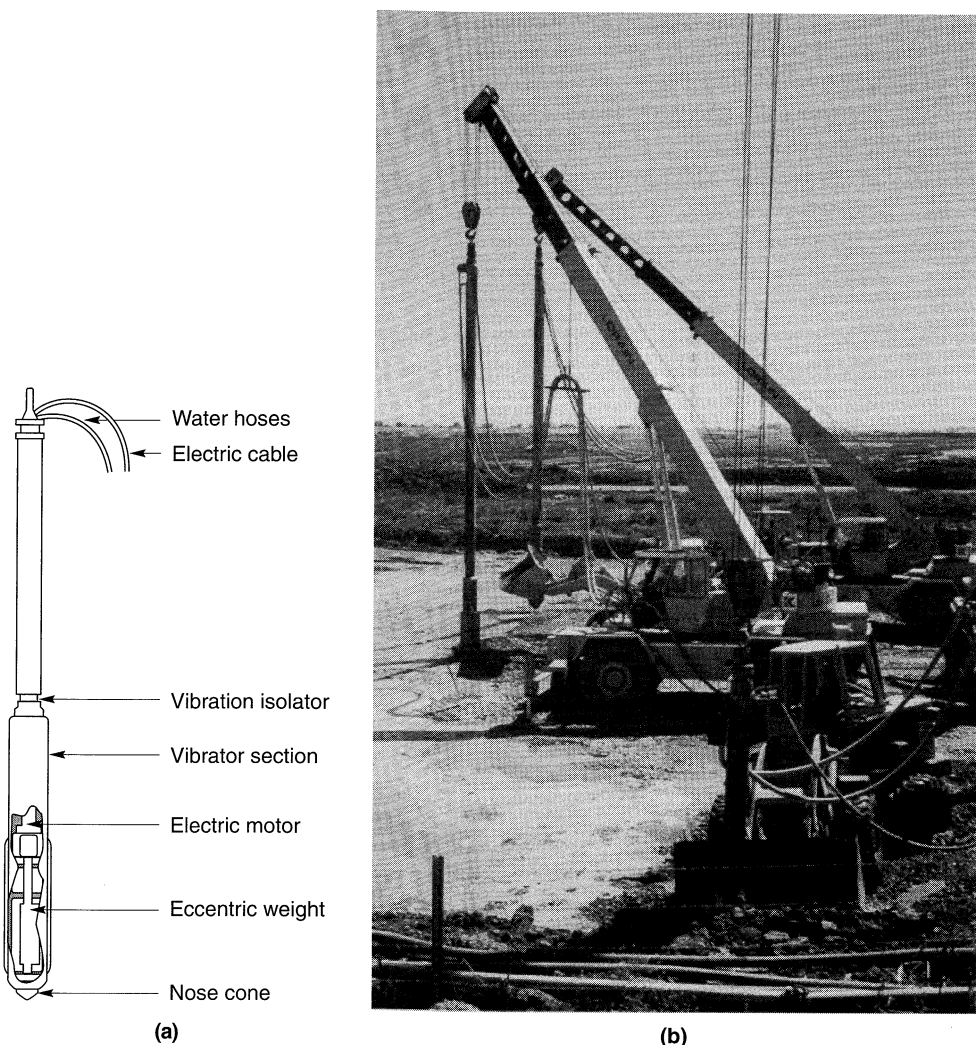


Figure 12.1 (a) Schematic illustration of a typical vibroflot (after Bell, 1993), and (b) vibroflots densifying liquefiable soils at a wastewater treatment facility in California (photo courtesy of Hayward Baker).

to densify soils to depths of up to 115 ft (35 m). Case histories of vibroflotation have been reported by Harder et al. (1984) and Dobson (1987).

12.2.1.2 Vibro Rod

Vibro rod systems use a vibratory pile driving hammer to vibrate a long probe into the soil. The probe is then withdrawn while still being vibrated to densify the soil. To minimize densification-induced settlement, additional soil may be introduced at the ground surface or

at depth. Several types of probes have been used in vibrocompaction. In the *Terraprobe* system, a 30-in. (76-cm) open-ended steel pipe is vibrated into the ground; the vibrations densify the soil both inside and outside the pipe. The *Vibro-Wing* consists of a central rod with diametrically opposed 31-in. (80-cm) "wings" spaced 19 in. (50 cm) apart along the length of the rod (Figure 12.2). The *Franki Y-probe* consists of three 19-in. (50-cm)-wide steel plates welded to a central rod at 120° angles from each other. Horizontal cross-ribs may be welded to the faces of the steel plates to facilitate densification. By adjusting the frequency of vibration, these probes can be "tuned" to the resonant frequency of the soil-probe system to increase vibration amplitudes and densify the soil more efficiently (Massarch, 1991).

Vibro rod systems are most effective in soils similar to those for which vibroflotation is most effective. Because vibro rods use vertical vibrations, their radius of influence is usually smaller than that observed for vibroflotation. As a result, the grid spacing for soil improvement by vibro rods is generally smaller than for vibroflotation. The effectiveness of vibro rods also appears to vary with depth (Janes, 1973). Case histories of vibro rod systems have been reported by Massarch (1991), Neely and Leroy (1991), and Senneset and Nestvold (1992).

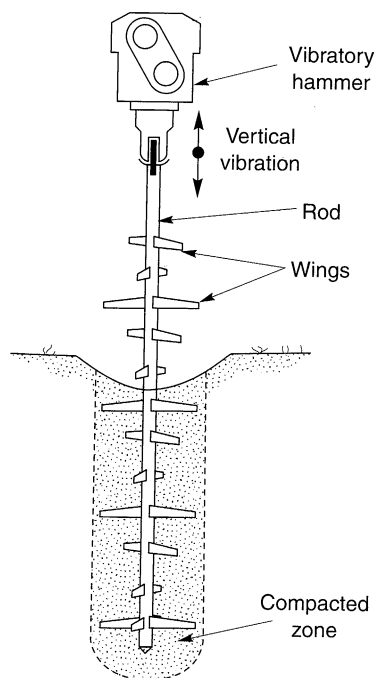


Figure 12.2 Vibro-wing system. Each pair of wings is oriented at a 120° angle to those located immediately above and below. After Broms (1991).

12.2.2 Dynamic Compaction

Dynamic compaction is performed by repeatedly dropping a heavy weight in a grid pattern on the ground surface (Figure 12.3). The weights, usually constructed of steel plates and/or reinforced concrete, generally range from 6 to 30 tons (53 to 267 kN), although weights of up to 170 tons (1500 kN) have been used. Drop heights usually range from about 35 to 100



Figure 12.3 Aerial view of site undergoing soil improvement by dynamic compaction. The grid pattern on which the dynamic compaction weight is dropped, and the need for subsequent regrading and surface compaction, are evident from this photograph. (Photo courtesy of Hayward Baker).

ft (10 to 30 m), although weights have been dropped from up to 130 ft (40 m). The weights are usually dropped three to eight times before moving to the next point on the grid. A detailed description of dynamic compaction was prepared by Lukas (1986).

At a particular site, dynamic compaction is generally performed in several stages, or passes. Empirical evidence suggests that the effective depth of influence (the depth to which significant improvement can be detected) increases with impact energy and that the greatest degree of improvement is usually observed at about half the effective depth of influence (Mayne et al., 1984). To avoid developing a shallow zone of dense soil that could inhibit the transmission of energy to greater depths, the deepest soil is densified first with a series of high-energy (heavy weight and/or high drop height) drops on a widely spaced grid. After the craters produced by the first pass have been filled (preferably with well-graded granular soil), soils at intermediate depth are then compacted using a greater number of drops from a smaller height at closer spacing (often half the spacing of the original grid). Finally, the

near-surface soils are compacted by dropping relatively light weights on a virtually continuous pattern to smooth or “iron” the ground surface. Additional smoothing by conventional surface grading and compaction equipment is usually required.

The kinetic energy of the weight at impact produces stress waves that travel through the soil. The total energy delivered to the soil is a function of the weight, drop height, grid spacing, and number of drops per grid point. When the groundwater table is near the surface, placement of a gravel or sand blanket may be required prior to compaction. Although dynamic compaction has been used successfully for cohesive soils, its most common use for mitigation of seismic hazards is for potentially liquefiable soils. At each grid point, a series of drops causes the porewater pressure to increase so that the soil particles can more easily move into a denser configuration. Dissipation of the excess porewater pressure results in further densification within a short period (1 to 2 days for sand and gravels; 1 to 2 weeks for sandy silts) after treatment.

Dynamic compaction is generally effective to depths of 30 to 40 ft (9 to 12 m), although extremely high impact energies may produce densification at greater depths. Because the process is rather intrusive—it can produce considerable noise, dust, flying debris, and vibration—it is rarely used near occupied or vibration-sensitive structures. Case histories of dynamic compaction of potentially liquefiable soil have been described by Hussin and Ali (1987), Keller et al. (1987), Koutsoftas and Kiefer (1990), Mitchell and Wentz (1991), and others.

12.2.3 Blasting

Loose granular soils have also been compacted by *blasting*. Blasting densification involves the detonation of multiple explosive charges vertically spaced 10 to 20 ft (3 to 6 m) apart in drilled or jetted boreholes. The boreholes are usually spaced between 15 to 50 ft (5 to 15 m) apart and backfilled prior to detonation. To increase the efficiency of the densification process, the charges at different elevations may be detonated at small time delays. Immediately after detonation, the ground surface rises and gas and water are expelled from fractures (Figure 12.4). The ground surface then settles as the excess gas and water pressure dissipates. Although the efficiency of densification decreases with each round of blasting, two or three rounds (with later rounds detonated at locations between those of the earlier rounds) are often used to achieve the desired degree of densification.

Blasting is most effective in loose sands that contain less than 20% silt and less than 5% clay. Even small amounts of clay, or small clay seams, can substantially reduce the effectiveness of blasting. Blasting can be effective in dry soils, but the effects of capillary tension and gas bubbles in partially saturated soils virtually negates its effectiveness. As a result, blasting is most commonly used to densify completely saturated soils. In such soils the shock wave produced by the charges produces localized, temporary liquefaction which allows the soil grains to move into a more dense configuration.

Although blasting is quite economical, its use is limited by several practical considerations. It produces strong vibrations that may damage nearby structures or produce significant ground movements. It requires the use of potentially hazardous explosives for which strict regulations on handling and storage usually apply. Finally, its effectiveness is difficult to predict in advance. Case histories of the use of blasting to mitigate seismic



Figure 12.4 Ground surface shortly after detonation of explosives during blast densification of loose soil beneath an abutment prior to construction of Coldwater Creek bridge near Mt. St. Helens in Washington state. (Photo by A. P. Kilian; used with permission).

hazards have been described by Klohn et al. (1981), Solymar and Reed (1986), LaFosse and von Rosenvinge (1992), and Hachey et al. (1994).

12.2.4 Compaction Grouting

Soft or weak soils can be densified by injecting a very low slump [generally less than 1 in. (2.5 cm)] grout into the soil under high pressure, a process known as *compaction grouting*. Because the grout is highly viscous, it forms an intact bulb or column that densifies the surrounding soil by displacement (Figure 12.5). Compaction grouting may be performed at a series of points in a grid or along a line. Grout point spacings ranging from 3 to 15 ft (1 to 4.6 m) have been used. Because higher overburden pressures allow the use of higher grout pressures, larger spacings are generally used when treating deeper soils. At shallow depths, compaction grouting may be used to lift settled slabs or structures; indeed, remediation of foundation settlement is probably the most common application of compaction grouting.

Compaction grouting may be performed from the top down (*downstage grouting*) or from the bottom up (*upstage grouting*). Upstage grouting is less expensive and more commonly used than downstage grouting. However, the downstage procedure is preferred (Stilley, 1982; Bell, 1993) for underpinning of structures or for sites where loose soils

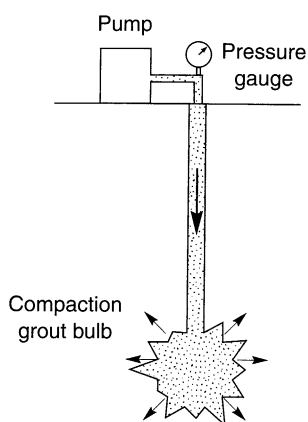


Figure 12.5 Compaction grouting. Low-slump grout is pumped under high pressure to form a bulb that displaces and densifies the surrounding soils. By raising the grout tube while pumping, a column of grout can be created in the soil. (After Hausmann, 1990.)

extend to the ground surface. By working from the top down, placement of an upper grout bulb reduces the possibility of subsequent grout escaping at the surface and grout heave, and also provides additional strength and confinement that allows the use of higher grouting pressures at greater depths.

Because it does not rely on vibration, compaction grouting can be used in all soil types. It is most commonly used in sands and nonplastic silts. Compaction grouting can be used to virtually any depth and can easily be used within a given range of depths. The size and shape of the grout bulb or column is influenced by the stiffness and strength of the soil and also by the rate and pressure at which the grout is injected. An important feature of compaction grouting is that its greatest effects occur where the soil is softest and weakest. Compaction grout masses with diameters greater than 3 ft (1 m) are not uncommon (Warner, 1982). Compaction grouting has been used to depths of 100 ft (30 m). Case histories of compaction grouting have been described by Salley et al. (1987), Warner (1982), Graf (1992), and Baez and Henry (1993).

12.2.5 Areal Extent of Densification

An important consideration in the densification of soils for construction of individual structures and foundations is the areal extent of soil improvement required for satisfactory performance during earthquakes. The areal extent should be evaluated on a case-by-case basis since site-specific soil conditions, performance requirements, and failure consequences must be addressed.

The required areal extent of improvement depends on the mechanism of failure that the improvement is intended to eliminate. For potential stability failures, the areal extent of improvement will depend on the degree of improvement that can be achieved and on the extent of the potential failure surface(s). By estimating the residual strength of the soil after improvement, stability analyses can be used to estimate the extent of improvement that will produce an acceptable level of stability. To minimize postearthquake settlement of a structure or foundation on loose, saturated sand, densification is usually performed within a zone defined by a 30 to 45° line from the edge of the structure, as illustrated in Figure 12.6. Available research and field experience indicates that this approach is likely to produce a satisfactory extent of improvement (Iai et al., 1988).

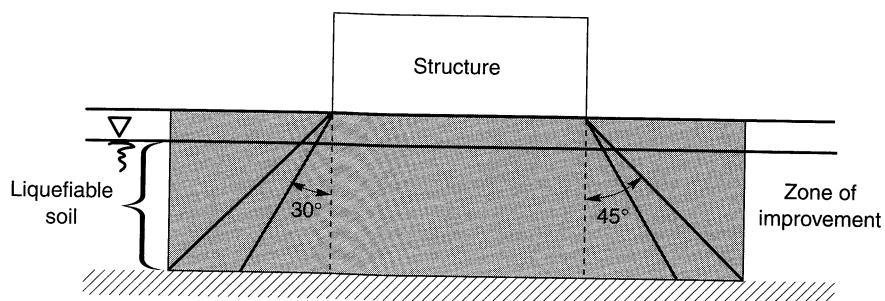


Figure 12.6 Typical areal extent of improvement for densification of potentially liquefiable soil beneath a structure.

12.3 REINFORCEMENT TECHNIQUES

In some cases it is possible to improve the strength and stiffness of an existing soil deposit by installing discrete inclusions that reinforce the soil. These inclusions may consist of structural materials, such as steel, concrete, or timber, and geomaterials such as densified gravel. Reinforcement of new engineered fills using geosynthetic or metallic reinforcement is beyond the scope of this chapter.

12.3.1 Stone Columns

Soil deposits can be improved by the installation of dense columns of gravel known as *stone columns*. Stone columns may be used in both fine- and coarse-grained soils. In fine-grained soils, stone columns are usually used to increase shear strength beneath structures and embankments by accelerating consolidation (by allowing radial drainage) and introducing columns of stronger material. For mitigation of seismic hazards, they are commonly used for improvement of liquefiable soil deposits.

Stone columns can be installed in a variety of ways. As discussed previously, stone columns may be constructed by introducing gravel during the process of vibroflotation (Brown, 1977). Several other methods of installation are also available. In the *Franki method*, a steel casing initially closed at the bottom by a gravel plug is driven to the desired depth by an internal hammer (Figure 12.7). At that depth, part of the plug is driven beyond the bottom of the casing to form a bulb of gravel. Additional gravel is then added and compacted as the casing is withdrawn. The diameter of the resulting stone column depends on the stiffness and compressibility of the surrounding soil; in loose sand, a 0.5- to 0.7-m (19 to 28 in.) casing will typically produce a 0.8-m (31 in.) diameter column. Casings with trap doors at the bottom have also been used to install stone columns (Solymar and Reed, 1986). The trap door allows the casing to be driven as a closed-end pile but also allows gravel to be placed during withdrawal of the casing. The gravel can be densified by pausing to redrive the casing at various intervals during the withdrawal process.

Stone columns combine at least four different mechanisms for improvement of liquefiable soil deposits. First, they improve the deposit by virtue of their own high density, strength, and stiffness—in this sense they reinforce the soil deposit. Second, they provide closely spaced drainage boundaries that inhibit the development of high excess porewater

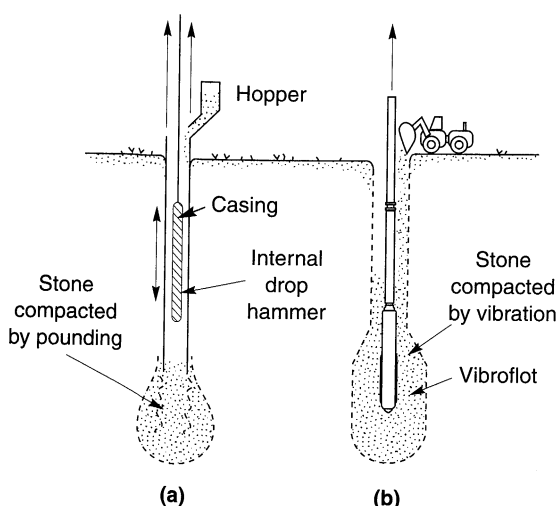


Figure 12.7 Methods of stone column installation: (a) Franki method; (b) by vibroflotation. (After Broms, 1991.)

pressures (Section 12.6). Third, the processes by which they are installed densify the surrounding soil by the combined effects of vibration and displacement. Finally, the installation process increases the lateral stresses in the soil surrounding the stone columns. These multiple benefits have made the use of stone columns very popular. Case histories of seismic hazard mitigation by stone columns have been presented by Priebe (1991), Hayden and Welch (1991), and Mitchell and Wentz, (1991).

12.3.2 Compaction Piles

Granular soils can be improved by the installation of *compaction piles*. Compaction piles are displacement piles, usually prestressed concrete or timber, that are driven into a loose sand or gravel deposit in a grid pattern (Figure 12.8) and left there. Compaction piles improve the seismic performance of a soil deposit by three different mechanisms. First, the flexural strength of the piles themselves provides resistance to soil movement (reinforcement). Second, the vibrations and displacements produced by their installation cause densification. Finally, the installation process increases the lateral stresses in the soil surrounding the piles.

Compaction piles generally densify the soil within a distance of 7 to 12 pile diameters (Robinsky and Morrison, 1964; Kishida, 1967), and consequently, are usually installed in a grid pattern. Between compaction piles, relative densities of up to 75 to 80% are usually achieved (Solymar and Reed, 1986). Improvement can be obtained with reasonable economy to depths of about 60 ft. Case histories describing the use of compaction piles have been presented by Lindqvist and Petaja (1981), Marcuson et al. (1991), Mitchell and Wentz (1991), and Kramer and Holtz (1991).

12.3.3 Drilled Inclusions

Structural reinforcing elements can also be installed in the ground by drilling or augering. Drilled shafts, sometimes with very large diameters, have been used to stabilize many slopes. Such shafts may be installed closely enough to form tangent or secant pile walls. Soil



Figure 12.8 Compaction piles driven into the upstream embankment of Sardis Dam to reduce liquefaction hazards. The contractor drove the piles to this level with a barge-mounted conventional hammer; the piles were later driven below the water surface with a different hammer. (Photo by T. D. Stark; used with permission.)

nails, tiebacks, micropiles, and root piles have also been used. The installation of such drilled inclusions can be quite difficult, however, in the loose granular soils that contribute to many seismic hazards. Although soil nailed walls performed well in the 1989 Loma Prieta earthquake (Felio et al., 1990), there is currently no consensus on their design for seismic loading.

12.4 GROUTING AND MIXING TECHNIQUES

The engineering characteristics of many soil deposits can be improved by injecting or mixing cementitious materials into the soil. These materials both strengthen the contacts between soil grains and fill the void space between the grains. *Grouting* techniques involve the injection of such materials into the voids of the soil or into fractures in the soil so that the particle structure of the majority of the soil remains intact. *Mixing* techniques introduce cementitious materials by physically mixing them with the soil, completely disturbing the particle structure of the soil. The mixing can be accomplished mechanically or hydraulically. Grouting and mixing techniques tend to be expensive but can often be accomplished with minimal settlement or vibration. As a result, grouting and mixing techniques can often be used in situations where other soil improvement techniques cannot.

12.4.1 Grouting

The term *grouting* is used to describe a variety of processes by which cementitious material is introduced into the ground. Grouting techniques are often classified according to the method by which the grout is placed in the ground (Hausmann, 1990). In this chapter, however, soil improvement techniques are classified according to the primary mechanisms by which they produce improvement. As a result, compaction grouting is described with other densification techniques in Section 12.3, and jet grouting is considered as a mixing technique in the following section. With this convention, there are two primary types of grouting techniques.

12.4.1.1 Permeation Grouting

Permeation grouting involves the injection of low-viscosity liquid grout into the voids of the soil without disturbing the soil structure (Figure 12.9). *Particulate grouts* (i.e., aqueous suspensions of cement, fly ash, bentonite, microfine cement, or some combination thereof) or *chemical grouts* (e.g., silica and lignin gels, or phenolic and acrylic resins) may be used.

The suitability of different types of grouts for different soil conditions is most strongly influenced by the grain size of the soil. Virtually any type of grout, even relatively viscous cement grouts, can be used in soil with large voids such as gravels and coarse sands. Chemical grouts generally exhibit lower viscosity than particulate grouts (although the viscosity of microfine cements grouts may be as low as some chemical grouts) and can therefore be used in fine sands. The presence of fines can significantly reduce the effectiveness of permeation grouting.

Grout pipes are typically installed in a grid pattern at spacings of 4 to 8 ft (1.2 to 2.4 m) (Hayden, 1994). The grout may be injected in different ways. In *stage grouting*, a boring is advanced a short distance before grout is injected through the end of the drill rod. After the grout sets up, the boring is advanced another short distance and grouted again. This process continues until grout has been placed to the desired depth. In the *tube-à-manchette* approach, a grout tube with injection ports every 12 to 24 in. (30 to 61 cm) along its length is installed in a borehole. Rubber sleeves (manchettes) that serve as one-way valves cover the injection ports on the outer surface of the grout tube and internal packer systems are used to control the depths at which grout is injected.

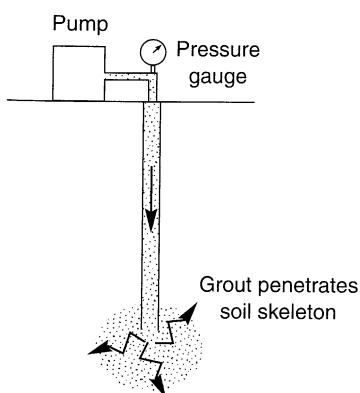


Figure 12.9 Permeation grouting. (After Hausmann, 1990).

Permeation grouting produces soil improvement by two primary mechanisms. First the grout tends to strengthen the contacts between individual soil grains, thereby producing a soil skeleton that is stronger and stiffer than that of the ungrouted soil. Second, the grout takes up space in the voids between soil particles, reducing the tendency for densification (or excess pore pressure generation) upon cyclic loading. Soils improved by permeation grouting can have shear strengths of 50 to 300 psi (345 to 2070 kPa). Case histories in which permeation grouting was used to mitigate seismic hazards were described by Zacher and Graf (1979), Graf (1992), and Bruce (1992).

12.4.1.2 Intrusion Grouting

In the process of *intrusion grouting*, fluid grout is injected under pressure to cause controlled fracturing of the soil (Figure 12.10). Because the grout is not intended to flow through the small voids between soil particles, relatively viscous (and strong) cement grouts can be used. In theory, the first fractures should be parallel to the minor principal stress planes, but observations show that they usually follow weak bedding planes. After allowing the initially placed grout to cure, repeated intrusion grouting fractures the soil along different planes. Eventually, a three-dimensional network of intersecting grout lenses can be formed. Some densification of the soil may occur, but the primary mechanism of improvement results from the increased stiffness and strength of the soil mass due to the hardened lenses of grout.

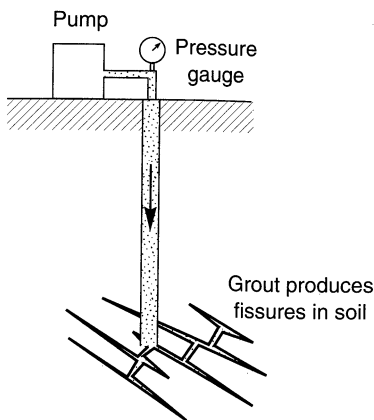


Figure 12.10 Intrusion grouting process.
(After Hausmann, 1990).

12.4.2 Mixing

Localized improvement of soil columns can be achieved by *in situ* mixing of the soil with cementitious material. Because the cementitious material is physically mixed with the soil, it need not have an extremely low viscosity—strong, cement slurries are commonly used. For mitigation of seismic hazards, this approach is most commonly accomplished by *soil mixing* and *jet grouting*.

12.4.2.1 Soil Mixing

The term *soil mixing* describes a specific technique in which cementitious material is mechanically mixed into the soil using a hollow stem auger and paddle arrangement (Figure 12.11). Soil mixing rigs may have single augers (0.5 to 4 m (1.6 to 13 ft) in diameter) or

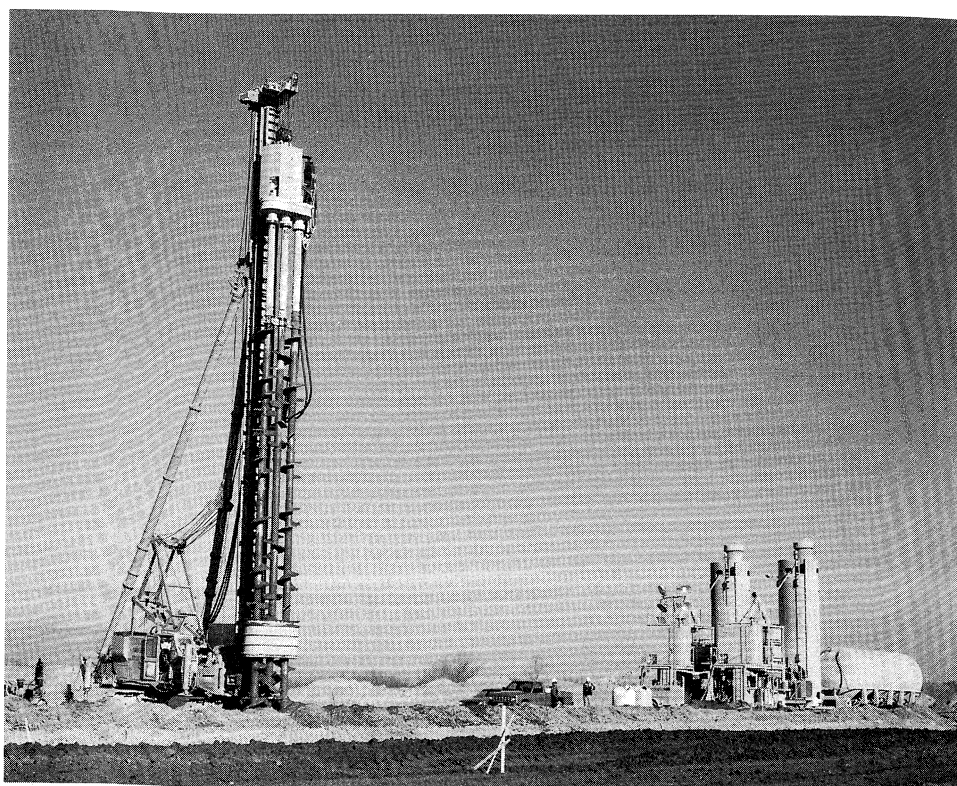


Figure 12.11 Triple auger soil mixing rig improving liquefiable soils at Jackson Lake Dam in Wyoming. Grout batch plant is at right (photo courtesy of SMW Seiko, Inc.)

gangs of two to eight augers (usually about 1 m (3.1 ft) in diameter). As the mixing augers are advanced into the soil, grout is pumped through their stems and injected into the soil at their tips. The grout is thoroughly mixed with the soil by the auger flights and mixing paddles. After the design depth has been reached, the augers are withdrawn while the mixing process continues. The soil mixing process leaves behind a uniform (constant width) column of soil–cement. By overlapping the columns before the grout cures, walls and cellular structures can be constructed below the ground surface.

Soil mixing can be used in virtually any type of inorganic soil. It has been used to depths of over 20 m (66 ft) in the United States and up to 60 m (200 ft) in Japan. The strength of the soil–cement mixture depends on the type of grout, type of soil, and degree of mixing; strengths of 200 psi (1380 kPa) or more are commonly achieved. Case histories involving the use of soil mixing for mitigation of seismic hazards have been presented by Ryan and Jasperse (1989), Babasaki et al. (1991), and Taki and Yang (1991).

12.4.2.2 Jet Grouting

In *jet grouting*, the soil is mixed with cement grout injected horizontally under high pressure in a previously drilled borehole (Figure 12.12). The injection nozzle is rotated to

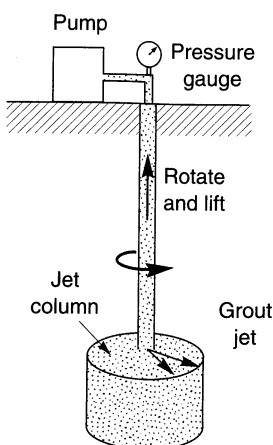


Figure 12.12 Jet grouting process. (After Hausmann, 1990).

allow the grout to be placed in all directions. Air or air and water may also be injected to aid in the mixing process. Jet grouting begins at the bottom of the borehole and proceeds to the top, leaving behind a relatively uniform column of mixed soil–cement. By overlapping the columns before the grout cures, walls and cellular structures can be constructed below the ground surface.

The diameter of a jet grouted column depends on the soil condition and the manner in which the jet grouting is performed. Column diameters are generally greater in coarse-grained soils than in fine-grained soils. By varying the air, water, and grout pressures and the rates of rotation and lifting of the grout tubes, a jet grouting operator can control the effective dimensions of the column. Diameters ranging from 0.4 to 0.5 m (16 to 20 in.) in clayey silt to 0.9 to 1.0 m (36 to 39 in.) in sandy gravel can be expected using a single-jet (grout only) system (Bell, 1993). Diameters of 0.8 to 1.0 m (31 to 39 in.) in clayey silt and 2.0 to 2.4 m (6.5 to 7.9 ft) in sandy gravel can be expected with a triple-jet (air, water, and grout) system. Jet grouting can be performed in any type of inorganic soil to depths limited only by the range of the drilling equipment. Case histories of the use of jet grouting for mitigation of seismic hazards have been presented by Hayden (1994).

12.5 DRAINAGE TECHNIQUES

Unacceptable movements of slopes, embankments, retaining structures, and foundations can frequently be eliminated by lowering the groundwater table prior to earthquake shaking. A number of dewatering techniques have been developed and proven useful in engineering practice. Procedures for the design of dewatering systems are well established and widely used (e.g., Cedergren, 1989; Powers, 1992). These standard techniques may be used to increase the stiffness and strength of a soil deposit for mitigation of seismic as well as nonseismic hazards.

The buildup of excess porewater pressure during earthquake shaking can be suppressed using drainage techniques, although drainage alone is rarely relied upon for the mitigation of liquefaction hazards. The installation of stone columns, for example, introduces

columns of freely draining gravel into a liquefiable soil deposit (though mixing of the gravel and the native soil during installation may reduce the permeability of the stone column). Earthquake-induced excess pore pressures may be rapidly dissipated by horizontal flow of porewater into the stone columns. The rate of pore pressure dissipation depends on the diameter and spacing of the stone columns and on the permeability and compressibility of the surrounding soil. Seed and Booker (1976, 1977) developed procedures for selecting the sizes and spacings of gravel drains (or stone columns) for mitigation of liquefaction hazards. The use of gravel drains for suppression of excess porewater pressure requires careful attention to drain permeability and filtration behavior of the drain–soil boundary. Even though drainage techniques can mitigate liquefaction hazards by suppressing excess porewater pressure buildup, postearthquake settlement may still occur. Case histories of the use of drainage techniques for mitigation of seismic hazards have been described by Ishihara et al. (1980), Aboshi et al. (1991), and Iai et al. (1994).

12.6 VERIFICATION OF SOIL IMPROVEMENT

All attempts at soil improvement should be checked to confirm that the desired improvement has taken place. The most direct way of verifying the effectiveness of a particular soil improvement technique is to measure the soil characteristic that was considered deficient both before and after improvement. For example, if the improvement was undertaken to increase the strength of the soil, measurement of the strength before and after improvement would provide the most direct verification of the effectiveness of the improvement process. However, it is not always feasible to measure the deficient characteristic directly. In such cases, verification is usually accomplished using related characteristics that are more easily measured.

Verification may be based on the results of laboratory or field tests. While laboratory tests have historically been commonly used for verification of soil improvement, recent advances in field testing techniques have provided additional means for verification. Field testing techniques may be divided into in situ testing techniques and geophysical testing techniques. Common verification techniques were summarized by Ledbetter (1985).

12.6.1 Laboratory Testing Techniques

Laboratory testing techniques have a number of advantages over other methods for verification of soil improvement, but they also suffer from drawbacks that can significantly limit their usefulness for certain types of soil improvement. The requirement of obtaining a sample of the improved soil leads directly to many of the advantages of using laboratory testing techniques and also to many of the disadvantages. Obtaining a sample of improved soil allows visual inspection of the effects of improvement. For many improvement techniques (e.g., permeation grouting, soil mixing, etc.), the ability to inspect the treated soil provides direct and valuable evidence of the effectiveness of the treatment. Laboratory tests allow greater control and more accurate measurement of stress, strain, and environmental conditions than are possible in field tests. In some cases this flexibility may allow more accurate characterization of the properties of the improved soil.

On the other hand, laboratory tests only provide verification at discrete points. When soil improvement is used to improve or eliminate localized zones or seams of weakness, verification by methods that require discrete sampling may be ineffective. Laboratory tests may also be influenced by the inevitable effects of sample disturbance, a problem that is particularly significant in the improvement of liquefiable soils. The density changes produced by even thin-walled samplers (Marcuson et al., 1977; Seko and Tobe, 1977; Singh et al., 1979) can lead to considerable uncertainty in the evaluation of improvement effectiveness.

12.6.2 In Situ Testing Techniques

Many of the limitations of laboratory testing based approaches to the verification of soil improvement effectiveness may be overcome by the use of in situ tests. Indeed, the use of in situ tests for verification of soil improvement effectiveness has increased dramatically in the past 15 to 20 years. Because many geotechnical seismic hazards are evaluated using in situ test parameters, those parameters can provide direct evidence of hazard mitigation. Indeed, soil improvement specifications may be written to require that a certain parameter value (e.g., a minimum SPT resistance) be achieved after improvement. Mitchell (1986) and Welsh (1986) described the use of in situ tests for verification of soil improvement effectiveness.

The SPT, CPT, PMT, and DMT (Section 6.3.1.2) can all be used for verification of soil improvement effectiveness. The SPT and CPT tests are performed relatively quickly and inexpensively compared to sampling and laboratory testing. The CPT is particularly useful because it provides a continuous record with depth. The PMT is more expensive, but it also allows measurement of lateral stresses and direct measurement of strength. For gravelly soils, the Becker hammer penetration test (Section 6.3.1.2) may be used for verification purposes.

Interpretation of soil improvement effectiveness from in situ test results must be performed carefully. The penetration resistance of granular soils, for example, is influenced not only by density and overburden stress, but also by lateral stress. Soil improvement techniques that result in increased lateral stress may produce unconservative estimates of the density of the improved soil if the postimprovement stress state is not carefully considered in the interpretation of penetration test results. Because time-dependent changes in strength, stiffness, and penetration resistance are often observed after densification (Mitchell and Solymar, 1984; Mitchell, 1986), in situ tests performed immediately after densification may not reflect the actual degree of improvement of the soil. Verification testing is usually performed at least 72 hours after densification has taken place. Many soil improvement techniques are applied at a grid of treatment points, and the degree of improvement usually decreases with distance from the treatment point. The relationship between the locations of in situ tests and the locations of treatment points should be considered in the interpretation of soil improvement effectiveness from in situ test results. In situ tests have limited effectiveness for verification of grouting effectiveness (Welsh, 1986).

12.6.3 Geophysical Testing Techniques

Many soil improvement techniques increase the stiffness of the treated soil. The effectiveness of these techniques can be verified using seismic geophysical techniques (Section 6.3.1.1). In most cases it is desirable to perform seismic tests both before and after improvement.

Cross-hole and downhole (including seismic cone) tests are most commonly used for verification of soil improvement. These techniques can measure p- or s-wave velocities over considerable distances, thereby providing spatially averaged stiffness measurements. However, each requires at least one borehole. For sites where soil improvement has been performed over a large area, seismic reflection and seismic refraction tests may be useful for verification purposes. SASW tests provide similar information without the need for boreholes. At sites where stiffness changes irregularly in two or three dimensions or sites that contain inclusions, the results of SASW tests may be very difficult to interpret. Such tests must also be performed when background noise (including that produced by on-going soil improvement work) will not adversely affect their results. Tests that measure average wave propagation velocities may not accurately reflect the degree of improvement of thin, loose zones unless the distance over which velocities are averaged is quite small.

12.7 OTHER CONSIDERATIONS

The application of soil improvement techniques to the mitigation of seismic hazards is relatively new. The theoretical underpinnings of many soil improvement techniques are poorly developed, and empirical observations of the performance of improved soil in actual earthquakes are rare. Because of these factors, it is particularly important to review the relevant geotechnical engineering literature before attempting to mitigate seismic hazards by soil improvement.

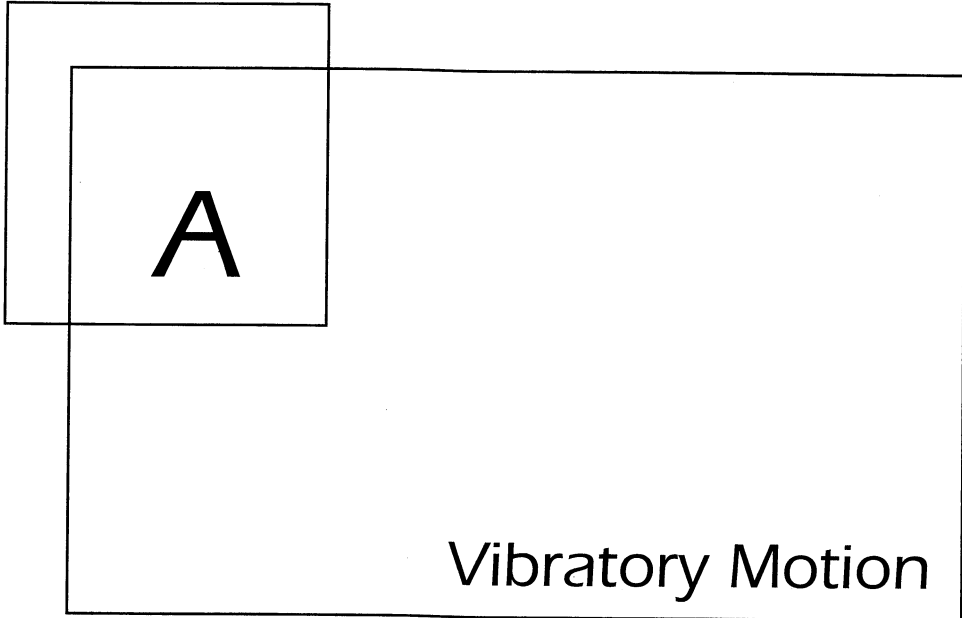
The effectiveness of many soil improvement techniques can be difficult to predict in advance for a particular site. Furthermore, the equipment, procedures, experience, and skill of the soil improvement contractor can strongly influence soil improvement effectiveness. For these reasons, it is frequently beneficial to construct *test sections* before beginning production work or even before final selection of a soil improvement technique. Test sections allow site- and procedure-specific evaluation of soil improvement effectiveness at a moderate cost; their use is advisable whenever possible.

12.8 SUMMARY

1. Unfavorable soil conditions can frequently be improved using soil improvement techniques. A variety of soil improvement techniques have been developed—some apply to long-term, static loading conditions and others also apply to seismic loading conditions.
2. The cost of different soil improvement techniques vary widely. Costs are influenced by the volume and extent of the soil to be treated, access to the site, site sensitivity to vibration and permanent ground movement, and other factors.
3. The presence of existing structures, pipelines, and other constructed facilities can eliminate many soil improvement techniques from consideration at a given site. The techniques that can be used at such sites tend to be among the more expensive.
4. Most soil improvement techniques are intended to increase the strength and stiffness of a soil deposit. Increased strength and stiffness is generally desirable for both static and seismic loading conditions.

5. Current soil improvement techniques can be divided into four broad categories: densification techniques, reinforcement techniques, grouting/mixing techniques, and drainage techniques. Not all techniques fall entirely within a single category; for example, stone columns can improve a soil deposit by densification, reinforcement, and drainage functions.
6. Several soil improvement techniques that are commonly used to mitigate seismic hazards are intended to reduce the tendency of loose, saturated granular soils to generate excess porewater pressure during earthquake shaking. These techniques typically involve densification of the soil.
7. Densification is probably the most commonly used soil improvement technique for mitigation of seismic hazards. Most densification techniques rely on the tendency of granular soils to densify when subjected to vibration. Densification can produce substantial settlement, although some procedures allow the introduction of new material to balance the volume change caused by densification.
8. Many densification techniques rely on vibrations that can be potentially damaging to structures, pipelines, and other constructed facilities. Such vibrations may also be too objectionable to people who live or work near sites that require improvement to allow their use.
9. Most vibratory techniques produce a temporary, localized zone of liquefaction in loose, saturated sand. Densification occurs as the sand particles are rearranged during reconsolidation. The presence of fines, particularly plastic fines, inhibits the development of high pore pressures and the rearrangement of soil particles. As a result, vibratory techniques may have limited effectiveness in soils with significant fines contents.
10. Reinforcement techniques introduce discrete inclusions that stiffen and strengthen a soil deposit. The high stiffness and strength of the inclusions also tend to reduce the stresses imposed on the weaker material between the inclusions.
11. Cementitious materials may be injected or mixed into a soil deposit. The materials improve the soil by strengthening the contacts between individual grains and filling the space between the grains.
12. Grouting techniques involve the injection of such materials into the voids of the soil or into fractures in the soil so that the particle structure of the majority of the soil remains intact. In permeation grouting, very low viscosity grouts are injected into the voids of the soil without disturbing the soil structure. In intrusion grouting, thicker and more viscous grouts are injected under pressure to cause controlled fracturing of the soil.
13. Mixing techniques introduce cementitious materials by physically mixing them with the soil, completely disturbing the particle structure of the soil. The mixing can be accomplished mechanically (soil mixing) or hydraulically (jet grouting). Both soil mixing and jet grouting leave behind relatively uniform columns of mixed soil-cement. By overlapping the columns, walls or cellular structures can be constructed below the ground surface.
14. Drainage techniques minimize the buildup of porewater pressure during earthquakes by shortening the drainage paths in a soil deposit. The installation of drains generally involves some degree of densification and the drains themselves may also provide some reinforcement.

15. Verification of the effectiveness of soil improvement is an important part of seismic hazard mitigation. Direct or indirect measurement of stiffness, strength, or density characteristics both before and after improvement can allow reliable evaluation of soil improvement effectiveness. These characteristics may be measured by laboratory, in situ, or geophysical tests. The relative advantages and limitations of these types of tests, discussed in detail in Chapter 6, apply to their use in verification applications.



A.1 INTRODUCTION

Many different types of dynamic loading can induce vibratory motion in soils and structures. To solve problems involving the dynamic response of soils and structures, it is necessary to be able to describe dynamic events. They can be described in different ways, and the geotechnical earthquake engineer must be familiar with each. This appendix provides a brief description of vibratory motion and introduces the nomenclature and mathematical forms by which it is usually described.

A.2 TYPES OF VIBRATORY MOTION

Vibratory motion can be divided into two broad categories: *periodic motion* and *nonperiodic motion*. Periodic motions are those which repeat themselves at regular intervals of time. Mathematically, a motion, $u(t)$, is periodic if there exists some period, T_f , for which $u(t + T_f) = u(t)$ for all t . The simplest form of periodic motion is *simple harmonic motion* in which displacement varies sinusoidally with time. *Nonperiodic motions*, which do not repeat themselves at constant intervals, can result from impulsive loads (e.g., explosions or falling weights), or from longer-duration transient loadings (e.g., earthquakes or traffic). Examples of periodic and nonperiodic motions are shown in Figure A.1.

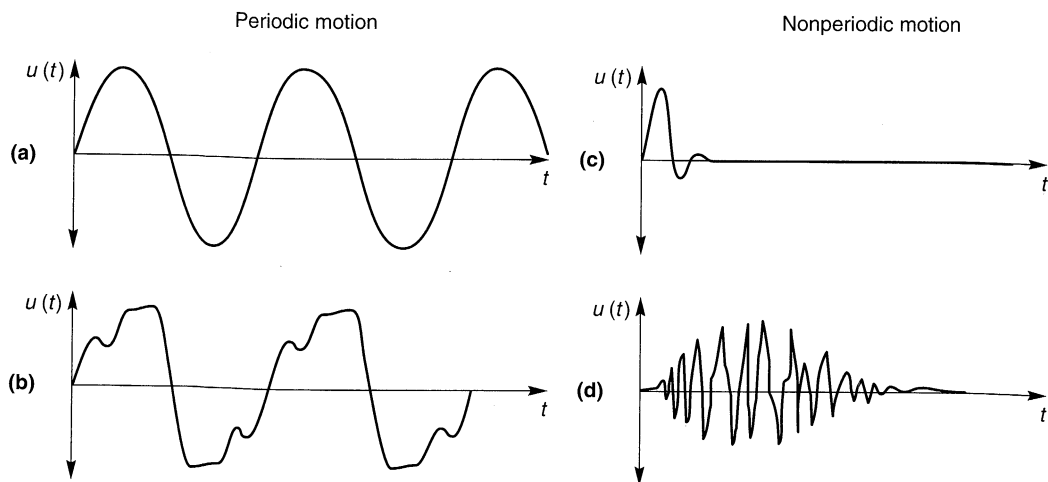


Figure A.1 Periodic and nonperiodic motion: (a) simple harmonic motion; (b) general periodic motion; (c) transient motion (response to impact loading); (d) transient motion (earthquake ground motion).

Some forms of periodic motion (e.g., Figure A.1b) may appear to be much more complex than simple harmonic motion, but with the use of mathematical techniques described later in this appendix, they can be expressed as the sum of a series of simple harmonic motions. Even transient, nonperiodic motions such as those of Figure A.1c and d can be represented as periodic motions by assuming that they repeat themselves after some “quiet” zone during which no motion occurs (Figure A.2). Using this technique, even a transient motion can also be expressed as a periodic motion. This becomes a very powerful tool for the dynamic analysis of linear systems, where the principle of superposition allows the response to transient loading to be expressed as the sum of the responses to a series of simple harmonic loads.

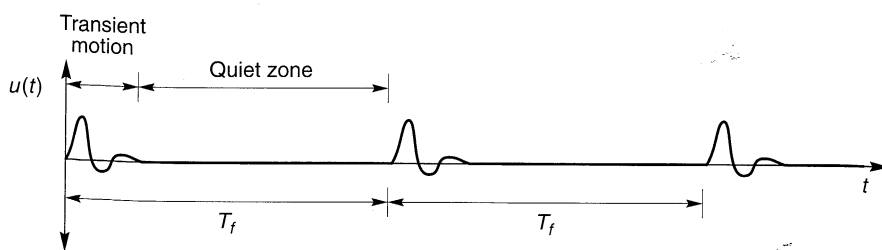


Figure A.2 Representation of a transient motion as a periodic motion using an artificial quiet zone. The motion repeats itself indefinitely at period T_f .

A.2.1 Simple Harmonic Motion

Simple harmonic motion can be characterized by sinusoidal motion at constant frequency. Its most important features can be defined by three quantities: *amplitude*, *frequency*, and

phase. Simple harmonic motion can be described in different ways, two of which will be presented in the following sections: using *trigonometric notation* or using *complex notation*. Both notations are equivalent and both are commonly used in geotechnical earthquake engineering.

A.2.2 Trigonometric Notation for Simple Harmonic Motion

In its simplest form, simple harmonic motion can be expressed in terms of a displacement, $u(t)$, using trigonometric notation: for example,

$$u(t) = A \sin(\omega t + \phi) \quad (\text{A.1})$$

where A represents the displacement *amplitude*, ω the *circular frequency*, and ϕ the *phase angle*. The time history of this simple harmonic displacement is shown in Figure A.3. The amplitude, A , is occasionally referred to as the *single amplitude* to distinguish it from the *double amplitude* (which represents the peak-to-peak displacement) referred to in some of the older geotechnical earthquake engineering literature. The circular frequency describes the rate of oscillation in terms of radians per unit time, where 2π radians corresponds to one cycle of motion. The phase angle describes the amount of time by which the peaks (and zero points) are shifted from those of a pure sine function, as illustrated in Figure A.4. The displacement will be zero when $\omega t + \phi = 0$ or, consequently, when $t = -\phi/\omega$. A positive phase angle indicates that the motion *leads* the sine function; it *lags* the sine function if the phase angle is negative. The concept of circular frequency is more easily understood by considering the motion of the

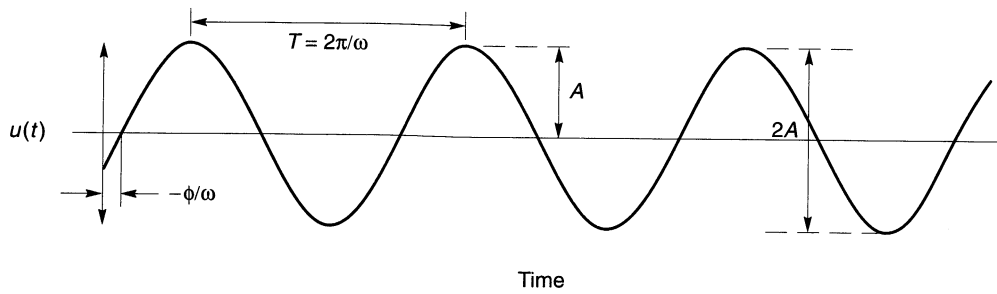


Figure A.3 Time history of simple harmonic displacement.

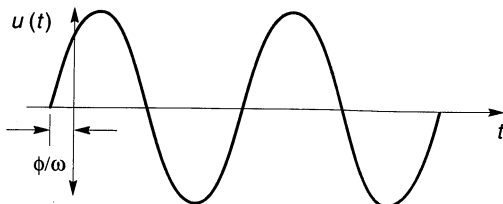


Figure A.4 Influence of phase angle on position of sinusoid.

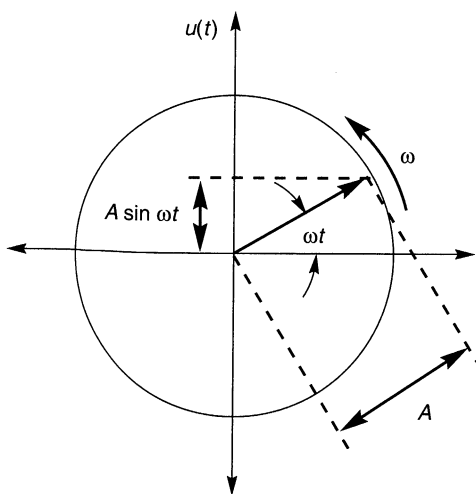


Figure A.5 Rotating vector representation of simple harmonic motion with zero phase angle.

rotating vector of length A shown in Figure A.5. If the vector rotates counterclockwise about its origin at an angular speed, ω , from its initial horizontal position, the displacement, $u(t)$, is given by the vertical component of the vector

$$u(t) = A \sin \omega t$$

The vertical component increases to a maximum value at $\omega t = \pi/2$, then decreases through zero (at $\omega t = \pi$) and reaches its maximum negative value at $\omega t = 3\pi/2$. It continues back to its original position and then repeats the entire process.

The time required for the rotating vector to make one full revolution is the time required for one *cycle* of the motion. This time is referred to as the *period of vibration*, T , and is related to the circular frequency by

$$T = \frac{\text{angular distance for one revolution}}{\text{angular speed}} = \frac{2\pi}{\omega} \quad (\text{A.2})$$

Another common measure of the frequency of oscillation is expressed in terms of the number of cycles that occur in a particular period of time. Since the period of vibration represents the time per cycle, the number of cycles per unit time must be its reciprocal, that is,

$$f = \frac{1}{T} = \frac{\omega}{2\pi} \quad (\text{A.3})$$

which is usually expressed in cycles per second or hertz (abbreviated Hz).

Simple harmonic motion can also be described as the sum of a sine function and a cosine function, that is,

$$u(t) = a \cos \omega t + b \sin \omega t \quad (\text{A.4})$$

As shown in Figure A.6, the sum of the sine and cosine functions is also a sinusoid that oscillates at circular frequency, ω . However, its amplitude is not the simple sum of the amplitudes of the sine and cosine functions, and its peaks do not occur at the same times as those of the sine or cosine functions. The rotating vector representation of this function is illustrated in

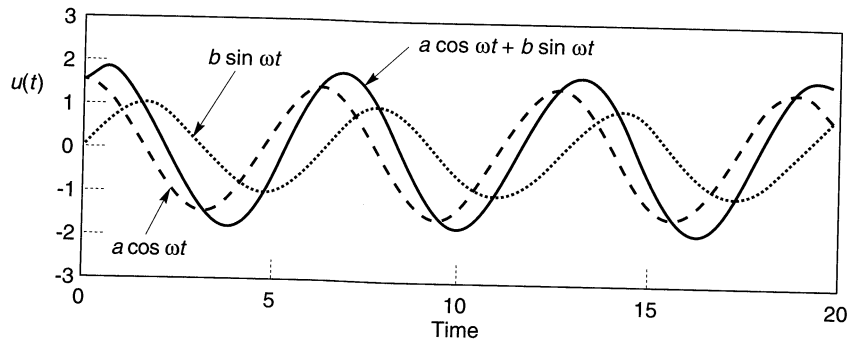


Figure A.6 Summation of sine and cosine functions of the same frequency produces a sinusoid of the same frequency. Amplitude and phase of the sinusoid depends on the amplitudes of the sine and cosine functions.

Figure A.7. Since $\cos \theta = \sin(\theta + 90^\circ)$, the rotating vector of length a must be 90° ahead of the vector of length b . The vertical components of vectors a and b are $a \cos \omega t$ and $b \sin \omega t$, respectively. As illustrated in Figure A.7a, the total value of $u(t)$ is given by $u(t) = a \cos \omega t + b \sin \omega t$. The motion can be expressed in a different form by considering the resultant of vectors a and b , as in Figure A.7b. The length of the resultant will be $\sqrt{a^2 + b^2}$ and it will lead b by an angle $\phi = \tan^{-1}(a/b)$. Accordingly, the vertical component of the resultant is

$$u(t) = A \sin(\omega t + \phi) \quad (\text{A.5})$$

where $A = \sqrt{a^2 + b^2}$ is the amplitude and $\phi = \tan^{-1}(a/b)$ is the phase angle of the motion.

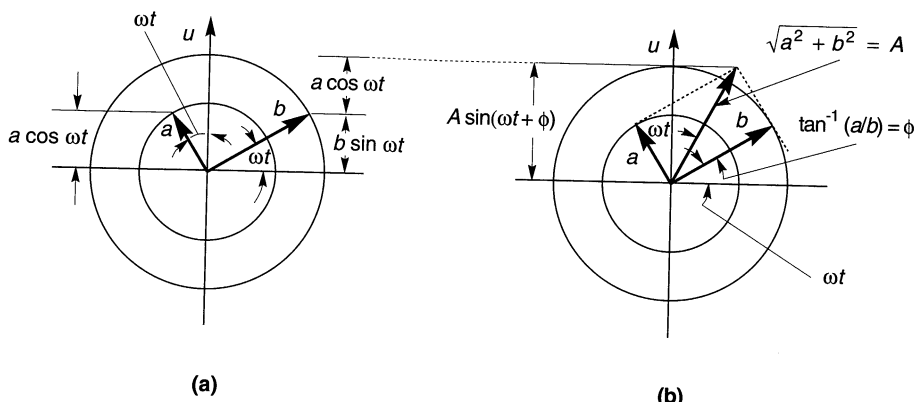


Figure A.7 Rotating vector representation of simple harmonic motion. Sum of vertical components of sine and cosine components in (a) is equal to vertical component of resultant of sine and cosine components in (b).

A.2.2.1 Complex Notation for Simple Harmonic Motion

Trigonometric descriptions of simple harmonic motion use familiar functions that are easy to visualize. For many dynamic analyses, however, the use of trigonometric notation

leads to very long and awkward equations. These analyses become much simpler when motions are described using complex notation (the word *complex* indicates that complex variables are used, not that the notation is particularly complicated). Complex notation can be derived directly from trigonometric notation using *Euler's law*:

$$e^{i\alpha} = \cos \alpha + i \sin \alpha \quad (\text{A.6})$$

where i is the imaginary number $i = \sqrt{-1}$. The quantity $e^{i\alpha}$ is a complex number; it has two parts, a *real part* and an *imaginary part*, which can be written as

$$\text{Re}(e^{i\alpha}) = \cos \alpha$$

$$\text{Im}(e^{i\alpha}) = \sin \alpha$$

Euler's law can be used to show that

$$\cos \alpha = \frac{e^{i\alpha} + e^{-i\alpha}}{2} \quad \sin \alpha = -i \frac{e^{i\alpha} - e^{-i\alpha}}{2} \quad (\text{A.7})$$

Substituting these expressions into the general expression for harmonic motion equation (A.4) gives

$$\begin{aligned} u(t) &= a \frac{e^{i\omega t} + e^{-i\omega t}}{2} - bi \frac{e^{i\omega t} - e^{-i\omega t}}{2} \\ &= \frac{a - ib}{2} e^{i\omega t} + \frac{a + ib}{2} e^{-i\omega t} \end{aligned} \quad (\text{A.8})$$

This form of the displacement may be visualized as a pair of rotating vectors in an *Argand diagram*. An Argand diagram represents a complex number graphically as a vector with orthogonal real and imaginary components. Although usually drawn with the real axis oriented horizontally, the rotated Argand diagram of Figure A.8a will help illustrate how this complex notation describes simple harmonic motion. In the Argand diagram, the term $e^{i\omega t}$

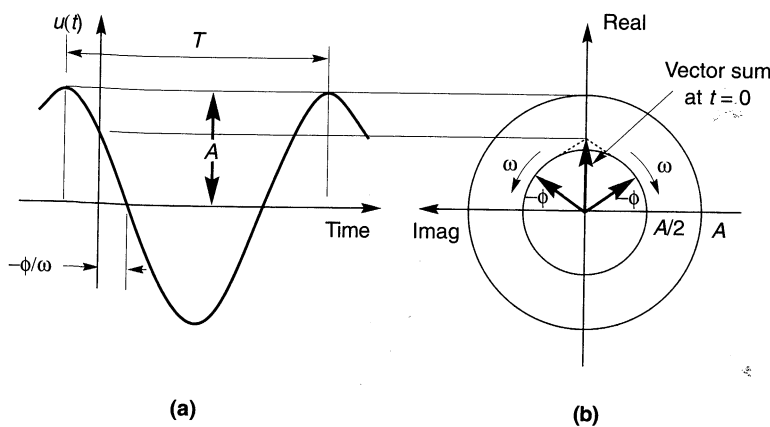


Figure A.8 How counterclockwise rotating vectors of length $A/2$ produce simple harmonic motion. Note that the phase angles are measured from the horizontal axis in the direction of vector rotation.

is represented by a vector of unit length rotating clockwise at an angular speed, ω . The term $e^{-i\omega t} = e^{i(-\omega)t}$ therefore can be represented by a unit vector rotating clockwise at angular speed, $-\omega$, which is equivalent to rotating counterclockwise at angular speed, ω . Accordingly, the first term in equation (A.8) can be represented by a vector of real part, $a/2$, and imaginary part, $-b/2$, rotating clockwise at ω , and the second term by another vector with the same real part, but an imaginary part, $b/2$, rotating counterclockwise at ω . The length of each vector is $\sqrt{(a/2)^2 + (b/2)^2} = \frac{1}{2}\sqrt{a^2 + b^2}$. As shown in Figure A.8a, the sum of the vectors is real (the imaginary parts always cancel each other). Figure A.8b shows how the vector sum describes a simple harmonic motion of amplitude $A = \sqrt{a^2 + b^2}$ and circular frequency ω .

A.2.3 Other Measures of Motion

Displacement is not the only parameter that can be used to describe vibratory motion. In fact, other parameters are often of greater interest. If the variation of displacement with time is known, however, the other parameters of interest can be determined. Differentiating the expression for simple harmonic displacement produces expressions for *velocity* and *acceleration*:

$$u(t) = A \sin(\omega t + \phi) \quad \text{displacement} \quad (\text{A.9a})$$

$$\dot{u}(t) = \frac{du}{dt} = \omega A \cos(\omega t + \phi) \quad \text{velocity} \quad (\text{A.9b})$$

$$\ddot{u}(t) = \frac{d^2u}{dt^2} = -\omega^2 A \sin(\omega t + \phi) = -\omega^2 u \quad \text{acceleration} \quad (\text{A.9c})$$

Note that when the *displacement amplitude* is A , the *velocity amplitude* is ωA , and the *acceleration amplitude* is $\omega^2 A$. Thus frequency and the displacement, velocity, and acceleration amplitudes of a harmonic motion are related in such a way that knowledge of the frequency and any one amplitude, or knowledge of any two amplitudes, allows calculation of all other quantities. This important and useful property of harmonic motions allows the use of *tripartite plots*, in which a harmonic motion can be completely described in terms of frequency and displacement, velocity, and acceleration amplitudes by a single point. Tripartite plots, an example of which is shown in Figure A.9, are commonly used to describe earthquake ground motions. It is important to note that these relationships apply only to harmonic motions and that the relationships between displacement, velocity, and acceleration for other types of motion must be obtained by differentiation and/or integration.

Examination of equations (A.8) reveals that in addition to having different amplitudes, the displacement, velocity, and acceleration are out of phase with each other (Figure A.10). The velocity can be seen to lead the displacement by $\pi/2$ radians, or 90° , and the acceleration to lead the velocity by the same amount. The relationships between displacement, velocity, and acceleration for harmonic motions, in both trigonometric and complex notation, are

$$u(t) = A \sin \omega t \quad u(t) = Ae^{i\omega t} \quad (\text{A.10a})$$

$$\dot{u}(t) = \omega A \cos \omega t = \omega A \sin(\omega t + \pi/2) \quad \dot{u}(t) = i\omega A e^{i\omega t} \quad (\text{A.10b})$$

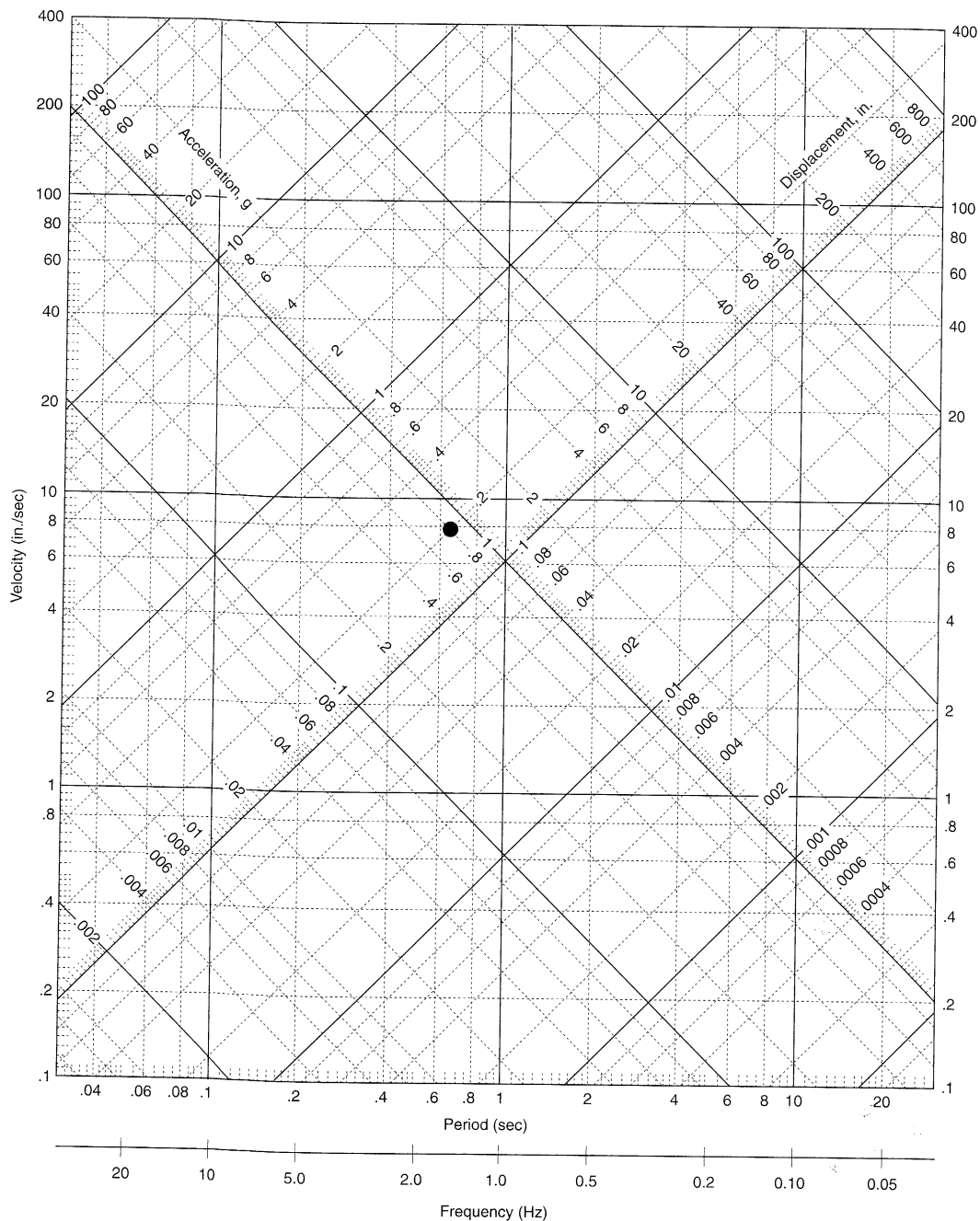


Figure A.9 Tripartite plot for harmonic motion. Point at center describes harmonic motion at a period of 0.65 sec with displacement amplitude of 0.8 in., velocity amplitude of 8.0 in./sec, and acceleration amplitude of 0.20g. (After Richart, et al., 1970.)

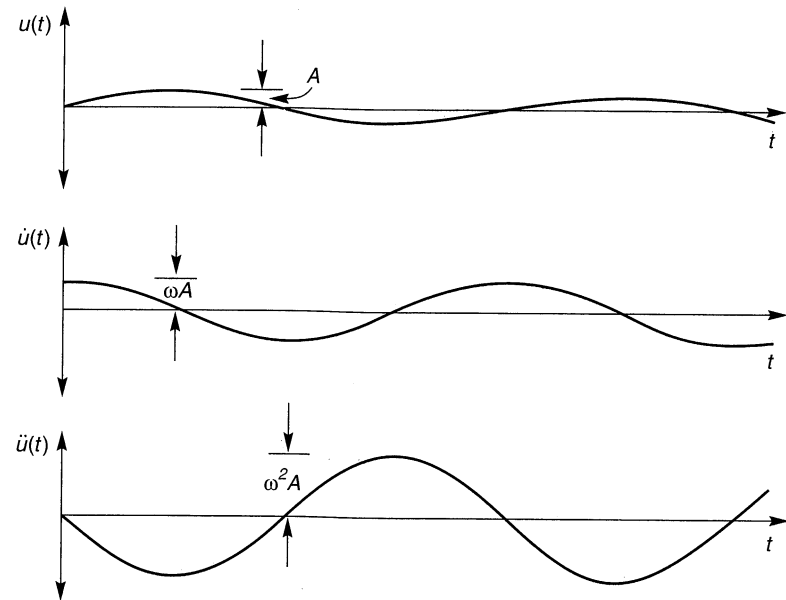


Figure A.10 Time histories of displacement, velocity, and acceleration. Note that acceleration leads velocity by one-quarter cycle and displacement by one-half cycle.

$$\ddot{u}(t) = -\omega^2 A \sin \omega t = \omega^2 A \sin(\omega t + \pi) \quad \ddot{u}(t) = i^2 \omega^2 A e^{i\omega t} = -\omega^2 A e^{i\omega t} \quad (\text{A.10c})$$

The relationship between harmonic displacements, velocities, and accelerations can be visualized in terms of three vectors rotating counterclockwise at an angular speed ω (Figure A.11). The acceleration vector is 90° (or $\pi/2$ radians) ahead of the velocity vector and 180° (or π radians) ahead of the displacement vector.

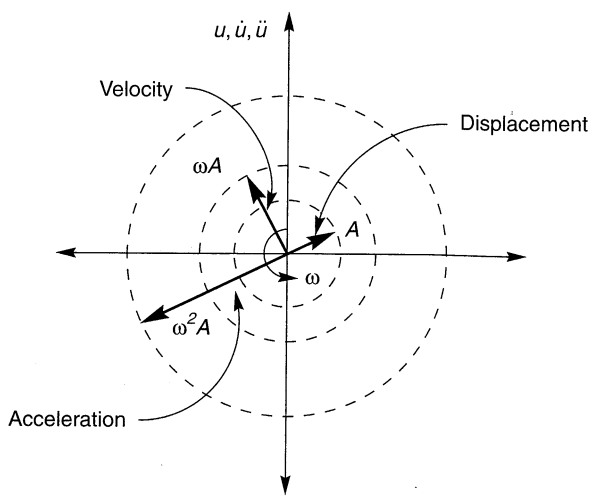


Figure A.11 Rotating vector representation of displacement, velocity, and acceleration. Note how acceleration leads velocity by 90° and displacement by 180° .

A.3 FOURIER SERIES

While studying heat flow problems in the early nineteenth century, the French mathematician J. B. J. Fourier showed that any periodic function that meets certain conditions can be expressed as the sum of a series of sinusoids of different amplitude, frequency, and phase. Since the conditions for existence of a Fourier series are nearly always met for functions that accurately describe physical processes (Ramirez, 1985), it is an extraordinarily useful tool in many branches of science and engineering.

Geotechnical earthquake engineering is no exception. By breaking down a complicated loading function such as that imposed by an earthquake ground motion into the sum of a series of simple harmonic loading functions, the principle of superposition allows available solutions for harmonic loading to be used to compute the total response (provided that the system is linear), as illustrated schematically in Figure A.12.

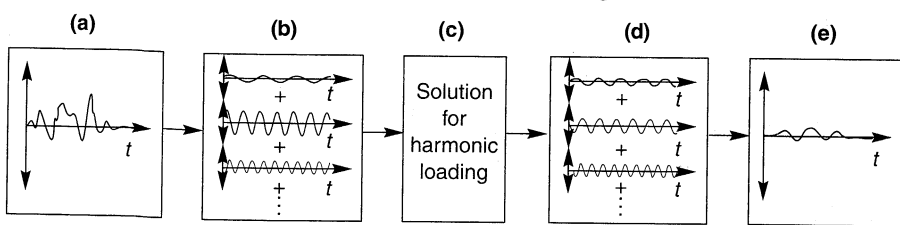


Figure A.12 Process by which Fourier series representation of complicated loading can allow relatively simple solutions for harmonic loading to be used to produce the total response: (a) time history of loading; (b) representation of time history of loading as sum of series of harmonic loads; (c) calculation of response for each harmonic load; (d) representation of response as sum of series of harmonic responses; (e) summation of harmonic responses to produce time history of response.

A.3.1 Trigonometric Form

Since a Fourier series is simply a summation of simple harmonic functions, it can be expressed using either trigonometric notation or complex notation. The general trigonometric form of the Fourier series for a function of period, T_f , is

$$x(t) = a_0 + \sum_{n=1}^{\infty} (a_n \cos \omega_n t + b_n \sin \omega_n t) \quad (\text{A.11})$$

where the *Fourier coefficients* are

$$a_0 = \frac{1}{T_f} \int_0^{T_f} x(t) dt$$

$$a_n = \frac{2}{T_f} \int_0^{T_f} x(t) \cos \omega_n t dt$$

$$b_n = \frac{2}{T_f} \int_0^{T_f} x(t) \sin \omega_n t dt$$

and $\omega_n = 2\pi n/T_f$. The term a_0 represents the average value of $x(t)$ over the range $t = 0$ to $t = T_f$; its value is zero in many geotechnical earthquake engineering applications. Note that the frequencies, ω_n , are not arbitrary; rather, they are evenly spaced at a constant frequency increment, $\Delta\omega = 2\pi/T_f$.

Example A.1

The Fourier coefficients are not difficult to calculate for simple functions. Consider the square-wave function shown in Figure EA.1. Over its period, T_f , the square wave is described by

$$x(t) = \begin{cases} +A & 0 < t \leq \frac{T_f}{4} \\ -A & \frac{T_f}{4} < t \leq \frac{3T_f}{4} \\ +A & \frac{3T_f}{4} < t \leq T_f \end{cases}$$

Since the average value of $x(t)$ is easily seen to be zero, the coefficient $a_0 = 0$. The value of a_1 can be computed as

$$\begin{aligned} a_1 &= \frac{2}{T_f} \int_0^{T_f} x(t) \cos \omega_1 t dt \\ &= \frac{2}{T_f} \left[A \int_0^{T_f/4} \cos \omega_1 t dt - A \int_{T_f/4}^{3T_f/4} \cos \omega_1 t dt + A \int_{3T_f/4}^{T_f} \cos \omega_1 t dt \right] \\ &= \frac{2A}{\omega_1 T_f} \left[\sin \frac{\omega_1 T_f}{4} - \left(\sin \frac{3\omega_1 T_f}{4} - \sin \frac{\omega_1 T_f}{4} \right) + \left(\sin \omega_1 T_f - \sin \frac{3\omega_1 T_f}{4} \right) \right] \end{aligned}$$

Substituting $\omega_1 T_f = 2\pi$ yields

$$a_1 = \frac{A}{\pi} (1 + 2 + 1) = \frac{4A}{\pi}$$

Repeating for all n yields

$$a_n = \begin{cases} \frac{+4A}{n\pi} & n = 1, 5, 9, \dots \\ \frac{-4A}{n\pi} & n = 3, 7, 11, \dots \\ 0 & n = \text{even integers} \end{cases}$$

$$b_n = 0 \quad \text{all } n$$

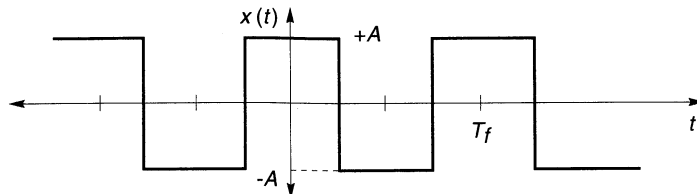


Figure EA.1 Square-wave function.

so the Fourier series is

$$x(t) = \frac{4A}{\pi} \left(\cos \omega_1 t - \frac{1}{3} \cos 3\omega_1 t + \frac{1}{5} \cos 5\omega_1 t - \frac{1}{7} \cos 7\omega_1 t + \dots \right)$$

where $\omega_1 = 2\pi/T_f$. The sine terms are all zero because the square wave, like the cosine function, is an *even function* [i.e., one for which $f(t) = f(-t)$]. For an *odd function* [$f(t) = -f(-t)$], the cosine terms are zero. For a function that is neither even nor odd, the Fourier series will contain both sine and cosine terms.

The Fourier series represents a function exactly only for $n = \infty$. If the series is truncated at some finite value of n , the Fourier series only approximates the function. For many functions, however, the approximation can be quite good even when n is relatively small. This characteristic is often used to great advantage in dynamic analyses of soils and structures.

From equations (A.5) and (A.11), it is apparent that the Fourier series can also be expressed as

$$x(t) = c_0 + \sum_{n=1}^{\infty} c_n \sin(\omega_n t + \phi_n) \quad (\text{A.12})$$

where $c_0 = a_0$, $c_n = \sqrt{a_n^2 + b_n^2}$, and $\phi_n = \tan^{-1}(a_n/b_n)$. In this form, c_n and ϕ_n are the amplitude and phase, respectively, of the n th harmonic. A plot of c_n versus ω_n is known as a *Fourier amplitude spectrum*; a plot of ϕ_n versus ω_n gives a *Fourier phase spectrum*. Fourier amplitude spectra are very useful in geotechnical earthquake engineering—as discussed in Chapter 3, they effectively describe the frequency content of an earthquake motion.

Example A.2

The Fourier amplitude and phase spectra for the square wave of Example A.1 are easily determined. The values of c_n and ϕ_n for the first eight terms of the series are

$$\begin{aligned} c_0 &= 0 \\ c_1 &= \frac{4A}{\pi} \quad \phi_1 = \frac{\pi}{2} \\ c_2 &= 0 \\ c_3 &= \frac{4A}{3\pi} \quad \phi_3 = -\frac{\pi}{2} \\ c_4 &= 0 \\ c_5 &= \frac{4A}{5\pi} \quad \phi_5 = \frac{\pi}{2} \\ c_6 &= 0 \\ c_7 &= \frac{4A}{7\pi} \quad \phi_7 = -\frac{\pi}{2} \end{aligned}$$

The spectra are plotted in Figure EA.2.

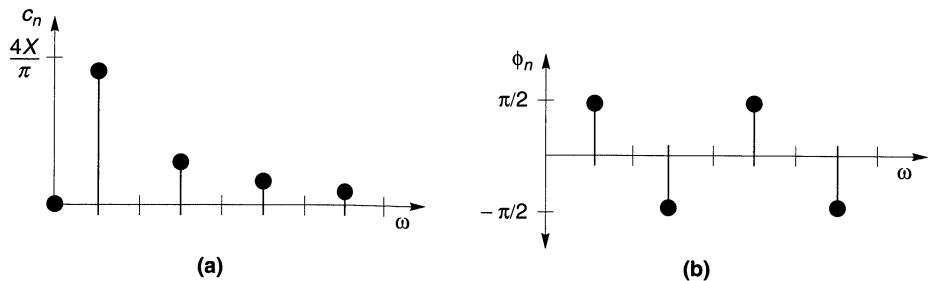


Figure EA.2 Fourier spectra for square wave of Example A.1: (a) Fourier amplitude spectrum; (b) Fourier phase spectrum.

A.3.2 Exponential Form

The Fourier series can also be expressed in exponential form. Substituting Equations A.7 into A.10 for all n gives

$$x(t) = a_0 + \sum_{n=1}^{\infty} \left(\frac{a_n - ib_n}{2} e^{i\omega_n t} + \frac{a_n + ib_n}{2} e^{-i\omega_n t} \right) \quad (\text{A.13})$$

Defining new Fourier coefficients,

$$\begin{aligned} c_0^* &= a_0 \\ c_n^* &= \frac{a_n - ib_n}{2} \\ c_{-n}^* &= \frac{a_n + ib_n}{2} \end{aligned}$$

where the * indicates the complex nature of the coefficient, the Fourier series can be rewritten as

$$x(t) = c_0^* + \sum_{n=1}^{\infty} (c_n^* e^{i\omega_n t} + c_{-n}^* e^{-i\omega_n t}) \quad (\text{A.14})$$

Since $\omega_{-n} = -\omega_n$, the limits of summation can be changed to write the Fourier series in the more compact form

$$x(t) = \sum_{n=-\infty}^{\infty} c_n^* e^{i\omega_n t} \quad (\text{A.15})$$

The complex Fourier coefficients, c_n^* , can be determined directly from $x(t)$ as

$$c_n^* = \frac{1}{T_f} \int_0^{T_f} x(t) e^{-i\omega_n t} dt \quad (\text{A.16})$$

Example A.3

Compute the complex Fourier coefficients for the square wave of Example A.1.

Solution Since the average value of the square wave is zero, $c_o^* = 0$. For $n = +1$, equation (A.16) gives

$$\begin{aligned} c_1^* &= \frac{1}{T_f} \left[X \int_0^{T_f/4} e^{i\omega_1 t} dt - X \int_{T_f/4}^{3T_f/4} e^{i\omega_1 t} dt + X \int_{3T_f/4}^{T_f} e^{i\omega_1 t} dt \right] \\ &= \frac{X}{i\omega_1 T_f} [e^{i\omega_1 T_f/4} - (e^{i3\omega_1 T_f/4} - e^{i\omega_1 T_f/4}) + (e^{i\omega_1 T_f} - e^{i3\omega_1 T_f/4})] \\ &= \frac{X}{i2\pi} (2e^{i\pi/2} - 2e^{i3\pi/2} + e^{i2\pi}) \\ &= \frac{X}{i2\pi} (2i + 2i + 0) = \frac{2X}{\pi} \end{aligned}$$

Note that although $c_0^* = c_0 = a_0$, the definitions of c_n^* and c_{-n}^* indicate that

$$\begin{aligned} |c_n^*| &= \sqrt{[\operatorname{Re}(c_n^*)]^2 + [\operatorname{Im}(c_n^*)]^2} = \sqrt{\left(\frac{a_n}{2}\right)^2 + \left(\frac{b_n}{2}\right)^2} = \frac{\sqrt{a_n^2 + b_n^2}}{2} = \frac{c_n}{2} \\ |c_{-n}^*| &= \sqrt{[\operatorname{Re}(c_{-n}^*)]^2 + [\operatorname{Im}(c_{-n}^*)]^2} = \sqrt{\left(\frac{a_n}{2}\right)^2 + \left(\frac{b_n}{2}\right)^2} = \frac{\sqrt{a_n^2 + b_n^2}}{2} = \frac{c_n}{2} \end{aligned} \quad (\text{A.17})$$

(i.e., in exponential form, half of the amplitude is associated with positive frequencies and half with negative frequencies). The phase angles at positive and negative frequencies are equal but of opposite sign; consequently, the imaginary parts cancel each other [as they must if $x(t)$ is a real function]. The complex Fourier coefficients are sometimes (although rarely in geotechnical earthquake engineering applications) used to plot *two-sided spectra* which are related to the more conventional *one-sided spectra* as shown in Figure EA.3.

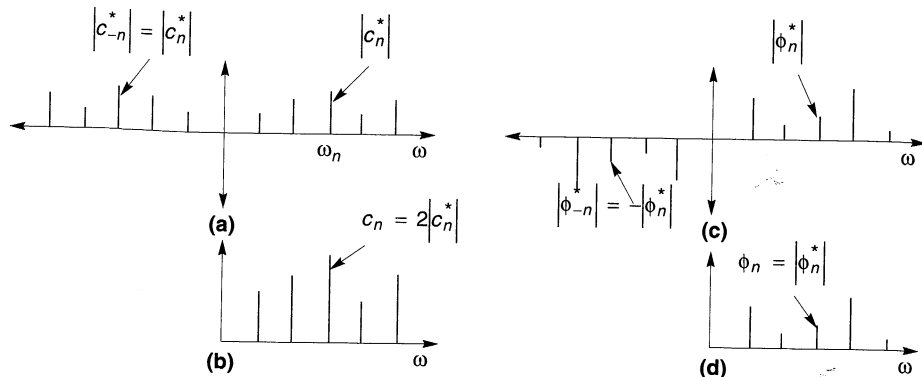


Figure EA.3 Comparison of one- and two-sided Fourier spectra. The two-sided Fourier amplitude spectrum (a) is symmetrical with amplitudes on each side of the $\omega = 0$ axis equal to half the amplitude of the one-sided spectrum (b). (The amplitude at $\omega = 0$ is the same for both.) The two-sided phase spectrum (c) is antisymmetric, but phase at positive frequencies is equal to phase of one-sided spectrum (d).

A.3.3 Discrete Fourier Transform

In many geotechnical earthquake engineering applications, loading or motion parameters are described by a finite number of data points rather than by an analytical function. In such cases the Fourier coefficients are obtained by summation rather than integration. For a variable $x(t_k)$, $k = 1, N$, where $t_k = k \Delta t$, the *discrete Fourier transform* (DFT) is given by

$$X(\omega_n) = \Delta t \sum_{k=1}^N x(t_k) e^{-i\omega_n t_k} \quad (\text{A.18a})$$

where $\omega_n = n \Delta\omega = 2\pi n/N \Delta t$. Using Euler's law, the DFT can also be written as

$$X(\omega_n) = \Delta t \sum_{k=1}^N [x(t_k) \cos \omega_n t_k - i x(t_k) \sin \omega_n t_k] \quad (\text{A.18b})$$

Note that the Fourier coefficients of the DFT have units of the original variable multiplied by time.

The DFT can also be inverted; that is, a set of data spaced at equal frequency intervals, $\Delta\omega$, can be expressed as a function of time, using the *inverse discrete Fourier transform* (IDFT):

$$x(t_k) = \Delta\omega \sum_{n=1}^N X(\omega_n) e^{i\omega_n t_k} \quad (\text{A.19a})$$

or

$$x(t_k) = \Delta\omega \sum_{n=1}^N [X(\omega_n) \cos \omega_n t_k + i X(\omega_n) \sin \omega_n t_k] \quad (\text{A.19b})$$

Either of these expressions can easily be programmed on a personal computer; since n takes on N different values, the summation operation will be performed N times. The time required for computation of a DFT (or IDFT), therefore, is proportional to N^2 .

A.3.4 Fast Fourier Transform

The DFT was developed long before computers were available, and its use, for even modest values of N , was extremely labor intensive. As early as 1805, the beginning of a more efficient approach to the DFT was described (Brigham, 1974). As digital computers were developed in the 1960s, Cooley and Tukey (1965) developed a computational algorithm for the case where N is a power of 2 that has become known as the *fast Fourier transform* (FFT). By performing repeated operations on groups that start with a single number and increase in size by a factor of 2 at each of j stages (where $N = 2^j$), the time required to complete the transform is proportional to $N \log_2 N$. Consequently, the FFT is much more efficient than the DFT. For example, at $N = 2048$, the FFT is more than 180 times faster than the DFT. The *inverse fast Fourier transform* (IFFT) operates with equal speed.

A.3.5 Power Spectrum

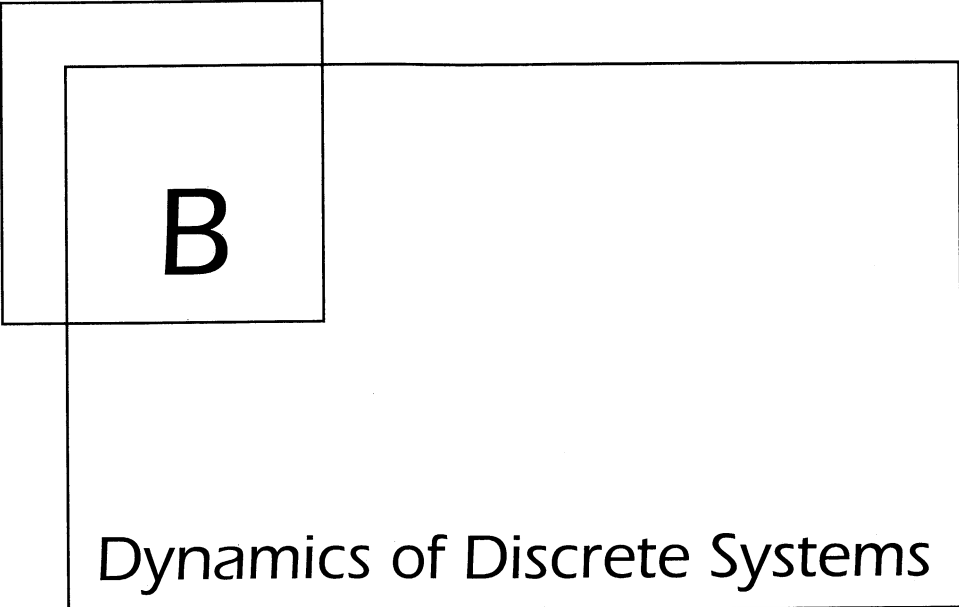
The Fourier amplitude spectrum illustrates how the strength of a quantity varies with frequency. This information can also be expressed in terms of *power*. The power of a signal, $x(t)$, that can be expressed in the form of equation (A.11) or (A.12), is defined as

$$P(\omega_n) = \frac{1}{2}(a_n^2 + b_n^2) = \frac{1}{2}c_n^2$$

Note that this definition of power can be applied to any signal (it is not related to mechanical—force times velocity—power). Power can be plotted as a function of frequency to obtain a power spectrum. The total power of the signal is the same whether it is computed in the time domain or the frequency domain:

$$\text{total power} = \sum_{n=1}^{\infty} P(\omega_n) = \int_0^{T_f} [x(t)]^2 dt = \frac{1}{2} \int_0^{\omega_n} c_n^2 d\omega$$

Power spectra are often used to describe earthquake-induced ground motions.



B

Dynamics of Discrete Systems

B.1 INTRODUCTION

Many vibrating systems consist of discrete elements such as masses and springs, or can at least be idealized as such. For most practical problems of structural dynamics, the structure is idealized as a system of rigid masses connected by massless springs. Even continuous systems such as soil deposits have been idealized as assemblages of many discrete elements, though that approach is seldom taken any more. Since the geotechnical earthquake engineer often provides input to the structural engineer, a firm understanding of the dynamic response of discrete systems is required. Also, many of the concepts and terminologies used in geotechnical earthquake engineering analyses are analogous to those of discrete system dynamics and are more easily introduced in that framework.

This appendix introduces the dynamics of discrete systems. It begins with very simple systems, and adds complicating factors such as damping, base motion, and nonlinearity. Analytical and numerical solutions in the time domain and frequency domain are presented. Finally, the response of multiple-degree-of-freedom systems is introduced. While many of the basic concepts of structural dynamics are presented, much more complete treatments may be found in a number of structural dynamics texts (e.g., Clough and Penzien, 1975; Paz, 1980; Berg, 1989; Chopra, 1995).

B.2 VIBRATING SYSTEMS

Vibrating systems can be divided into two broad categories: *rigid systems* and *compliant systems*. A rigid system is one in which no strains occur. All points within a rigid system move in phase with each other, and the description of rigid-body motion is a relatively simple matter of kinematics. In compliant systems, however, different points within the system may move differently (and out of phase) from each other. A given physical system may behave very nearly as a rigid system under certain conditions and as a compliant system under other conditions. Since neither soils nor structures are rigid, the dynamic response of compliant systems is central to the study of soil and structural dynamics and to earthquake engineering.

Compliant systems can be characterized by the distribution of their mass. *Discrete systems* are those whose mass can be considered to be concentrated at a finite number of locations, where the mass of a *continuous system* is distributed throughout the system. The number of independent variables required to describe the position of all the significant masses of a system is the number of *dynamic degrees of freedom* of the system. Systems of interest in earthquake engineering may have anywhere from 1 to an infinite number of degrees of freedom. Figure B.1 illustrates several commonly encountered systems with varying numbers of degrees of freedom (DOF). Discrete systems have a finite number of degrees of freedom; the number of degrees of freedom of a continuous system is infinite. Certain types of analyses idealize continuous systems as discrete systems with large numbers of degrees of freedom, and other types represent discrete systems with many degrees of freedom as continuous systems.

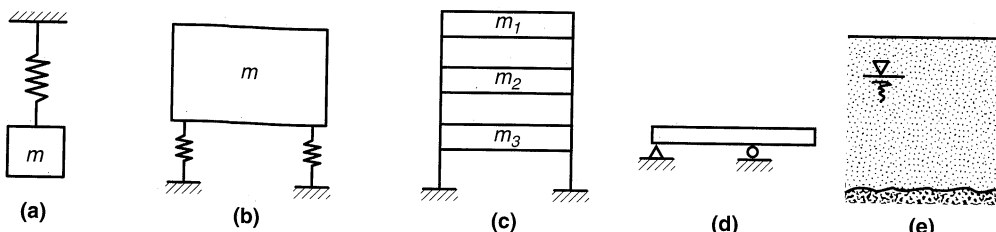


Figure B.1 Vibrating systems with various numbers of degrees of freedom: (a) one DOF, vertical translation; (b) two DOF, vertical translation and rocking; (c) three DOF, horizontal translation; (d) infinite DOF; (e) infinite DOF.

B.3 SINGLE-DEGREE-OF-FREEDOM SYSTEMS

A discrete system whose position can be described completely by a single variable is known as a *single-degree-of-freedom* (SDOF) system. That single degree of freedom may represent translational displacement, as in the SDOF systems of Figure B.2a–c, or rotational displacement, as in the case of the pendulum of Figure B.2d.

A typical SDOF system is one in which a rigid *mass*, m , is connected in parallel to a *spring* of stiffness, k , and a *dashpot* of viscous damping coefficient, c , and subjected to some external load, $Q(t)$, as shown in Figure B.3. The spring and dashpot are assumed to be massless and the displacement origin to coincide with the static equilibrium position.

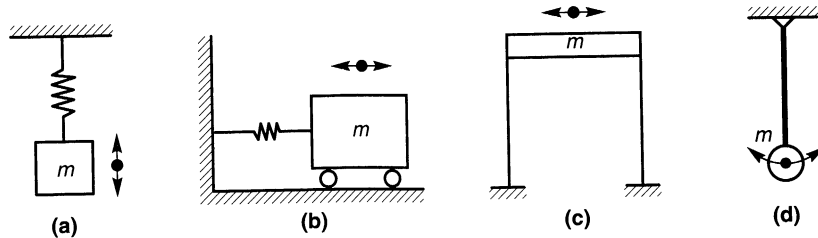


Figure B.2 Various SDOF systems. The degrees of freedom are (a) vertical translation, (b) and (c) horizontal translation, and (d) rotation.

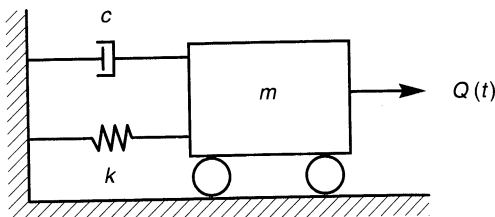


Figure B.3 Damped SDOF system subjected to external dynamic load, $Q(t)$.

B.4 EQUATION OF MOTION FOR SDOF SYSTEM

Many SDOF systems are acted upon by externally applied loads. In earthquake engineering, dynamic loading often results from another source—movement of the supports of the system. The dynamic response of a SDOF system such as that shown in Figure B.3 is governed by an *equation of motion*. The equation of motion can be derived in a number of ways; a simple, force equilibrium approach will be used here.

B.4.1 Equation of Motion: External Loading

When a dynamic load is applied to the mass of a SDOF system (Figure B.3), the tendency for motion is resisted by the inertia of the mass and by forces that develop in the dashpot and spring. Thus the external load, $Q(t)$, acting in the positive x -direction is opposed by three forces (Figure B.4) that act in the negative x -direction: the *inertial force*, f_I , the *viscous damping force*, f_D , and the *elastic spring force*, f_S . The equation of motion can be expressed in terms of the dynamic equilibrium of these forces:

$$f_I(t) + f_D(t) + f_S(t) = Q(t) \quad (\text{B.1})$$

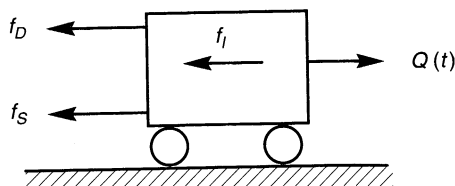


Figure B.4 Dynamic forces acting on mass from Figure B.3.

These forces can also be expressed in terms of the motion of the mass. Newton's second law states that the inertial force acting on a mass is equal to its rate of change of momentum, which for a system of constant mass produces

$$f_I(t) = \frac{d}{dt} \left(m \frac{du(t)}{dt} \right) = m \frac{d^2 u(t)}{dt^2} = m \ddot{u}(t) \quad (\text{B.2a})$$

For a viscous dashpot, the damping force is proportional to the velocity of the mass:

$$f_D(t) = c \frac{du(t)}{dt} = c \dot{u}(t) \quad (\text{B.2b})$$

and the force provided by the spring is simply the product of its stiffness and the amount by which it is displaced

$$f_S(t) = k u(t) \quad (\text{B.2c})$$

The behavior of these forces is illustrated graphically in Figure B.5. The inertial force is proportional to the acceleration and the constant of proportionality is the mass. Similarly, the viscous damping force and the elastic spring force are proportional to the velocity and displacement with the damping and spring coefficients serving as the respective constants of proportionality.

Substituting equations (B.2) into equation (B.1), the equation of motion for the SDOF system can be written as

$$m \ddot{u}(t) + c \dot{u}(t) + k u(t) = Q(t) \quad (\text{B.3})$$

This second-order differential equation is commonly used to describe the behavior of oscillating systems ranging from the mechanical systems considered in earthquake engineering problems to electrical circuits. The differential equation of motion is linear (i.e., all of its terms have constant coefficients). This linearity allows a closed-form analytical solution to be readily obtained and, importantly, it allows the principle of superposition to be used. When any of the coefficients are not constant, the behavior is not linear and the solution becomes considerably more difficult. In most cases, the response of nonlinear systems must be evaluated numerically (Section B.7).

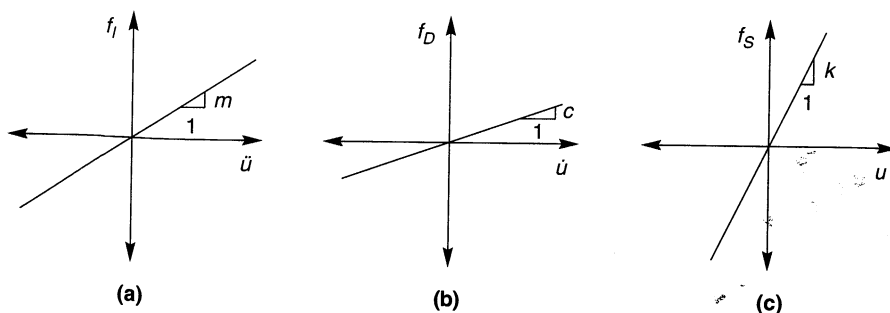


Figure B.5 Variation of (a) inertial, (b) viscous, and (c) elastic forces with acceleration, velocity, and displacement, respectively.

B.4.2 Equation of Motion: Vibration of Supports (Base Shaking)

For earthquake engineering problems, dynamic loading often results from vibration of the supports of a system rather than from dynamic external loads. To evaluate the response of such systems, it is necessary to develop an equation of motion for loading caused by base shaking. Consider the damped SDOF system shown in Figure B.6a. When subjected to dynamic base shaking, $u_b(t)$, it will deform into a configuration that might look like that shown in Figure B.6b at a particular time, t . The total displacement of the mass, $u_t(t)$, can be broken down as the sum of the base displacement, $u_b(t)$, and the displacement of the mass relative to the base, $u(t)$. The inertial force will depend on the total acceleration of the mass, while the viscous damping and elastic spring forces will depend on the relative velocity and displacement, respectively. Using the notation shown in Figure B.6b, the equation of motion can be written as

$$m\ddot{u}_t + c\dot{u}_t + ku_t = 0$$

or substituting $\ddot{u}_t(t) = \ddot{u}_b(t) + \ddot{u}(t)$ and rearranging,

$$m\ddot{u} = c\dot{u} + ku = -m\ddot{u}_b \quad (\text{B.4})$$

In other words, the response of the system to base shaking is equivalent to the response that the system would have if its base was fixed and the mass was subjected to an external load $Q(t) = -m\ddot{u}_b(t)$. Thus any solutions for the response of an SDOF system subjected to external load can be used to evaluate the response of the system to base shaking.

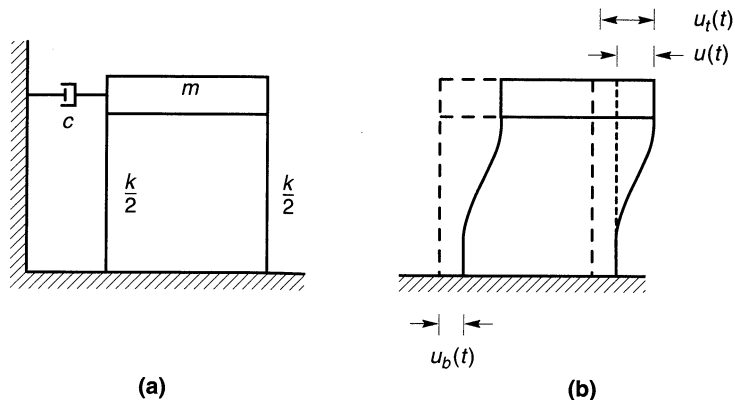


Figure B.6 Damped SDOF system subjected to base shaking.

B.5 RESPONSE OF LINEAR SDOF SYSTEMS

In order to evaluate the dynamic response of a linear SDOF system, the differential equation of motion must be solved. There are several types of conditions under which the dynamic response of SDOF systems are commonly calculated. *Forced vibration* occurs when the mass

is subjected to some external loading, $Q(t)$. The loading may be periodic or nonperiodic and it may correspond to an actual physical force applied to the mass or to some known level of base shaking. *Free vibration* occurs in the absence of external loading or base shaking. It may result from the release of the mass from some initial displacement or may occur after some transient forced vibration has ended. The following sections will develop solutions to the equation of motion for cases in which damping is and is not present, and for cases in which external loading is and is not present. The resulting four permutations of these conditions are

1. Undamped free vibrations: $c = 0, Q(t) = 0$
2. Damped free vibrations: $c > 0, Q(t) = 0$
3. Undamped forced vibrations: $c = 0, Q(t) \neq 0$
4. Damped forced vibrations: $c > 0, Q(t) \neq 0$

The solution of the equation of motion for each of these conditions will be presented in turn.

B.5.1 Undamped Free Vibrations

A SDOF system undergoes free vibration when it oscillates without being acted upon by any external loads. When damping is not present ($c = 0$) the equation of motion (for undamped free vibration) reduces to

$$m\ddot{u} + ku = 0 \quad (\text{B.5})$$

or after dividing both sides by the mass,

$$\ddot{u} + \frac{k}{m}u = 0 \quad (\text{B.6})$$

The solution to this simple differential equation can be found in any elementary text on differential equations as

$$u = C_1 \sin \sqrt{\frac{k}{m}}t + C_2 \cos \sqrt{\frac{k}{m}}t \quad (\text{B.7})$$

where the values of the constants C_1 and C_2 depend on the initial conditions of the system. The quantity $\sqrt{k/m}$ is very important—it represents the *undamped natural circular frequency* of the system

$$\omega_0 = \sqrt{\frac{k}{m}} \quad (\text{B.8})$$

Then the *natural frequency*, f_0 , and *natural period of vibration*, T_0 , can be written as

$$f_0 = \frac{\omega_0}{2\pi} = \frac{1}{2\pi} \sqrt{\frac{k}{m}} \quad (\text{B.9})$$

$$T_0 = \frac{2\pi}{\omega_0} = 2\pi \sqrt{\frac{m}{k}} \quad (\text{B.10})$$

Substituting equation (B.8) into the solution for the equation of motion [equation (B.7)] yields

$$u = C_1 \sin \omega_0 t + C_2 \cos \omega_0 t \quad (\text{B.11})$$

which indicates that an undamped system in free vibration will oscillate harmonically at its undamped natural frequency. C_1 and C_2 , can be evaluated by assuming the initial ($t = 0$) conditions to be represented by an initial displacement, u_0 , and initial velocity, \dot{u}_0 . Then

$$\begin{aligned} u_0 &= C_1 \sin(0) + C_2 \cos(0) = C_2 \\ \dot{u}_0 &= \omega_0 C_1 \cos(0) - \omega_0 C_2 \sin(0) = \omega_0 C_1 \end{aligned}$$

Therefore, $C_1 = \dot{u}_0/\omega_0$ and $C_2 = u_0$, so the complete solution to the undamped free vibration response of an SDOF system is given by

$$u = \frac{\dot{u}_0}{\omega_0} \sin \omega_0 t + u_0 \cos \omega_0 t \quad (\text{B.12})$$

The response of such a system is shown in Figure B.7.

Referring back to equation (A.5), the free vibration response can also be expressed as

$$u = A \sin(\omega_0 t + \phi) \quad (\text{B.13})$$

where the amplitude, A , and phase angle, ϕ , are given by

$$A = \sqrt{u_0^2 + \left(\frac{\dot{u}_0}{\omega_0}\right)^2}$$

$$\phi = \tan^{-1} \frac{u_0 \omega_0}{\dot{u}_0}$$

The solution to the equation of motion of an undamped system indicates that the response of the system depends on its initial displacement and velocity. Note that the amplitude remains constant with time. Because no energy is lost in an undamped system, it will continue to oscillate forever. Obviously, truly undamped systems do not exist in the real world; however, some systems can have such low damping that their response over short periods of time may approximate that of an undamped system.

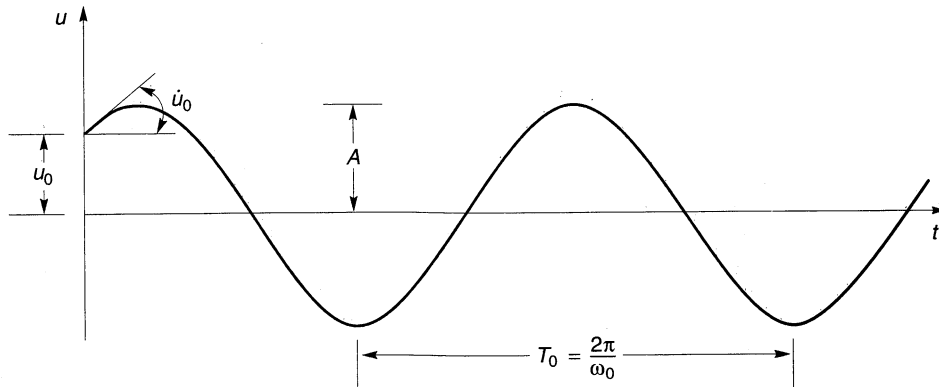
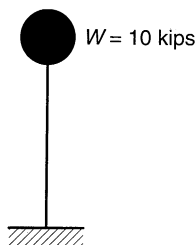


Figure B.7 Time history of displacement for undamped free vibration with initial displacement u_0 and initial velocity \dot{u}_0 .

Example B.1

The SDOF structure shown in Figure EB.1a consists of a 10-kip weight supported by a massless column. Application of a 5-kip static horizontal force to the weight produces a horizontal deflection of 0.04 in. Compute (a) the natural circular frequency, (b) the natural period of vibration, and (c) the time history of response if the horizontal force was suddenly removed.

**Figure EB.1a**

Solution (a) The problem statement indicates that the stiffness of the column is

$$k = \frac{5 \text{ kips}}{0.04 \text{ in.}} = 125 \text{ kips/in.}$$

The natural circular frequency is given by

$$\omega_0 = \sqrt{\frac{k}{m}} = \sqrt{\frac{kg}{W}} = \sqrt{\frac{(125 \text{ kips/in.})(12 \text{ in./ft})(32.2 \text{ ft/sec}^2)}{10 \text{ kips}}} = 69.5 \text{ rad/sec}$$

(b) The natural period would be

$$T_0 = \frac{2\pi}{\omega_0} = \frac{2\pi \text{ rad}}{69.5 \text{ rad/sec}} = 0.09 \text{ sec}$$

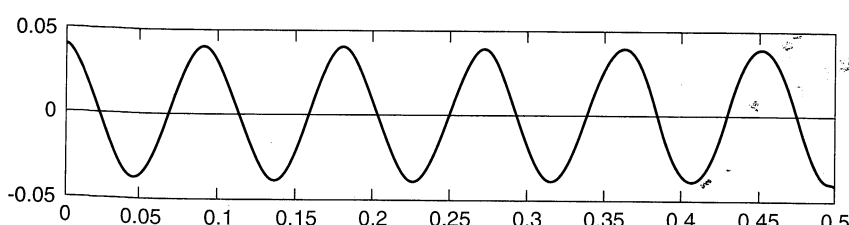
(c) The horizontal force produced a static deflection of 0.04 in. Consequently, the initial conditions for free vibration would be

$$u_0 = 0.04 \text{ in.} \quad \dot{u}_0 = 0$$

Then

$$u(t) = \frac{\dot{u}_0}{\omega_0} \sin \omega_0 t + u_0 \cos \omega_0 t = (0.04 \text{ in.}) \cos (69.5t)$$

The response is plotted in Figure EB.1b.

**Figure EB.1b**

B.5.2 Damped Free Vibrations

In real systems, energy may be lost as a result of friction, heat generation, air resistance, or other physical mechanisms. Hence the free vibration response of a damped SDOF system will diminish with time. For damped free vibrations, the equation of motion is written as

$$m\ddot{u} + c\dot{u} + ku = 0 \quad (\text{B.14})$$

or, dividing by m and substituting [from equation (B.17)] $k = m\omega_0^2$, we have

$$\ddot{u} + 2\frac{c}{2\sqrt{km}}\omega_0 u + \omega_0^2 u = 0 \quad (\text{B.15})$$

The quantity $2\sqrt{km}$, called the *critical damping coefficient*, c_c , allows the *damping ratio*, ξ , to be defined as the ratio of the damping coefficient to the critical damping coefficient, that is,

$$\xi = \frac{c}{c_c} = \frac{c}{2\sqrt{km}} = \frac{c}{2m\omega_0} = \frac{c\omega_0}{2k} \quad (\text{B.16})$$

With this notation, the equation of motion can be expressed as

$$\ddot{u} + 2\xi\omega_0\dot{u} + \omega_0^2 u = 0 \quad (\text{B.17})$$

The solution of this differential equation of motion depends on the value of the damping ratio. When $\xi < 100\%$ ($c < c_c$), the system is said to be *underdamped*. When $\xi = 100\%$ ($c = c_c$) the system is *critically damped*, and when $\xi > 100\%$ ($c > c_c$) the system is *over-damped*. Separate solutions must be obtained for each of the three cases, but structures of interest in earthquake engineering are virtually always underdamped.

For the case in which damping is less than critical, the solution to the equation of motion is of the form

$$u = e^{-\xi\omega_0 t} \left[C_1 \sin(\omega_0 \sqrt{1 - \xi^2} t) + C_2 \cos(\omega_0 \sqrt{1 - \xi^2} t) \right] \quad (\text{B.18})$$

Note the exponential term by which the term in brackets is multiplied. This exponential term gets smaller with time and eventually approaches zero, indicating that the response of an underdamped system in free vibration decays exponentially with time. The rate of decay depends on the damping ratio—for small ξ the response decays slowly and for larger ξ the response decays more quickly. Defining the *damped natural circular frequency* of the system as $\omega_d = \omega_0 \sqrt{1 - \xi^2}$ the solution can be expressed as

$$u = e^{-\xi\omega_0 t} (C_1 \sin \omega_d t + C_2 \cos \omega_d t) \quad (\text{B.19})$$

The natural frequency of a damped system is always lower than that of an undamped system, and it decreases with increasing damping ratio.

The coefficients C_1 and C_2 can be determined from the initial conditions in the same manner as for the undamped case. The initial displacement and velocity are

$$\begin{aligned} u_0 &= e^{-\xi\omega_0(0)} [C_1 \sin(0) + C_2 \cos(0)] = C_2 \\ \dot{u}_0 &= e^{-\xi\omega_0(0)} [\omega_d C_1 \cos \omega_d(0) - \omega_d C_2 \sin \omega_d(0)] - \xi \omega_0 e^{-\xi\omega_0(0)} [C_1 \sin \omega_d(0) + C_2 \cos \omega_d(0)] \\ &= \omega_d C_1 - \xi \omega_0 C_2 \end{aligned}$$

Therefore, $C_1 = (\dot{u}_0 + \xi\omega_0 u_0)/\omega_d$ and $C_2 = u_0$, so the solution for damped free vibrations can be expressed as

$$u = e^{-\xi\omega_0 t} \left(\frac{\dot{u}_0 + \xi\omega_0 u_0}{\omega_d} \sin \omega_d t + u_0 \cos \omega_d t \right) \quad (B.20)$$

The free vibration response of an underdamped system is shown in Figure B.8. Note the exponential decay of displacement amplitude with time. The ratio of the amplitudes of any two successive peaks will be

$$\frac{u_n}{u_{n+1}} = \exp\left(2\pi\xi\frac{\omega_0}{\omega_d}\right) \quad (B.21)$$

Defining the *logarithmic decrement* as $\delta = \ln(u_n/u_{n+1})$; then

$$\delta = 2\pi\xi\frac{\omega_0}{\omega_d} = \frac{2\pi\xi}{\sqrt{1-\xi^2}} \quad (B.22)$$

Rearranging allows the damping ratio to be determined from the logarithmic decrement

$$\xi = \frac{\delta}{\sqrt{4\pi^2 + \delta^2}} \quad (B.23)$$

For small values of δ , $\xi \approx \delta/2\pi$. Therefore, a simple way to estimate the damping ratio of an SDOF system is to perform a *free vibration test*, in which the logarithmic decrement is measured when a system is displaced by some initial displacement, u_0 , and released with initial velocity $\dot{u}_0 = 0$.

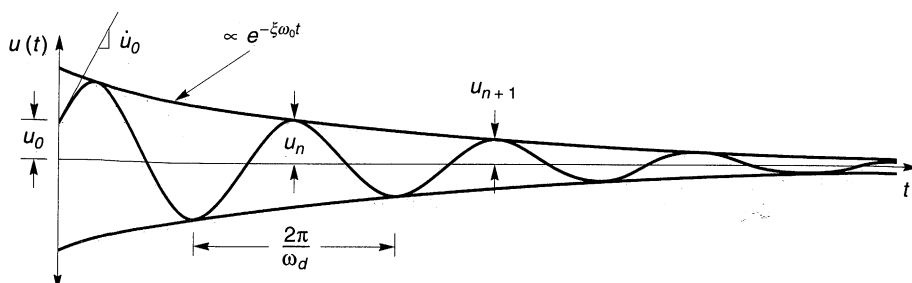


Figure B.8 Time history of damped free vibration with initial displacement u_0 and initial velocity \dot{u} .

Example B.2

The structure shown in Figure EB.2a is released from an initial displacement of 1 cm with an initial velocity of -5 cm/sec. Compute (a) the damped natural frequency and (b) the time history of response of the mass.

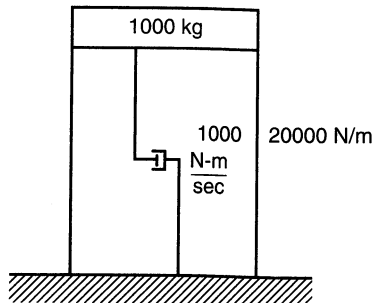


Figure EB2.a

Solution (a) The undamped natural frequency is

$$f_0 = \frac{\omega_0}{2\pi} = \frac{1}{2\pi\sqrt{\frac{k}{m}}} = \frac{1}{2\pi\sqrt{\frac{20000 \text{ N/m}}{1000 \text{ kg}}}} = 0.71 \text{ Hz}$$

and the damping ratio is

$$\xi = \frac{c}{2\sqrt{km}} = \frac{1000 \text{ N-m/sec}}{2\sqrt{(20000 \text{ N/m})(1000 \text{ kg})}} = 0.118$$

Then

$$f_d = f_0\sqrt{1 - \xi^2} = (0.71 \text{ Hz})\sqrt{1 - (0.118)^2} = 0.70 \text{ Hz}$$

(b) The undamped and damped natural circular frequencies will be $\omega_0 = 2\pi f_0 = 4.47$ rad/sec and $\omega_d = f_d/2\pi = 0.70/2\pi = 0.118$ rad/sec, respectively. From equation (B.20), the displacement response is

$$\begin{aligned} u &= e^{-\xi\omega_0 t} \left(\frac{\dot{u}_0 + \xi\omega_0 u_0}{\omega_d} \sin \omega_d t + u_0 \cos \omega_d t \right) \\ &= \exp[-(0.118)(4.47)t] \left[\frac{-0.05 + (0.118)(4.47)(0.01)}{4.47} \sin(4.47t) + (1) \cos(4.47t) \right] \\ &= e^{-0.527t} [\cos(4.47t) - 0.010 \sin(4.47t)] \end{aligned}$$

which is plotted in Figure EB.2b.

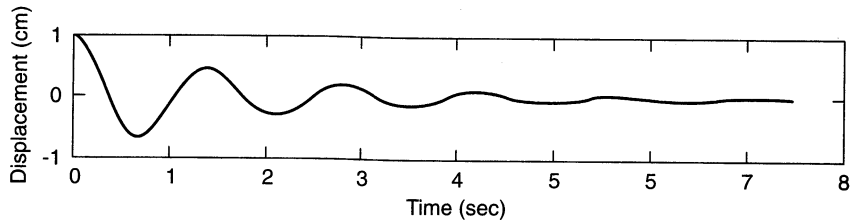


Figure EB.2b

B.5.3 Response of SDOF Systems to Harmonic Loading

A SDOF system is said to undergo forced vibration when acted upon by some external dynamic force, $Q(t)$. Dynamic loading may come from many different sources and may be

periodic or nonperiodic. For problems of soil and structural dynamics, the response to harmonic loading is very important. One form of simple harmonic loading $Q(t)$ can be expressed as $Q(t) = Q_0 \sin \bar{\omega}t$, where Q_0 is the amplitude of the harmonic load and $\bar{\omega}$ is the circular frequency at which the load is applied.

B.5.3.1 Undamped Forced Vibrations

The equation of motion for an undamped system subjected to such simple harmonic loading is

$$m\ddot{u} + ku = Q_0 \sin \bar{\omega}t \quad (\text{B.24})$$

The general solution to this equation of motion is given by the sum of the *complementary solution* (for the homogeneous case in which the right side of the equation is zero) and the *particular solution* [which must satisfy the right side of equation (B.24)].

The homogeneous equation is

$$m\ddot{u} + ku = 0$$

so the complementary solution is simply the solution to the undamped free vibration problem

$$u_c(t) = C_1 \sin \omega_0 t + C_2 \cos \omega_0 t \quad (\text{B.25})$$

The portion of the response described by the complementary solution is that which results from the initial conditions of the system. It consists of a simple harmonic oscillation at the undamped natural frequency of the system.

The particular solution describes the portion of the response caused by the external loading. This portion of the response can be assumed to be of the same form and to be in phase with the harmonic loading; thus

$$u_p(t) = U_0 \sin \bar{\omega}t \quad (\text{B.26})$$

where U_0 is the amplitude of the harmonic response. Substituting equation (B.26) into equation (B.24) yields

$$-m\bar{\omega}^2 U_0 \sin \bar{\omega}t + kU_0 \sin \bar{\omega}t = Q_0 \sin \bar{\omega}t \quad (\text{B.27})$$

Substituting $k/m = \omega_0^2$ and rearranging gives

$$U_0 = \frac{Q_0/k}{1 - \bar{\omega}^2/\omega_0^2} = \frac{Q_0/k}{1 - \beta^2} \quad (\text{B.28})$$

where $\beta = \bar{\omega}/\omega_0$ is referred to as the *tuning ratio*. Now the general solution of the equation of motion can be obtained by combining the complementary and particular solutions:

$$u(t) = u_c(t) + u_p(t) = C_1 \sin \omega_0 t + C_2 \cos \omega_0 t + \frac{Q_0/k}{1 - \beta^2} \sin \bar{\omega}t \quad (\text{B.29})$$

The general solution must satisfy the initial conditions. From equation (B.29), the velocity can be written as

$$\dot{u}(t) = \frac{du}{dt} = \omega_0 C_1 \cos \omega_0 t - \omega_0 C_2 \sin \omega_0 t + \bar{\omega} \frac{Q_0/k}{1 - \beta^2} \cos \bar{\omega}t \quad (\text{B.30})$$

For a given initial displacement, u_0 , and initial velocity, \dot{u}_0 ,

$$u_0 = C_1 \sin \omega_0(0) + C_2 \cos \omega_0(0) + \frac{Q_0/k}{1 - \beta^2} \sin \bar{\omega}(0) = C_2 \quad (\text{B.31})$$

and

$$\begin{aligned} \dot{u}_0 &= \omega_0 C_1 \cos \omega_0(0) - \omega_0 C_2 \sin \omega_0(0) + \bar{\omega} \frac{Q_0/k}{1 - \beta^2} \cos \bar{\omega}(0) = \omega_0 C_1 \\ &\quad + \bar{\omega} \frac{Q_0/k}{1 - \beta^2} \end{aligned} \quad (\text{B.32})$$

from which

$$C_1 = \frac{\dot{u}_0 - \bar{\omega}[(Q_0/k)/(1 - \beta^2)]}{\omega_0} = \frac{\dot{u}_0}{\omega_0} - \frac{Q_0 \beta}{k(1 - \beta^2)} \quad (\text{B.33})$$

Now the general response can finally be written as

$$u = \left[\frac{\dot{u}_0}{\omega_0} - \frac{Q_0 \beta}{k(1 - \beta^2)} \right] \sin \omega_0 t + u_0 \cos \omega_0 t + \frac{Q_0/k}{1 - \beta^2} \sin \bar{\omega} t \quad (\text{B.34})$$

It is interesting to consider the case in which the system is initially at rest in its equilibrium position, (i.e., $u_0 = \dot{u}_0 = 0$). For this case the response is given by

$$u = \frac{Q_0}{k} \frac{1}{1 - \beta^2} (\sin \bar{\omega} t - \beta \sin \omega_0 t) \quad (\text{B.35})$$

which indicates that the response has two components. One component occurs in response to the applied loading and occurs at the frequency of the applied loading. The other is a free vibration effect induced by the initial conditions; it occurs at the natural frequency of the system. It is useful to realize that the term Q_0/k in equation (B.35) represents the displacement of the mass that would occur if the load Q_0 was applied statically. The term $1/(1 - \beta^2)$ can then be thought of as a magnification factor that describes the amount by which the static displacement amplitude is magnified by the harmonic load. The magnification factor varies with the tuning ratio, β , as shown in Figure B.9. Note that the displacement amplitude is greater than the static displacement for loading frequencies lower than $\sqrt{2} \omega_0$. At higher loading frequencies, the displacement amplitude is less than the static displacement and can become very small at high frequencies. However, the response of an undamped SDOF system becomes very large as $\bar{\omega}$ approaches ω_0 . When harmonic loading is applied at the natural frequency of an undamped SDOF system, the response goes to infinity indicating *resonance* of the system. However, since truly undamped systems do not exist, true resonance is never really achieved. The concept of the tuning ratio that relates the frequency of loading to the natural frequency of the system is an important one, as evidenced by its strong influence on the response.

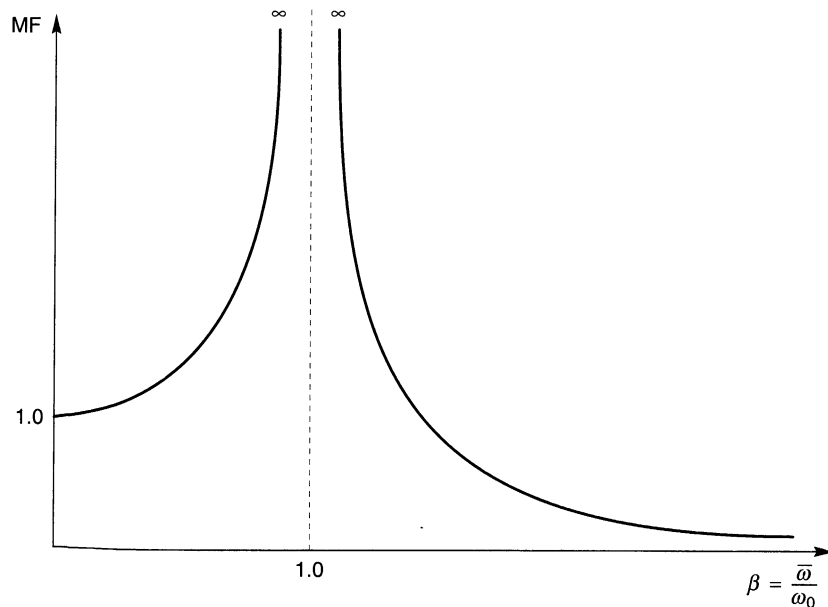


Figure B.9 Variation of magnification factor with tuning ratio for undamped SDOF system.

Example B.3

From an initial stationary state, the undamped SDOF system of Example B.1 is subjected to a harmonic base acceleration of $0.20g$ at a frequency of 2 Hz. Compute the response of the system.

Solution Expressing the base motion as

$$\ddot{u}_b(t) = (0.2)(32.2 \text{ ft/sec}^2) \sin 4\pi t = 6.44 \sin 4\pi t$$

the equivalent external force would be

$$Q(t) = -\frac{W}{g} \ddot{u}_b(t) = -\frac{10,000 \text{ lb}}{32.2 \text{ ft/sec}^2} (6.44 \text{ ft/sec}^2) \sin 4\pi t = -(2000 \text{ lb}) \sin 4\pi t$$

The tuning ratio would be

$$\beta = \frac{\bar{\omega}}{\omega_0} = \frac{2\pi f}{\omega_0} = \frac{2\pi(2)}{69.5} = 0.181$$

Then, from equation (B.35),

$$\begin{aligned} u(t) &= \frac{Q_0}{k} \frac{1}{1-\beta^2} (\sin \bar{\omega}t - \beta \sin \omega_0 t) \\ &= \frac{-2 \text{ kips}}{1500 \text{ kips/ft}} \frac{1}{1-(0.181)^2} [\sin 4\pi t - 0.181 \sin (69.5t)] \\ &= 0.00138 \sin 4\pi t - 0.00025 \sin 69.5t \end{aligned}$$

which is plotted in Figure EB.3.

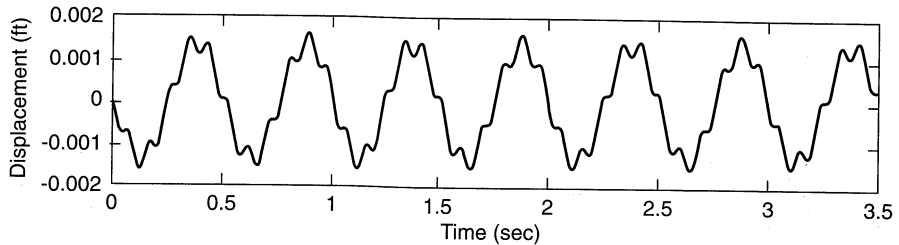


Figure EB.3

B.5.3.2 Damped Forced Vibrations

The most general case is that of a damped system subjected to forced harmonic loading. Each of the three prior cases can be considered as a subset of this one since their equations of motion can be obtained by setting various terms of the equation of motion for damped forced vibrations shown below to zero. The equation of motion for a damped SDOF system subjected to simple harmonic loading of the form $Q(t) = Q_0 \sin \bar{\omega}t$ is

$$m\ddot{u} + c\dot{u} + ku = Q_0 \sin \bar{\omega}t \quad (\text{B.36})$$

After dividing by m and using the relationships $\xi = c/2m\omega_0$ and $\omega_0^2 = k/m$, equation (B.36) can be rewritten as

$$\ddot{u} + 2\xi\omega_0\dot{u} + \omega_0^2 u = \frac{Q_0}{m} \sin \bar{\omega}t \quad (\text{B.37})$$

The complementary solution represents the damped free vibration response, which was expressed for an underdamped system by equation (B.19).

$$u_c(t) = e^{-\xi\omega_0 t} (C_1 \sin \omega_d t + C_2 \cos \omega_d t)$$

Since the response of a damped SDOF system is generally out of phase with the external loading, a harmonic particular solution of the form

$$u_p(t) = C_3 \sin \bar{\omega}t + C_4 \cos \bar{\omega}t \quad (\text{B.38a})$$

can be assumed. The corresponding velocity and acceleration are

$$\dot{u}_p(t) = C_3 \bar{\omega} \cos \bar{\omega}t - C_4 \bar{\omega} \sin \bar{\omega}t \quad (\text{B.38b})$$

$$\ddot{u}_p(t) = -\bar{\omega}^2 C_3 \sin \bar{\omega}t - \bar{\omega}^2 C_4 \cos \bar{\omega}t \quad (\text{B.38c})$$

Substituting equations (B.38) into the equation of motion [equation (B.37)] and grouping the $\sin \bar{\omega}t$ and $\cos \bar{\omega}t$ terms gives

$$(C_3 \omega_0^2 - C_3 \bar{\omega}^2 - 2\xi\omega_0 C_4 \bar{\omega}) \sin \bar{\omega}t + (C_4 \omega_0^2 - C_4 \bar{\omega}^2 + C_3 \bar{\omega} 2\xi\omega_0) \cos \bar{\omega}t = \frac{Q_0}{m} \sin \bar{\omega}t \quad (\text{B.39})$$

Now, at the instances where $\bar{\omega}t = 0 + n\pi$ (where n is any positive integer), $\sin \bar{\omega}t = 0$ and $\cos \bar{\omega}t = 1$. Thus the relationship

$$C_4\omega_0^2 - C_4\bar{\omega}^2 + C_3\bar{\omega}2\xi\omega_0 = 0 \quad (\text{B.40a})$$

must be satisfied. Further, at $\bar{\omega}t = \pi/2 + n\pi$, $\cos \bar{\omega}t = 0$ and $\sin \bar{\omega}t = 1$, which means that

$$C_3\omega_0^2 - C_3\bar{\omega}^2 - 2\xi\omega_0C_4\bar{\omega} = \frac{Q_0}{m} \quad (\text{B.40b})$$

must also be satisfied. Equations (B.40) represent two simultaneous equations with the two unknowns C_3 and C_4 . Solving for the unknowns yields

$$C_3 = \frac{Q_0}{k} \frac{1 - \beta^2}{(1 - \beta^2)^2 + (2\xi\beta)^2} \quad (\text{B.41a})$$

$$C_4 = \frac{Q_0}{k} \frac{-2\xi\beta}{(1 - \beta^2)^2 + (2\xi\beta)^2} \quad (\text{B.41b})$$

The general solution to the equation of motion for damped forced vibration can now be obtained by combining the complementary and particular solutions

$$\begin{aligned} u(t) &= e^{-\xi\omega_0 t} (C_1 \sin \omega_d t + C_2 \cos \omega_d t) \\ &\quad + \frac{Q_0}{k} \frac{1}{(1 - \beta^2)^2 + (2\xi\beta)^2} [(1 - \beta^2) \sin \bar{\omega}t - 2\xi\beta \cos \bar{\omega}t] \end{aligned} \quad (\text{B.42})$$

where the constants C_1 and C_2 depend on the initial conditions. There are several important characteristics of this solution. Note that the complementary solution (which represents the effects of the initial conditions) decays with time. The complementary solution therefore describes a *transient response* caused by the requirement of satisfying the initial conditions. After the transient response dies out, only the *steady-state response* described by the particular solution remains. The steady-state response occurs at the frequency of the applied harmonic loading but is out of phase with the loading.

Example B.4

The SDOF system shown in Figure EB.4a is at rest when the sinusoidal load is applied. Determine the transient, steady state, and total motion of the system.

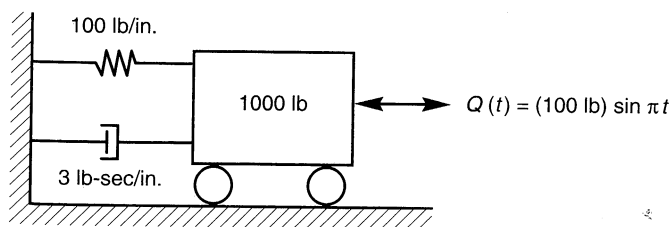


Figure EB.4a

Solution From equation (B.42), the total response is given by

$$u(t) = e^{-\xi\omega_0 t} (C_1 \sin \omega_d t + C_2 \cos \omega_d t) + \frac{Q_0}{k} \frac{1}{(1-\beta^2)^2 + (2\xi\beta)^2} [(1-\beta^2) \sin \bar{\omega}t - 2\xi\beta \cos \bar{\omega}t]$$

For zero initial displacement,

$$\begin{aligned} u(t=0) &= 0 \\ &= e^{-\xi\omega_0(0)} [C_1 \sin \omega_d(0) + C_2 \cos \omega_d(0)] \\ &\quad + \frac{Q_0}{k} \frac{1}{(1-\beta^2)^2 + (2\xi\beta)^2} [(1-\beta^2) \sin \bar{\omega}(0) - 2\xi\beta \cos \bar{\omega}(0)] \\ &= C_2 + \frac{Q_0}{k} \frac{-2\xi\beta}{(1-\beta^2)^2 + (2\xi\beta)^2} \end{aligned}$$

or

$$C_2 = \frac{Q_0}{k} \frac{2\xi\beta}{(1-\beta^2)^2 + (2\xi\beta)^2}$$

For zero initial velocity,

$$\begin{aligned} \dot{u} &= 0 \\ &= \omega_d e^{-\xi\omega_0(0)} [C_1 \cos \omega_d(0) - C_2 \sin \omega_d(0)] - \xi\omega_0 e^{-\xi\omega_0 t} [C_1 \sin \omega_d(0) - C_2 \cos \omega_d(0)] \\ &\quad + \frac{Q_0}{k} \frac{\bar{\omega}}{(1-\beta^2)^2 + (2\xi\beta)^2} [(1-\beta^2) \cos \bar{\omega}(0) + 2\xi\beta \sin \bar{\omega}(0)] \\ &= \omega_d C_1 - \xi\omega_0 C_2 + \frac{Q_0}{k} \frac{\bar{\omega}(1-\beta^2)}{(1-\beta^2)^2 + (2\xi\beta)^2} \end{aligned}$$

or

$$C_1 = \frac{Q_0}{k} \frac{\bar{\omega}}{\omega_d} \frac{\beta^2 - 1}{(1-\beta^2)^2 + (2\xi\beta)^2}$$

Then the transient motion is given by

$$u_c(t) = \frac{Q_0}{k} \frac{1}{(1-\beta^2)^2 + (2\xi\beta)^2} e^{-\xi\omega_0 t} \left[\frac{\bar{\omega}}{\omega_d} (\beta^2 + 2\xi^2 - 1) \sin \omega_d t + 2\xi\beta \cos \omega_d t \right]$$

and the steady-state motion by

$$u_p(t) = \frac{Q_0}{k} \frac{1}{(1-\beta^2)^2 + (2\xi\beta)^2} [(1-\beta^2) \sin \bar{\omega}t - 2\xi\beta \cos \bar{\omega}t]$$

The total motion is the sum of the transient and steady-state motions. For the system shown in Figure EB.1a,

$$\omega_0 = \sqrt{\frac{k}{m}} = \sqrt{\frac{kg}{W}} = \sqrt{\frac{(100 \text{ lb/in.})(12 \text{ in./ft})(32.2 \text{ ft/sec/sec})}{1000 \text{ lb}}} = 6.22 \text{ rad/sec}$$

$$\xi = \frac{c}{2m\omega_0} = \frac{cg}{2W\omega_0} = \frac{(3 \text{ lb-sec/in.})(12 \text{ in./ft})(32.2 \text{ ft/sec/sec})}{2(1000 \text{ lb})(6.22 \text{ rad/sec})} = 0.093$$

$$\omega_d = \omega_0 \sqrt{1 - \xi^2} = \sqrt{1 - (0.092)^2} = 6.19 \text{ rad/sec}$$

$$\beta = \frac{\bar{\omega}}{\omega_0} = \frac{\pi \text{ rad/sec}}{6.22 \text{ rad/sec}} = 0.505$$

Substituting these values into the solutions gives the response shown in Figure EB.4b

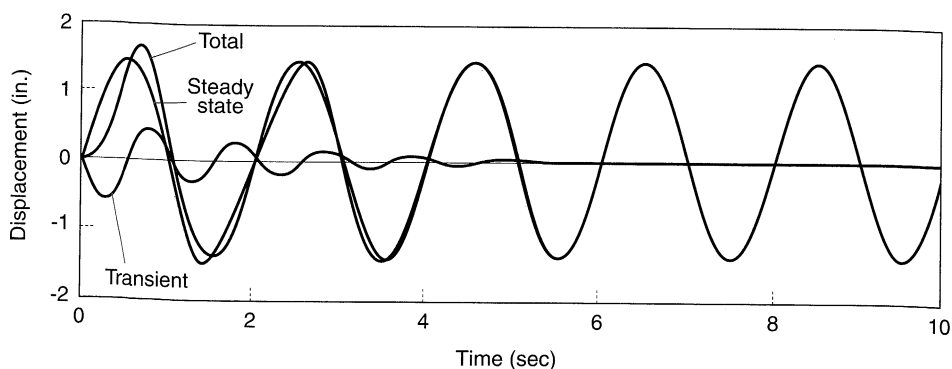


Figure EB.4b

The steady-state response could also be described by

$$u = A \sin(\bar{\omega}t + \phi) \quad (\text{B.43})$$

where

$$A = \frac{Q_0}{k} \frac{1}{\sqrt{(1-\beta^2)^2 + (2\xi\beta)^2}}$$

$$\phi = \tan^{-1}\left(-\frac{2\xi\beta}{1-\beta^2}\right)$$

The steady-state response can be visualized with the aid of rotating vectors, both for the response and for the forces induced in the system, as shown in Figure B.10. Note that the spring, dashpot, and inertial forces act opposite to the displacement, velocity and acceleration vectors, and that the displacement lags the applied loading vector by the negative phase

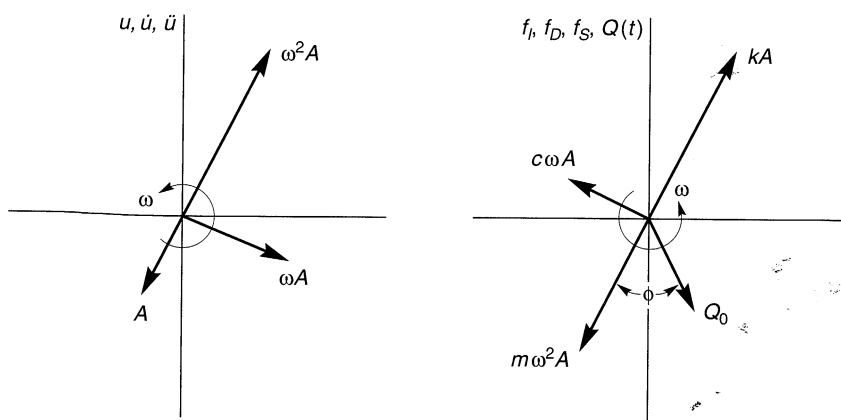


Figure B.10 Rotating vector representation of response and forces in vibrating SDOF system.

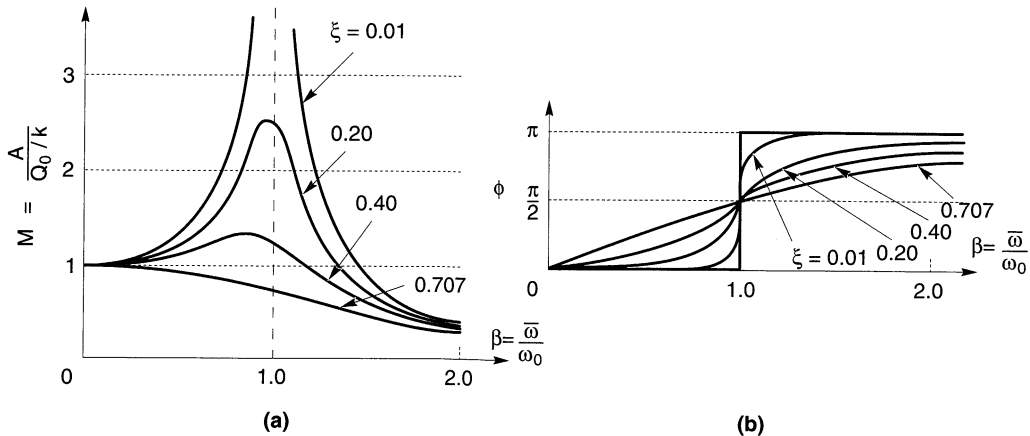


Figure B.11 Variation of (a) magnification factor, and (b) phase angle with damping ratio and tuning ratio.

angle, ϕ . For harmonic loading the phase angle varies with both damping ratio and tuning ratio, as shown in Figure B.11a.

The influence of the tuning ratio can be illustrated by the use of the magnification factor, again defined as the ratio of the amplitude to the static displacement:

$$M = \frac{A}{Q_0/k} = \frac{1}{\sqrt{(1-\beta^2)^2 + (2\xi\beta)^2}} \quad (\text{B.44})$$

The variation of the magnification factor with tuning ratio and damping ratio is shown in Figure B.11b. The damping ratio influences the peak magnification factor and also the variation of magnification factor with frequency. The magnification factor curves broaden with increasing damping ratio. Note that the magnification is unbounded (resonance) only for $\xi = 0$ and $\beta = 1$. For nonzero damping, there is some maximum magnification, M_{\max} ,

$$M_{\max} = \frac{1}{2\xi\sqrt{1-\xi^2}} \quad (\text{B.45})$$

which occurs when the tuning ratio $\beta = \sqrt{1-2\xi^2}$. The shape of the magnification curve is obviously controlled by the damping ratio. Although a system with low damping may produce large magnification at a tuning ratio near 1, it will exhibit significant magnification over a smaller range of frequencies than a system with higher damping.

B.5.4 Response of SDOF Systems to Periodic Loading

The solutions for the response of a SDOF system to harmonic loading developed in the preceding section can be used to develop solutions for the more general case of periodic loading. As shown in Appendix A, periodic loading can be approximated by a Fourier series (i.e., as the sum of a series of harmonic loads). The response of a SDOF system to the periodic loading, using the principle of superposition, is simply the sum of the responses to each term in the loading series. The required calculations can be performed using trigonometric or exponential notation.

B.5.4.1 Trigonometric Notation

From equation (A.11) a periodic load, $Q(t)$, can be expressed by the Fourier series

$$Q(t) = a_0 + \sum_{n=1}^{\infty} a_n \cos \omega_n t + b_n \sin \omega_n t$$

where the *Fourier coefficients* are

$$\begin{aligned} a_0 &= \frac{1}{T_f} \int_0^{T_f} Q(t) dt \\ a_n &= \frac{2}{T_f} \int_0^{T_f} Q(t) \cos \omega_n t dt \\ b_n &= \frac{2}{T_f} \int_0^{T_f} Q(t) \sin \omega_n t dt \end{aligned}$$

and $\omega_n = 2\pi n/T_f$. Using the steady-state portion of equation (B.42), the response to each sine term in the Fourier series is

$$u_{n, \sin}(t) = \frac{b_n}{k} \frac{1}{(1 - \beta_n^2)^2 + (2\xi\beta_n)^2} [(1 - \beta_n^2) \sin \bar{\omega}t - 2\xi\beta_n \cos \bar{\omega}t]$$

where $\beta_n = \omega_n T_f / 2\pi$. In the same way, the steady-state response to each cosine term can be shown to be

$$u_{n, \cos}(t) = \frac{a_n}{k} \frac{1}{(1 - \beta_n^2)^2 + (2\xi\beta_n)^2} [(1 - \beta_n^2) \cos \bar{\omega}t + 2\xi\beta_n \sin \bar{\omega}t]$$

Since the steady-state response to the constant load term is the static displacement, $u_0 = a_0/k$, the total steady-state response is given by

$$\begin{aligned} u(t) &= u_0 + \sum_{n=1}^{\infty} u_{n, \sin}(t) + u_{n, \cos}(t) \\ &= \frac{1}{k} \left(a_0 + \sum_{n=1}^{\infty} \frac{1}{(1 - \beta_n^2)^2 + (2\xi\beta_n)^2} \{ [a_n 2\xi\beta_n + b_n (1 - \beta_n^2)] \sin \omega_n t \right. \\ &\quad \left. + [a_n (1 - \beta_n^2) - b_n 2\xi\beta_n] \cos \omega_n t \} \right) \end{aligned} \quad (\text{B.46})$$

B.5.4.2 Exponential Notation

Periodic loading can also be described by the Fourier series in exponential form. Using equation (A.15), a periodic load can be expressed as

$$Q(t) = \sum_{n=-\infty}^{\infty} q_n^* e^{i\omega_n t}$$

The complex Fourier coefficients, q_n^* , can be determined directly from $Q(t)$ as

$$q_n^* = \frac{1}{T_f} \int_0^{T_f} Q(t) e^{-i\omega_n t} dt$$

The response of a SDOF system loaded by the n th harmonic would be governed by the equation of motion

$$m\ddot{u}_n(t) + (c\dot{u}_n(t) + ku_n(t)) = q_n^* e^{i\omega_n t} \quad (\text{B.47})$$

The response of the system can be related to the loading by

$$u_n(t) = H(\omega_n) q_n^* e^{i\omega_n t} \quad (\text{B.48})$$

where $H(\omega_n)$ is a *transfer function* [i.e., a function that relates one parameter (in this case, the displacement of the oscillator) to another (the external load)]. Substituting equation (B.48) into the equation of motion gives

$$-m\omega_n^2 H(\omega_n) q_n^* e^{i\omega_n t} + ic\omega_n H(\omega_n) q_n^* e^{i\omega_n t} + kH(\omega_n) q_n^* e^{i\omega_n t} = q_n^* e^{i\omega_n t}$$

or

$$H(\omega_n) = \frac{1}{-m\omega_n^2 + ic\omega_n + k} = \frac{1}{k(-\beta_n^2 + 2i\beta_n\xi + 1)} \quad (\text{B.49})$$

Since $A^* = a + ib = Ae^{i\theta}$, where the *modulus*, $A = \sqrt{a^2 + b^2}$, and the *argument*, $\theta = \tan^{-1}(b/a)$, the transfer function can also be written as

$$H(\omega_n) = \frac{1/k}{\sqrt{(1 - \beta_n^2)^2 + (2\xi\beta_n)^2}} \exp\left(i \tan^{-1} \frac{2\xi\beta_n}{\beta_n^2 - 1}\right)$$

Note the close relationship between the modulus of the transfer function and the magnification factor of equation (B.44). Because the transfer function can be used for any frequency in the series, the principle of superposition gives the total response as

$$u(t) = \sum_{n=-\infty}^{\infty} H(\omega_n) q_n^* e^{i\omega_n t} \quad (\text{B.50})$$

Many different transfer functions can be developed. For example, a transfer function relating the acceleration of the SDOF system to the external load could have been developed just as easily. The advantages of the transfer function approach lie in its simplicity and in the ease with which it allows computation of the response to complicated loading patterns.

The transfer function may be viewed as a *filter* that acts upon some input signal to produce an output signal. In the case just considered, the input signal was the time history of loading, $Q(t)$, and the output was the displacement, $u(t)$. If the input signal has Fourier amplitude and phase spectra, $F_i(\omega_n)$ and $\phi_i(\omega_n)$, the Fourier amplitude spectra of the output signal will be given by

$$F_o(\omega_n) = H(\omega_n) F_i(\omega_n) \quad (\text{B.51a})$$

$$\phi_o(\omega_n) = H(\omega_n) \phi_i(\omega_n) \quad (\text{B.51b})$$

Thus the procedure for Fourier analysis of SDOF system response can be summarized in the following steps:

1. Obtain the Fourier series for the applied loading (or base motion). In doing so, the loading (or base motion) is expressed as a function of frequency rather than a function of time.
2. Multiply the Fourier series coefficients by the appropriate value of the transfer function at each frequency, ω_n . This will produce the Fourier series of the output motion.
3. Express the output motion in the time domain by obtaining the inverse Fourier transform of the output motion.

It is precisely this approach that forms the backbone of several of the most commonly used methods for analysis of ground response and soil–structure interaction. These methods are presented in Chapter 7.

B.5.5 Response of SDOF Systems to General Loading

Not all loading is harmonic or even periodic. To determine the response of SDOF systems to general loading conditions, a more general solution of the equation of motion is required.

B.5.5.1 Response to Step Loading

Consider a damped SDOF system subjected to a step load of intensity, Q_0 , which is applied instantaneously at $t = 0$ and removed instantaneously at $t = t_1$ as shown in Figure B.12. For $t \leq t_1$, the complementary solution to the equation of motion for this system [equation (B.19)],

$$u_c(t) = e^{-\xi\omega_0 t} [C_1 \sin \omega_d t + C_2 \cos \omega_d t]$$

describes the transient response of the system. The equation of motion for the steady-state condition is given by

$$m\ddot{u}_p + c\dot{u}_p + ku_p = Q_0$$

Since the applied load does not vary with time, the steady-state response will be a constant displacement,

$$u_p(t) = \frac{Q_0}{k}$$

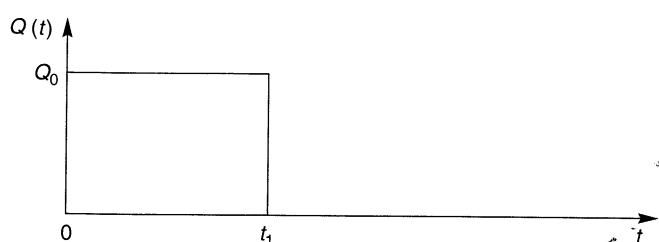


Figure B.12 Time history of step loading.

The general solution to the step loading problem for $t \leq t_1$ can then be written as

$$u(t) = \frac{Q_0}{k} + e^{-\xi\omega_0 t} (C_1 \sin \omega_d t + C_2 \cos \omega_d t) \quad (\text{B.52})$$

with free vibration occurring at $t > t_1$ (when no external load is applied). The constants are determined by the initial conditions, u_0 and \dot{u}_0 . At $t = 0$,

$$\begin{aligned} u_0 &= \frac{Q_0}{k} + e^{-\xi\omega_0(0)} [C_1 \sin \omega_d(0) + C_2 \cos \omega_d(0)] = \frac{Q_0}{k} + C_2 \\ \dot{u}_0 &= e^{-\xi\omega_0(0)} [\omega_d C_1 \cos \omega_d(0) - \omega_d C_2 \sin \omega_d(0)] \\ &\quad - \xi\omega_0 e^{-\xi\omega_0(0)} [C_1 \sin \omega_d(0) + C_2 \cos \omega_d(0)] = \omega_d C_1 - \xi\omega_0 C_2 \end{aligned}$$

from which

$$\begin{aligned} C_1 &= \frac{\dot{u}_0 + \xi\omega_0(u_0 - Q_0/k)}{\omega_d} \\ C_2 &= u_0 - \frac{Q_0}{k} \end{aligned}$$

so that

$$u(t) = \frac{Q_0}{k} + e^{-\xi\omega_0 t} \left[\frac{\dot{u}_0 + \xi\omega_0(u_0 - Q_0/k)}{\omega_d} \sin \omega_d t + \left(u_0 - \frac{Q_0}{k} \right) \cos \omega_d t \right] \quad (\text{B.53})$$

describes the response of the system up to the beginning of free vibration at $t = t_1$.

B.5.5.2 Dirac Pulse

A particular type of step loading can be described using a Dirac delta function. A Dirac delta function is one whose value is zero at all values of u except one at which it goes to infinity in such a way that the area under the function is unity. Mathematically, the Dirac delta function satisfies the conditions

$$\delta(x) = \begin{cases} 0 & \text{for } x \neq a \\ \infty & \text{for } x = a \end{cases} \quad (\text{B.54a})$$

$$\int_{-\infty}^{\infty} \delta(x) dx = 1 \quad (\text{B.54b})$$

Define a Dirac pulse as a constant force Q_0 applied over a duration t_1 that approaches zero as shown in Figure B.13. From impulse-momentum principles, $Q_0 t_1 = m\dot{u}_0(t_1)$. As t_1 approaches zero, the effect of the Dirac pulse is to cause an initial velocity $\dot{u}_0 = Q_0 t_1 / m$, with no initial displacement. Thus the steady-state response occurs only over an infinitesimal period of time, and the system is immediately set into free vibration. From equation (B.20), the response to a Dirac pulse disturbance at $t = 0$ is given by

$$u(t) = e^{-\xi\omega_0 t} \left(\frac{Q_0 t_1}{m\omega_d} \sin \omega_d t \right) \quad (\text{B.55})$$



Figure B.13 Dirac pulse loading.

B.5.5.3 Duhamel Integral

A general loading function such as that shown in Figure B.14 can be thought of as a train of load pulses, each of infinitesimal duration. Looking at one of these pulses, the pulse of duration $d\tau$ occurring at $t = \tau$ (Figure B.14), the response it causes at a later time, $t = \tilde{t}$, follows from equation (B.55):

$$du(\tilde{t}) = e^{-\xi\omega_0(\tilde{t}-\tau)} \frac{Q_0(\tau)d\tau}{m\omega_d} \sin \omega_d(\tilde{t}-\tau) \quad (\text{B.56})$$

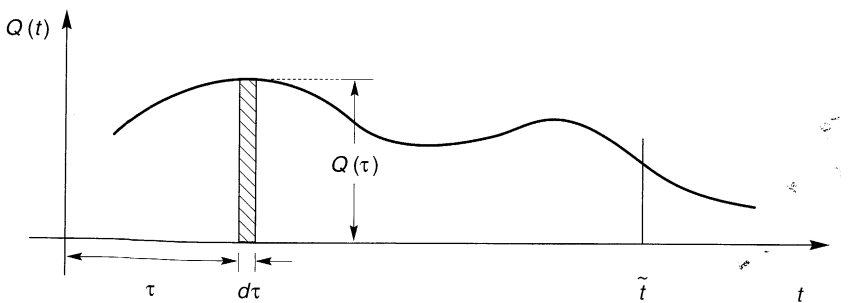
The response induced by the entire train of load pulses can be obtained by summing the responses of all of the individual pulses up to the time $t = \tilde{t}$, that is,

$$u(\tilde{t}) = \frac{1}{m\omega_d} \sum_{i=1}^n Q(\tau_i) \sin \omega_d(\tilde{t}-\tau_i) d\tau \quad (\text{B.57})$$

where n is the total number of pulses up to $t = \tilde{t}$. As dt approaches zero, the summation becomes an integral with which the total response can be calculated as

$$u(\tilde{t}) = \frac{1}{m\omega_d} \int_0^{\tilde{t}} Q(\tau) e^{-\xi\omega_0(\tilde{t}-\tau)} \sin \omega_d(\tilde{t}-\tau) d\tau \quad (\text{B.58})$$

This equation describing the response of a linear system is known as *Duhamel's integral*. It is usually very difficult to solve analytically, but can be integrated numerically by a variety of procedures. Its use, however, is constrained to linear systems.

Figure B.14 Pulse of duration $d\tau$ occurring at $t = \tau$.

B.6 DAMPING

Energy is dissipated in soils and structures by several mechanisms, including friction, heat generation, and plastic yielding. For specific soils and structures, however, the operative mechanisms are not understood sufficiently to allow them to be explicitly modeled. As a result, the effects of the various energy loss mechanisms are usually lumped together and represented by some convenient damping mechanism.

B.6.1 Viscous Damping

The most commonly used mechanism for representing energy dissipation is viscous damping. When a viscous damped SDOF system such as that shown in Figure B.3 is subjected to a harmonic displacement

$$u(t) = u_0 \sin \bar{\omega}t$$

the net force exerted on the mass by the spring and dashpot is

$$F(t) = ku(t) + c\dot{u}(t) = ku_0 \sin \bar{\omega}t + c\bar{\omega}u_0 \cos \bar{\omega}t$$

Evaluating these functions from time t_0 to time $t_0 + 2\pi/\bar{\omega}$ yields the force–displacement values for one cycle of a *hysteresis loop*. When the viscous damping coefficient, c , is zero, the force and displacement are in phase and proportional to each other, implying a linear elastic stress–strain relationship. For nonzero damping, however, the hysteresis loop is elliptical, as shown in Figure B.15. Note that when the displacement is zero, the spring force is zero and the net force comes entirely from the dashpot. Similarly, when the velocity is zero (at $\bar{\omega}t = \pi/2 + n\pi$), the dashpot force vanishes and the net force consists entirely of the spring force. The aspect ratio of the hysteresis loop decreases with increasing damping; the loop becomes a circle when $c = k/\bar{\omega}$.

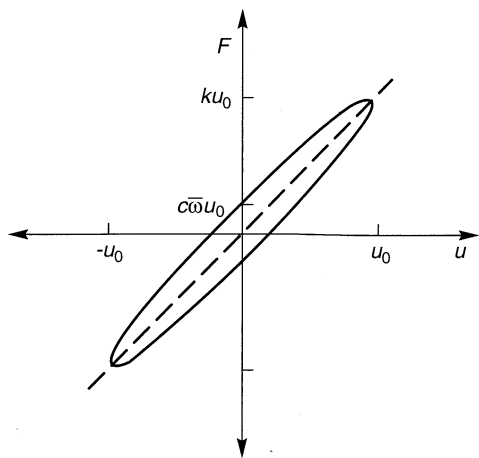


Figure B.15 Stress–strain behavior implied by viscous damping. Hysteresis loop is elliptical.

Obviously, the shape of the hysteresis loop depends on the viscous damping coefficient and therefore on the damping ratio. Hence we should be able to determine the damping ratio from a known hysteresis loop. The energy dissipated in one cycle of oscillation is given by the area inside the hysteresis loop and can be obtained from

$$W_D = \int_{t_0}^{t_0 + 2\pi/\bar{\omega}} F \frac{du}{dt} dt = \pi c \bar{\omega} u_0^2 \quad (\text{B.59})$$

At maximum displacement, the velocity is zero and the strain energy stored in the system is given by

$$W_S = \frac{1}{2} k u_0^2 \quad (\text{B.60})$$

Equations (B.59) and (B.60) show that $c = W_D / (\pi \bar{\omega} u_0^2)$ and $k = 2W_S / u_0^2$. Substituting these into equation (B.16) with $\bar{\omega} = \omega_0$ gives an expression

$$\xi = \frac{W_D}{4\pi W_S}$$

that is commonly used for graphical determination of the damping ratio from a measured hysteresis loop. Referring to Figure B.16, the damping ratio is taken as the ratio of the area of the hysteresis loop to the area of the shaded triangle, all divided by 4π . This graphical evaluation of the damping ratio is commonly used in the interpretation of many of the laboratory tests discussed in Chapter 6.

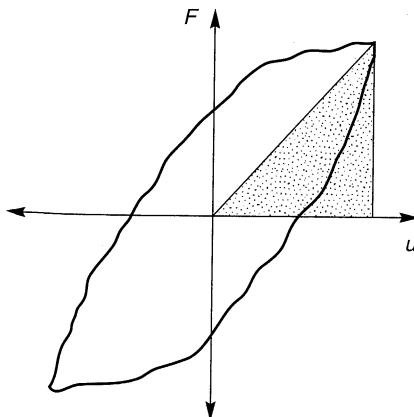


Figure B.16 Graphical evaluation of damping ratio from measured hysteresis loop. The damping ratio is proportional to the ratio of the shaded area to the area of the hysteresis loop.

The damping characteristics of a linear system can also be evaluated from its frequency response characteristics. Setting the magnification factor expression [equation (B.44)] equal to $M_{\max}/\sqrt{2}$, the *half-power tuning ratios*, shown in Figure B.17, can be approximated as

$$\beta_1 \approx 1 - \xi - \xi^2$$

$$\beta_2 \approx 1 + \xi - \xi^2$$

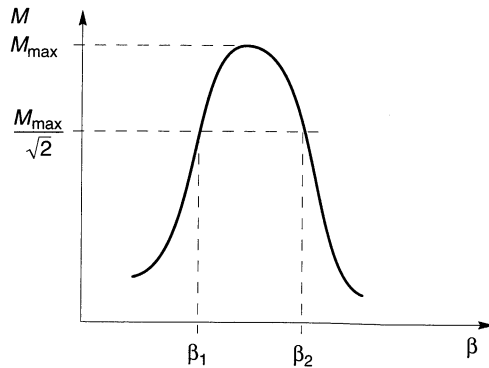


Figure B.17 Half-power tuning ratios for evaluation of damping ratio from magnification curve.

Therefore, the damping ratio is given by half the difference between the half-power tuning ratios

$$\xi \approx \frac{\beta_2 - \beta_1}{2} \quad (\text{B.61})$$

or, when the response is expressed in terms of frequency, where $\omega_1 = \beta_1 \omega_0$ and $\omega_2 = \beta_2 \omega_0$,

$$\xi \approx \frac{\omega_2 - \omega_1}{\omega_2 + \omega_1} \quad (\text{B.62})$$

Thus the damping ratio of a system can be measured by exciting the system at different frequencies and determining the amplitude of the magnification factor at each frequency.

B.6.2 Other Measures of Energy Dissipation

In addition to the damping ratio, ξ , a number of other parameters have been used to describe energy dissipation characteristics. Seismologists, for example, often work with the *quality factor*

$$Q = \frac{1}{2\xi} \quad (\text{B.63})$$

In vibration analysis, the *loss factor*

$$\eta = 2\xi \quad (\text{B.64})$$

and *specific damping capacity*

$$\psi = 2\pi\xi \quad (\text{B.65})$$

are often used (Goodman, 1988).

It is important to remember that the damping ratio, and any of these other parameters, are simply parameters used to describe the effects of phenomena that are often poorly understood. They allow the effects of energy dissipation to be represented in a mathematically convenient manner. For most soils and structures, however, energy is dissipated hysteretically (i.e., by yielding or plastic straining of the material). In such cases the behavior is more accurately characterized by evaluating the nonlinear response of the system.

B.6.3 Complex Stiffness

A viscously damped system can be represented conveniently in a different but equivalent way for a class of techniques known as *complex response analysis*. Consider a damped SDOF system subjected to simple harmonic loading of amplitude Q_0 and loading frequency $\bar{\omega}$. The loading can be represented by

$$Q(t) = Q_0 e^{i\bar{\omega}t} \quad (\text{B.66})$$

Assuming that $u(t) = U_0 e^{i\bar{\omega}t}$, the steady-state solution to the equation of motion

$$m\ddot{u} + c\dot{u} + ku = Q_0 e^{i\bar{\omega}t} \quad (\text{B.67})$$

is

$$u(t) = \frac{Q_0}{k - m\bar{\omega}^2 + ic\bar{\omega}} e^{i\bar{\omega}t} \quad (\text{B.68})$$

Now consider the SDOF system of Figure B.18, which has no dashpot but which has a spring of *complex stiffness* $k^* = k_1 + ik_2$. The equation of motion for this system is

$$m\ddot{u} + k^* u = Q_0 e^{i\bar{\omega}t} \quad (\text{B.69})$$

Again assuming that $u(t) = U_0 e^{i\bar{\omega}t}$, the steady-state solution can be expressed as

$$u(t) = \frac{Q_0}{k^* - \bar{\omega}^2 m} e^{i\bar{\omega}t} \quad (\text{B.70})$$

Comparing equations (B.68) and (B.70), it is apparent that

$$k^* = k + ic\bar{\omega} \quad (\text{B.71})$$

By the appropriate choice of k^* , the displacement amplitude of equation (B.70) can be made equal to that of equation (B.68), (although a small phase difference between the two solutions will remain). To accomplish this, the complex stiffness is represented as

$$k^* = k(1 - 2\xi^2 + 2i\xi\sqrt{1 - \xi^2}) \quad (\text{B.72})$$

where $\xi \leq 1$. For the usual small damping ratios considered in earthquake engineering problems, the ξ^2 terms can be neglected so that $k^* \approx k(1 + 2i\xi)$. Using this expression for k^* , the error in phase angle between the responses given by equations (B.68) and (B.70) is $\Delta\theta \approx 2\xi/(1 + \beta)$. As a result, a viscously damped system can be represented as an undamped system with complex stiffness. The use of this approach, however, is restricted to cases of harmonic motion. For problems in which loading is characterized as periodic (and therefore as the sum of a series of harmonic loads), the use of complex stiffness greatly simplifies calculation of the response of damped systems.

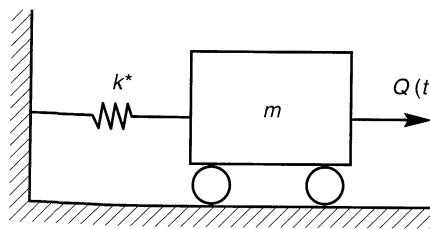


Figure B.18 SDOF system with spring of complex stiffness.

For small damping ratios, the complex stiffness then consists of real and imaginary parts

$$\operatorname{Re}(k^*) = k \quad (\text{B.73a})$$

$$\operatorname{Im}(k^*) = 2k\xi \quad (\text{B.73b})$$

Consequently, the damping ratio can be expressed as

$$\xi = \frac{\operatorname{Im}(k^*)}{2\operatorname{Re}(k^*)} \quad (\text{B.74})$$

which is useful to remember in the interpretation of quantities such as complex impedance functions, which are usually expressed in terms of their real and imaginary parts.

B.7 RESPONSE SPECTRA

For earthquake-resistant design, the entire time history of response may not be required. Instead, earthquake-resistant design may be based on the maximum (absolute) value of the response of a structure to a particular base motion. Obviously, the response will depend on the mass, stiffness, and damping characteristics of the structure and on the characteristics of the base motion.

The *response spectrum* describes the maximum response of a single-degree-of-freedom (SDOF) system to a particular input motion as a function of the natural frequency (or natural period) and damping ratio of the SDOF system (Figure B.19). The response may be expressed in terms of acceleration, velocity, or displacement. The maximum values of each of these parameters depend only on the natural frequency and damping ratio of the SDOF

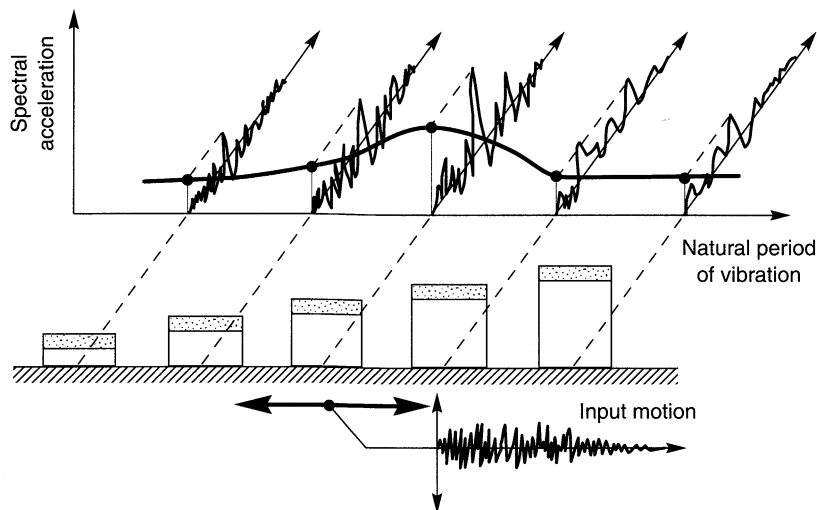


Figure B.19 Response spectrum. Spectral accelerations are the maximum acceleration amplitudes of SDOF systems in response to the same input motion. The response system is obtained by plotting the spectral accelerations against the periods of vibrations of the SDOF systems.

system (for a particular input motion). The maximum values of acceleration, velocity, and displacement are referred to as the spectral acceleration (S_a), spectral velocity (S_v), and spectral displacement (S_d), respectively. Note that a SDOF system of zero natural period (infinite natural frequency) would be rigid, and its spectral acceleration would be equal to the peak ground acceleration.

Application of the Duhamel integral to a linear elastic SDOF system produces expressions for the acceleration, velocity, and displacement time histories that are proportional (by a factor of ω), except for a phase shift. Because the phase shift does not significantly influence the maximum response values, the spectral acceleration, velocity, and displacement can be approximately related to each other by the following simple expressions:

$$S_d = |u|_{\max} \quad (\text{B.75a})$$

$$S_v = |\dot{u}|_{\max} \approx \omega_0 S_d = \text{PSV} \quad (\text{B.75b})$$

$$S_a = |\ddot{u}|_{\max} \approx \omega_0^2 S_d = \omega_0 \cdot \text{PSV} = \text{PSA} \quad (\text{B.75c})$$

where u and ω_0 are the displacement and natural frequency of the SDOF system, PSV is the *pseudospectral velocity*, and PSA is the *pseudospectral acceleration*. Although the PSV and PSA are not the true maximum values of velocity and acceleration, they are usually very close to the maxima for recorded strong ground motions. In practice, the pseudospectral values are generally assumed to be equal to the spectral values.

B.8 RESPONSE OF NONLINEAR SDOF SYSTEMS TO GENERAL LOADING

Numerical integration of the Duhamel integral is very useful for calculation of the response of linear systems to general loading. Many systems for which the seismic response is to be calculated, however, exhibit nonlinear behavior. In such systems the mass is usually constant, but the damping coefficient and/or the stiffness may vary with time, deflection, or velocity. It will be useful to develop methods for analysis of the response of nonlinear systems, recognizing that they will be appropriate for linear systems as well when damping and stiffness values are held constant.

The most common approach to nonlinear analysis is the direct integration of *incremental equations of motion* that govern the response of the system over small time increments. The response is calculated for each time increment after adjusting the stiffness and damping at the beginning of the increment. By using the conditions at the end of one time increment as the initial conditions for the next time increment, the nonlinear system is approximated as an incrementally changing linear system.

B.8.1 Incremental Equation of Motion

Consider the SDOF system shown in Figure B.20, which has a nonlinear spring and dashpot (i.e., the spring force is not proportional to displacement and the dashpot force is not proportional to velocity). Dynamic equilibrium at time τ requires that

$$f_I(\tau) + f_D(\tau) + f_S(\tau) = Q(\tau) \quad (\text{B.76})$$

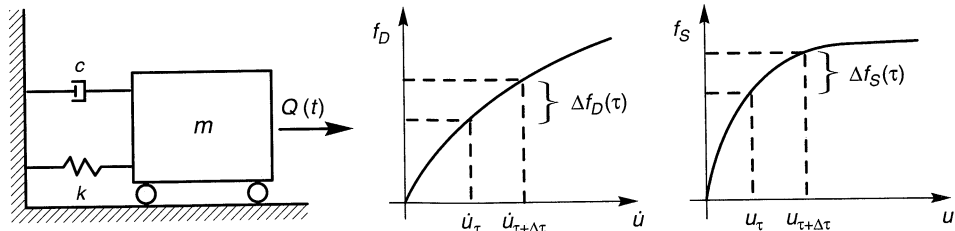


Figure B.20 SDOF system with nonlinear damping and spring forces.

and that

$$f_I(\tau + \Delta\tau) + f_D(\tau + \Delta\tau) + f_S(\tau + \Delta\tau) = Q(\tau + \Delta\tau) \quad (\text{B.77})$$

at time $\tau + \Delta\tau$. Defining

$$\Delta f_I(\tau) = f_I(\tau + \Delta\tau) - f_I(\tau)$$

$$\Delta f_D(\tau) = f_D(\tau + \Delta\tau) - f_D(\tau)$$

$$\Delta f_S(\tau) = f_S(\tau + \Delta\tau) - f_S(\tau)$$

$$\Delta Q(\tau) = Q(\tau + \Delta\tau) - Q(\tau)$$

and subtracting equation (B.76) from equation (B.77), the incremental equation of motion for the time interval from t to $\tau + \Delta\tau$ is

$$\Delta f_I(\tau) + \Delta f_D(\tau) + \Delta f_S(\tau) = \Delta Q(\tau) \quad (\text{B.78})$$

or expressing the incremental forces in terms of incremental displacements, velocities, and accelerations, as

$$m \Delta \ddot{u}(\tau) + c(\tau) \Delta \dot{u}(\tau) + k(\tau) \Delta u(\tau) = \Delta Q(\tau) \quad (\text{B.79})$$

By integrating this incremental equation of motion in a series of small time steps, the response of the nonlinear system can be obtained. It should be noted that this approach can be used to calculate the response of linear elastic, nonlinear elastic, or nonlinear inelastic materials with stress-strain behaviors shown in Figure B.21. The third of these is particularly important because it allows representation of the hysteretic damping displayed by cyclically loaded soils.

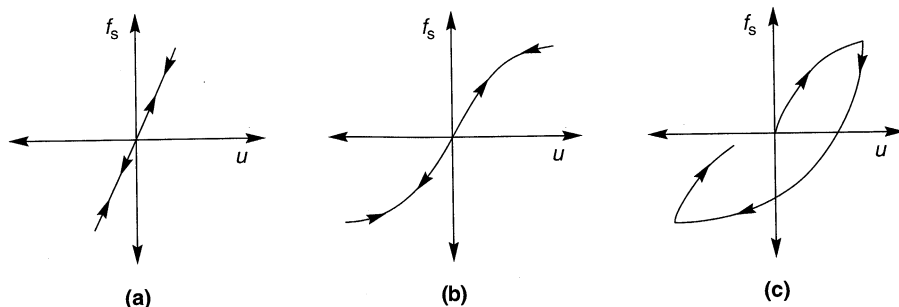


Figure B.21 Stress-strain behavior of (a) linear elastic, (b) nonlinear elastic, and (c) nonlinear inelastic materials under cyclic loading conditions.

B.8.2 Numerical Integration

There are many ways to numerically integrate the incremental equation of motion. One of the simplest and most easily coded of these is the *linear acceleration method*. It is based on the assumption that the acceleration varies linearly within each time increment. If the acceleration in the time increment varies linearly, the velocity and displacement will vary quadratically and cubically, respectively, as shown in Figure B.22. Therefore, expressions for the incremental velocity and displacement can be written in terms of the incremental acceleration, that is,

$$\Delta \ddot{u}(\tau) = \ddot{u}(\tau)\Delta t + \Delta \dot{u}(\tau) \frac{\Delta t}{2} \quad (\text{B.80})$$

$$\Delta u(\tau) = \dot{u}(\tau)\Delta t + \Delta \dot{u}(\tau) \frac{\Delta t^2}{2} + \Delta \ddot{u}(\tau) \frac{\Delta t^2}{6} \quad (\text{B.81})$$

Rearranging, the incremental acceleration and velocity can be expressed in terms of the incremental displacement

$$\Delta \ddot{u}(\tau) = \frac{6}{\Delta t^2} \Delta u(\tau) - \frac{6}{\Delta t} \dot{u}(\tau) - 3 \ddot{u}(\tau) \quad (\text{B.82a})$$

$$\Delta \dot{u}(\tau) = \frac{3}{\Delta t} \Delta u(\tau) - 3 \dot{u}(\tau) - \frac{\Delta t}{2} \ddot{u}(\tau) \quad (\text{B.82b})$$

Substituting equations (B.82) into the incremental equation of motion gives

$$m \left[\frac{6}{\Delta t^2} \Delta u(\tau) - \frac{6}{\Delta t} \dot{u}(\tau) - 3 \ddot{u}(\tau) \right] + c(\tau) \left[\frac{3}{\Delta t} \Delta u(\tau) - 3 \dot{u}(\tau) - \frac{\Delta t}{2} \ddot{u}(\tau) \right] + k(\tau) \Delta u(\tau) = \Delta Q(\tau) \quad (\text{B.83})$$

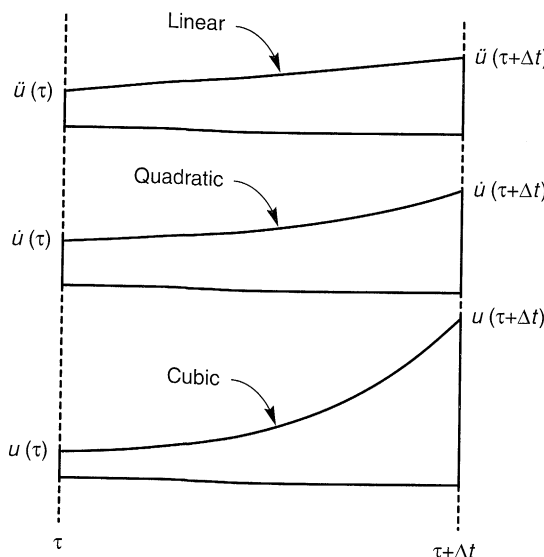


Figure B.22 Variation of acceleration, velocity, and displacement over time increment.

which can be solved for the unknown incremental displacement

$$\Delta u(\tau) = \frac{\Delta Q(\tau) + m [(6/\Delta t)\dot{u}(\tau) + 3\ddot{u}(\tau)] + c(\tau) [3\dot{u}(\tau) + (\Delta t/2)\ddot{u}(\tau)]}{k(\tau) + (6/\Delta t^2)m + (3/\Delta t)c(\tau)} \quad (B.84)$$

Equation (B.84) shows that if the displacement, velocity, and acceleration at time τ are known, the incremental displacement during the succeeding time increment $\Delta\tau$ based on the loading and the stiffness and damping during that time increment can be calculated. From this incremental displacement, the incremental velocity and acceleration, and from these the displacement, velocity, and acceleration at the end of the time increment, can be determined. The conditions at the end of the time increment are then taken as the initial conditions for the next time increment and are used to calculate the appropriate stiffness and damping values for the next time increment. To prevent the accumulation of errors resulting from the assumptions of the linear acceleration method, the acceleration at the beginning of each time step should be calculated by subtracting the damping and spring forces from the total external load and dividing the result by the mass. This will ensure that total equilibrium is satisfied at each step of the analysis.

For numerical stability, it is necessary that the time steps be relatively small, typically less than about 55% of the undamped natural period of the system. These small time steps can lead to considerable computational effort, particularly when such direct integration methods are applied to multiple-degree-of-freedom systems. A number of other numerical integration techniques are available; Berg (1989) describes the application of several to structural dynamics problems.

B.9 MULTIPLE-DEGREE-OF-FREEDOM SYSTEMS

In most physical systems, the motion of the significant masses cannot be described by a single variable; such systems must be treated as *multiple-degree-of-freedom* (MDOF) systems. With the exception of only the simplest cases, the types of buildings, bridges, and other structures that are of interest in earthquake engineering have multiple degrees of freedom. Some structures can be idealized with only a few degrees of freedom; others may require hundreds or even thousands.

In many respects, the response of MDOF systems is similar to the response of SDOF systems, and procedures for analysis are analogous to those described previously for SDOF systems. Although the additional degrees of freedom complicate the algebra, the procedures are conceptually quite similar. In fact, a very useful approach to the response of linear MDOF systems allows their response to be computed as the sum of the responses of a series of SDOF systems.

B.9.1 Equations of Motion

In evaluating the response of an MDOF system, dynamic equilibrium of all masses must be ensured simultaneously. Consider the idealized two-story structure shown in Figure B.23. The structure has two degrees of freedom: horizontal translation of the upper mass and horizontal translation of the lower mass. For each mass the externally applied load must be balanced by the inertial, damping, and elastic forces that resist motion:

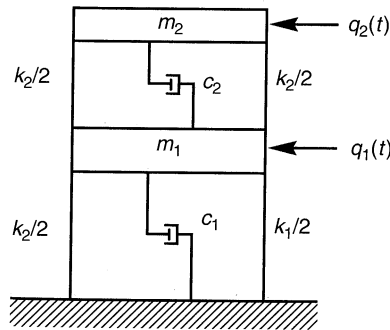


Figure B.23 Two-degree-of-freedom system. Displacements of masses 1 and 2 from equilibrium positions are \$u_1\$ and \$u_2\$, respectively.

$$f_{I1} + f_{D1} + f_{S1} = q_1(t) \quad (\text{B.85a})$$

$$f_{I2} + f_{D2} + f_{S2} = q_2(t) \quad (\text{B.85b})$$

or, in matrix form,

$$\mathbf{f}_I + \mathbf{f}_D + \mathbf{f}_S = \mathbf{q}(t) \quad (\text{B.86})$$

If the structure exhibits linear behavior, the principle of superposition is valid. Then the forces that resist motion at each level can be expressed in terms of coefficients by which the motion parameter at all levels are multiplied. For example, the elastic force resisting motion at level 1 can be expressed as

$$f_{S1} = k_{11}u_1 + k_{12}u_2$$

where the stiffness coefficients \$k_{ij}\$ represent the force induced at level \$i\$ due to a unit displacement at level \$j\$ (with the displacements at all levels except \$j\$ held equal to zero). In matrix form

$$\begin{Bmatrix} f_{S1} \\ f_{S2} \end{Bmatrix} = \begin{bmatrix} k_{11} & k_{12} \\ k_{21} & k_{22} \end{bmatrix} \begin{Bmatrix} u_1 \\ u_2 \end{Bmatrix}$$

or

$$\mathbf{f}_S = \mathbf{K}\mathbf{u}$$

in which \$\mathbf{K}\$ is the *stiffness matrix* of the structure.

Similarly, a *damping matrix* and a *mass matrix* can be developed in which the elements \$c_{ij}\$ (or \$m_{ij}\$) represent the damping (or inertial) forces resisting motion at level \$i\$ due to a unit velocity (or acceleration) of level \$j\$. Dynamic equilibrium of the MDOF system can then be described by a set of simultaneous equations of motion, which can be expressed in matrix form as

$$\mathbf{m}\ddot{\mathbf{u}} + \mathbf{c}\dot{\mathbf{u}} + \mathbf{K}\mathbf{u} = \mathbf{q}(t) \quad (\text{B.87})$$

MDOF systems also respond to base motions. The equation of motion for the case of base shaking is easily developed following the same procedure applied to the SDOF case in Section B.4.2. The resulting equation of motion is

$$\mathbf{m}\ddot{\mathbf{u}} + \mathbf{c}\dot{\mathbf{u}} + \mathbf{K}\mathbf{u} = -\mathbf{m}_1\ddot{u}_b(t) \quad (\text{B.88})$$

Equation (B.95) indicates that the response of an N -story structure to base motion is equal to the response to equivalent external loads, where $q_i = -m_i \ddot{u}_b(t)$ ($i = 1, N$) is the load applied to the i th floor.

B.9.2 Undamped Free Vibrations

For undamped free vibrations, all terms of the damping matrix are zero, so the equations of motion reduce to

$$\mathbf{m}\ddot{\mathbf{u}} + \mathbf{k}\mathbf{u} = \mathbf{0} \quad (\text{B.89})$$

Assuming that the response of each mass (degree of freedom) is harmonic, we have

$$\mathbf{u}(t) = \mathbf{U} \sin(\omega t + \theta) \quad (\text{B.90})$$

where \mathbf{U} is a vector containing the displacement amplitudes and θ is a vector containing the phase angles at each level of the structure (or for each degree of freedom). Differentiating equation (B.90) twice gives

$$\ddot{\mathbf{u}}(t) = -\omega^2 \mathbf{U} \sin(\omega t + \theta) = -\omega^2 \mathbf{u}(t) \quad (\text{B.91})$$

Substituting the expressions for displacement [equation (B.90)] and acceleration [equation (B.91)] into the equation of motion [equation (B.89)] yields

$$-\mathbf{m}\omega^2 \mathbf{U} \sin(\omega t + \theta) + \mathbf{k}\mathbf{U} \sin(\omega t + \theta) = \mathbf{0}$$

or

$$[\mathbf{k} - \omega^2 \mathbf{m}] \mathbf{U} = \mathbf{0} \quad (\text{B.92})$$

which is a set of linear algebraic equations with unknown \mathbf{U} . A nontrivial solution (one that gives values other than $\mathbf{U} = \mathbf{0}$) can be obtained only if

$$\det(\mathbf{k} - \omega^2 \mathbf{m}) = |\mathbf{k} - \omega^2 \mathbf{m}| = 0 \quad (\text{B.93})$$

Equation (B.93) is the *frequency equation* (or *characteristic equation*) of the system, which for a system of N degrees of freedom, will give a polynomial of N th degree in ω^2 . The N roots of the frequency equations $\{\omega_1^2, \omega_2^2, \omega_3^2, \dots, \omega_N^2\}$ represent the frequencies at which the undamped system can oscillate in the absence of external forces. These frequencies are called the *natural circular frequencies* of the system.

Example B.5

Compute the natural frequencies of the three-story structure shown in Figure EB.5.

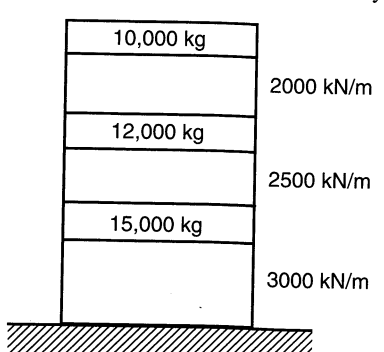


Figure EB.5

Solution The mass matrix for this simple structure is

$$\mathbf{m} = 1000 \begin{bmatrix} 10 & 0 & 0 \\ 0 & 12 & 0 \\ 0 & 0 & 15 \end{bmatrix} \text{ kg}$$

The stiffness matrix can be determined by applying a unit displacement to each floor (with zero displacement at the other floors) and evaluating the resulting forces. By this procedure the stiffness matrix is

$$\mathbf{k} = 1,000,000 \begin{bmatrix} 5.5 & -2.5 & 0 \\ -2.5 & 4.5 & -2.0 \\ 0 & -2.0 & 2.0 \end{bmatrix} \text{ N/m}$$

Then

$$\mathbf{k} - \omega^2 \mathbf{m} = 1,000,000 \begin{bmatrix} 5.5 - 10\alpha & -2.5 & 0 \\ -2.5 & 4.5 - 12\alpha & -2.0 \\ 0 & -2.0 & 2.0 - 15\alpha \end{bmatrix} \quad \text{where } \alpha = \frac{\omega^2}{1000}$$

Setting the determinant $|\mathbf{k} - \omega^2 \mathbf{m}| = 0$ gives the frequency equation

$$1800\alpha^3 - 1905\alpha^2 + 459.5\alpha - 15 = 0$$

The roots of the frequency equation are $\alpha_1 = 0.0386$, $\alpha_2 = 0.3000$, and $\alpha_3 = 0.7197$. Consequently,

$$\begin{Bmatrix} \omega_1^2 \\ \omega_2^2 \\ \omega_3^2 \end{Bmatrix} = \begin{Bmatrix} 38.6 \\ 300.0 \\ 719.7 \end{Bmatrix} \Rightarrow \begin{Bmatrix} \omega_1 \\ \omega_2 \\ \omega_3 \end{Bmatrix} = \begin{Bmatrix} 6.21 \\ 17.62 \\ 26.83 \end{Bmatrix} \frac{\text{rad}}{\text{sec}} \Rightarrow \begin{Bmatrix} f_1 \\ f_2 \\ f_3 \end{Bmatrix} = \begin{Bmatrix} 0.99 \\ 2.76 \\ 4.27 \end{Bmatrix} \text{ Hz}$$

Each natural frequency is associated with a *mode of vibration* of the system. At the natural frequencies, the amplitude of the displacement vector, \mathbf{U} , is indeterminate [scaling the displacements up or down by a constant factor will still satisfy equation (B.92)]. The vector \mathbf{U} does describe the shape of the vibrating system, which is different at each natural frequency. This shape is often made dimensionless by dividing the elements of \mathbf{U} by one (often the first, sometimes the largest) element. The resulting vector describes the mode shape; the *mode shape* for the n^{th} mode of vibration would be

$$\Phi_n^T = [\phi_{1n} \ \phi_{2n} \ \cdots \ \phi_{Nn}] = \frac{1}{U_{Nn}} [U_{1n} \ U_{2n} \ \cdots \ 1] \quad (\text{B.94})$$

All mode shapes satisfy the relationship, $|\mathbf{k} - \omega_n^2 \mathbf{m}| \Phi_n = \mathbf{0}$ for $n = [1, N]$. The values of the vector Φ_n at each natural frequency describe the mode shape of the corresponding mode of vibration. Thus a system of N degrees of freedom will have N natural frequencies corresponding to N modes of vibration. Each mode of vibration occurs at a particular natural frequency and causes the structure to deform with a particular mode shape. The mode corresponding to the lowest natural frequency is called the first mode or *fundamental mode*, the second lowest natural frequency is called the second mode, and so on. The mode shapes can be shown to be *orthogonal*, that is, for $m \neq n$

$$\Phi_m^T \mathbf{m} \Phi_n = 0$$

$$\Phi_m^T \mathbf{k} \Phi_n = 0$$

Example B.6

Compute the mode shapes for the structure shown in Example B.5.

Solution Substituting the fundamental frequency into equation (B.99) yields

$$1,000,000 \begin{bmatrix} 5.114 & -2.5 & 0 \\ -2.5 & 4.037 & -2.0 \\ 0 & -2.0 & 1.421 \end{bmatrix} \begin{Bmatrix} U_{11} \\ U_{21} \\ U_{31} \end{Bmatrix} = \begin{Bmatrix} 0 \\ 0 \\ 0 \end{Bmatrix}$$

Normalizing by the top floor displacement, U_{31} , the mode shape

$$\Phi_1 = \frac{1}{U_{31}} \begin{Bmatrix} U_{11} \\ U_{21} \\ U_{31} \end{Bmatrix} = \begin{Bmatrix} \phi_{11} \\ \phi_{21} \\ 1 \end{Bmatrix}$$

must satisfy $[\mathbf{k} - \omega_1^2 \mathbf{m}] \Phi_1 = \mathbf{0}$. Then, using the known value of $\phi_{31} = 1$, ϕ_{11} and ϕ_{21} can be determined. The process can be repeated to yield the mode shapes of all three modes of vibration:

$$\Phi_1 = \begin{Bmatrix} 0.347 \\ 0.711 \\ 1.000 \end{Bmatrix} \quad \Phi_2 = \begin{Bmatrix} -1.250 \\ -1.250 \\ 1.000 \end{Bmatrix} \quad \Phi_3 = \begin{Bmatrix} 6.479 \\ -4.398 \\ 1.000 \end{Bmatrix}$$

The mode shapes are shown graphically in Figure EB.6.

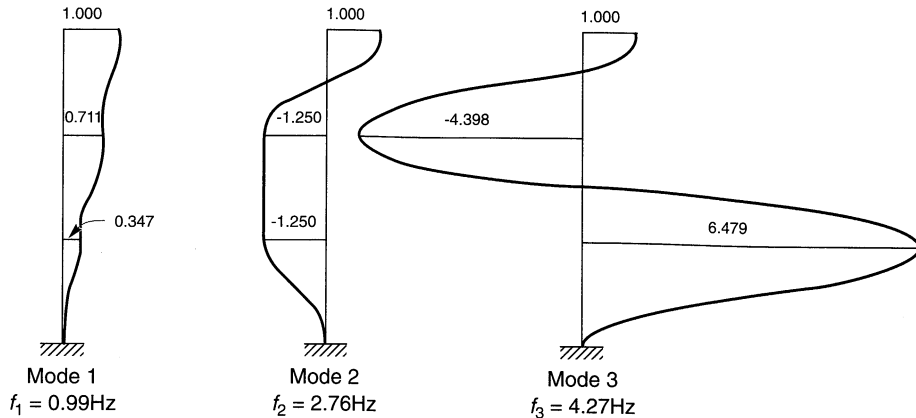


Figure EB.6

B.9.3 Mode Superposition Method

For linear structures with certain types of damping, the response in each mode of vibration can be determined independently of the response in the other modes. The independent modal responses can then be combined to determine the total response. This is the basis of the *mode superposition method*.

Recalling that the mode shape vector, Φ_n , describes only the shape of the n th mode, the displacements can be expressed as the product of the mode shape and the modal amplitude, y_n :

$$\mathbf{U}_n(t) = \boldsymbol{\Phi}_n y_n(t) \quad (\text{B.95})$$

Then, by substituting equation (B.95) into equation (B.87) and premultiplying each term by $\boldsymbol{\Phi}_n^T$, the equation of motion can be written for the n th mode of vibration as

$$M_n \ddot{y}_n + C_n \dot{y}_n + K_n y_n = Q_n(t) \quad (\text{B.96})$$

where $M_n = \boldsymbol{\Phi}_n^T \mathbf{m} \boldsymbol{\Phi}_n$, $C_n = \boldsymbol{\Phi}_n^T \mathbf{c} \boldsymbol{\Phi}_n$, $K_n = \boldsymbol{\Phi}_n^T \mathbf{k} \boldsymbol{\Phi}_n$, and $Q_n(t) = \boldsymbol{\Phi}_n^T \mathbf{q}(t)$. This equation of motion is based on the assumption that the damping matrix is orthogonal (i.e., that $\boldsymbol{\Phi}_m^T \mathbf{c} \boldsymbol{\Phi}_n = 0$ for $m \neq n$). *Rayleigh damping*, in which the damping matrix can be broken into a component proportional to the mass matrix and a component proportional to the stiffness matrix, satisfies the orthogonality requirement. Other procedures are described in standard structural dynamics texts. Alternatively, the equation of motion can be written as

$$\ddot{y}_n + 2\xi_n \omega_n \dot{y}_n + \omega_n^2 y_n = \frac{Q_n(t)}{M_n} \quad (\text{B.97})$$

For the case of base shaking, the equation of motion can be expressed as

$$\ddot{y}_n + 2\xi_n \omega_n \dot{y}_n + \omega_n^2 y_n = -\frac{L_n}{M_n} \ddot{u}_b(t) \quad (\text{B.98})$$

$$\text{where } L_n = \sum_{j=1}^N m_j \phi_{jn}.$$

By this process, the system of N simultaneous equations (the original equations of motion) is transformed to a system of N independent equations. Each of these independent equations can be solved for $y_n(t)$ using the SDOF procedures described earlier in this appendix. Then the total displacement is obtained by superposition of the modal contributions:

$$\mathbf{u}(t) = \boldsymbol{\Phi}_1 y_1(t) + \boldsymbol{\Phi}_2 y_2(t) + \cdots + \boldsymbol{\Phi}_N y_N(t) \quad (\text{B.99})$$

Once the displacements are known, they can be used to compute forces, stresses, and other parameters of interest. The displacements can also be used to compute a set of *equivalent lateral forces*, $\mathbf{f}(t)$, which would produce the displacements $u(t)$ if they were applied as static loads:

$$\mathbf{f}(t) = \mathbf{k} \boldsymbol{\Phi}_1 y_1(t) + \mathbf{k} \boldsymbol{\Phi}_2 y_2(t) + \cdots + \mathbf{k} \boldsymbol{\Phi}_N y_N(t) \quad (\text{B.100})$$

Internal forces can be computed by static analysis of the structure subjected to the equivalent lateral forces. These internal forces can be used for design of the various elements of the structure.

Example B.7

Compute the response of the structure shown in Example B.4 to the Gilroy No. 2 E-W earthquake motion using the mode superposition method. Assume 5% damping for all modes.

Solution The Gilroy No. 2 earthquake motion, illustrated in Figure 3.1, was recorded on the surface of a thick deposit of stiff soil in the 1989 Loma Prieta earthquake. Use of the mode superposition method requires evaluation of the modal equations of motion. For the first mode,

$$M_1 = \Phi_1^T \mathbf{m} \Phi_1 = (1000 \text{ kg}) \begin{Bmatrix} 0.347 & 0.711 & 1.000 \end{Bmatrix} \begin{bmatrix} 10 & 0 & 0 \\ 0 & 12 & 0 \\ 0 & 0 & 15 \end{bmatrix} \begin{Bmatrix} 0.347 \\ 0.711 \\ 1.000 \end{Bmatrix} = 22,270 \text{ kg}$$

$$\begin{aligned} L_1 &= m_1\phi_{11} + m_2\phi_{21} + m_3\phi_{31} \\ &= (10,000)(0.347) + (12,000)(0.711) + (15,000)(1.000) \\ &= 27,002 \text{ kg} \end{aligned}$$

so the equation of motion [equation (B.98)] is

$$\ddot{y}_1 + 0.621\dot{y}_1 + 38.56y_1 = -1.212\ddot{u}_b(t)$$

Repeating this process for the second and third modes gives

$$\begin{aligned} \ddot{y}_2 + 1.732\dot{y}_2 + 300.0y_2 &= 0.253\ddot{u}_b(t) \\ \ddot{y}_3 + 2.683\dot{y}_3 + 719.8y_3 &= -0.041\ddot{u}_b(t) \end{aligned}$$

B.9.4 Response Spectrum Analysis

The mode superposition method produces the entire time history of the response of the structure. For design purposes, however, the entire time history may not be needed; the maximum response values may be sufficient. Because each mode of vibration can be treated as an independent SDOF system, maximum values of modal response can be obtained from the response spectrum. The modal maxima can then be combined to estimate the maximum total response.

B.9.4.1 Calculation of Modal Response Maxima

Let S_{dn} , S_{vn} , and S_{an} denote the spectral displacement, velocity, and acceleration associated with the n th mode of vibration, respectively (these values would be obtained from the response spectrum at a period, $T_n = 2\pi/\omega_n$). Then the maximum modal displacement is given by

$$(y_n)_{\max} = \frac{L_n}{M_n} S_{dn} = \frac{L_n T_n^2}{4\pi^2 M_n} S_{an} \quad (\text{B.101})$$

Using equation (B.95), the maximum displacement of the j th floor would be

$$(U_{jn})_{\max} = \frac{L_n}{M_n} S_{dn} \Phi_{jn} = \frac{L_n T_n^2}{4\pi^2 M_n} S_{an} \Phi_{jn} \quad (\text{B.102})$$

The maximum value of the equivalent lateral force at the j th floor is

$$(f_{jn})_{\max} = \frac{L_n}{M_n} m_j \Phi_{jn} S_{an} \quad (\text{B.103})$$

Maximum values of the internal forces can be computed by static analysis of the structure subjected to the maximum equivalent lateral forces.

B.9.4.2 Combination of Modal Response Maxima

Section B.9.4.1 showed how the response spectrum can be used to predict maximum values of various modal response parameters. The mode superposition method showed that

time histories of modal response can be combined by simple superposition to obtain the total time history of response. However, combination of modal response maxima to obtain the maximum total response is not as straightforward.

The exact value of the maximum total response cannot be obtained directly from the modal maxima because the modal maxima occur at different times. Direct superposition of the modal maxima, which implies that the maxima do occur simultaneously, produces an upper bound to the maximum total response; for any response parameter $r(t)$,

$$r_{\max} \leq \sum_{n=1}^N (r_n)_{\max} \quad (\text{B.104})$$

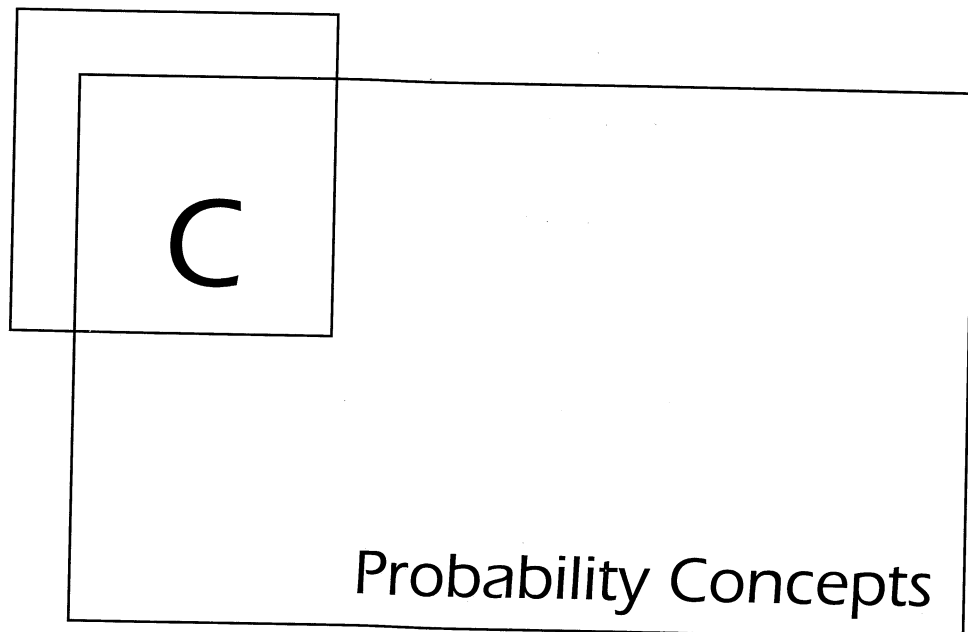
This upper bound value is usually too conservative and is rarely used for design. Instead, modal combination procedures based on random vibration theory are used. The simplest of these is the root-sum-square value

$$r_{\max} = \sqrt{\sum_{n=1}^N (r_n)_{\max}^2} \quad (\text{B.105})$$

The root-sum-square procedure provides a good estimate of maximum total response when the natural periods are well separated (by a factor of about 1.5 or more for 5% damping). Procedures that account for correlation between modes are available (Newmark and Rosenblueth, 1971; Chopra, 1995) for cases of closely spaced modes.

B.9.5 Discussion

The mode superposition method and response spectrum analysis procedures both rely on representation of a MDOF system by a set of SDOF systems. The characteristics of the set of SDOF systems are such that those corresponding to the lower natural frequencies contribute more to the total response than those corresponding to the higher natural frequencies. For practical purposes, the response of a MDOF system can be computed with reasonable accuracy by considering only the lower modes that contribute significantly to the total response of the structure. For some structures, only a small number of modes may need to be considered. All of the analyses described in this section apply to linear structures. Procedures for analysis of nonlinear MDOF structures are available but are well beyond the scope of this appendix.



C.1 INTRODUCTION

Geotechnical earthquake engineering problems are fraught with uncertainty. At a particular site, earthquake-induced loading depends on the size and location of the earthquake—none of which can be predicted with certainty. Because of the inherent variability of soils and the inevitable limits on exploration of subsurface conditions, the resistance of the soil to that loading is not known with certainty. When both loading and resistance are uncertain, the resulting effects are uncertain as well. A number of geotechnical earthquake engineering analyses attempt to quantify the uncertainty in the various input parameters for a particular problem, and compute the resulting uncertainty in the output.

In this appendix we provide a brief introduction to some basic concepts of probability and describe several probability distributions that are used in the body of the book. More detailed information on these topics can be found in texts such as Benjamin and Cornell (1970), Ang and Tang (1975a,b, 1984), and Harr (1987).

C.2 SAMPLE SPACES AND EVENTS

Probability theory deals with the results, or outcomes, of processes that are usually described in a general sense as *experiments*. The set of all possible outcomes of an experiment is called the *sample space*, and each outcome of an experiment is called a *sample*.

point. The sample space therefore consists of all possible sample points. The sample space may be *continuous*, in which case the number of sample points is infinite, or it may be *discrete*, as when the number of sample points are finite and countable.

An *event* is a subset of a sample space, and therefore represents a set of sample points. A *single event* consists of a single sample point, and a *compound event* consists of more than one sample point. If Ω represents a sample space and A represents an event, the *complementary event*, \bar{A} , is the set of all sample points in Ω that are not in A . The interrelationships among sets can be conveniently illustrated by means of a *Venn diagram* (Figure C.1). In Figure C.1 the sample space is represented by the rectangle Ω and the event A by the circle. Thus A is a subset of Ω . The complementary event \bar{A} corresponds to the part of the rectangle that lies outside the circle. Because no sample points are in both A and \bar{A} , the *intersection* of A and \bar{A} is the *null set*, ϕ (i.e., $A \cap \bar{A} = \phi$). Similarly, all sample points are in either A or \bar{A} , so the *union* of A and \bar{A} is Ω (i.e., $A \cup \bar{A} = \Omega$). Two events, A and B , are said to be *mutually exclusive* if they share no common sample points (i.e., $A \cap B = \phi$).

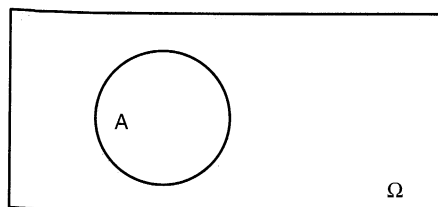


Figure C.1 Venn diagram illustrating event A in sample space Ω .

Example C.1

Consider the Venn diagram for the three events, A , B , and C , shown in Figure EC.1.

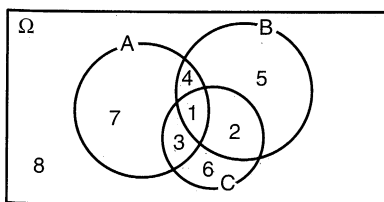


Figure EC.1

$$A \cap B = \text{regions 1 and 4}$$

$$B \cap C = \text{regions 1, 2, 3, 4, 5, and 6}$$

$$A \cap B \cap C = \text{region 1}$$

$$A \cap \bar{B} = \text{regions 3 and 7}$$

$$(A \cup B) \cap C = \text{regions 1, 2, and 3}$$

$$\bar{A} \cap \bar{B} \cap \bar{C} = \text{region 8}$$

C.3 AXIOMS OF PROBABILITY

A probability measure, P , can be assigned to each sample point or set of sample points in a sample space. The probability of an event A is denoted by the symbol $P[A]$. The entire theory of probability is based on the following three fundamental axioms.

Axiom 1. The probability of an event is represented by a number greater than or equal to zero but less than or equal to 1:

$$0 \leq P[A] \leq 1 \quad (\text{C.1a})$$

Axiom 2. The probability of an event equal to the entire sample space Ω is 1:

$$P[\Omega] = 1 \quad (\text{C.1b})$$

Axiom 3. The probability of an event representing the union of two mutually exclusive events is equal to the sum of the probabilities of the events:

$$P[A \cup B] = P[A] + P[B] \quad (\text{C.1c})$$

These axioms can be used to develop the rules and theorems that comprise the mathematical theory of probability.

C.4 PROBABILITIES OF EVENTS

Probabilities are often thought of in terms of relative frequencies of occurrence. If the existence of a water content greater than the optimum water content in a compacted fill is considered to be an event, the probability of that event can be estimated by determining the relative frequency of water content measurements that exceed the water content. If the total number of water content measurements is small, the relative frequency may only approximate the actual probability, but as the number of measurements becomes large, the relative frequency will approach the actual probability. This frequentist point of view is not very helpful, however, for situations in which an experiment cannot be repeated. In such cases, probabilities can be viewed as relative likelihoods (or degrees of belief), as in the probability that a newly discovered fault is capable of producing maximum earthquake magnitudes of 7.0 or 7.5. The latter interpretation lends itself to the subjective evaluation of probability.

Regardless of how probabilities are interpreted, the axioms of probability allow statements to be made about the probabilities of occurrence of single or multiple events. These can be visualized with the help of *Venn diagrams* drawn such that the area of the rectangle representing the sample space Ω is 1 and the areas of all events within the sample space are equal to their probabilities. Consider the nonexclusive events A and B in Figure C.2. The event $A \cap B$ (which means that *both A and B occur*) is represented by the shaded region in Figure C.2a; $P[A \cap B]$ is given by the area of the shaded region. The event $A \cup B$ (which means that either A or B occurs) is represented by the shaded region in Figure C.2b; $P[A \cup B]$ is given by the area of that shaded region, or

$$P[A \cup B] = P[A] + P[B] - P[A \cap B] \quad (\text{C.2})$$

In many instances, the probability of one event depends on the occurrence of another event. The *conditional probability* of event A given the occurrence of event B is denoted $P[A|B]$ and is defined (for $P[B > 0]$) by

$$P[A|B] = \frac{P[A \cap B]}{P[B]} \quad (\text{C.3})$$

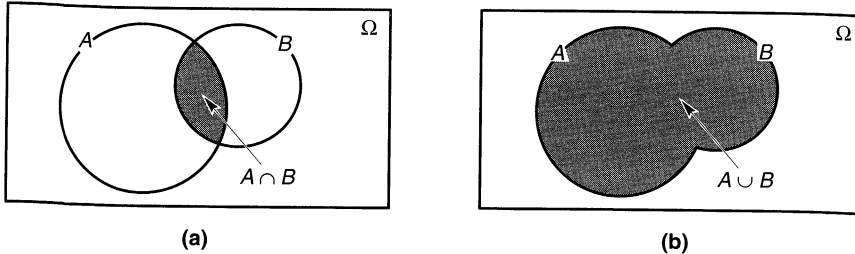


Figure C.2 Venn diagrams for events A and B in sample space Ω . (a) The set $A \cap B$ is given by the shaded area; if the area of Ω is 1, $P[A \cap B]$ is equal to the area that is shaded. (b) The set $A \cup B$ is given by the shaded area; $P[A \cup B]$ is equal to the shaded area.

The conditional probability is easily visualized with the Venn diagram (Figure C.2a) as the ratio of the area of $A \cap B$ to the area of B . Event A is *statistically independent* of event B if the occurrence of B does not affect the probability of occurrence of A ; that is,

$$P[A|B] = P[A] \quad (C.4)$$

Rearranging equation (C.2), the probability that both A and B occur, is given by

$$P[A \cap B] = P[A|B]P[B] \quad (C.5)$$

which if A and B are statistically independent becomes

$$P[A \cap B] = P[A]P[B] \quad (C.6)$$

This is known as the *multiplication rule* and can be extended to the multiple, mutually independent events A, B, C, \dots, N by

$$P[A \cap B \cap C \cap \dots \cap N] = P[A]P[B]P[C] \dots P[N] \quad (C.7)$$

The multiplication rule states that the probability of joint occurrence of statistically independent events is equal to the product of their individual probabilities.

Example C.2

Consider the rolling of a single fair die as an experiment. Then the resulting sample space, $\Omega = \{1, 2, 3, 4, 5, 6\}$, is the set of all possible outcomes of the experiment. Let the following three events be defined as

$$\begin{aligned} A &= \{1\} && \text{(a single roll produces a 1)} \\ B &= \{1, 3, 5\} && \text{(a single roll produces an odd number)} \\ C &= \{4, 5, 6\} && \text{(a single roll produces a number greater than 3)} \end{aligned}$$

Define the sets $A \cap B$, $A \cup B$, and $B \cup C$, and compute their probabilities.

Solution The set $A \cap B$ includes all outcomes that are in both A and B (i.e., $A \cap B = \{1\}$). The set $A \cup B$ includes all outcomes that are in either A or B (i.e., $A \cup B = \{1, 3, 5\}$). The set $B \cup C$ includes all outcomes that are in either B or C (i.e., $B \cup C = \{1, 3, 4, 5, 6\}$). The probabilities of each set can be computed as

$$\begin{aligned} P[A \cap B] &= P[A|B]P[B] = \left(\frac{1}{3}\right)\left(\frac{1}{2}\right) = \frac{1}{6} \\ P[A \cup B] &= P[A] + P[B] - P[A \cap B] = \frac{1}{6} + \frac{1}{2} - \frac{1}{6} = \frac{1}{2} \\ P[B \cup C] &= P[B] + P[C] - P[B \cap C] = \frac{1}{2} + \frac{1}{2} - \frac{1}{6} = \frac{5}{6} \end{aligned}$$

Example C.3

One hundred field compaction tests were performed in the early stages of construction of an earth dam. The results of the tests are presented in terms of the numbers that satisfied specifications for minimum relative compaction and for compaction water content in the table below.

| Water Content | Relative Compaction | |
|----------------|---------------------|----------------|
| | Acceptable | Not Acceptable |
| Acceptable | 80 | 10 |
| Not acceptable | 6 | 4 |

Assume that the contractor's performance in the future will be the same as in the first 100 tests and that the fill material does not change. Estimate the probability that the relative compaction specification will be satisfied in the next test if the water content specification is satisfied. Estimate that probability for the case in which the water content specification is not satisfied.

Solution Define two events, R and W , such that

$$R = \text{relative compaction specification satisfied}$$

$$W = \text{water content specification satisfied}$$

From the table the probability that both the relative compaction and water content specifications are satisfied can be estimated as $P[W \cap R] = 80/100$. Then the probability that the relative compaction specification will be satisfied in the next test if the water content specification is satisfied is the conditional probability $P[R|W]$, which can be computed as

$$P[R|W] = \frac{P[W \cap R]}{P[W]} = \frac{80/100}{80/100 + 10/100} = \frac{80}{90} = 0.889$$

The probability that the relative compaction specification is satisfied given that the water content specification is not satisfied can be estimated as $P[R|\bar{W}]$, or

$$P[R|\bar{W}] = \frac{P[\bar{W} \cap R]}{P[\bar{W}]} = \frac{6/100}{6/100 + 4/100} = \frac{6}{10} = 0.600$$

For a set of events, B_1, B_2, \dots, B_N , which are mutually exclusive ($B_i \cap B_j = \emptyset$ for all $i \neq j$) but collectively exhaustive ($B_1 \cup B_2 \cup \dots \cup B_N = \Omega$), like that shown in the Venn diagram of Figure C.3, the probability of another event A can be expressed as

$$P[A] = P[A \cap B_1] + P[A \cap B_2] + \dots + P[A \cap B_N] \quad (C.8)$$

Using equation (C.5) for each term on the right side of equation (C.8) yields

$$\begin{aligned} P[A] &= P[A|B_1]P[B_1] + P[A|B_2]P[B_2] + \dots + P[A|B_N]P[B_N] \\ &= \sum_{i=1}^N P[A|B_i]P[B_i] \end{aligned} \quad (C.9)$$

which is known as the *total probability theorem*. The total probability theorem forms the backbone of the probability calculations required for probabilistic seismic hazard analyses (Chapter 4).

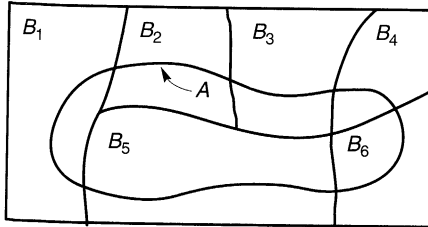


Figure C.3 Intersection of event A with mutually exclusive but collectively exhaustive events B_i .

Example C.4

A structural engineer has determined that a structure will collapse in an earthquake that produces a peak acceleration of $0.3g$. The probability that a given earthquake on fault A, B, or C would be strong enough to cause the structure to collapse are 0.5, 0.2, and 0.1, respectively. The probabilities that that such earthquakes will occur on faults A, B, and C during the life of the building are 0.01, 0.05, and 0.08, respectively. What is the probability that the structure will collapse in an earthquake?

Solution Define the following events as

$$A = \text{the structure collapses in an earthquake}$$

$$D_1 = \text{an earthquake capable of collapsing the structure occurs on fault A}$$

$$D_2 = \text{an earthquake capable of collapsing the structure occurs on fault B}$$

$$D_3 = \text{an earthquake capable of collapsing the structure occurs on fault C}$$

Then the probability that the structure collapses in an earthquake is given by

$$\begin{aligned} P[A] &= P[A|D_1]P[D_1] + P[A|D_2]P[D_2] + P[A|D_3]P[D_3] \\ &= (0.5)(0.01) + (0.2)(0.05) + (0.1)(0.10) \\ &= 0.025 \end{aligned}$$

C.5 RANDOM VARIABLES

All fields of science and engineering attempt to describe various quantities or phenomena with numerical values. In most cases, the precise numerical value cannot be predicted in advance of some process, or experiment, of interest. In such cases, a particular quantity or phenomenon is described by a *random variable*. The random variable is used to describe an event in a sample space in quantitative terms.

A *continuous random variable* can take on any value within one or more intervals. Because a continuous random variable can take on any of an infinite number of values, the probability of it taking on any specific value is $1/\infty = 0$. The probability distribution of a continuous random variable can also be described by its *probability density function* or PDF, $f_X(x)$, which must satisfy the conditions

$$f_X(x) \geq 0 \quad \text{for all } x$$

$$\int_{-\infty}^{\infty} f_X(x) dx = 1$$

$$P[a \leq X \leq b] = \int_a^b f_X(x) dx$$

According to these conditions, the area under the PDF between two values a and b represents the probability that the random variable will have a value in the interval bounded by a and b . The probability distribution of a random variable can also be described by its *cumulative distribution function* (CDF), which is given by

$$F_X(x) = P[X \leq x] = \int_{-\infty}^x f_X(x) dx \quad (\text{C.10})$$

Therefore, the probability that a random variable, X , falls between two values a and b is

$$P[a \leq X \leq b] = F_X(b) - F_X(a) \quad (\text{C.11})$$

Obviously, the PDF and CDF are closely related—one can be obtained from the other by integration or differentiation. The PDF and CDF of a typical probability distribution are shown in Figure C.4.

From the total probability theorem and the definition of the PDF, the probability of the random variable Y having some value y given that the random variable X is between two values, a and b , can be expressed as

$$\begin{aligned} P[Y = y] &= P[Y = y | a \leq X \leq x_2] P[x_1 \leq X \leq x_2] \\ &= \int_a^b P[Y = y | a \leq X \leq x_2] f_X(X) dx \end{aligned} \quad (\text{C.12})$$

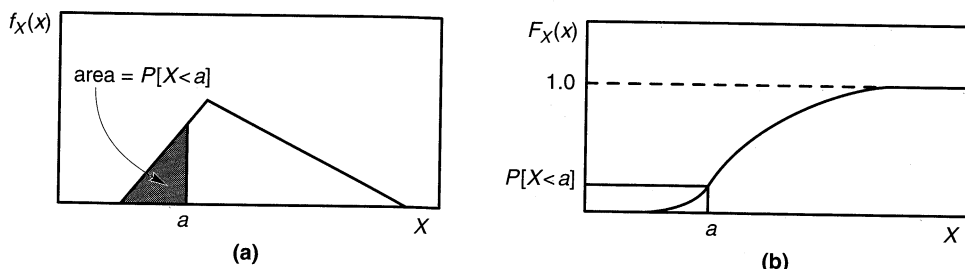


Figure C.4 (a) PDF for a random variable, X . The probability that $X < a$ is given by the area under the PDF to the left of a . (b) CDF for the same random variable. The probability that $X < a$ is given by the value of the CDF at $X = a$.

C.6 EXPECTED VALUES AND STANDARD DEVIATIONS

The uncertainty of a random variable can often be characterized with reasonable accuracy by a few statistical parameters. The *mean*, or *expected value*, of a continuous random variable, X , is given by

$$\bar{x} = \int_{-\infty}^{\infty} x f_X(x) dx \quad (\text{C.13})$$

The mean is a very useful measure of the central tendency of the random variable. By itself, however, it does not adequately describe the shape of the PDF. The dispersion of the random

variable about the mean is also very important. This dispersion is usually characterized by the *variance*

$$\sigma_x^2 = \int_{-\infty}^{\infty} (x - \bar{x})^2 f_X(x) dx \quad (\text{C.14})$$

or the *standard deviation*

$$\sigma_x = \sqrt{\sigma_x^2} \quad (\text{C.15})$$

Both of these parameters reflect how widely the random variable is dispersed about the mean. Because its units are the same as those of the random variable, the standard deviation is more commonly used than the variance. This characteristic also allows the dispersion to be expressed in dimensionless form by the coefficient of variation

$$\text{COV}_x = \frac{\sigma_x}{\bar{x}} \quad (\text{C.16})$$

The mean and standard deviation (or mean and coefficient of variation) go far toward describing the uncertainty in a random variable. Many simple probability distributions, including those most commonly used in geotechnical earthquake engineering, are completely described by these two parameters. Other distributions may require additional parameters to characterize their symmetry, limits, and/or other characteristics.

C.7 COMMON PROBABILITY DISTRIBUTIONS

The results of statistical experiments often exhibit the same general type of behavior. As a result, the random variables associated with those experiments can be described by essentially the same PDF. Many probability density functions exist, but only a few are required for the geotechnical earthquake engineering analyses described in this book.

C.7.1 Uniform Distribution

The simplest probability distribution is one in which all possible values of the random variable are equally likely. Such a random variable is described by a *uniform distribution*. The PDF for a continuous random variable, X , that is uniformly distributed between two values a and b is

$$f_X(x) = \begin{cases} 0 & \text{for } x \leq a \\ \frac{1}{b-a} & \text{for } a < x \leq b \\ 0 & \text{for } x > b \end{cases} \quad (\text{C.17})$$

The PDF and CDF for a uniform distribution are illustrated in Figure C.5.

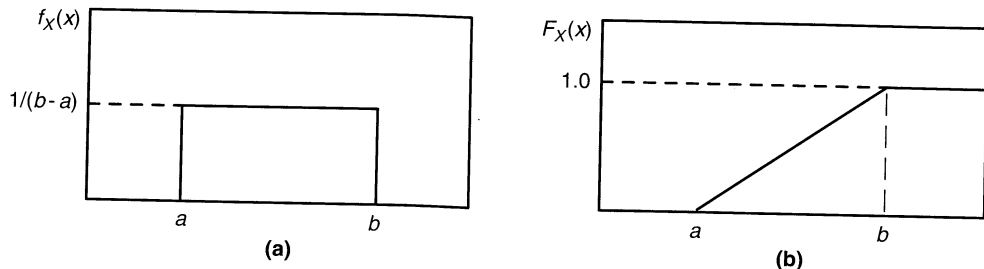


Figure C.5 Uniform distribution: (a) probability density function; (b) cumulative distribution function.

C.7.2 Normal Distribution

The most commonly used probability distribution in statistics is the *normal distribution* (or *Gaussian distribution*). Its PDF, which plots as the familiar bell-shaped curve of Figure C.6a, describes sets of data produced by a wide variety of physical processes. The normal distribution is completely defined by two parameters: the mean and standard deviation. Mathematically, the PDF of a normally distributed random variable X with mean \bar{x} and standard deviation σ_x is given by

$$f_X(x) = \frac{1}{\sqrt{2\pi}\sigma_x} \exp\left[-\frac{1}{2}\left(\frac{x-\bar{x}}{\sigma_x}\right)^2\right] \quad (\text{C.18})$$

The PDF and CDF for a normal distribution are illustrated in Figure C.6. Examples of normal pdf's for random variables with different means and standard deviations are shown in Figure C.7.

Integration of the PDF of the normal distribution does not produce a simple expression for the CDF, so values of the normal CDF are usually expressed in tabular form. The

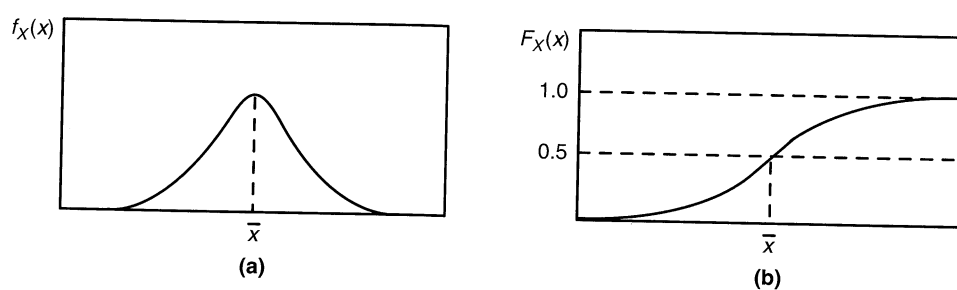


Figure C.6 Normal distribution: (a) probability density function; (b) cumulative distribution function.

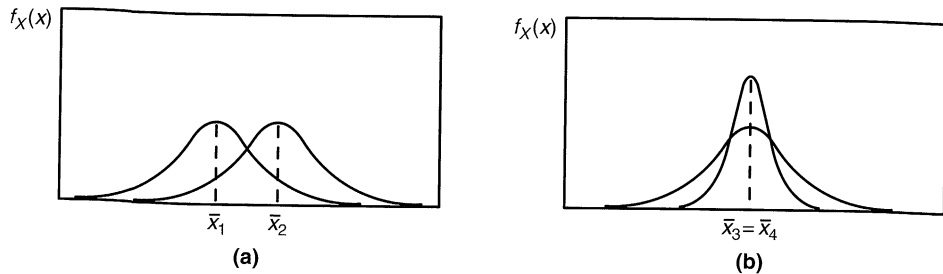


Figure C.7 Normal distributions for (a) two random variables, X_1 and X_2 , with different means but the same standard deviation, and (b) two random variables, X_3 and X_4 , with the same mean but different standard deviations.

normal CDF is most efficiently expressed in terms of the *standard normal variable*, Z , which can be computed for any random variable, X , using the transformation

$$Z = \frac{X - \bar{x}}{\sigma_x} \quad (\text{C.19})$$

Whenever X has a value, x , the corresponding value of Z is $z = (x - \bar{x})/\sigma_x$. Thus, the mean value of Z is $\bar{z} = 0$ and the standard deviation is $\sigma_z = 1$. Tabulated values of the standard normal CDF are presented in Table C-1.

Example C.5

Given a normally distributed random variable, X , with $\bar{x} = 270$ and $\sigma_x = 40$, compute the probability that (a) $X < 300$, (b) $X > 350$, and (c) $200 < X < 240$.

Solution (a) For $X = 300$,

$$Z = \frac{X - \bar{x}}{\sigma_x} = \frac{300 - 270}{40} = 0.75$$

Then

$$P[X < 300] = P[Z < 0.75] = F_z(0.75) = 1 - F_z(-0.75) = 1 - 0.2266 = 0.7734$$

(b) For $X = 350$,

$$Z = \frac{X - \bar{x}}{\sigma_x} = \frac{350 - 270}{40} = 2.0$$

Then

$$P[X > 350] = P[Z > 2.0] = 1 - F_z(2.0) = F_z(-2.0) = 0.0228$$

(c) For $X = 200$,

$$Z = \frac{X - \bar{x}}{\sigma_x} = \frac{200 - 270}{40} = -1.75$$

For $X = 240$,

$$Z = \frac{X - \bar{x}}{\sigma_x} = \frac{240 - 270}{40} = -0.75$$

Then

$$\begin{aligned} P[200 < X < 240] &= P[-1.75 < Z < -0.75] = F_z(-0.75) - F_z(-1.75) \\ &= 0.2266 - 0.0401 = 0.1865 \end{aligned}$$

TABLE C-1 Values of the CDF of the standard normal distribution, $F_Z(z) = 1 - F_{Z'}(-z)$

| z | 0.00 | 0.01 | 0.02 | 0.03 | 0.04 | 0.05 | 0.06 | 0.07 | 0.08 | 0.09 |
|------|--------|--------|--------|--------|--------|--------|--------|--------|--------|--------|
| -3.4 | 0.0003 | 0.0003 | 0.0003 | 0.0003 | 0.0003 | 0.0003 | 0.0003 | 0.0003 | 0.0003 | 0.0002 |
| -3.3 | 0.0005 | 0.0005 | 0.0005 | 0.0004 | 0.0004 | 0.0004 | 0.0004 | 0.0004 | 0.0004 | 0.0003 |
| -3.2 | 0.0007 | 0.0007 | 0.0006 | 0.0006 | 0.0006 | 0.0006 | 0.0005 | 0.0005 | 0.0005 | 0.0005 |
| -3.1 | 0.0010 | 0.0009 | 0.0009 | 0.0009 | 0.0008 | 0.0008 | 0.0008 | 0.0008 | 0.0007 | 0.0007 |
| -3.0 | 0.0013 | 0.0013 | 0.0013 | 0.0012 | 0.0012 | 0.0011 | 0.0011 | 0.0011 | 0.0010 | 0.0010 |
| -2.9 | 0.0019 | 0.0018 | 0.0017 | 0.0017 | 0.0016 | 0.0016 | 0.0015 | 0.0015 | 0.0014 | 0.0014 |
| -2.8 | 0.0026 | 0.0025 | 0.0024 | 0.0023 | 0.0023 | 0.0022 | 0.0021 | 0.0021 | 0.0020 | 0.0019 |
| -2.7 | 0.0035 | 0.0034 | 0.0033 | 0.0032 | 0.0031 | 0.0030 | 0.0029 | 0.0028 | 0.0027 | 0.0026 |
| -2.6 | 0.0047 | 0.0045 | 0.0044 | 0.0043 | 0.0041 | 0.0040 | 0.0039 | 0.0038 | 0.0037 | 0.0036 |
| -2.5 | 0.0062 | 0.0060 | 0.0059 | 0.0057 | 0.0055 | 0.0054 | 0.0052 | 0.0051 | 0.0049 | 0.0048 |
| -2.4 | 0.0082 | 0.0080 | 0.0078 | 0.0075 | 0.0073 | 0.0071 | 0.0069 | 0.0068 | 0.0066 | 0.0064 |
| -2.3 | 0.0107 | 0.0104 | 0.0102 | 0.0099 | 0.0096 | 0.0094 | 0.0091 | 0.0089 | 0.0087 | 0.0084 |
| -2.2 | 0.0139 | 0.0136 | 0.0132 | 0.0129 | 0.0125 | 0.0122 | 0.0119 | 0.0116 | 0.0113 | 0.0110 |
| -2.1 | 0.0179 | 0.0174 | 0.0170 | 0.0166 | 0.0162 | 0.0158 | 0.0154 | 0.0150 | 0.0146 | 0.0143 |
| -2.0 | 0.0228 | 0.0222 | 0.0217 | 0.0212 | 0.0207 | 0.0202 | 0.0197 | 0.0192 | 0.0188 | 0.0183 |
| -1.9 | 0.0287 | 0.0281 | 0.0274 | 0.0268 | 0.0262 | 0.0256 | 0.0250 | 0.0244 | 0.0239 | 0.0233 |
| -1.8 | 0.0359 | 0.0352 | 0.0344 | 0.0336 | 0.0329 | 0.0322 | 0.0314 | 0.0304 | 0.0301 | 0.0294 |
| -1.7 | 0.0446 | 0.0436 | 0.0427 | 0.0418 | 0.0409 | 0.0401 | 0.0392 | 0.0384 | 0.0375 | 0.0367 |
| -1.6 | 0.0548 | 0.0537 | 0.0526 | 0.0516 | 0.0505 | 0.0495 | 0.0485 | 0.0475 | 0.0465 | 0.0455 |
| -1.5 | 0.0668 | 0.0655 | 0.0643 | 0.0630 | 0.0618 | 0.0606 | 0.0594 | 0.0582 | 0.0571 | 0.0559 |
| -1.4 | 0.0808 | 0.0793 | 0.0778 | 0.0764 | 0.0749 | 0.0735 | 0.0722 | 0.0708 | 0.0694 | 0.0681 |
| -1.3 | 0.0968 | 0.0951 | 0.0934 | 0.0918 | 0.0901 | 0.0885 | 0.0859 | 0.0853 | 0.0838 | 0.0823 |
| -1.2 | 0.1151 | 0.1131 | 0.1112 | 0.1093 | 0.1075 | 0.1056 | 0.1038 | 0.1020 | 0.1003 | 0.0985 |
| -1.1 | 0.1357 | 0.1335 | 0.1314 | 0.1292 | 0.1271 | 0.1251 | 0.1230 | 0.1210 | 0.1190 | 0.1170 |
| -1.0 | 0.1587 | 0.1562 | 0.1539 | 0.1515 | 0.1492 | 0.1469 | 0.1446 | 0.1423 | 0.1401 | 0.1379 |
| -0.9 | 0.1841 | 0.1814 | 0.1788 | 0.1762 | 0.1736 | 0.1711 | 0.1685 | 0.1660 | 0.1635 | 0.1611 |
| -0.8 | 0.2119 | 0.2090 | 0.2061 | 0.2033 | 0.2005 | 0.1977 | 0.1949 | 0.1922 | 0.1894 | 0.1867 |
| -0.7 | 0.2420 | 0.2389 | 0.2358 | 0.2327 | 0.2296 | 0.2266 | 0.2236 | 0.2206 | 0.2177 | 0.2148 |
| -0.6 | 0.2743 | 0.2709 | 0.2676 | 0.2643 | 0.2611 | 0.2578 | 0.2546 | 0.2514 | 0.2483 | 0.2451 |
| -0.5 | 0.3085 | 0.3050 | 0.3015 | 0.2981 | 0.2946 | 0.2912 | 0.2877 | 0.2843 | 0.2810 | 0.2776 |
| -0.4 | 0.3446 | 0.3409 | 0.3372 | 0.3336 | 0.3300 | 0.3264 | 0.3228 | 0.3192 | 0.3156 | 0.3121 |
| -0.3 | 0.3821 | 0.3783 | 0.3745 | 0.3707 | 0.3669 | 0.3632 | 0.3594 | 0.3557 | 0.3520 | 0.3483 |
| -0.2 | 0.4207 | 0.4168 | 0.4129 | 0.4090 | 0.4052 | 0.4013 | 0.3974 | 0.3936 | 0.3897 | 0.3859 |
| -0.1 | 0.4602 | 0.4562 | 0.4522 | 0.4483 | 0.4443 | 0.4404 | 0.4365 | 0.4325 | 0.4286 | 0.4247 |
| -0.0 | 0.5000 | 0.4960 | 0.4920 | 0.4880 | 0.4840 | 0.4801 | 0.4761 | 0.4721 | 0.4681 | 0.4641 |

C.7.3 Lognormal Distribution

Some problems, particularly those involving ground motion parameters (Chapter 3), are formulated in terms of the logarithm of a parameter rather than the parameter itself. If X is a random variable, then $Y = \ln X$ is also a random variable. If Y is normally distributed, then X is *lognormally distributed*. In other words, a random variable is lognormally distributed if its logarithm is normally distributed. The PDF of a lognormally distributed random variable X is given by

$$f_X(x) = \frac{1}{x\sqrt{2\pi}\sigma_{\ln x}} \exp\left[-\frac{1}{2}\left(\frac{\ln x - \bar{\ln}x}{\sigma_{\ln x}}\right)^2\right] \quad (\text{C.20})$$

The shape of the lognormal distribution is shown in Figure C.8. Note that the PDF is not symmetric, and that it assigns zero probability to negative values of the random variable. These characteristics can be very useful for some random variables [the normal distribution, for example, assigns nonzero probabilities for values ranging from $-\infty$ to $+\infty$; when applied to a random variable such as soil density, it can assign some (hopefully small) probability that the soil will have a negative density].

Values of the CDF of the lognormal distribution are usually obtained from Table C-1, using the modified transformation

$$Z = \frac{\ln X - \bar{\ln}x}{\sigma_{\ln x}} \quad (\text{C.21})$$

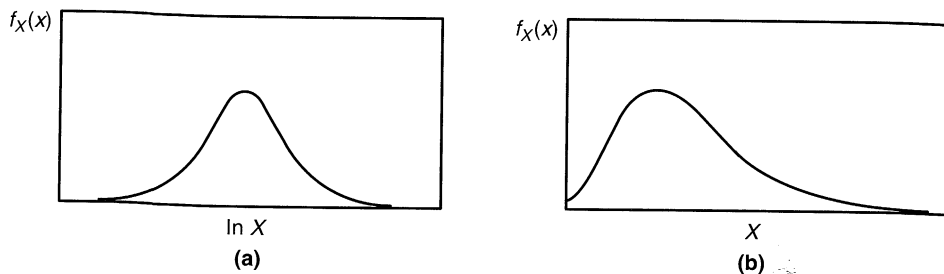


Figure C.8 Two views of the lognormal distribution. (a) Because the logarithm of a lognormally distributed random variable, X , is normally distributed, the probability density function of $\ln X$ is a bell-shaped curve. (b) The probability density function of X itself has no negative values and is not symmetric.

Example C.6

A random variable, X , is lognormally distributed with $\bar{\ln}x = 5$ and $\sigma_{\ln x} = 1.2$. Compute (a) the probability that $X < 100$, and (b) the value of X that has a 10% probability of being exceeded.

Solution (a) For $X = 100$,

$$Z = \frac{\ln X - \bar{\ln}x}{\sigma_{\ln x}} = \frac{\ln 100 - 5}{1.2} = -0.33$$

From Table C-1,

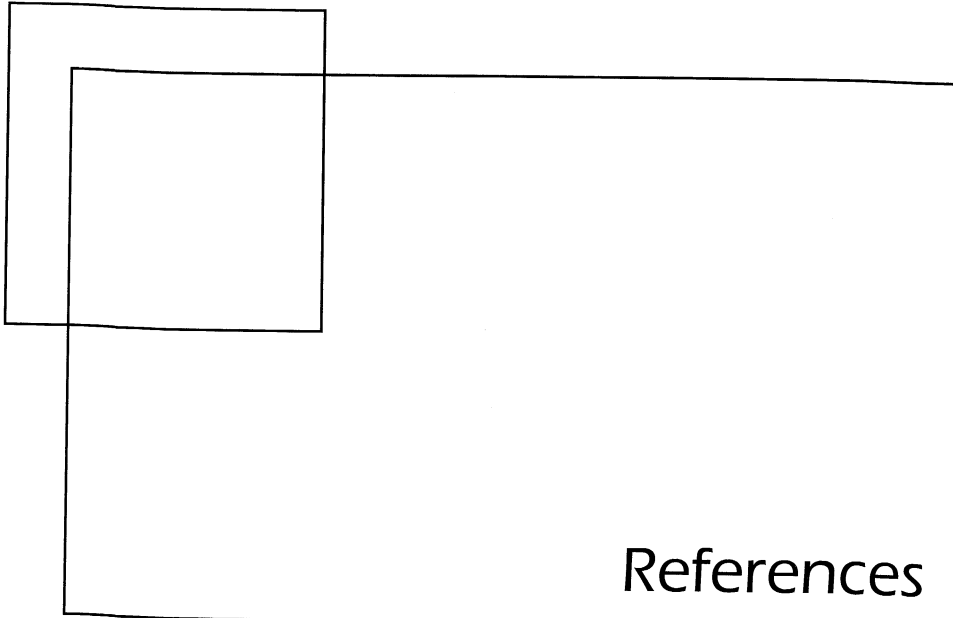
$$P[X < 100] = P[Z < -0.33] = F_z(-0.33) = 0.3707$$

(b) From Table C-1, the value of Z that would have a 10% probability of exceedance is 1.282 [i.e., $F_Z(1.282) = 0.90$]. Then, rearranging equation (C.21) yields

$$\ln X = Z\sigma_{\ln x} + \bar{\ln x} = (1.282)(1.2) + 5 = 6.54$$

so

$$X = e^{6.54} = 691$$



References

- AASHTO (1991). *Interim Specification: Bridges - 1991*, American Association of State Highway and Transportation Officials, Washington, D.C., 470 pp.
- ABDEL-GHAFFAR, A.M. AND SCOTT, R.F. (1979). "Shear moduli and damping factors of earth dam," *Journal of the Geotechnical Engineering Division*, ASCE, Vol. 105, No. GT12, pp. 1405-1426.
- ABOSHI, H., MIZUNO, Y., AND KUWABARA, M. (1991). Present state of sand compaction pile in Japan, *Deep Foundation Improvements: Design, Construction, and Testing*, ASTM STP 1089, M.I. Esrig and R.C. Bachus, eds., ASTM, Philadelphia, pp. 32-46.
- ABRAHAMSON, N.A. (1991). "Spatial coherency of ground motion from the SMART 1 array," *Geotechnical News*, Vol. 9, No. 1, pp. 31-34.
- ABRAHAMSON, N.A. AND LITEHISER, J.J. (1989). "Attenuation of vertical peak acceleration," *Bulletin of the Seismological Society of America*, Vol. 79, pp. 549-580.
- ABRAHAMSON, N.A. AND SINGH, J.P. (1986). "Importance of phasing of strong ground motion in the estimation of structural response," *Proceedings, 3rd Engineering Mechanics Specialty Conference on Dynamic Response of Structures*, ASCE, Los Angeles.
- ABRAHAMSON, N.A., SCHNEIDER, J.F., AND STEPP, J.C. (1991). "Empirical spatial coherency functions for application to soil-structure interaction analyses," *Earthquake Spectra*, Vol. 7, No. 1, pp. 1-28.
- ACHARAYA, H.K. (1979). "Regional variations in the rupture-length magnitude relationships and their dynamical significance," *Bulletin of the Seismological Society of America*, Vol. 69, No. 6, pp. 2063-2084.

- ADAIR, M.J. (1979). "Geologic evaluation of a site for a nuclear power plant," in A.W. Hatheway and C.R. McClure, eds., *Geology in the Siting of Nuclear Power Plants*, Geological Society of America Reviews in Engineering Geology, Boulder, Colorado, Vol. 4, pp. 27-39.
- AIREY, D.W. AND WOOD, D.M. (1987). "An evaluation of direct simple shear tests on clay," *Geotechnique*, Vol. 37, No. 1, pp. 25-35.
- AKI, K. (1969). Analysis of the seismic coda of local earthquakes as scattered waves, *Journal of Geophysical Research*, Vol. 74, pp. 615-631.
- AKI, K. (1979). "Characterization of barriers on an earthquake fault," *Journal of Geophysical Research*, Vol. 86, pp. 6140-6148.
- AKI, K. (1984). "Asperities, barriers, characteristic earthquakes, and strong motion prediction," *Journal of Geophysical Research*, Vol. 89, pp. 5867-5872.
- AKI, K. (1988). Local site effects on strong ground motion, *Proceedings, Earthquake Engineering and Soil Dynamics II - Recent Advances in Ground Motion Evaluation*, ASCE, Geotechnical Special Publication No. 20, pp. 103-155.
- AKI, K. (1993). "Local site effects on weak and strong ground motion," *Tectonophysics*, Vol. 218, No. 1-3, pp. 93-112.
- AKI, K. AND RICHARDS, P.G. (1980). *Quantitative Seismology: Theory and Methods*, Volumes 1 and 2, W.H. Freeman, San Francisco, California.
- AL-SANAD, H. AND AGGOUR, M.S. (1984). "Dynamic soil properties from sinusoidal and random vibrations," *Proceedings, 8th World Conference on Earthquake Engineering*, San Francisco, Vol. 3, pp. 15-22.
- ALAMPALLI, S. AND ELGAMEL, A.-W. (1990). "Dynamic response of retaining walls including supported soil backfill: A computational model," *Proceedings, 4th U.S. National Conference on Earthquake Engineering*, Earthquake Engineering Research Institute, Palm Springs, California, Vol. 3, pp. 623-632.
- ALARCON-GUZMAN, A., LEONARDS, G.A., and CHAMEAU, J.L. (1988). "Undrained monotonic and cyclic strength of sands," *Journal of Geotechnical Engineering*, ASCE, Vol. 114, No. 10, pp. 1089-1108.
- ALGERMISSEN, S.T., PERKINS, D.M., THENHAUS, P.C., HANSON, S.L., AND BENDER, B.L. (1982). "Probabilistic estimates of maximum acceleration and velocity in rock in the contiguous United States," *Open-File Report 82-1033*, U.S. Geological Survey, Washington, D.C., pp. 99.
- ALGERMISSEN, S.T., PERKINS, D.M., THENHAUS, P.C., HANSON, S.L., AND BENDER, B.L. (1990). Probabilistic earthquake acceleration and velocity maps for the United States and Puerto Rico, Miscellaneous Field Studies Map MF-2120, U.S. Geological Survey, Washington, D.C.
- ALLEN, C.R. (1975). "Geologic criteria for evaluating seismicity," *Bulletin of the Geological Society of America*, Vol. 86, No. 8, pp. 1041-1057.
- AMBRASEYS, N.N. (1960). "On the shear response of a two-dimensional truncated wedge subjected to an arbitrary disturbance," *Bulletin of the Seismological Society of America*, Vol. 50, No. 1, pp. 45-56.
- AMBRASEYS, N.N. (1971). "Value of historical records of earthquakes," *Nature*, Vol. 232, pp. 375-379.
- AMBRASEYS, N.N. (1978). "Middle East - A reappraisal of the seismicity," *Quarterly Journal of Engineering Geology*, Vol. 11, pp. 19-32.
- AMBRASEYS, N.N. (1988). "Engineering seismology," *Earthquake Engineering and Structural Dynamics*, Vol. 17, pp. 1-105.
- AMBRASEYS, N.N. AND MENU, J.M. (1988). "Earthquake-induced ground displacements," *Earthquake Engineering and Structural Dynamics*, Vol. 16, pp. 985-1006.
- ANAGNOS, T., AND KRREMIDJIAN, A.S. (1982). Stochastic time-predictable model for earthquake occurrences, *Bulletin of the Seismological Society of America*, Vol. 74, No. 6, pp. 2593-2611.

- ANDERSEN, K.H., KLEVEN, A., AND HEIEN, D. (1988). "Cyclic soil data for design of gravity structures," *Journal of Geotechnical Engineering*, ASCE, Vol. 114, No. 5, pp. 517-539.
- ANDERSON, D.G. AND STOKOE, K.H. (1978). "Shear modulus: A time-dependent soil property," *Dynamic Geotechnical Testing*, ASTM STP 654, ASTM, Philadelphia, pp. 66-90.
- ANDERSON, D.G. AND WOODS, R.D. (1975). "Comparison of field and laboratory shear modulus," *Proceedings, ASCE Conference on In Situ Measurement of Soil Properties*, Vol. 1, pp. 69-92.
- ANDERSON, D.G. AND WOODS, R.D. (1976). "Time-dependent increase in shear modulus of clay," *Journal of the Geotechnical Engineering Division*, ASCE, Vol. 102, No. GT5, pp. 525-537.
- ANDERSON, J.G. (1991). "Guerrero accelerograph array: Seismological and geotechnical lessons," *Geotechnical News*, Vol. 9, No. 1, pp. 34-37.
- ANDERSEN, A. AND BJERRUM, L. (1968). "Slides in subaqueous slopes in loose sand and silt," *Publication 81*, Norwegian Geotechnical Institute, Publication 8, Oslo, pp. 1-9.
- ANG, A.H.S. (1990). Reliability bases for seismic safety assessment and design, *Proceedings, Fourth U.S. National Conference on Earthquake Engineering*, Earthquake Engineering Research Institute, Palm Springs, Vol. 1, pp. 29-45.
- ANG, A.H.S. AND TANG, W.H. (1975a). *Probability Concepts in Engineering Planning and Design*, Vol. I: *Basic Principles*, Wiley, New York.
- ANG, A.H.S. AND TANG, W.H. (1975b). *Probability Concepts in Engineering Planning and Design*, Vol. II: *Decision, Risk, and Reliability*, Wiley, New York.
- APPLEGATE, J.K. (1974). "A torsional seismic source," Thesis, Colorado School of Mines, Boulder, Colorado.
- ATC (1978). "Tentative provisions for the development of seismic regulations for buildings, ATC 3-06, Applied Technology Council, Palo Alto, California.
- ARIAS, A. (1970) "A measure of earthquake intensity," in R.J. Hansen, ed. *Seismic Design for Nuclear Power Plants*, MIT Press, Cambridge, Massachusetts, pp. 438-483.
- ARULMOLI, K., ARULANANDAN, K., AND SEED, H.B. (1985). "New method for evaluating liquefaction potential," *Journal of Geotechnical Engineering*, ASCE, Vol. 111, No. 1, pp. 95-114.
- ATWATER, T. AND SVERINGHAUS, J. (1989). "Tectonic map of the north Pacific," in E.L. Winterer, D.M. Hussong, and R.W. Decker, eds., *DNAG: The Eastern Pacific Ocean and Hawaii*, Geologic Society of America Publication, Boulder, Colorado, Vol. N, pp. 15-20.
- ATWATER, B.F. (1987). Evidence for great Holocene earthquakes along the outer coast of Washington state" *Science*, Vol. 236, pp. 942-944.
- ATWATER, B.F., HULL, A.G., AND BEVIS, K.A. (1987). "Aperiodic Holocene recurrence of widespread, probably coseismic subsidence in southwestern Washington," *Eos*, Vol. 68, 1468 pp.
- AULD, B. (1977). "Cross-hole and down-hole v_s by mechanical impulse," *Journal of the Geotechnical Engineering Division*, ASCE, Vol. 103, No. GT12, pp. 1381-1398.
- BABASAKI, R., SUZUKI, K., SAITO, S., SUZUKI, Y., AND TOKITOH, K. (1991). "Construction and testing of deep foundation improvement using the deep cement mixing method," *Deep Foundation Improvements: Design Construction and Testing*, ASTM STP 1089, ASTM, Philadelphia, pp. 224-233.
- BAEZ, J.I. AND HENRY, J.F. (1993). "Reduction of liquefaction potential by compaction grouting at Pinoplis Dam, South Carolina," *Geotechnical Practice in Dam Rehabilitation*, Geotechnical Special Publication 35, ASCE, New York, pp. 430-466.
- BALDI, G., BELLOTTI, R., GHIONNA, V., JAMIOLKOWSKY, M., MARCHETTI, S., AND PASQUELINI, E. (1986). "Flat dilatometer tests in calibration chambers," *Proceedings, In Situ '86*, Geotechnical Special Publication 6, ASCE, New York, pp. 431-446.

- BALDI, G., BRUZZI, D., SUPERBO, S., BATTAGLIO, M. AND JAMIOLKOWSKY, M. (1988). "Seismic cone in Po River sand," *Penetration Testing 1988, ISOPT-1 Symposium*, Orlando, Florida, Vol. 2, pp. 643-650.
- BALDI, G., BELLOTTI, R., GHIONNA, V., JAMIOLKOWSKY, M., AND LO PRESTI, D.C.F. (1989). "Modulus of sands from CPT's and DMT's," *Proceedings, 12th International Conference on Soil Mechanics and Foundation Engineering*, Rio de Janeiro, Brazil, Vol. 1, pp. 165-170.
- BARD, P.Y. AND GARIEL, J.C. (1986). "The seismic response of two-dimensional sedimentary deposits with large vertical velocity gradients," *Bulletin of the Seismological Society of America*, Vol. 76, pp. 343-356.
- BARTLETT, S.F. AND YOUD, T.L. (1992). "Empirical analysis of horizontal ground displacement generated by liquefaction-induced lateral spread," *Technical Report NCEER-92-0021*, National Center for Earthquake Engineering Research, Buffalo, New York.
- BATH, M. (1979). *Introduction to seismology*, Birkhauser, Boston, 428 pp.
- BATHE, K.J. (1982). *Finite Element Procedures in Engineering Analysis*, Prentice Hall, Englewood Cliffs, New Jersey, 735 pp.
- BAYLOR, J.L. (1974). "TRANL: a 3-D finite element code for transient nonlinear analysis," *DNA 3501F*, Weidlinger Associates, New York.
- BAZIAR, M.H., DOBRY, R., AND ELGAMEL, A.W.M. (1992). "Engineering evaluation of permanent ground deformations due to seismically-induced liquefaction," *Technical Report NCEER-92-0007*, National Center for Earthquake Engineering Research, State University of New York, Buffalo.
- BEEN, K. AND JEFFRIES, M.G. (1985). "A state parameter for sands," *Geotechnique*, Vol. 35, No. 2, pp. 99-112.
- BEEN, K., CROOKS, J.H.A., BECKER, D.E., AND JEFFRIES, M.G. (1986). "The cone penetration test in sands; Part I: State parameter interpretation," *Geotechnique*, Vol. 36, No. 2, pp. 239-249.
- BEEN, K., JEFFRIES, M.G., CROOKS, J.H.A., AND ROTHENBURG, L. (1987). "The cone penetration test in sands, Part II: General inference of state," *Geotechnique*, Vol. 37, No. 3, pp. 285-300.
- BELL, F.G. (1993). *Engineering treatment of soils*, E & FN Spon, London, 302 pp.
- BELLOTTI, R., GHIONNA, V., JAMIOLKOWSKY, M., LANCELLOTTA, R., AND MANFREDINI, G. (1986). "Deformation characteristics of cohesionless soils in insitu tests," *Proceedings, In Situ '86, Geotechnical Special Publication 6*, ASCE, New York, pp. 47-73.
- BEN-MENACHEM, A. (1961). "Radiation patterns of seismic surface waves from finite moving sources," *Bulletin of the Seismological Society of America*, Vol. 51, pp. 401-435.
- BENDER, B. (1984). "Incorporating acceleration variability into seismic hazard analysis," *Bulletin of the Seismological Society of America*, Vol. 74, No. 4, pp. 1451-1462.
- BENIOFF, H. (1955). "Mechanism and strain characteristics of the White Wolf fault as indicated by the aftershock sequence," *Earthquakes in Kern County, California During 1955*, California Division of Mines, Bulletin 171, G.B. Oakeshott, ed., pp. 199-202.
- BENJAMIN, J.R. AND ASSOCIATES (1988). "A criterion for determining exceedance of the Operating Basis Earthquake," *EPRI Report NP-5930*, Electric Power Research Institute, Palo Alto, California.
- BENJAMIN, J.R., AND CORNELL, C.A. (1970). *Probability, Statistics, and Decision for Civil Engineers*, McGraw-Hill, New York.
- BERG, G.V. (1983). *Seismic design codes and procedures*, Earthquake Engineering Research Institute, Berkeley, California, 119 pp.
- BERG, G.V. (1989). *Elements of Structural Dynamics*, Prentice Hall, Englewood Cliffs, New Jersey, 268 pp.

- BERGER, J., BAKER, L.M., BRUNE, J.N., FLETCHER, J.B., HANKS, T.C. AND VERNON, F.L. (1984). "The Anza array: A high-dynamic-range, broadband, digitally radiotelemetered seismic array," *Bulletin of the Seismological Society of America*, Vol. 74, No. 4, pp 1469-1481.
- BERLIN, G.L. (1980). *Earthquakes and the Urban Environment*, CRC Press, Boca Raton, Florida, Vol. 1, 211 pp.
- BISHOP, A.W. (1955). "The use of the slip circle in the stability analysis of slopes," *Geotechnique*, Vol. 5, No. 1, pp. 7-17.
- BJERRUM, L., (1971). "Subaqueous slope failures in Norwegian fjords," *Publication 88*. Norwegian Geotechnical Institute, Oslo.
- BOLT, B. A. (1969) "Duration of strong motion," *Proceedings of the 4th World Conference on Earthquake Engineering*, Santiago, Chile, pp. 1304-1315.
- BOLT, B.A. (1975). *Nuclear Explosions and Earthquakes*, W.H. Freeman, San Francisco.
- BOLT, B.A. (1988). *Earthquakes*, W.H. Freeman and Company, New York, 282 pp.
- BOLT, B.A. (1989). The nature of earthquake ground motion, in F. Naeim, ed., *The Seismic Design Handbook*, Van Nostrand Reinhold, New York.
- BOLT, B.A. (1993). *Earthquakes*, W.H. Freeman, New York, 331 pp.
- BONILLA, M.G. AND BUCHANAN, J.M. (1970). "Interim report on world-wide historic surface faulting," *Open-File Report*, U.S. Geological Survey, Reston, Virginia, 32 pp.
- BONILLA, M.G., MARK, R.K. AND LIENKAEMPER, J.J. (1984). "Statistical relations among earthquake magnitude, surface rupture length, and surface fault displacement," *Bulletin of the Seismological Society of America*, Vol. 74, pp. 2379-2411.
- BOORE, D.M. (1977). The motion of the ground during earthquakes, *Scientific American*, Vol. 237, No. 6, pp. 68-78.
- BOORE, D.M. (1983). "Stochastic simulation of high-frequency ground motions based on seismological models of the radiated spectra," *Bulletin of the Seismological Society of America*, Vol. 73, pp. 1865-1884.
- BOORE, D.M., JOYNER, W.B., AND FUMAL, T.E. (1993). Estimation of response spectra and peak accelerations from western North America earthquakes: An interim report, *Open-File-Report 93-509*, U.S. Geological Survey, Reston, Virginia, 72 pp.
- BORCHERDT, R. D., FLETCHER, J. B., JENSEN, E. G., MAXWELL, G. L., VAN SCHAAK, J. R., WARRICK, R. E., CRANSWICK, E., JOHNSON, M.J.S., AND McCLEARN, R. (1985) "A general earthquake observation system, *Bulletin of the Seismological Society of America*, 75, 1783-1825.
- BOULANGER, R.W., CHAN, C.K., SEED, H.B., SEED, R.B., AND SOUSA, J. (1993). "A low-compliance bi-directional cyclic simple shear apparatus," *Geotechnical Testing Journal*, ASTM, Vol. 16, No. 1, pp. 36-45.
- BRIGHAM, E.O. (1974). *The Fast Fourier Transform*, Prentice Hall, Englewood Cliffs, New Jersey, 252 pp.
- BROMS, B. (1991). "Deep compaction of granular soil," in H.-Y. Fang, ed., *Foundation Engineering Handbook*, 2nd ed., Van Nostrand Reinhold, New York, pp. 814-832.
- BROMS, B. AND BENNERMARK, H. (1967). Free discussion, *Proceedings, Geotechnical Conference*, Vol. 2, Oslo, Norway, pp. 118-120.
- BROWN, R.E. (1977). "Vibroflotation compaction of cohesionless soils," *Journal of the Geotechnical Engineering Division*, ASCE, Vol. 103, No. GT12, pp. 1437-1451.
- BRUCE, D.A. (1992). "Progress and development in dam rehabilitation by grouting," *Grouting, Soil Improvement, and Geosynthetics*, Geotechnical Special Publication 30, ASCE, New York, Vol. 1, pp. 601-613.

- BRUNE, J.N. (1970). "Tectonic stress and the spectra of seismic shear waves from earthquakes," *Journal of Geophysical Research*, Vol. 75, pp. 4997-5009.
- BRUNE, J.N. (1971). "Correction," *Journal of Geophysical Research*, Vol. 76, p. 5002.
- BSSC (1994A). *NEHRP Recommended Provisions for the Development of Seismic Regulations for New Buildings, Part I: Provisions*, Building Seismic Safety Council, Federal Emergency Management Agency, Washington, D.C.
- BSSC (1994B). *NEHRP Recommended Provisions for the Development of Seismic Regulations for New Buildings, Part II: Commentary*, Building Seismic Safety Council, Federal Emergency Management Agency, Washington, D.C.
- BULLARD, E.C., EVERETT, J.E., AND SMITH, A.G. (1965). "Fit of Continents around Atlantic, in P.M.S. Blackett, *On Continental Drift. Philosophical Transactions of the Royal Society of London, Series A*, Vol. 258, pp. 41-75.
- BULLEN, K.E. (1953). *An introduction to the theory of seismology*, Cambridge University Press, London, 296 pp.
- BULLEN, K.E. (1975). *The Earth's Density*, Chapman & Hall, London.
- BULLEN, K.E. AND BOLT, B.A. (1985). *An Introduction to the Theory of Seismology*, Cambridge University Press, Cambridge.
- BURLAND, J.B. AND SYMES, M.J. (1982) "A simple axial displacement gauge for use in the triaxial apparatus," *Geotechnique*, Vol. 32, No. 1, pp. 62-65.
- BUTLER, K.K., SLOGLUND, G.R., AND LANDERS, G.B. (1978). "Crosshole: An interpretive computer code for crosshole seismic test results, Documentation and examples," *Miscellaneous Paper S-78-6*, U.S. Army Corps of Engineers Waterways Experiment Station, Vicksburg, Mississippi.
- BYCROFT, G. N. (1978) "The effect of soil-structure interaction on seismometer readings," *Bulletin of the Seismological Society of America*, Vol. 68, pp. 823-843.
- BYRNE, P.M. (1991). "A model for predicting liquefaction induced displacement," *Proceedings, 2nd International Conference on Recent Advances in Geotechnical Earthquake Engineering and Soil Dynamics*, St. Louis, Missouri, Vol. 2, pp. 1027-1035.
- BYRNE, P.M., IMRIE, A.S., AND MORGENSTERN, N.R. (1993). "Results and implications of seismic response studies - Duncan Dam," *Proceedings, 46th Annual Canadian Geotechnical Conference*, Saskatoon, Saskatchewan, pp. 271-281.
- BYRNE, P.M., JITNO, H., AND SALGADO, R. (1992). "Earthquake-induced displacements of soil-structures systems," *Proceedings, 10th World Conference on Earthquake Engineering*, Madrid, Vol. 3, pp. 1407-1412.
- BYRNE, P.M., MORRIS, D.V., AND CALDWELL, J.A. (1984). "Seismic stability of a tailings impoundment on soft clayey silt deposits," *Proceedings, 8th World Conference on Earthquake Engineering*, San Francisco, Vol. 3.
- BYRNE, P.M., SALGADO, F., AND HOWIE, J.A. (1991). " G_{max} from pressuremeter tests: theory, chamber tests, and field measurements," *Proceedings, 2nd International Conference on Recent Advances in Geotechnical Earthquake Engineering and Soil Dynamics*, St. Louis, Missouri, Vol. 1, pp. 57-63.
- CAMPBELL, K. W. (1981) "Near source attenuation of peak horizontal acceleration," *Bulletin of the Seismological Society of America*, 71, 2039-2070.
- CAMPBELL, K.W. (1985). Strong ground motions attenuation relations: A ten-year perspective, *Earthquake Spectra*, Vol. 1, No. 4, pp. 759-804.
- CAMPBELL, K.W. AND BOZORGNA, Y. (1994). Near-source attenuation of peak horizontal acceleration from worldwide accelerograms recorded from 1957 to 1993, *Proceedings, Fifth U.S. National*

- Conference on Earthquake Engineering*, Earthquake Engineering Research Institute, Berkeley, California, Vol. 1, pp. 283-292.
- CAMPBELL, K.W. AND DUKE, C.M. (1974). Bedrock intensity, attenuation, and site factors from San Fernando earthquake records, *Bulletin of the Seismological Society of America*, Vol. 64, No. 1, pp. 173-185.
- CAQUOT, A. AND KERISEL, F. (1948). *Tables for the calculation of passive pressure, active pressure and bearing capacity of foundations*, Gauthier-Villars, Paris.
- CARTER, D.P. AND SEED, H.B. (1988). "Liquefaction potential of sand deposits under low levels of excitation," *Report UCB/EERC-88/11*, Earthquake Engineering Research Center, University of California, Berkeley, 309 pp.
- CASAGRANDE, A. (1936). "Characteristics of cohesionless soils affecting the stability of slopes and earth fills," *Journal of the Boston Society of Civil Engineers*, reprinted in *Contributions to Soil Mechanics*, Boston Society of Civil Engineers, 1940, pp.257-276.
- CASAGRANDE, A. (1976). "Liquefaction and cyclic mobility of sands: a critical review," *Harvard Soil Mechanics Series 88*, Harvard University, Cambridge, Massachusetts.
- CASTRO, G. (1969). "Liquefaction of sands," *Harvard Soil Mechanics Series 87*, Harvard University, Cambridge, Massachusetts.
- CASTRO, G. (1975). "Liquefaction and cyclic mobility of sands," *Journal of the Geotechnical Engineering Division*, ASCE, Vol. 101, No. GT6, pp. 551-569.
- CASTRO, G. (1991). "On the behavior of soils during earthquakes - liquefaction," *Proceedings, NSF/EPRI Workshop on Dynamic Soil Properties and Site Characterization*, EPRI NP-7337, Vol. 2, Electric Power Research Institute, Palo Alto, California, pp. 1-36.
- CASTRO, G. AND CHRISTIAN, J.T. (1976). "Shear strength of soils and cyclic loading," *Journal of the Geotechnical Engineering Division*, ASCE, Vol. 102, No. GT9, pp. 887-894.
- CASTRO, G. AND POULOS, S.J. (1977). "Factors affecting liquefaction and cyclic mobility," *Journal of the Geotechnical Engineering Division*, ASCE, Vol. 106, No. GT6, pp. 501-506.
- CASTRO, G. AND TRONCOSO, J. (1989). "Effects of 1989 Chilean earthquake on three tailings dams," *Proceedings, 5th Chilean Conference on Seismology and Earthquake Engineering*, Santiago, Chile.
- CASTRO, R.R., ANDERSON, J.G., AND SINGH, S.K. (1990). "Site response, attenuation and source spectra of s-waves along the Guerrero, Mexico, subduction zone," *Bulletin of the Seismological Society of America*, Vol. 80, No. 6, pp. 1489-1523.
- CEDERGREN, H. (1989). *Seepage, Drainage, and Flow Nets*, 3rd ed., Wiley, New York, 465 pp.
- CHAMEAU, J.L. AND CLOUGH, G.W. (1983). "Probabilistic pore pressure analysis for seismic loading," *Journal of Geotechnical Engineering*, ASCE, Vol. 109, No. 4, pp. 507-524.
- CHANG, C.-Y., MOK, C.M., POWER, M.S., TANG, Y.K., TANG, H.T., AND STEPP, J.C. (1991). "Development of shear modulus reduction curves based on Lotung downhole ground motion data," *Proceedings, 2nd International Conference on Recent Advances in Geotechnical Earthquake Engineering and Soil Dynamics*, St. Louis, Missouri, Vol. 1, pp. 111-118.
- CHANG, C.-Y., POWER, M.S., IDRISI, I.M., SOMERVILLE, P.G., SILVA, W., AND CHEN, P.C. (1986). "Engineering characterization of ground motion, Task II: Observational data on spatial variations of earthquake ground motions," *Report NUREG/CR-3805*, Vol. 3, U.S. Nuclear Regulatory Commission, Washington, D.C.
- CHANG, C.Y., POWER, M.S., MOK, C.M., TANG, Y.K., AND TANG, H.T. (1990). "Analysis of dynamic lateral earth pressures recorded on Lotung reactor containment model structure," *Proceedings, 4th U.S. National Conference on Earthquake Engineering*, Earthquake Engineering Research Institute, Palm Springs, California, Vol. 3, pp. 643-652.

- CHANG, F. K. AND KRINITZSKY, E. L. (1977) "Duration, spectral content, and predominant period of strong motion earthquake records from western United States," *Miscellaneous Paper 5-73-1*, U.S. Army Corps of Engineers Waterways Experiment Station, Vicksburg, Mississippi.
- CHANG, K.T. (1978). "An Analysis of Damage of Slope Sliding by Earthquake on the Paiho Main Dam and its Earthquake Strengthening," Tseng-hua Design Section, Dept. of Earthquake-Resistant Design and Flood Control Command of Miyna Reservoir, Peoples Republic of China.
- CHANG, M., KWIATOWSKI, H., NAU, R., OLIVER, R. AND PISTER, K. (1982). "ARMA models for earthquake ground motions," *Earthquake Engineering and Structural Dynamics*, Vol. 10, pp. 651-662.
- CHANG, N.Y., JUANG, M.J., LIEN, B.H., AND CHANG, F.K. (1986). "EQGEN: a user-friendly artificial earthquake simulation program," *Proceedings, 3rd U.S. National Conference on Earthquake Engineering*, Charleston, South Carolina, Vol. 1, pp. 439-450.
- CHEN, D. (1984). "Some empirical formulae for hazard analysis in China," *Proceedings, 8th World Conference on Earthquake Engineering*, San Francisco, Vol. 1, pp. 173-180.
- CHOPRA, A.K. (1966). "Earthquake effects on dams," Ph.D. dissertation, University of California, Berkeley.
- CHOPRA, A.K. (1995). *Dynamics of Structures*. Prentice Hall, Englewood Cliffs, New Jersey, 729 pp.
- CHOWDHURY, R.N. (1978). *Slope analysis*, Elsevier, New York, 423 pp.
- CHRISTIAN, J.T. (1988). "Developing design ground motions in practice," in *Geotechnical Special Publication 20, Earthquake Engineering and Soil Dynamics II: Recent Advances in Ground Motion Evaluation*, Geotechnical Special Publication 20, ASCE, New York, pp. 405-429.
- CHRISTIAN, J.T. AND SWIGER, W.F. (1973). "Statistic of liquefaction and SPT results," *Journal of the Geotechnical Engineering Division*, ASCE, Vol. 101, No. GT11, pp. 1135-1150.
- CHRISTIAN, J.T., ROESSET, J.M., AND DESAI, C.S. (1977). "Two- and three-dimensional dynamic analyses," Chapter 20 in *Numerical Methods in Geotechnical Engineering*, C.S. Desai and J.T. Christian, eds., McGraw Hill Book Company, New York, New York, pp. 683-718.
- CHRISTIAN, J.T., BORJESON, R.W., AND TRINGALE, P.T. (1978). "Probabilistic evaluation of OBE for nuclear plant," *Journal of the Geotechnical Engineering Division*, ASCE, Vol. 104, No. GT7, pp. 907-919.
- CHRISTOPHER, B.R., GILL, S.A., GIROUD, J.-P., JURAN, I., MITCHELL, J.K., SCHLOSSER, F., AND DUNNCLIFF, J. (1990). "Reinforced soil structures - design and construction guidelines," *Report FHWA-RD-89-043*, Vol. 1, Federal Highway Administration, Washington, D.C., 285 pp.
- CLOSE, U. AND MCCORMICK, E. (1922). "Where the mountains walked," *National Geographic*, Vol. 41, No. 5, pp. 445-464.
- CLOUGH, G.W. AND DUNCAN, J.M. (1971). Finite element analyses of retaining wall behavior, *Journal of the Soil Mechanics and Foundations Division*, ASCE, Vol. 97, No. SM12, pp. 1657-1674.
- CLOUGH, R.W. AND PENZIEN, J. (1975). *Dynamics of Structures*, McGraw-Hill, New York, 634 pp.
- CLUFF, L.S. AND CLUFF, J.L. (1984). "Importance of assessing degrees of fault activity for engineering decisions," *Proceedings, 8th World Conference on Earthquake Engineering*, San Francisco, Vol. 2, pp. 629-636.
- CLUFF, L.S., HANSON, W.R., TAYLOR, C.L., WEAVER, K.D., BROGAN, G.E., IDRISI, I.M., MCCLURE, F.E., AND BLAYNEY, J.A. (1972). "Site evaluation in seismically active regions: an interdisciplinary approach," *Proceedings, First International Conference on Microzonation*, Seattle, Washington, Vol. 2, pp. 957-987.
- CLUFF, L.S., PATARDHAN, A.S., AND COPPERSMITH, K.J. (1980). "Estimating the probability of occurrences of surface faulting earthquakes on the Wasatch fault zone," *Bulletin of the Seismological Society of America*, Vol. 70, No. 5, pp. 1463-1478.

- Code of Federal Regulations* (1978). "Title 10, Energy; Part 100 [10 CFR 100] *Reactor Site Criteria*; Appendix A, Seismic and geologic siting criteria for nuclear power plants," Nuclear Regulatory Commission, Washington, D.C.
- COMMITTEE ON EARTHQUAKE ENGINEERING RESEARCH (1982). *Earthquake engineering research - 1982*, National Research Council, National Academy Press, Washington, D.C., 266 pp.
- COMMITTEE ON NUCLEAR STRUCTURES AND MATERIALS (1979). *Analyses for Soil-Structure Interaction Effects for Nuclear Power Plants*, ASCE, New York, 155 pp.
- COMMITTEE ON SEISMIC RISK (1984). "Glossary of terms for probabilistic seismic-risk and hazard analysis," *Earthquake Spectra*, Vol. 1, No. 1, pp. 33-40.
- CONLON, R. (1966). "Landslide at Toulnustouc River, Quebec," *Canadian Geotechnical Journal*, Vol. 3, No. 3, pp. 113-144.
- CONSTANTINOU, M. AND GAZETAS, G. (1984). "Probabilistic seismic sliding deformations of earth dams and slopes," *Proceedings, 4th ASCE Specialty Conference on Probabilistic Mechanics and Structural Reliability*, pp. 318-321.
- CONVERSE, A.M. (1992). "BAP: Basic strong-motion accelerogram processing software, Version 1.0" *Open-File Report 92-296A*, U. S. Geological Survey, U.S. Department of the Interior, Denver, Colorado.
- COOLEY, P.M., AND TUKEY, J.W. (1965). An algorithm for the machine computation of complex Fourier series, *Mathematics of Computation*, Vol. 19, No. 4, pp. 297-301.
- COPPERSMITH, K.J. (1981). "Probabilities of earthquake occurrences on the San Andreas fault based on geologic risk," *EOS*, Vol. 62, No. 17, p. 322.
- COPPERSMITH, K.J. AND YOUNGS, R.R. (1986). "Capturing uncertainty in probabilistic seismic hazard assessments with intraplate tectonic environments," *Proceedings, 3rd U.S. National Conference on Earthquake Engineering*, Charleston, South Carolina, Vol. 1, pp. 301-312.
- CORNELL, C.A. (1968). Engineering seismic risk analysis, *Bulletin of the Seismological Society of America*, Vol. 58, pp. 1583-1606.
- CORNELL, C.A. AND WINTERSTEIN, S.R. (1986). "Applicability of the Poisson earthquake-occurrence model," in *Seismic Hazard Methodology for the Central and Eastern United States*, EPRI Research Report NP-4726, Electric Power Research Institute, Palo Alto, California.
- CORNELL, C.A. AND WINTERSTEIN, S.R. (1988). "Temporal and magnitude dependence in earthquake recurrence models, *Bulletin of the Seismological Society of America*, Vol. 78, pp. 1522-1537.
- CORNELL, C.A., BANON, H., AND SHAKAL, A.F. (1979). Seismic motion and response prediction alternatives, *Earthquake Engineering and Structural Dynamics*, Vol. 7, No. 4, pp. 295-315.
- CORNFORTH, D.H., WORTH, E.G. AND WRIGHT, W.L., (1975). "Observations and analysis of a flow slide in sand fill," in British Geotechnical Society, *Field Instrumentation in Geotechnical Engineering*, Wiley, New York, 136-151.
- CORPS OF ENGINEERS (1979). "Geophysical exploration," *Engineer Manual 1110-1-1802*, U. S. Department of the Army, Corps of Engineers.
- COULOMB, C.A. (1776). "Essai sur une application des regles des maximis et minimis a quelques problemes de statique relatifs a l'architecture," *Memoires de l'Academie Royale prés Divers Savants*, Vol. 7.
- COULTER, M. AND MIGLIACCIO, L. (1966). "Effects of the earthquake of March 27, 1964 at Valdez, Alaska." *Professional Paper 542-C*, U.S. Geological Survey , U.S. Department of the Interior, Washington, D.C.
- CROUSE, C. B. AND HUSHMAND, B. (1989). "Soil-structure interaction at CDMG and USGS accelerograph stations," *Bulletin of the Seismological Society of America*, Vol. 79, No. 1, pp. 1-14.

- CROUSE, C. B., LIANG, G. C., AND MARTIN, G. R. (1984). "Experimental study of soil-structure interaction at an accelerograph station," *Bulletin of the Seismological Society of America*, Vol. 74, pp. 1995-2013.
- CROUSE, C.B. (1991). "Ground motion attenuation equations for earthquakes on the Cascadia subduction zone," *Earthquake Spectra*, Vol. 7, No. 2, pp. 201-236.
- CROUSE, C.B. AND HUSHMAND, B. (1989). Soil-structure interaction at CDMG and USGS accelerograph stations, *Bulletin of the Seismological Society of America*, Vol. 79, No. 1, pp. 1-14.
- CUNDALL, P.A. AND STRACK, O.D.L. (1979). "A discrete numerical model for granular assemblies," *Geotechnique*, Vol. 29, No. 1, pp. 47-65.
- DADDAZIO, R.P., ETTOUNEY, M.M., AND SANDLER, I.S. (1987). "Nonlinear dynamic slope stability analysis," *Journal of Geotechnical Engineering*, ASCE, Vol. 113, No. 4, pp. 285-298.
- DAFALIAS, Y.F. AND HERRMANN, L.R. (1982). "Bounding surface formulation of soil plasticity," Chapter 10 in G.N. Pande and O.C. Zienkiewicz, eds., *Soil Mechanics: Transient and Cyclic Loads*, Wiley, New York, pp. 253-282.
- DAFALIAS, Y.F. AND POPOV, E.P. (1979). "A model for nonlinearly hardening materials for complex loading," *Acta Mechanica*, Vol. 21, No. 3, pp. 173-192.
- DAKOULAS, P. (1985). "Contributions to seismic analysis of earth dams," Ph.D. dissertation, Renssalaer Polytechnic Institute, Troy, New York.
- DAKOULAS, P. AND GAZETAS, G. (1985). "A class of inhomogeneous shear models for seismic response of dams and embankments," *Soil Dynamics and Earthquake Engineering*, Vol. 4, No. 4, pp. 166-182.
- DAKOULAS, P. AND GAZETAS, G. (1986). "Seismic lateral vibration of embankment dams in semi-cylindrical valleys," *Earthquake Engineering and Structural Dynamics*, Vol. 13, No. 1, pp. 19-40.
- DAKOULAS, P. AND GAZETAS, G. (1986). "Seismic shear strains and seismic coefficients in dams and embankments," *Soil Dynamics and Earthquake Engineering*, Vol. 5, No. 2, pp. 75-83.
- DAVIS, J.L. (1986). *Finite Difference Methods in Dynamics of Continuous Media*, Macmillan, New York, 238 pp.
- DAVIS, R.O. AND BERRILL, J.B. (1982). "Energy dissipation and seismic liquefaction in sands," *Earthquake Engineering and Structural Dynamics*, Vol. 10, No. 1, pp. 59-68.
- DBAIBO, N.T. (1989). "Investigation of collapse surface behavior of sands," *M.S.E. Thesis*, Department of Civil Engineering, University of Washington, Seattle, Washington, 268 pp.
- DE ALBA, P. AND PYKE, R.M. (1987). "Behavior of embankments on soft soils under earthquake loading," *Proceedings*, International Symposium on Geotechnical Engineering of Soft Soils, Mexico City, Vol. 2, pp. 125-141.
- DE ALBA, P., BALDWIN, K., JANOO, V., ROE, G. AND CELIKKEL, B. (1984). "Elastic-wave velocities and liquefaction potential," *Geotechnical Testing Journal*, ASTM, Vol. 7, No. 2, pp. 77-88.
- DE ALBA, P. (1983). "Pile settlement in a liquefying soil deposit," *Journal of Geotechnical Engineering*, ASCE, Vol. 109, No. 9, pp. 1165-1180.
- DE ALBA, P., CHAN, C.K., AND SEED, H.B. (1975). "Determination of soil liquefaction characteristics by large-scale laboratory tests," *Report EERC 75-14*, Earthquake Engineering Research Center, University of California, Berkeley.
- DENG, N., ASHFORD, S.A., AND LYSMER, J. (1995). GROUND2D: A two-dimensional seismic site response analysis program, *Report*, Earthquake Engineering Research Center, University of California, Berkeley.
- DENNEHY, K.T. (1985). Seismic vulnerability, analysis, and design of anchored bulkheads, *Ph.D. Dissertation*, Renssalaer Polytechnic Institute, Troy, New York.

- DER-KIUREGHIAN, A. AND ANG, A.H.S. (1977). "A fault-rupture model for seismic risk analysis," *Bulletin of the Seismological Society of America*, Vol. 67, No. 4, pp. 1173-1194.
- DESAI, C.S. AND ABEL, J.F. (1972). *Introduction to the Finite Element Method*, Van Nostrand Reinhold, New York.
- DESAI, C.S. AND SIRIWARDANE, H.J. (1984). *Constitutive Laws for Engineering Materials, with Emphasis on Geologic Materials*, Prentice Hall, Englewood Cliffs, New Jersey, 468 pp.
- DEWEY, J.W. (1979). "A consumer's guide to instrumental methods for determination of hypocenters," A.W. Hatheway and C.R. McClure, Jr., eds., *Geology in the Siting of Nuclear Power Plants, Geologic Society of America Reviews in Engineering Geology*, Vol. 4, pp. 109-117.
- DIKMEN, S.U. AND GHABOSSI, J. (1984). "Effective stress analysis of seismic response and liquefaction, theory," *Journal of Geotechnical Engineering*, ASCE, Vol. 110, No. 5, pp. 628-644.
- DOBRY, R. AND LADD, R.S. (1980). Discussion to "Soil liquefaction and cyclic mobility evaluation for level ground during earthquakes," by H.B. Seed and "Liquefaction potential: science versus practice," by R.B. Peck, *Journal of the Geotechnical Engineering Division*, ASCE, Vol. 106, No. GT6, pp. 720-724.
- DOBRY, R. AND VUCETIC, M. (1987). "Dynamic properties and seismic response of soft clay deposits," *Proceedings, International Symposium on Geotechnical Engineering of Soft Soils*, Mexico City, Vol. 2, pp. 51-87.
- DOBRY, R., IDRISI, I.M., AND NG, E. (1978). "Duration characteristics of horizontal components of strong motion earthquake records," *Bulletin of the Seismological Society of America*, Vol. 68, No. 5, pp. 1487-1520.
- DOBRY, R., LADD, R.S., YOKEL, F.Y., CHUNG, R.M., AND POWELL, D. (1982). "Prediction of pore water pressure buildup and liquefaction of sands during earthquakes by the cyclic strain method," *NBS Building Science Series 138*, National Bureau of Standards, Gaithersburg, Maryland, 150 pp.
- DOBRY, R., MOHAMAD, R., DAKOULAS, P., AND GAZETAS, G. (1984). "Liquefaction evaluation of earth dams - a new approach," *Proceedings, 8th World Conference on Earthquake Engineering*, Vol. 3, pp. 333-340.
- DOBRY, R., VASQUEZ-HERRERA, A., MOHAMMAD, R. AND VUCETIC, M. (1985). "Liquefaction flow failure of silty sand by torsional cyclic tests," *Advances in the Art of Testing Soils Under Cyclic Loading Conditions*, ASCE, New York, pp. 29-50.
- DOBSON, T. (1987). "Case histories of the vibro systems to minimize the risk of liquefaction," in *Soil Improvement: A Ten Year Update*, Geotechnical Special Publication 12, ASCE, New York, pp. 167-183.
- DOUGLAS, B.J., OLSEN, R.S., AND MARTIN, G.R. (1981). Evaluation of the cone penetrometer test for SPT liquefaction assessment, *Proceedings, In Situ Testing to Evaluate Liquefaction Susceptibility*, ASCE, New York.
- DRNEVICH, V.P. (1967). "Effect of strain history on the dynamic properties of sand," Ph.D. Dissertation, University of Michigan, 151 pp.
- DRNEVICH, V.P. (1972). "Undrained cyclic shear of saturated sand," *Journal of the Soil Mechanics and Foundations Division*, ASCE, Vol. 98, No. SM8, pp. 807-825.
- DRNEVICH, V.P. AND RICHART, F.E. JR. (1970). "Dynamic prestraining of dry sand," *Journal of the Soil Mechanics and Foundations Division*, ASCE, Vol. 96, No. SM2, pp. 453-469.
- DUNCAN, J.M. (1992). "State-of-the-art: static stability and deformation analysis," in R.B. Seed and R.W. Boulanger, eds., *Proceedings, Specialty Conference on Stability and Performance of Slopes and Embankments*, II, ASCE, New York, Vol. 1, pp. 222-266.

- DUNCAN, J.M. AND CHANG, C.Y. (1970). "Nonlinear analysis of stress and strain in soils," *Journal of the Soil Mechanics and Foundations Division*, ASCE, Vol. 96, No. SM5, pp. 1629-1653.
- DUNCAN, J.M., BYRNE, P.M., WONG, K.S., AND MABRY, P. (1980). "Strength, stress-strain, and bulk modulus parameters for finite element analysis of stresses and movements in soil masses," *Report UCB/GT/80-01*, University of California, Berkeley.
- DUNCAN, J.M., CLOUGH, G.W., AND EBELING, R.M. (1990). "Behavior and design of gravity earth retaining structures," *Proceedings, ASCE Specialty Conference on Design and Performance of Earth Retaining Structures*, Special Technical Publication 25, Cornell University, Ithaca, New York, pp. 251-277.
- DUSSOM, K.B., HADJ-HAMOU, T., AND BAKER, R. (1991). "QUAKE: An expert system for the selection of design earthquake accelerogram," *Computers and Structures*, Vol. 40, No. 1, pp. 161-167.
- DYVIK, R. AND MADSHUS, C. (1985). "Laboratory measurements of G_{\max} using bender elements," *Advances in the Art of Testing Soils Under Cyclic Conditions*, ASCE, New York, pp. 186-196.
- EBELING, R.M. AND MORRISON, E.E. (1993). "The seismic design of waterfront retaining structures," *NCEL Report R-939*, Naval Civil Engineering Laboratory, Port Hueneme, California, 256 pp.
- ECKERSLEY, J.D. (1985). "Flowslides in stockpiled coal," *Engineering Geology*, Vol 22, No. 1, pp. 13-22.
- EIBY, G.A. (1980). *Earthquakes*, Van Nostrand Reinhold, New York.
- EILER, E.E. AND WHITTIER, R.M. (1988). "Piezoelectric and piezoresistive transducers," Chapter 12 in *Shock and Vibration Handbook*, 3rd edition, C.M. Harris, editor, McGraw Hill Book Company, New York.
- ELGAMAL, A.M., SCOTT, R.F., SUCCARIEH, M.F., AND YAN, L.P. (1990). "La Villita Dam response during five earthquake including permanent deformation," *Journal of Geotechnical Engineering*, ASCE, Vol. 116, No. 10, pp. 1443-1462.
- ELGAMAL, A.W., ABDEL-GHAFFAR, M., AND PREVOST, J.H. (1985). "Elasto-plastic earthquake shear response of one-dimensional earth dam models," *Earthquake Engineering and Structural Dynamics*, Vol. 13, pp. 617-633.
- ELGHADAMSI, F. E., MOHRAZ, B., LEE, C. T. AND MOAYYAD, P. (1988) "Time dependent power spectral density of earthquake motion," *International Journal of Soil Dynamics and Earthquake Engineering*, 7 No. (1), pp. 15-21.
- EPRI (1986). "Seismic hazard methodology for the central and eastern United States," *Report NP-4726*, Electric Power Research Institute, Palo Alto, California.
- EPRI (1993). *Guidelines for determining design basis ground motions*, Electric Power Research Institute, Palo Alto, California, Vol. 1, pp. 8-1 through 8-69.
- ESTEVA, L. (1970). "Seismic risk and seismic design decisions," in R.J. Hansen, ed., *Seismic Design of Nuclear Power Plants*, MIT Press, Cambridge, Massachusetts.
- EVANS, M.D. AND SEED, H.B. (1987). "Undrained cyclic triaxial testing of gravels: the effect of membrane compliance," *Report UCB/EERC-87/08*, Earthquake Engineering Research Center, University of California, Berkeley, California.
- EWING, M., JARDESKY, W. AND PRESS, F. (1957). *Elastic Waves in Layered Media*, McGraw-Hill, New York, 380 pp.
- FACCIOLI, E. (1991). "Seismic amplification in the presence of geological and topographic irregularities," *Proceedings, 2nd International Conference on Recent Advances in Geotechnical Earthquake Engineering and Soil Dynamics*, St. Louis, Missouri, Vol. 2, pp. 1779-1797.
- FARDIS, M.N. AND VENEZIANO, D. (1982). "Probabilistic analysis of deposit liquefaction," *Journal of the Geotechnical Engineering Division*, ASCE, Vol. 108, No. GT3, pp. 395-417.

- FELIO, G., VUCETIC, M., HUDSON, M., BARAR, P. AND CHAPMAN, R. (1990). "Performance of soil nailed walls during the October 17, 1989 Loma Prieta earthquake," *Proceedings, 43rd Canadian Geotechnical Conference*, Quebec City, Vol. 1, pp. 165-173.
- FELLENIUS, B. (1953). "The landslide at Guntorp," *Geotechnique*, Vol. 5, No. 1, pp. 120-125.
- FELLENIUS, W. (1927). *Erdstatische Berechnungen mit Reibung und Kohäsion*, Ernst, Berlin.
- FERRITTO, J.M. (1992). "Optimized earthquake time history and response spectra, User's guide," *Report UG-0025*, Naval Civil Engineering Laboratory, Port Hueneme, California, 14 pp.
- FIEGEL, G.L. AND KUTTER, B.L. (1992). "The mechanism of liquefaction in layered soils," *Report CR92.009*, Naval Civil Engineering Laboratory, Port Hueneme, California, 34 pp.
- FIGUEROA, J.L. AND DAHISARIA, N. (1991). "An energy approach in defining soil liquefaction," *Proceedings, 2nd International Conference on Recent Advances in Geotechnical Earthquake Engineering and Soil Dynamics*, St. Louis, Missouri, Vol. 1, pp. 407-410.
- FINN, W.D.L. (1988). "Dynamic analysis in geotechnical engineering," *Earthquake Engineering and Soil Dynamics II: Recent Advances in Ground-Motion Evaluation*, Geotechnical Special Publication 20, ASCE, New York, pp. 523-591.
- FINN, W.D.L. (1990). "Analysis of post-liquefaction deformations in soil structures," *Proceedings, H. Bolton Seed Memorial Symposium*, University of California, Berkeley, Vol. 2, pp. 291-312.
- FINN, W.D.L. (1991). "Assessment of liquefaction potential and post-liquefaction behavior of earth structures: Developments 1981-1991 (State-of-the-art paper)," *Proceedings, 2nd International Conference on Recent Advances in Geotechnical Earthquake Engineering and Soil Dynamics*, St. Louis, Missouri, Vol. 3, pp. 1833-1850.
- FINN, W.D.L. (1991). "Geotechnical engineering aspects of microzonation," *Proceedings, 4th International Conference on Microzonation*, Earthquake Engineering Research Institute, Stanford University, Palo Alto, California, Vol. 1, pp. 199-259.
- FINN, W.D.L. AND BHATIA, S.K. (1981). "Prediction of seismic pore-water pressures," *Proceedings, 10th International Conference on Soil Mechanics and Foundation Engineering*, Rotterdam, The Netherlands, Vol. 3, pp. 201-206.
- FINN, W.D.L. AND YOGENDRAKUMAR, M. (1989). *TARA-3FL - Program for analysis of liquefaction induced flow deformations*, Department of Civil Engineering, University of British Columbia, Vancouver, British Columbia.
- FINN, W.D.L., BRANSBY, P.L., AND PICKERING, D.J. (1970). "Effect of strain history on liquefaction of sands," *Journal of the Soil Mechanics and Foundations Division*, ASCE, Vol. 96, No. SM6, pp. 1917-1934.
- FINN, W.D.L., PICKERING, D.J., AND BRANSBY, P.L. (1971). "Sand liquefaction in triaxial and simple shear tests," *Journal of the Soil Mechanics and Foundations Division*, ASCE, Vol. 97, No. SM4, pp. 639-659.
- FINN, W.D.L., LEE, K.W., AND MARTIN, G.R. (1977). "An effective stress model for liquefaction," *Journal of the Geotechnical Engineering Division*, ASCE, Vol. 103, No. GT6, pp. 517-533.
- FINN, W.D.L., YOGENDRAKUMAR, M., YOSHIDA, M., AND YOSHIDA, N. (1986). *TARA-3: A Program to Compute the Response of 2-D Embankments and Soil-Structure Interaction Systems to Seismic Loadings*, Department of Civil Engineering, University of British Columbia, Vancouver.
- FINN, W.D.L., LEDBETTER, R.H., FLEMING, R.L., JR., TEMPLETON, A.E., FORREST, T.W., AND STACY, S.T. (1991). "Dam on liquefiable foundation: Safety assessment and remediation," *Proceedings, 17th International Conference on Large Dams*, Vienna, pp. 531-553.

- FINN, W.D.L., WU, G., AND YOSHIDA, N. (1992). "Seismic response of sheet pile walls," *Proceedings, 10th World Conference on Earthquake Engineering*, Madrid, Vol. 3, pp. 1689-1694.
- FINN, W.D.L., LEDBETTER, R.H., AND WU, G. (1994). "Liquefaction in silty soils: Design and analysis," *Ground Failures under Seismic Conditions*, Geotechnical Special Publication 44, ASCE, New York, pp. 51-76.
- FLORIN, V.A. AND IVANOV, P.L. (1961). "Liquefaction of saturated sand soil," *Proceedings, 5th International Conference on Soil Mechanics and Foundation Engineering*, Paris.
- FOSTER, R. J. (1971). *Physical Geology*, Charles E. Merrill, Columbus, Ohio.
- FOWLER, C.M.R. (1990). *The solid earth. An introduction to global geophysics*, Cambridge University Press, Cambridge, England, 472 pp.
- FRAGASZY, R.J., ALI, A., DENBY, G., AND KILIAN, A.P. (1987). "Seismic response of tieback walls," *Transportation Research Record*, Transportation Research Board, Washington, D.C.
- FRANKLIN, A.G. AND CHANG, F.K. (1977). Permanent displacements of earth embankments by Newmark sliding block analysis, *Report 5, Miscellaneous Paper S-71-17*, U.S. Army Corps of Engineers Waterways Experiment Station, Vicksburg, Mississippi.
- FRENCH ASSOCIATION FOR EARTHQUAKE ENGINEERING (1990). *Recommendations AFPS90 for the reduction of rules relative to the structures and installations built in regions prone to earthquakes*, Saint-Remy-les-Chevreuse, France.
- GAO, Z., HO, B., AND CHANG, D. (1983). "Some geological considerations for the damage during the Tangshan earthquake," *North China Earthquake Sciences*, Vol. 1, pp. 64-72 (in Chinese).
- GARFUNKEL, Z. (1975). "Growth, shrinking, and long-term evolution of plates and their implications for flow patterns in the mantle," *Journal of Geophysical Research*, Vol. 80, p. 4425.
- GAZETAS, G. (1982). "Shear vibrations of vertically inhomogeneous earth dams," *International Journal for Numerical and Analytical Methods in Geomechanics*, Vol. 6, No. 1, pp. 219-241.
- GAZETAS, G. (1987). "Seismic response of earth dams; some recent developments," *Soil Dynamics and Earthquake Engineering*, Vol. 6, No. 1, pp. 3-47.
- GAZETAS, G. (1991). Foundation vibrations, Chapter 15 in *Foundation Engineering Handbook*, 2nd edition, H.-Y. Fang, ed., Van Nostrand Reinhold, New York, pp. 553-593.
- GAZETAS, G., DAKOULAS, P., AND DENNEHY, K. (1990). Empirical seismic design method for waterfront anchored sheetpile walls, *Proceedings, ASCE Specialty Conference on Design and Performance of Earth Retaining Structures*, Geotechnical Specialty Publication 25, pp. 232-250.
- GELI, L., BARD, P.Y., AND JULLIEN, B. (1988). "The effect of topography on earthquake ground motion: A review and new results," *Bulletin of the Seismological Society of America*, Vol. 78, No. 1, pp. 42-63.
- GILBERT, F. AND DZIEWONSKI, A.M. (1975). "An application of normal mode theory to the retrieval of structural parameters and source mechanisms from seismic spectra," *Phil. Trans. R. Soc. Lond.*, 278, 187-269.
- GLASER, S. (1995). System identification and its application to estimating soil properties, *Journal of Geotechnical Engineering*, Vol. 121, No. 7, pp. 553-560.
- GLEN, W. (1975). *Continental Drift and Plate Tectonics*, Charles E. Merrill, Columbus, Ohio.
- GOODMAN, L.E. (1988). Material damping and slip damping, Chapter 36 in C.M. Harris, ed., *Shock and Vibration Handbook*, 3rd ed., McGraw-Hill, New York.
- GOTO, S., TATSUOKA, F., SHIBUYA, S., KIM, Y.-S., AND SATO, S. (1991). "A simple gauge for local small strain measurements in the laboratory," *Soils and Foundations*, Vol. 31, No. 1, pp. 169-180.

- GOULOIS, A.M., WHITMAN, R.V., AND HOEG, K. (1985). "Effect of sustained shear stress on the cyclic degradation of clay," *Proceedings, Symposium on Strength Testing of Marine Sediments*, R.C. Chaney and K.R. Demars, eds., ASTM STP 883, ASTM, Philadelphia, pp. 336-351.
- GRAF, E.D. (1992). "Earthquake support grouting in sands," in *Grouting, Soil Improvement, and Geosynthetics*, Geotechnical Special Publication 30, ASCE, New York, Vol. 2, pp. 879-888.
- GRIFFITHS, D.H. AND KING, R.F. (1965). *Applied geophysics for engineers and geologists*, Pergamon Press, New York, 223 pp.
- GRIFFITHS, D.V. AND PREVOST, J.H. (1988). "Two- and three-dimensional finite element analyses of the Long Valley Dam," *Technical Report NCEER-88-0015*, National Center for Earthquake Engineering Research, Buffalo, New York.
- GUAGENTI-GRANDORI, E. AND MOLINA, D. (1984). "Semi-Markov processes in seismic risk analysis," *Proceedings, International Symposium of Semi-Markov Processes and Their Applications*, Brussels.
- GUBBINS, D. (1990). *Seismology and Plate Tectonics*, University Press, Cambridge, 339 pp.
- GUCUNSKI, N. AND WOODS, R.D. (1991). "Use of Rayleigh modes in interpretation of SASW test," *Proceedings, 2nd International Conference on Recent Advances in Geotechnical Earthquake Engineering and Soil Dynamics*, St. Louis, Missouri, Vol. 2, pp. 1399-1408.
- GUTENBERG, B. (1927). *Grundlagen der Erdbebeneukunde*, Berlin.
- GUTENBERG, B. (1945). "Magnitude determination for deep-focus earthquakes," *Bulletin of the Seismological Society of America*, Vol. 35, pp. 117-130.
- GUTENBERG, B., AND RICHTER, C.F. (1936). "On Seismic Waves (third paper)", *Gelands Bietraege zur Geophysik*, Vol. 47, pp. 73-131.
- GUTENBERG, B. AND RICHTER, C.F. (1942). "Earthquake magnitude, intensity, energy, and acceleration," *Bulletin of the Seismological Society of America*, Vol. 32, pp. 163-191.
- GUTENBERG, B. AND RICHTER, C. F. (1944). "Frequency of Earthquakes in California," *Bulletin of the Seismological Society of America*, Vol. 34, No. 4, pp. 1985-1988.
- GUTENBERG, B. AND RICHTER, C.F. (1954). *Seismicity of the Earth and Related Phenomena*, Princeton University Press, Princeton, New Jersey, 310 pp.
- GUTENBERG, B. AND RICHTER, C.F. (1956). "earthquake magnitude: intensity, energy, and acceleration," *Bulletin of the Seismological Society of America*, Vol. 46, pp. 104-145.
- HACHEY, J.E., PLUM, R.L., BYRNE, R.J., KILIAN, A.P., AND JENKINS, D.V. (1994). Blast densification of a thick, loose debris flow at Mt. St. Helen's, Washington, *Proceedings, Vertical and Horizontal Deformations of Fundations and Embankments*, Geotechnical Special Publication No. 40, ASCE, College Station, Texas, pp. 502-512.
- HAGER, B.H. (1978). "Oceanic plate driven by lithospheric thickening and subducted slabs," *Nature*, Vol. 276, pp. 156-159.
- HAGIWARA, Y. (1974). "Probability of earthquake occurrence as obtained from a Weibull distribution analysis of crustal strain," *Tectonophysics*, Vol. 23, No. 3, pp. 313-318.
- HALDAR, A. AND TANG, W.H. (1979). "Probabilistic evaluation of liquefaction potential," *Journal of the Geotechnical Engineering Division*, ASCE, Vol. 105, No. GT2, pp. 145-163.
- HALDAR, A. AND TANG, W.H. (1981). "Statistical study of uniform cycles in earthquakes," *Journal of the Geotechnical Engineering Division*, ASCE, Vo. 107, No. GT5, pp. 577-589.
- HALL, W.J. (1988). "Part I: Vibration of structures induced by ground motion," Chapter 24 in *Shock and Vibration Handbook*, 3rd edition, C.M. Harris, editor, McGraw Hill Book Company, New York.
- HAMADA, M., YASUDA, S., ISOYAMA, R., AND EMOTO, K. (1986). "Study on liquefaction induced permanent ground displacements," *Report for the Association for the Development of Earthquake Prediction*.

- HAMADA, M. AND O'ROURKE, T.D. (1992). Case histories of liquefaction and lifeline performance during past earthquakes, *Technical Report NCEER-92-0001*, National Center for Earthquake Engineering Research, Buffalo, New York, 2 Vol.
- HANKS, T.C. (1982). "f_{max}," *Bulletin of the Seismological Society of America*, Vol. 72, pp. 1867-1879.
- HANKS, T.C. AND KANAMORI, H. (1979). "A moment magnitude scale," *Journal of Geophysical Research*, Vol. 84, pp. 2348-2350.
- HANKS, T. C. AND MCGUIRE, R. K. (1981) "The character of high-frequency strong ground motion," *Bulletin of the Seismological Society of America*, Vol. 71, pp. 2071-2095.
- HANZAWA, H., ITOH, Y., AND SUZUKI, K. (1979). "Shear characteristics of a quick sand in the Arabian Gulf," *Soils and Foundations*, Vol., 19, No. 4, pp.1-15.
- HAO, H., OLIVEIRA, C.S., AND PENZIEN, J. (1989). "Multiple station ground motion processing and simulation based on SMART-1 array data," *Nuclear Engineering and Design*, Vol. 111, pp. 293-310.
- HARDER, L. F. AND SEED, H.B. (1986). "Determination of penetration resistance for coarse-grained soils using the Becker hammer drill," *Report UCB/EERC-86/06*, Earthquake Engineering Research Center, University of California, Berkeley, 126 pp.
- HARDER, L.F., JR., HAMMOND, W.D., AND ROSS, P.S. (1984). "Vibroflotation compaction at Thermalito Afterbay," *Journal of Geotechnical Engineering*, ASCE, Vol. 110, No. 1, pp. 57-72.
- HARDIN, B.O. (1978). "The nature of stress-strain behavior of soils," *Proceedings, Earthquake Engineering and Soil Dynamics*, ASCE Pasadena, California, Vol. 1, pp. 3-89.
- HARDIN, B.O. AND BLACK, W.L. (1968). "Vibration modulus of normally consolidated clay," *Journal of the Soil Mechanics and Foundations Division*, ASCE, Vol. 94, No. SM2, pp. 353-369.
- HARDIN, B.O. AND DRNEVICH, V.P. (1972a). "Shear modulus and damping in soils: Measurement and parameter effects," *Journal of the Soil Mechanics and Foundations Division*, ASCE, Vol. 98, No. SM6, pp. 603-624.
- HARDIN, B.O. AND DRNEVICH, V.P. (1972b). "Shear modulus and damping in soils: design equations and curves," *Journal of the Soil Mechanics and Foundations Division*, ASCE, Vol. 98, No. SM7, pp. 667-692.
- HARICHARAN, R.S. AND VANMARCKE, E.H. (1986). "Stochastic variation of earthquake ground motion in space and time," *Journal of Engineering Mechanics*, Vol. 112, No. 2, pp. 154-174.
- HART, M.E. (1987). *Reliability-based Design in Civil Engineering*, McGraw-Hill, New York.
- HARTZELL, S. (1978). "Earthquake aftershocks as Green's functions," *Geophysical Research Letters*, Vol. 5, No. 1, pp. 1-4.
- HASKELL, N.H. (1953). "The dispersion of surface waves in multilayered media," *Bulletin of the Seismological Society of America*, Vol. 43, pp. 17-34.
- HATANAKA, M. (1952). "3-dimensional consideration on the vibration of earth dams," *Journal of the Japanese Society of Civil Engineers*, Vol. 37, No. 10.
- HATHEWAY, A.W. AND LEIGHTON, F.B. (1979). "Trenching as an exploratory method," in A.W. Hatheway and C.R. McClure eds. *Geology in the Siting of Nuclear Power Plants*, Reviews in Engineering Geology, Geological Society of America, Vol. 4, pp. 169-198.
- HAUSMANN, M.R. (1990). *Engineering Principles of Ground Modification*, McGraw-Hill, New York, 632 pp.
- HAYDEN, R.F. (1994). "Utilization of liquefaction countermeasures in North America," *Proceedings, 5th U.S. National Conference on Earthquake Engineering*, Chicago, Vol. 4, pp. 149-158.

- HAYDEN, R.F. AND WELCH, J.P. (1991). "Design and installation of stone columns at naval air station," in M.I. Esrig and R.C. Bachus, eds., *Deep Foundation Improvement: Design, Construction, and Testing*, ASTM STP 1089, ASTM, Philadelphia, pp. 172-184.
- HEATON, T.H. AND KANAMORI, H. (1984). "Seismic potential associated with subduction in the northwestern United States," *Bulletin of the Seismological Society of America*, Vol. 73, No. 3, pp. 933-941.
- HEIDARI, M. AND JAMES, R.G. (1982). "Centrifuge modelling of earthquake induced liquefaction in a column of sand," *Proceedings, Conference on Soil Dynamics and Earthquake Engineering*, A.A. Balkema, Rotterdam, The Netherlands, Vol. 1, pp. 271-281.
- HEISEY, J.S., STOKOE, K.H., AND MEYER, A.H. (1982). "Moduli of pavement systems from spectral analysis of surface waves," *Transportation Research Record 853*, Transportation Research Board Washington, D.C.
- HENKE, W. AND HENKE, R. (1991). "In situ torsional cylindrical shear test - laboratory results," *Proceedings, 2nd International Conference on Recent Advances in Geotechnical Earthquake Engineering and Soil Dynamics*, St. Louis, Missouri, Vol. 1, pp. 131-136.
- HERSHBERGER, J. (1956). "A comparison of earthquake accelerations with intensity ratings," *Bulletin of the Seismological Society of America*, Vol. 46, pp. 317-320.
- Hertz, H. (1881). "Über die Beruhrung fester elastischer Körper," *Journal Für die Reine und Angewandte Mathematik*, Vol. 92, pp. 156-171.
- HETTLER, A. AND GUDEHUS, G. (1985). "A pressure-dependent correction for displacement results from 1 g model tests with sand," *Geotechnique*, Vol. 35, No. 4, pp. 497-510.
- HEUKELOM, W. AND FOSTER, C.R. (1960). "Dynamic testing of pavements," *Journal of the Soil Mechanics and Foundations Division, ASCE*, Vol. 86, No. SM1), pp. 1-28.
- HILTUNEN, D.R. AND WOODS, R.D. (1988). "SASW and crosshole test results compared," *Proceedings, Earthquake Engineering and Soil Dynamics II: Recent Advances in Ground Motion Evaluation*, Geotechnical Special Publication 20, ASCE, New York, pp. 279-289.
- HO, C.L., DENBY, G.M., AND FRAGASZY, R.J. (1990). Seismic performance of tied-back walls, *Proceedings, ASCE Specialty Conference on Design and Performance of Earth Retaining Structures*, Geotechnical Specialty Publication No. 25, pp. 843-853.
- HOAR, R.J. AND STOKOE, K.H. (1984). "Field and laboratory measurements of material damping of soil in shear" *Proceedings, 8th World Conference on Earthquake Engineering*, San Francisco, Vol. 3, pp. 47-54.
- HOLTZ, R.D. AND KOVACS, W.D. (1981). *An Introduction to Geotechnical Engineering*, Prentice Hall, Englewood Cliffs, New Jersey, 733 pp.
- HORN, H.M. (1978). "North American experience in soil sampling and its influence on dynamic laboratory testing," Preprint Session No. 79, ASCE Annual Convention, Chicago.
- HOU, S. (1968). "Earthquake simulation models and their applications," *Report R68-17*, Department of Civil Engineering, Massachusetts Institute of Technology, Cambridge, Massachusetts.
- HOUSNER, G.W. (1947). "Characteristics of strong-motion earthquakes," *Bulletin of the Seismological Society of America*, Vol. 37, No. 1, pp. 19-31.
- HOUSNER, G. W. (1959) "Behavior of structures during earthquakes," *Journal of the Engineering Mechanics Division, ASCE*, Vol. 85, No. EM14, 109-129.
- HOUSNER, G.W. ET AL. (1990). *Competing Against Time*, Report to the Governor, Governor's Board of Inquiry, State of California.
- HOUSTON, W.N. AND HERRMANN, H.G. (1980). Undrained cyclic strength of marine soil, *Journal of the Geotechnical Engineering Division, ASCE*, Vol. 106, No. GT6, pp. 691-712.

- HRYCIW, R.D. (1989). "Ray-path curvature in shallow seismic investigations," *Journal of Geotechnical Engineering*, ASCE, Vol. 115, No. 9, pp. 1268-1284.
- HRYCIW, R.D. (1990). Small-strain-shear modulus of soil by dilatometer, *Journal of Geotechnical Engineering*, ASCE, Vol. 116, No. 11, pp. 1700-1716.
- HRYCIW, R.D., VITTON, S., AND THOMANN, T.G. (1990). "Liquefaction and flow failure during seismic exploration," *Journal of Geotechnical Engineering*, ASCE, Vol. 116, No. 12, pp. 1881-1889.
- HUANG, Y.H. (1983). *Stability Analysis of Earth Slopes*, Van Nostrand Reinhold, New York, 305 pp.
- HUDSON, D.E. (1958). "The Wilmot survey type strong-motion earthquake recorder," *Earthquake Engineering Laboratory Research Report*, California Institute of Technology, Pasadena, California.
- HUDSON, D.E. (1979). *Reading and Interpreting Strong Motion Accelerograms*, Earthquake Engineering Research Institute, Berkeley, California, 112 pp.
- HUDSON, D.E. (1984). "Strong motion accelerograph systems - problems and prospects," *Proceedings, 8th World Conference on Earthquake Engineering*, Vol. 2, pp. 39-45.
- HUNGR, O. AND MORGENSTERN, N.R. (1984). "High velocity ring shear tests on sand," *Geotechnique*, Vol. 34, No. 3, pp. 415-421.
- HUSSIN, J.D. AND ALI, S. (1987). "Soil improvement of the Trident submarine facility," in *Soil Improvement: A Ten Year Update*, Geotechnical Special Publication 12, ASCE, New York, pp. 215-231.
- HVORSLEV, M.J. (1949). *Subsurface Exploration and Sampling of Soils for Civil Engineering Purposes*, Report of Committee on Sampling and Testing, Soil Mechanics and Foundations Division, ASCE, New York, 521 pp.
- HYNES-GRIFFIN, M.E. AND FRANKLIN, A.G. (1984). "Rationalizing the seismic coefficient method," *Miscellaneous Paper GL-84-13*, U.S. Army Corps of Engineers Waterways Experiment Station, Vicksburg, Mississippi, 21 pp.
- IAI, S. (1989). "Similitude for shaking table tests on soil-structure-fluid model in 1g gravitational field," *Soils and Foundations*, Vol. 29, No. 1, pp. 105-118.
- IAI, S. AND KAMEOKA, T. (1993). "Finite element analysis of earthquake induced damage to anchored steel sheet pile quay walls," *Soils and Foundations*, Vol. 33, No. 1, pp. 71-91.
- IAI, S., NODA, S., AND TSUCHIDA, H. (1988). "Basic consideration for designing the area of the ground compaction as a remedial measure against liquefaction," *Proceedings, U.S.-Japan Joint Workshop on Remedial Measures for Liquefiable Soils*.
- IAI, S., MATSUNAGA, Y., MORITA, T., MIYODA, M., SAKURAI, H., OISHI, H., OGURA, H., ANDO, Y., TANAKA, Y., AND KATO, M. (1994). "Effects of remedial measures against liquefaction at 1993 Kushiro-Oki earthquake," *Proceedings, 5th Japan-U.S. Workshop on Earthquake Resistant Design of Lifeline Facilities and Countermeasures for Soil Liquefaction*, Snowbird, Utah.
- ICBO, (1994). *Uniform Building Code, 1991*, International Conference of Building Officials, Whittier, California.
- Idriss, I.M. (1985). "Evaluating seismic risk in engineering practice," *Proceedings of the 11th International Conference on Soil Mechanics and Foundation Engineering*, San Francisco, Vol. 1, 255-320.
- IDRISS, I.M. (1990). "Response of soft soil sites during earthquakes," in J.M. Duncan, ed., *Proceedings, H. Bolton Seed Memorial Symposium*, BiTech Publishers, Vancouver, British Columbia, Vol. 2, pp. 273-289.
- IDRISS, I.M. (1991). "Earthquake ground motions at soft soil sites," *Proceedings, 2nd International Conference on Recent Advances in Geotechnical Earthquake Engineering and Soil Dynamics*, Vol. III, pp. 2265-2271.

- IDRISS, I.M. AND SEED, H.B. (1968). "An analysis of ground motions during the 1957 San Francisco earthquake," *Bulletin of the Seismological Society of America*, Vol. 58, No. 6, pp. 2013-2032.
- IDRISS, I.M. and Sun, J.I. (1992). "SHAKE91: a computer program for conducting equivalent linear seismic response analyses of horizontally layered soil deposits," *User's Guide*, University of California, Davis, 13 pp.
- IDRISS, I.M., DOBRY, R., AND SINGH, R.D. (1978). "Nonlinear behavior of soft clays during cyclic loading," *Journal of the Geotechnical Engineering Division*, ASCE, Vol. 104, No. GT12, pp. 1427-1447.
- IDRISS, I.M., MORIWAKI, Y., WRIGHT, S.G., DOYLE, E.H., AND LADD, R.S. (1980). "Behavior of normally consolidated clay under simulated earthquake and ocean wave loading conditions, Proceedings, International Symposium on Soils under Cyclic and Transient Loading", Swansea, United Kingdom, Vol. 1, pp. 437-445.
- IIDA, K., COX, D.C., AND PARARAS-CARAYANNIS, G. (1967). "Preliminary catalog of tsunamis occurring in the Pacific Ocean," *Report No. HIG-67-10*, Hawaii Institute of Geophysics, University of Hawaii, Honolulu, Hawaii.
- IMAI, T. AND TONOUCHI, K. (1982). "Correlation of N-value with s-wave velocity and shear modulus," *Proceedings, 2nd European Symposium on Penetration Testing*, Amsterdam, pp. 57-72.
- ISENHOWER, W.M. AND STOKOE, K.H. (1981). Strain rate dependent shear modulus of San Francisco Bay Mud, *Proceedings, Internatinoal Conference on Recent Advances in Geotechnical Earthquake Engineering and Soil Dynamics*, St. Louis, Missouri, Vol. 2, pp. 597-602.
- ISHIBASHI, I. (1992). Discussion to "Effect of soil plasticity on cyclic response," by M. Vucetic and R. Dobry, *Journal of Geotechnical Engineering*, ASCE, Vol. 118, No. 5, pp. 830-832.
- ISHIBASHI, I. AND ZHANG, X. (1993). "Unified dynamic shear moduli and damping ratios of sand and clay," *Soils and Foundations*, Vol. 33, No. 1, pp. 182-191.
- ISHIHARA, K. (1984). "Post-earthquake failure of a tailings dam due to liquefaction of the pond deposit," *Proceedings, International Conference on Case Histories in Geotechnical Engineering*, University of Missouri, St. Louis, Vol. 3, pp. 1129-1143.
- ISHIHARA, K. (1985). "Stability of natural deposits during earthquakes," *Proceedings, 11th International Conference on Soil Mechanics and Foundation Engineering*, Vol. 1, pp. 321-376.
- ISHIHARA, K. (1993). Liquefaction and flow failure during earthquakes, *Geotechnique*, Vol. 43, No. 3, pp. 351-415.
- ISHIHARA, K. AND KOSEKI, J. (1989). Discussion of "Cyclic shear strength of fines-containing sands," *Earthquake Geotechnical Engineering, 12th International Conference on Soil Mechanics and Foundation Engineering*, Rio de Janeiro, pp. 101-106.
- ISHIHARA, K. AND LI, S. (1972). "Liquefaction of saturated sand in triaxial torsion shear test," *Soils and Foundations*, Vol. 12, No. 2, pp. 19-39.
- ISHIHARA, K. AND TOWHATA, I. (1980). "One-dimensional soil response analysis during earthquakes based on effective stress model," *Journal of the Faculty of Engineering*, University of Tokyo, Vol. 35, No. 4.
- ISHIHARA, K. AND YOSHIMINE, M. (1992). "Evaluation of settlements in sand deposits following liquefaction during earthquakes," *Soils and Foundations*, Vol. 32, No. 1, pp. 173-188.
- ISHIHARA, K., TATSUOKA, F., AND YASUDA, S. (1975). "Undrained deformation and liquefaction of sand under cyclic stresses," *Soils and Foundations*, Vol. 15, No. 1, pp. 29-44.
- ISHIHARA, K., KAWASE, Y., AND NAKAJIMA, M. (1980). Liquefaction characteristics of sand deposits at an oil tank site during the 1978 Miyagiken-Oki earthquake, *Soils and Foundation*, Vol. 20, No. 2, pp. 97-111.
- ISHIMOTO, M. (1932). "Echelle d'intensité sismique et accélération maxima," *Bulletin of the Earthquake Research Institute*, Tokyo University, Vol.10, pp. 614-626.

- IVERSON, R.M. AND DENLINGER, R.P. (1987). "The physics of debris flows: a conceptual assessment," in R.L. Beschta, T. Blinn, G.E. Grant, G.G. Ice, and F.J. Swanson, eds. *Proceedings, Erosion and Sedimentation in the Pacific Rim*, International Association of Hydrological Science, Corvallis, Oregon, pp. 155-165.
- IVERSON, R.M. AND LAHUSEN, R.G. (1993). "Friction in debris flows: Inferences from large-scale flume experiments," *Proceedings, Hydraulics Engineering '93*, ASCE, San Francisco, pp. 1604-1609.
- IWAN, W.D. (1967). "On a class of models for the yielding behavior of continuous and composite systems," *Journal of Applied Mechanics*, Vol. 34, No. E3, pp. 612-617.
- IWASAKI, T., TATSUOKA, F., AND TAKAGI, Y. (1978). "Shear modulus of sands under torsional shear loading," *Soils and Foundations*, Vol. 18, No. 1, pp. 39-56.
- JACOB, K.H. (1991). "Seismoc zonation and site response: Are building-code soil-factors adequate to account for variability of site conditions across the US?" *Proceedings, 4th International Conference on Microzonation*, Earthquake Engineering Research Institute, Stanford University, Palo Alto, California, Vol. 1, pp. 695-702.
- JAKOBSEN, B. (1952). "The landslide at Surte on the Gota River, September 29, 1952," *Proceedings 5*, Royal Swedish Geotechnical Institute, Stockholm.
- JAMIOLKOWSKY, M. AND LOPRESTI, D.C.F. (1992). Discussion of "Correlation between liquefaction resistance and shear wave velocity," by K. Tokimatsu and A. Uchida, *Soils and Foundations*, Vol. 32, No. 2, pp. 145-148.
- JAMIOLKOWSKI, M., LEROUEIL, S., AND LOPRESTI, D.C.F. (1991). "Theme lecture: Design parameters from theory to practice," *Proceedings, Geo-Coast '91*, Yokohama, Japan, pp. 1-41.
- JANBU, N. (1968). "Slope stability computations," *Soil Mechanics and Foundation Engineering Report*, Technical University of Norway, Trondheim.
- JANES, H.W. (1973). Densification of sand for drydock by Terra-probe, *Journal of the Soil Mechanics and Foundations Division*, ASCE, Vol. 99, No. SM6, pp. 451-470.
- JAPAN SOCIETY OF CIVIL ENGINEERS (1980). "Earthquake resistant design of quaywalls and piers in Japan," *Earthquake Resistant Design for Civil Engineering Structures*, Earth Structures and Foundations, pp. 31-85.
- JENNINGS, J.E. (1979). "The failure of a slimes dam at Bafokeng," *Civil Engineering in South Africa*, Vol. 6, pp. 135-140.
- JENNINGS, P.C. (1985). "Ground motion parameters that influence structural damage," in R.E. Scholl and J.L. King, eds. *Strong Ground Motion Simulation and Engineering Applications*, EERI Publication 85-02, Earthquake Engineering Research Institute, Berkeley, California.
- JEYAPALAN, J.K. (1980). "Analyses of flow failures of mine tailings impoundments," Ph.D. Dissertation, University of California, Berkeley, 298 pp.
- JEYAPALAN, J.K., DUNCAN, J.M., AND SEED, H.B. (1981). "Summary of research on flow failures of mine tailings impoundments," *Information Circular 8857*, Technology Transfer Workshop on Mine Waste Disposal Techniques, U.S. Bureau of Mines, Denver, Colorado, pp. 54-63.
- JIBSON, R. (1987). "Summary of research on the effects of topographic amplification of earthquake shaking on slope stability," *Open-File Report 87-268*, U.S. Geological Survey, Menlo Park, California.
- JIBSON, R. (1994). "Predicting earthquake-induced landslide displacements using Newmark's sliding block analysis," *Transportation Research Record 1411*, Transportation Research Board, Washington, D.C., pp. 9-17.
- JOHNSON, A.M. (1970). *Physical Processes in Geology*, Freeman, Cooper, San Francisco, 577 pp.

- JOHNSON, H.V. (1982). "The effects of end platens, methods of loading and specimen size in monotonic triaxial R tests," *Miscellaneous Paper GL-82-10*, U.S. Army Engineering Waterways Experiment Station, Vicksburg, MS.
- JOHNSON, L.R. AND SILVA, W. (1981). "The effects of unconsolidated sediments upon the ground motion during local earthquakes," *Bulletin of the Seismological Society of America*, Vol. 71, No. 1, pp. 127-142.
- JOHNSON, S.A., GREENLEAF, J.F., RITMAN, E.L., HARRIS, L.D., AND RAJAGOPALAN, B. (1978). "Three-dimensional analysis and display of rock and soil masses for site characterization: potential contributions from medical imaging techniques," *Proceedings, Specialty Workshop on Site Characterization and Exploration*, Northwestern University, Evanston, Illinois, pp. 322-334.
- JOHNSTON, A.C. (1990). "An earthquake strength scale for the media and the public," *Earthquakes and Volcanoes*, Vol. 22, No. 5, pp. 214-216.
- JOYNER, W.B. (1977). "NONLI3: A Fortran program for calculating nonlinear ground response," *Open File Report 77-761*, U.S. Geological Survey, Menlo Park, California.
- JOYNER, W. B. AND BOORE, D. M. (1981) "Peak horizontal acceleration and velocity from strong-motion records including records from the 1979 Imperial Valley, California earthquake," *Bulletin of the Seismological Society of America*, 71, 2011-2038.
- JOYNER, W.B. AND BOORE, D.M. (1982). "Prediction of earthquake response spectra," *Proceedings, 51st Annual Convention of the Structural Engineers of California*, also *USGS Open-File Report 82-977*, 16 pp.
- JOYNER, W.J. AND BOORE, D.M. (1991). Strong earthquake ground motion and engineering design, *Geotechnical News*, Vol. 9, No. 1, pp. 21-26.
- JOYNER, W. B. AND BOORE, D.M. (1988) "Measurement, characterization, and prediction of strong ground motion," in *Earthquake Engineering and Soil Dynamics II - Recent Advances in Ground-Motion Evaluation*, Geotechnical Special Publication 20, ASCE, New York, pp. 43-102.
- JOYNER, W.B. AND CHEN, A.T.F. (1975) "Calculation of nonlinear ground response in earthquakes," *Bulletin of the Seismological Society of America*, Vol. 65, pp. 1315-1336.
- JOYNER, W.B., WARRICK, R.E., AND OLIVER, A.A., III (1976). "Analysis of seismograms from a downhole array in sediments near San Francisco Bay," *Bulletin of the Seismological Society of America*, Vol. 66, No. 5, pp. 937-958.
- KAGAWA, T. (1977). "Shaking table tests and analysis of soil-structure systems," Ph.D. Dissertation, University of California, Berkeley.
- KAGAWA, T., MEJIA, L., SEED, H.B., AND LYSMER, J. (1981). "TLUSH: a computer program for three-dimensional dynamic analysis of earth dams," *Report UCB/EERC-81/14*, University of California, Berkeley.
- KANAI, K. (1957) "Semi-empirical formula for the seismic characteristics of the ground," *Bulletin of the Earthquake Research Institute*, Tokyo University, Vol. 35, pp. 308-325.
- KANAMORI, H. (1977). "The Energy Release in Great Earthquakes," *Journal of Geophysical Research*, Vol. 82, pp. 2981-2987.
- KANAMORI, H. (1983). Magnitude scale and quantification of earthquakes, *Tectonophysics*, Vol. 93, pp. 185-199.
- KANAMORI, H. (1988). "Importance of historical seismograms for geophysical research," in W.H.K. Lee, H. Meyers, and K. Shimazaki, eds. *Historical Seismograms and Earthquakes of the World*, Academic Press, San Diego, California, pp. 16-31.

- KANAMORI, H. AND STEWART, G.S. (1978). "Seismological aspects of the Guatemala earthquake of February 4, 1976," *Journal of Geophysical Research*, Vol. 83, pp. 3427-3434.
- KATAYAMA, I. (1991). "Wave scattering effect in soil-structure interaction," *Proceedings, 11th International Conference on Structural Mechanics in Reactor Technology*, Tokyo, Vol. K, pp. 153-158.
- KATAYAMA, T. AND SATO, N. (1982). "Ground strain measurement by a very densely located seismometer array," *Proceedings, 6th Japan Earthquake Engineering Symposium*, pp. 241-248.
- KAVAZANJIAN, E., ECHEZURIA, H., AND MCCANN, M.W. (1985). "RMS acceleration hazard for San Francisco," *Soil Dynamics and Earthquake Engineering*, Vol. 4, No. 3, pp.
- KAVAZANJIAN, E., JR., SNOW, M.S., MATASOVIC, N., PORAN, C., AND SATOH, T. (1994). "Non-intrusive Rayleigh wave investigations at solid waste landfills," *Proceedings, First International Conference on Environmental Geotechnics*, Edmonton, Alberta, Canada.
- KAWAI, T. (1985). DIANA - Dynamic interaction approach and non-linear analysis, *Summary Report*, Science University of Tokyo.
- KAWASUMI, H. (1951). "Measures of earthquake danger and expectancy of maximum intensity throughout Japan as inferred from the seismic activity in historical times," *Bulletin of the Earthquake Research Institute*, Tokyo University, Vol. 29, pp. 469-482.
- KAYEN, R.E., MITCHELL, J.K., SEED, R.B., LODGE, A., NISHIO, S., AND COTINHO, R. (1992). Evaluation of SPT-, CPT-, and shear wave-based methods for liquefaction potential assessment using Loma Prieta data, *Proceedings, 4th U.S. - Japan Workshop on Earthquake Resistant Design of Lifeline Facilities and Countermeasures for Soil Liquefaction*, Vol. 1, pp. 177-204.
- KEAREY, P. AND VINE, F.J. (1990). *Global Tectonics*, Blackwell, Oxford, 302 pp.
- KEEFER, D.K. (1984). "Landslides caused by earthquakes," *Geologic Society of America Bulletin*, Vol. 95, No. 2, pp. 406-421.
- KELLER, T.O., CASTRO, G., AND ROGERS, J.H. (1987). "Steel Creek Dam foundation densification," in *Soil Improvement: A Ten Year Update*, Geotechnical Special Publication 12, ASCE, New York, pp. 136-166.
- KENNEDY, R.P. (1980). "Ground motion parameters useful in structural design," presented at the Conference on Evaluation of Regional Seismic Hazards and Risk, Santa Fe, New Mexico.
- KHOURI, N.Q. (1984). "Dynamic properties of soils," *Masters Thesis*, Department of Civil Engineering, Syracuse University, Syracuse, New York.
- KING, J.L. AND TUCKER, B.E. (1984). "Dependence of sediment-filled valley response on the input amplitude and the valley properties," *Bulletin of the Seismological Society of America*, Vol. 74, No. 1, pp. 153-165.
- KIREMIDJIAN, A. AND ANAGNOS, T. (1984). "Stochastic slip-predictable model for earthquake occurrences," *Bulletin of the Seismological Society of America*, Vol. 74, pp. 739-755.
- KISHIDA, H. (1967). "Ultimate bearing capacity of piles driven into loose sand," *Soils and Foundations*, Vol. 7, No. 3, pp. 20-29.
- KITAJIMA, S. AND UWABE, T. (1979). "Analysis of seismic damage in anchored sheet-piling bulkheads," *Report of the Japanese Port and Harbor Research Institute*, Vol. 18, No. 1, pp. 67-130 (in Japanese).
- KLEINER, D.E. (1976). "Design and construction of an embankment dam to impound gypsum wastes," *Proceedings, 12th International Congress on Large Dams, International Commission on Large Dams*, Mexico City, pp. 235-249.
- KLEYN, A.H. (1983). *Seismic Reflection Interpretation*, Applied Science Publishers, London, 269 pp.

- KLOHN, E.J., GARGA, V.K., AND SHUKIN, W. (1981). "Densification of sand tailings by blasting," *Proceedings, 10th International Conference on Soil Mechanics and Foundation Engineering*, Stockholm, Vol. 3, pp. 725-730.
- KOBAYASHI, Y. (1981). "Causes of fatalities in recent earthquakes in Japan," *Journal of Disaster Science*, Vol. 3, pp. 15-22.
- KOERNER, R.M. (1994). *Designing with geosynthetics*, Prentice Hall, Englewood Cliffs, New Jersey, 783 pp.
- KOESTER, J.P. (1994). The influence of fines type and content on cyclic strength, *Ground Failures Under Seismic Conditions*, Geotechnical Special Report No. 44, ASCE, New York, pp. 17-33.
- KOKUSHO, T. (1980). "Cyclic triaxial test of dynamic soil properties for wide strain range," *Soils and Foundations*, Vol. 20, No. 2, pp. 45-60.
- KOKUSHO, T., YOSHIDA, Y., AND ESASHI, Y. (1982). "Dynamic properties of soft clay for wide strain range," *Soils and Foundations*, Vol. 22, No. 4, pp. 1-18.
- KOLSKY, H. (1963). *Stress waves in solids*, Dover Publications, New York, 213 pp.
- KONDNER, R.L. (1963). "Hyperbolic stress-strain response: cohesive soils," *Journal of the Soil Mechanics and Foundations Division*, ASCE, Vol 89, No. SM1, pp. 115-.
- KONDNER, R.L. AND ZELASKO, J.S. (1963). "A hyperbolic stress-strain formulation of sands," *Proceedings, 2nd Pan American Conference on Soil Mechanics and Foundation Engineering*, Brazil, Vol. 1, p. 281.
- KONNO, T., SUZUKI, Y., TATOISHI, A., ISHIHARA, K., AKINO, K., AND SATSUO, I. (1993). "Gravelly soil properties by field and laboratory tests," *Proceedings, 3rd International Conference on Case Histories in Geotechnical Engineering*, St. Louis, Missouri, Vol. 1, pp. 575-594.
- KONRAD, J.-M. (1988). "Interpretation of flat plate dilatometer tests in sands in terms of the state parameter," *Geotechnique*, Vol. 38, No. 2, pp. 263-278.
- KOPPEJAN, A.W., WAMELAN, B.M. AND WEINBERG, L.J. (1948), "Coastal flowslides in the Dutch Province of Zeeland," *Proceedings, 2nd International Conference on Soil Mechanics and Foundation Engineering*, Vol. 5, pp. 89-96.
- KOUTSOFTAS, D.C. (1978). "Effect of cyclic loads on undrained strength of two marine clays," *Journal of the Geotechnical Engineering Division*, ASCE, Vol. 104, No. GT5.
- KOUTSOFTAS, D.C. AND KIEFER, M.L. (1990). "Improvement of mine spoils in southern Illinois," in *Geotechnics of Waste Fills*, Special Technical Publication 1070, ASTM, Philadelphia, pp. 153-167.
- KOVACS, W.D. AND LEO, E. (1981). "Cyclic simple shear of large-scale sand samples: Effects of diameter to height ratio," *Proceedings, International Conference on Recent Advances in Geotechnical Earthquake Engineering and Soil Dynamics*, St. Louis, Vol. 3, pp. 897-907.
- KOVACS, W.D. AND SALOMONE, L.A. (1982). "SPT hammer energy measurement," *Journal of the Geotechnical Engineering Division*, ASCE, Vol. 108, No. GT4, pp. 599-620.
- KOVACS, W.D., EVANS, J.C., AND GRIFFITH, A.H. (1977). "Toward a more standardized SPT," *Proceedings, 9th International Conference on Soil Mechanics and Foundation Engineering*, Tokyo, Vol. 2, pp. 269-276.
- KOZIN, F. (1988). "Autoregressive moving average models of earthquake records," *Journal of Probabilistic Engineering Mechanics*, Vol. 3, No. 2.
- KRAMER, S.L. (1985). "Liquefaction of sands due to non-seismic loading," *Ph.D. Dissertation*, University of California, Berkeley, California.
- KRAMER, S.L. (1988). "Triggering of liquefaction flow slides in coastal soil deposits," *Engineering Geology*, Vol. 26, No. 1, pp. 17-31.

- KRAMER, S.L. (1989). "Uncertainty in Steady State Liquefaction Evaluation Procedures," *Journal of Geotechnical Engineering*, ASCE, Vol. 115, No. 10, pp. 1402-1419.
- KRAMER, S.L. AND HOLTZ, R.D. (1991). *Soil improvement and foundation remediation with emphasis on seismic hazards*, University of Washington, Seattle, Washington, 106 pp.
- KRAMER, S.L. AND SEED, H.B. (1988). "Initiation of soil liquefaction under static loading condition," *Journal of Geotechnical Engineering*, ASCE, Vol. 114, No. 4, pp. 412-430.
- KRAMER, S.L. AND SIVANESWARAN, N. (1989a). "A non-destructive, specimen-specific method for measurement of membrane penetration in the triaxial test," *Geotechnical Testing Journal*, ASTM, Vol. 12, No. 1, pp. 50-59.
- KRAMER, S.L. AND SIVANESWARAN, N. (1989b). "Stress-path-dependent correction for membrane penetration," *Journal of Geotechnical Engineering*, ASCE, Vol. 115, No. 12, pp. 1787-1804.
- KRINITZSKY, E.L. AND CHANG, F.K. (1979). "State-of-the-art for assessing earthquake hazards in the United States: specifying peak motions for design earthquakes," *Miscellaneous Paper S-73-1, Report 7*, U.S. Army Corps of Engineers Waterways Experiment Station, Vicksburg, Mississippi.
- KRINITZSKY, E.L. AND CHANG, F.K. (1987). "Parameters for specifying intensity-related earthquake ground motions," *Miscellaneous Paper S-73-1, Report 25*, U.S. Army Corps of Engineers Waterways Experiment Station, Vicksburg, Mississippi, 43 pp.
- KRINITZSKY, E.L., GOULD, J.P., AND EDINGER, P.H. (1993). *Fundamentals of Earthquake-Resistant Construction*, John Wiley and Sons, New York, 299 pp.
- KUHLEMAYER, R.L. AND LYSMER, J. (1973). Finite element method accuracy for wave propagation problems, *Journal of the Soil Mechanics and Foundations Division*, ASCE, Vol. 99, No. SM5, pp. 421-427.
- KULKARNI, R. B., SUDIGH, K., AND IDRISI, I. M. (1979) "Probabilistic evaluation of seismic exposure," *Proceedings, 8th World Conference on Earthquake Engineering*, San Francisco, pp. 90-98.
- KULKARNI, R.B., YOUNGS, R.R., AND COPPERSMITH, K.J. (1984). "Assessment of confidence intervals for results of seismic hazard analysis," *Proceedings, 8th World Conference on Earthquake Engineering*, San Francisco, Vol. 1, pp. 263-270.
- KUTTER, B.L. AND JAMES, R.G. (1989). "Dynamic centrifuge model tests on clay embankments," *Geotechnique*, Vol. 39, No. 1, pp. 91-106.
- LADD, C.C. AND FOOTT, R. (1974). "New design procedure for stability of soft clays," *Journal of the Geotechnical Engineering Division*, ASCE, Vol. 100, No. GT7, pp. 763-786.
- LADD, R.J. AND DUTKO, P. (1985). "Small-strain measurements using triaxial apparatus," in V. Koschla, ed., *Advances in the Art of Testing Soils Under Cyclic Conditions*, ASCE, New York, pp. 148-166.
- LADD, R.S. (1974). "Specimen preparation and liquefaction of sands," *Journal of the Geotechnical Engineering Division*, ASCE, Vol. 100, No. GT10, pp. 1180-1184.
- LADE, P.V. (1988). "Effects of voids and volume changes on the behaviour of frictional materials," *International Journal for Numerical and Analytical Methods in Geomechanics*, Vol. 12, pp. 351-370.
- LADE, P.V. (1992). "Static instability and liquefaction of loose fine sandy slopes," *Journal of Geotechnical Engineering*, ASCE, Vol. 118, No. 1, pp. 51-71.
- LADE, P.V. AND HERNANDEZ, S.B. (1977). "Membrane penetration effects in undrained tests," *Journal of the Geotechnical Engineering Division*, ASCE, Vol. 103, No. GT2, pp. 109-125.
- LAFOSSE, U. AND VON ROSENVINGE, T. (1992). "Densification of loose sands by blasting," *Grouting, Soil Improvement, and Geosynthetics*, Geotechnical Special Publication 30, ASCE, New York, Vol. 2, pp. 954-968.

- LAI, C.D. (1977). "A two-dimensional 'immigration-branching' model with application to earthquake occurrence times and energies," *Journal of Applied Probability*, Vol. 14, pp. 464-474.
- LAI, S.P. (1982). "Statistical characterization of strong motions using power spectral density function," *Bulletin of the Seismological Society of America*, Vol. 72, No. 1, pp 259-274.
- LAMBE, T.W. AND WHITMAN, R.V. (1969). *Soil Mechanics*, Wiley, New York.
- LAW, K.T., CAO, Y.L., AND HE, G.N. (1990). "An energy approach for assessing seismic liquefaction potential," *Canadian Geotechnical Journal*, Vol. 27, No. 3, pp. 320-329.
- LAWRENCE, F.V. JR. (1963). "Propagation velocity of ultrasonic waves through sand," *MIT Research Report R63-8*, Massachusetts Institute of Technology, Cambridge, Massachusetts.
- LAY, T. AND WALLACE, T.C. (1995). *Modern Global Seismology*, Academic Press, San Diego, 521 pp.
- LEDEBTER, R.H. (1985). "Improvement of liquefiable foundation conditions beneath existing structures," *Technical Report REMR-GT-2*, U.S. Army Corps of Engineers, Waterways Experiment Station, Vicksburg, Mississippi, 51 pp.
- LEE, K.L. (1974). Seismic permanent deformations in earth dams, *Report No. UCLA-ENG-7497*, School of Engineering and Applied Science, University of California at Los Angeles.
- LEE, K.L. AND ALBAISA, A. (1974). "Earthquake induced settlements in saturated sands," *Journal of the Soil Mechanics and Foundations Division*, ASCE, Vol. 100, No. GT4.
- LEE, K.L. AND FOCHT, J.A. (1976). "Strength of clay subjected to cyclic loading," *Marine Geotechnology*, Vol. 1, No. 3.
- LEE, M.K.W AND FINN, W.D.L. (1978). "DESRA-2, Dynamic effective stress response analysis of soil deposits with energy transmitting boundary including assessment of liquefaction potential," *Soil Mechanics Series No. 38*, University of British Columbia, Vancouver.
- LEMOS, L.J.L. AND COELHO, P.A.L.F. (1991). Displacements of slopes under earthquake loading, *Proceedings, 2nd International Conference on Recent Advances in Geotechnical Earthquake Engineering and Soil Dynamics*, St. Louis, Missouri, Vol. 2, pp. 1051-1056.
- LEMOS, L.J.L., SKEMPTON, A.W., AND VAUGHAN, P.R. (1985). "Earthquake loading of shear surfaces in slopes," *Proceedings, 11th International Conference on Soil Mechanics and Foundation Engineering*, San Francisco, Vol. 4, pp. 1955-1958.
- LI, T. (1990). "Landslide management in mountain areas of China," *Occasional Paper 15*, International Centre for Integrated Mountain Development, Kathmandu, Nepal, 50 pp.
- LIAO, S.S.C. AND WHITMAN, R.V. (1986). "Overburden correction factors for SPT in sand," *Journal of Geotechnical Engineering*, ASCE, Vol. 112, No. 3, pp. 373-377.
- LIAO, S.S.C., VENEZIANO, D., AND WHITMAN, R.V. (1988). "Regression models for evaluating liquefaction probability," *Journal of Geotechnical Engineering*, ASCE, Vol. 114, No. 4, pp. 389-411.
- LIN, J.S. AND WHITMAN, R.V. (1986). "Earthquake induced displacements of sliding blocks," *Journal of Geotechnical Engineering*, ASCE, Vol. 112, No. 1, pp. 44-59.
- LINDQVIST, L. AND PETAJA, J. (1981). "Experience in the evaluation of the bearing capacity of tapered friction piles in postglacial sand and silt strata," *Proceedings, 10th International Conference on Soil Mechanics and Foundation Engineering*, Stockholm, Vol. 2, pp. 759-766.
- LIU, H. AND QIAO, T. (1984). "Liquefaction potential of saturated sand deposits underlying foundation of structure," *Proceedings, 8th World Conference on Earthquake Engineering*, San Francisco, Vol. 3, pp. 199-206.
- LIU, S.C. (1970). "Evolutionary power spectral density of strong-motion earthquakes," *Bulletin of the Seismological Society of America*, Vol. 60, No. 3, pp. 891-900.

- LODDE, P.F. (1982). "Dynamic response of San Francisco Bay mud," *M.S. Thesis*, University of Texas, Austin, Texas.
- LOMNITZ-ADLER, J. AND LOMNITZ, C. (1979). "A modified form of the Gutenberg-Richter magnitude-frequency law," *Bulletin of the Seismological Society of America*, Vol. 63, pp. 1999-2003.
- LOVE, A.E.H. (1927). *The Mathematical Theory of Elasticity*, 4th Ed., University Press, Cambridge.
- LUCIA, P.C., DUNCAN, J.M., AND SEED, H.B. (1981). "Summary of research on case histories of flow failures of mine tailings impoundments," *Information Circular 8857*, Technology Transfer Workshop on Mine Waste Disposal Techniques, U.S. Bureau of Mines, Denver, Colorado, pp. 46-53.
- LUCO, J.E. AND WONG, H.L. (1982). "Response of structures to nonvertically incident seismic waves," *Bulletin of the Seismological Society of America*, Vol. 72, No 1, pp. 265-302.
- LUCO, J.E. AND WONG, H.L. (1986). "Response of a rigid foundation to a spatially random ground motion," *Earthquake Engineering and Structural Dynamics*, Vol. 14, pp. 891-908.
- LUKAS, R.G. (1986). "Dynamic compaction for highway construction, Vol. I: Design and construction guidelines," *Report FHWA/RD-86/133*, Federal Highway Administration, Washington, D.C.
- LYSMER, J., UDAKA, T., SEED, H.B., AND HWANG, R. (1974). "LUSH: a computer program for complex response analysis of soil-structure systems," *Report EERC 74-4*, Earthquake Engineering Research Center, University of California, Berkeley.
- LYSMER, J., UDAKA, T., TSAI, C.F., AND SEED, H.B. (1975). "FLUSH: a computer program for approximate 3-D analysis of soil-structure interaction problems," *Report EERC 75-30*, Earthquake Engineering Research Center, University of California, Berkeley, 83 pp.
- LYSMER, J., TABATABAIE, M., TAJIRIAN, F., VAHDANI, S., AND OSTDADAN, F. (1981). "SASSI: a system for analysis of soil-structure interaction," *Report UCB/GT81-02*, University of California, Berkeley.
- LYTLE, R.J. (1978). "Geophysical characterization using advanced data processing," *Proceedings, Specialty Workshop on Site Characterization and Exploration*, Northwestern University, Evanston, Illinois, pp. 291-300.
- MACMURDO, J. (1824). "Papers relating to the earthquake which occurred in India in 1819," *Philosophical Magazine*, Vol. 63, pp. 105-177.
- MAIR, R.J. AND WOOD, D.M. (1987). *Pressuremeter Testing: Methods and Interpretation*, Butterworth, London, 160 pp.
- MAKDISI, F.I. AND SEED, H.B. (1978). "Simplified procedure for estimating dam and embankment earthquake-induced deformations," *Journal of the Geotechnical Engineering Division*, ASCE, Vol. 104, No. GT7, pp. 849-867.
- MALLET, R. (1862). *Great Neapolitan Earthquake of 1857*, London, 2 vols.
- MARCHETTI, S. (1980). "In situ tests by flat dilatometer," *Journal of the Geotechnical Engineering Division*, ASCE, Vol. 106, No. GT3, pp. 299-321.
- MARCHETTI, S. (1982). "Detection of liquefiable sand layers by means of quasi-static penetration tests," *Proceedings, 2nd European Symposium on Penetration Testing*, Amsterdam, Vol. 2, pp. 458-482.
- MARCUSON, W.F., III (1981). "Moderator's report for session on 'Earth dams and stability of slopes under dynamic loads,'" *Proceedings, International Conference on Recent Advances in Geotechnical Earthquake Engineering and Soil Dynamics*, St. Louis, Missouri, Vol. 3, p. 1175.
- MARCUSON, W.F. III, COOPER, S.S., AND BIEGANOUSKY, W.A. (1977). "Laboratory sampling study conducted on fine sands," *Proceedings of Specialty Session 2, 9th International Conference on Soil Mechanics and Foundation Engineering*, Tokyo, pp. 15-22.
- MARCUSON, W.F. AND HYNES, M.E. (1990). Stability of slopes and embankments during earthquakes, *Proceedings, ASCE/Pennsylvania Department of Transportation Geotechnical Seminar*, Hershey, Pennsylvania.

- MARCUSON, W.F., III, BALLARD, R.F., JR., AND LEDBETTER, R.H. (1979). "Liquefaction failure of tailings dams resulting from the Near Izu Oshima earthquake, 14 and 15 January, 1978," *Proceedings, 6th Pan American Conference on Soil Mechanics and Foundation Engineering*, Lima, Peru.
- MARCUSON, W.F. III, HYNES, M.E., AND FRANKLIN, A.G. (1990). Evaluation and use of residual strength in seismic safety analysis of embankments, *Earthquake Spectra*, Vol. 6, No. 3, pp. 529-572.
- MARCUSON, W.F. III, HADALA, P.F., AND LEDBETTER, R.H. (1991). "Seismic rehabilitation of earth dams," *Geotechnical Practice in Dam Rehabilitation*, Geotechnical Special Publication 35, ASCE, New York, pp. 430-466.
- MARK, R.K. AND BONILLA, M.G. (1977). "Regression analysis of earthquake magnitude and surface fault length using the 1970 data of Bonilla and Buchanan," Open File Report, U.S. Geological Survey, 10 pp.
- MARTIN, G.R. (1992). Evaluation of soil properties for seismic stability analysis of slopes, *Proceedings, Stability and Performance of Slopes and Embankments*, Geotechnical Special Publication No. 31, ASCE, Vol. 1, pp. 116-142.
- MARTIN, G.R., FINN, W.D.L., AND SEED, H.B. (1978). "Effects of system compliance on liquefaction tests," *Journal of Geotechnical Engineering*, ASCE, Vol. 104, No. GT4, pp. 463-479.
- MARTIN, G.R., FINN, W.D.L., AND SEED, H.B. (1975). "Fundamentals of liquefaction under cyclic loading," *Journal of the Geotechnical Engineering Division*, ASCE, Vol. 101, No. GT5, pp. 423-438.
- MARTIN, G.R., LAM, I.P., MCCASKIE, S.L., AND TSAI, C.-F. (1981). "A parametric study of an effective stress liquefaction model," *Proceedings, International Conference on Geotechnical Earthquake Engineering and Soil Dynamics*, St. Louis, Missouri, Vol. 2, pp. 699-705.
- MARTIN, P.P. AND SEED, H.B. (1978). "MASH - A computer program for the nonlinear analysis of vertically propagating shear waves in horizontally layered soil deposits," *Report No. UCB/EERC-78/23*, Earthquake Engineering Research Center, University of California, Berkeley, California.
- MASING, G. (1926). "Eigenspannungen und Verfertigung beim Messing," *Proceedings, 2nd International Congress on Applied Mechanics*, Zurich.
- MASSARCH, K.R. (1991). "Deep soil compaction using vibratory probes," in M.I. Esrig and R.C. Bachus, eds., *Deep Foundation Improvement: Design, Construction, and Testing*, ASTM STP 1089, ASTM, Philadelphia, pp. 297-319.
- MATSUZAWA, H., ISHIBASHI, I., AND KAWAMURA, M. (1985). Dynamic soil and water pressures of submerged soils, *Journal of Geotechnical Engineering*, ASCE, Vol. 111, No. 10, pp. 1161-1176.
- MATTHIESSEN, J., ET AL. (1982). "Recommendations concerning seismic design of zonation," *Critical Aspects of Earthquake Ground Motion and Building Damage Potential*, ATC-10-1, Applied Technology Council, Redwood City, California, pp. 213-246.
- MAYNE, P.W. AND RIX, G.J. (1993). " G_{\max} - q_c relationship for clays," *Geotechnical Testing Journal*, ASTM, Vol. 16, No. 1, pp. 54-60.
- MAYNE, P.W., JONES, J.S., AND DUMAS, J.C. (1984). Ground response to dynamic compaction, *Journal of Geotechnical Engineering*, Vol. 110, No. 6, pp. 757-774.
- MCCAMY, K., MEYER, R.P., AND SMITH, T.J. (1962). "Generally applicable solutions of Zeppritz' amplitude equations," *Bulletin of the Seismological Society of America*, Vol. 52, No. 4, pp. 923-955.
- MCCANN, M.W. AND SHAH, H. C. (1979) "Determining strong motion duration of earthquakes," *Bulletin of the Seismological Society of America*, Vol. 69, No.4, pp. 1253-1265.
- MCGUIRE, R. K. (1977) "Seismic design spectra and mapping predreus using hazard analysis based directly on oscillator response," *Journal of Earthquake Engineering and Structural Dynamics*, 5, 211-234.
- MCGUIRE, R. K. (1978) "Seismic ground motion parameter relations," *Journal of the Geotechnical Engineering Division*, ASCE, Vol. 104, No. GT4, pp. 481-490.

- MC GUIRE, R.K. AND ARABASZ, W.J. (1990). "An introduction to probabilistic seismic hazard analysis," in S.H. Ward, ed. *Geotechnical and Environmental Geophysics*, Society of Exploration Geophysicists, Vol. 1, pp. 333-353.
- MC GUIRE, R.M. AND HANKS, T.C. (1980). "RMS accelerations and spectral amplitudes of strong ground motion during the San Fernando, California earthquake," *Bulletin of the Seismological Society of America*, Vol. 70, pp. 1907-1919.
- MC GUIRE, R.K., BECKER, A.M., AND DONOVAN, N.C. (1984). "Spectral estimates of seismic shear waves," *Bulletin of the Seismological Society of America*, Vol. 74, No. 4, pp. 1427-1440.
- MCKENZIE, D.P. (1970). "Plate tectonics of the Mediterranean region," *Nature, London*, pp-226-239.
- MEDVEDEV, S.V. AND SPONHEUR, V. (1969). "Scale of seismic intensity," *Proceedings, 4th World Conference on Earthquake Engineering*, Santiago, Chile, pp. 143-153.
- MEIMON, Y. AND HICHER, P.Y. (1980). "Mechanical behavior of clays under cyclic loading," in G.N. Pande and O.C. Zienkiewicz, eds., *Proceedings, International Symposium on Soils Under Cyclic and Transient Loading*, Balkema, Vol. 1, Rotterdam, The Netherlands.
- MEJIA, L.H. AND SEED, H.B. (1981). "Three-dimensional dynamic response analysis of earth dams," *Report No. UCB/EERC-81/15*, Earthquake Engineering Research Center, University of California, Berkeley, 238 pp.
- MERZ, H. A. AND CORNELL, C. A. (1973a). "Seismic risk based on a quadratic magnitude-frequency law," *Bulletin of the Seismological Society of America*, Vol. 73, No. 6, pp. 1949-2006.
- MERZ, H. A. AND CORNELL, C. A. (1973b). "Aftershocks in engineering seismic risk analysis," *Report R73-25*, Department of Civil Engineering, Massachusetts Institute of Technology, Cambridge, Massachusetts.
- MIDDLEBROOKS, T.A. (1942) "Fort Peck Slide," *Transactions, ASCE*, Vol. 107, pp. 723-764.
- MILLER, G.F. AND PURSEY, H. (1955). "On the partition of energy between elastic waves in a semi-infinite solid," *Proceedings of the Royal Society, London, Series A*, Vol. 233, pp. 55-69.
- MINDLIN, R.D. AND DERESIEWICZ, H. (1953). "Elastic spheres in contact under varying oblique forces," *Journal of Applied Mechanics, ASME*, Vol. 20, pp. 327-344.
- MITCHELL, D.E. (1984). "Liquefaction slides in hydraulically placed sands," *Proceedings, 4th International Symposium on Landslides*, Toronto.
- MITCHELL, J.K. (1986). "Ground improvement evaluation by insitu tests," *Proceedings, In Situ '86*, Geotechnical Special Publication 6, ASCE, New York, pp. 221-236.
- MITCHELL, J.K. AND SOLYMAR, Z.V. (1984). "Time-dependent strength gain in freshly deposited or densified sand," *Journal of Geotechnical Engineering, ASCE*, Vol. 110, No. 11, pp. 1559-1576.
- MITCHELL, J.K. AND TSENG, D.-J. (1990). "Assessment of liquefaction potential by cone penetration resistance," in J.M. Duncan ed., *Proceedings, H. Bolton Seed Memorial Symposium*, Berkeley, California, Vol. 2, pp. 335-350.
- MITCHELL, J.K. AND VILLET, W.C.B. (1987). Reinforcement of earth slopes and embankments, *National Cooperative Highway Research Program Report 290*, Transportation Research Board, Washington, D.C., 323 pp.
- MITCHELL, J.K. AND WENTZ, F.L. (1991). "Performance of improved ground during the Loma Prieta earthquake," *Report UCB/EERC-91/12*, Earthquake Engineering Research Center, University of California, Berkeley.
- MIZUNO, E. AND CHEN, W.F. (1982). "Plasticity models for seismic analysis of slopes," *Report CE-STR-82-2*, School of Civil Engineering, Purdue University, West Lafayette, Indiana.
- MOGAMI, T., AND KUBU, K. (1953). The behavior of soil during vibration, *Proceedings, 3rd International Conference on Soil Mechanics and Foundation Engineering*, Zurich, Vol. 1, pp. 152-155.

- MOHAMAD, R. AND DOBRY, R. (1986). "Undrained monotonic and cyclic triaxial strength of sand," *Journal of Geotechnical Engineering*, ASCE, Vol. 112, No. 10, pp. 941-958.
- MOHRAZ, B. AND ELGHADAMSI, F. E. (1989) "Earthquake ground motion and response spectra," in *The Seismic Design Handbook*, F. Naeim, ed., Van Nostrand Reinhold, New York, 32-80.
- MOK, Y.-J., SANCHEZ-SALINERO, I., STOKOW, K.H., AND ROESSET, J.M. (1988). "In situ damping measurements by crosshole seismic method," *Proceedings, Earthquake Engineering and Soil Dynamics II: Recent Advances in Ground Motion Evaluation*, Geotechnical Special Publication 20, ASCE, New York, pp. 305-320.
- MONONOBE, H.A. ET AL. (1936). "Seismic stability of the earth dam," *Proceedings, 2nd Congress on Large Dams*, Washington, D.C., Vol. 4.
- MONONOBE, N. AND MATSUO, H. (1929). "On the determination of earth pressures during earthquakes," *Proceedings, World Engineering Congress*, 9 p.
- MORGENSTERN, N.R. AND PRICE, V.E. (1965). "The analysis of the stability of general slip surfaces," *Geotechnique*, Vol. 15, No. 1, pp. 79-93.
- MOSELY, M.P., ED. (1993). *Ground Improvement*, Blackie, London, 218 pp.
- MROZ, Z. (1967). "On the description of anisotropic work hardening," *Journal of Mechanics and Physics of Solids*, Vol. 15, pp. 163-175.
- MULILIS, J.P., CHAN, C.K. AND SEED, H.B. (1975). "The effects of method of sample preparation on the cyclic stress-strain behavior of sands," *Report EERC 75-18*, Earthquake Engineering Research Center, University of California, Berkeley.
- MURPHY, J.R. AND O'BRIEN, L.J. (1977). The correlation of peak ground acceleration amplitude with seismic intensity and other physical parameters, *Bulletin of the Seismological Society of America*, Vol. 67, pp. 877-915.
- NACCI, V.A. AND TAYLOR, K.J. (1967). "Influence of clay structure on elastic wave velocities," *Proceedings, International Symposium on Wave Propagation and Dynamic Properties of Earth Materials*, Albuquerque, New Mexico, pp. 491-502.
- NADIM, F. (1980). "Tilting and sliding of gravity retaining walls," *S.M. Thesis*, Department of Civil Engineering, Massachusetts Institute of Technology, Cambridge, Massachusetts.
- NADIM, F. (1982). "A numerical model for evaluation of seismic behavior of gravity retaining walls," Sc.D. thesis, *Research Report R82-33*, Department of Civil Engineering, Massachusetts Institute of Technology, Cambridge, Massachusetts.
- NADIM, F. AND WHITMAN, R.V. (1984). "Coupled sliding and tilting of gravity retaining walls during earthquakes," *Proceedings, 8th World Conference on Earthquake Engineering*, San Francisco, Vol. 3, pp. 477-484.
- NAEIM, F. AND LEW, M. (1995). On the use of design-spectrum compatible time histories, *Earthquake Spectra*, Vol. 11, No. 1, pp. 111-127.
- NATIONAL RESEARCH COUNCIL (1976). Landslides, analysis and control, *Special Report 176*, R.L. Schuster and R.J. Krizek, eds., Transportation Research Board, Washington, D.C., 234 pp.
- NATIONAL RESEARCH COUNCIL (1985). *Liquefaction of Soils during Earthquakes*, National Academy Press, Washington, D.C., 240 pp.
- NATIONAL RESEARCH COUNCIL (1988). *Probabilistic Seismic Hazard Analysis*, National Academy Press, Washington, D.C., 97 pp.
- NAVFAC (1982). "Foundations and earth structures," *Design Manual 7.2*, Naval Facilities Engineering Command, Department of the Navy, Alexandria, Virginia, 244 pp.
- NAZARIAN, S. (1984). "In situ determination of elastic moduli of soil deposits and pavement systems by spectral-analysis-of-surface-waves method," Ph.D. dissertation, University of Texas, Austin, 458 pp.

- NAZARIAN, S. AND STOKOE, K.H. (1983). "Use of spectral analysis of surface waves for determination of moduli and thicknesses of pavement systems, *Transportation Research Record 954*, Transportation Research Board, Washington, D.C.
- NEELY, W.J. AND LEROY, D.A. (1991). "Densification of sand using a variable frequency vibratory probe," in M.I. Esrig and R.C. Bachus, eds., *Deep Foundation Improvement: Design, Construction, and Testing*, ASTM STP 1089, ASTM, Philadelphia, pp. 320-332.
- NEHRP (1993) *Building for the future*, Fiscal Years 1991-1992 Report to Congress, National Earthquake Hazard Reduction Program, Washington, D.C., 123 pp.
- NEMAT-NASSER, S. AND SHOKOOGH, A. (1979). "A unified approach to densification and liquefaction of cohesionless sand in cyclic shearing," *Canadian Geotechnical Journal*, Vol. 16, No. 4, pp. 649-678.
- NEWMARK, N. (1965). "Effects of earthquakes on dams and embankments," *Geotechnique*, Vol. 15, No. 2, pp. 139-160.
- NEWMARK, N.M. (1973) "A Study of Vertical and Horizontal Earthquake spectra," N.M. Newmark Consulting Engineering Services, Directorate of Licensing, U.S. Atomic Energy Commission, Washington, D.C.
- NEWMARK, N.M. AND HALL, W.J. (1973). "Procedures and criteria for earthquake-resistant design," *Building Practices for Disaster Mitigation*, Washington, D.C., Building Science Series 46, U.S. Department of Commerce, pp. 209-236.
- NEWMARK, N.M. AND HALL, W.J. (1978). "Development of criteria for earthquake resistant design," *Report NUREG/CR-0098*, Nuclear Regulatory Commission, Washington, D.C., 49 pp.
- NEWMARK, N.M. AND HALL, W.J. (1982). *Earthquake Spectra and Design*, EERI Monograph, Earthquake Engineering Research Institute, Berkeley, California, 103 pp.
- NEWMARK, N.M. AND ROSENBLUETH, E. (1971). *Fundamentals of Earthquake Engineering*, Prentice Hall, Englewood Cliffs, New Jersey, 640 pp.
- NG, T.-T. AND DOBRY, R. (1994). "Numerical simulations of monotonic and cyclic loading of granular soil," *Journal of Geotechnical Engineering*, ASCE, Vol. 20, No. 2, pp. 388-403.
- NIGBOR, R.L. AND IMAI, T. (1994). The suspension p-s velocity logging method, *Geophysical Characterization of Sites*, R.D. Woods, ed., A.A. Balkema, Rotterdam, pp. 57-61.
- NISHIOKA, T. AND SHAH, H.C. (1980). "Application of the Markov chain on probability of earthquake occurrences," *Proceedings of the Japanese Society of Civil Engineering*, Vol. 1, pp. 137-145.
- NOSON, L.L., QAMAR, A., AND THORSEN, G.W. (1988). Washington state earthquake hazards, *Information Circular 85*, Washington Division of Geology and Earth Resources, Olympia, Washington.
- NOVAK, M., SHETA, M., EL-HIFNAWY, L., EL-MARSAFAWI, H., AND RAMADAN, O. (1993). "DYNA4: a computer program for calculation of foundation response to dynamic loads" *Report GEOP 93-01*, Geotechnical Research Centre, The University of Western Ontario, London, Ontario.
- NUTTLI, O.W. (1973). Seismic wave attenuation and magnitude relations for eastern North America, *Journal of Geophysical Research*, Vol. 78, pp. 876-885.
- NUTTLI, O.W. (1979). "The relation of sustained maximum ground acceleration and velocity to earthquake intensity and magnitude," *Miscellaneous Paper S-73-1*, Report 16, U.S. Army Corps of Engineers Waterways Experiment Station, Vicksburg, Mississippi, 74 pp.
- NUTTLI, O.W. AND HERRMANN, R.B. (1984). "Ground motion of Mississippi Valley earthquakes," *Journal of Technical Topics in Civil Engineering*, ASCE, Vol. 110, pp. 54-69.
- O'BRIEN, J.S. AND JULIEN, P.Y. (1988). "Laboratory analysis of mudflow properties," *Journal of Hydraulic Engineering*, ASCE, Vol. 114, pp. 877-887.
- O'REILLY, M.P. (1991). "Cyclic load testing of soils," in M.P. O'Reilly and S.F. Brown, eds., *Cyclic Loading of Soils*, Blackie, London, pp. 70-121.

- O'ROURKE, T.D., GOWDY, T.E., STEWART, H.E., AND PEASE, J.W. (1991). "Lifeline and geotechnical aspects of the 1989 Loma Prieta earthquake," *Proceedings, 2nd International Conference on Recent Advances in Geotechnical Earthquake Engineering and Soil Dynamics*, St. Louis, Missouri, Vol. 2, pp. 1601-1612.
- OHSAKI, Y. (1969). "The effects of local soil conditions upon earthquake damage," *Proceedings of Specialty Session 2, 7th International Conference on Soil Mechanics and Foundation Engineering*, Mexico City.
- OHSAKI, Y. (1970). "Effects of sand compaction on liquefaction during Tokachioki earthquake," *Soils and Foundations*, Vol. 10, No. 2, pp. 112-128.
- OHSAKI, Y. (1979). "On the significance of phase content in earthquake ground motion," *Earthquake Engineering and Structural Dynamics*, Vol. 7, pp. 427-439.
- OHTA, Y. AND GOTO, N. (1976). Estimation of s-wave velocity in terms of characteristic indices of soil, *Butsuri-Tanko*, Vol. 29, No. 4, pp. 34-41.
- OKABE, S. (1926). "General theory of earth pressures," *Journal of the Japan Society of Civil Engineering*, Vol. 12, No. 1.
- OKAMOTO, S. (1973). *Introduction to Earthquake Engineering*, John Wiley, New York, New York.
- ORPHAL, D. L. AND LAHOUD, J. A. (1974) "Prediction of peak ground motion from earthquakes," *Bulletin of the Seismological Society of America*, 64, 1563-1574.
- PAGE, R.A., BOORE, D.M., HOUNER, W.B., AND CAULTER, H.W. (1972). "Geound motion values for use in the seismic design of the Trans-Alaska pipeline system," *USGS Circular 672*, U.S. Geological Survey, Reston, Virginia.
- PAPAGEORGIOU, A.S. AND AKI, K. (1983). "A specific barrier for the quantitative description of inhomogeneous faulting and the prediction of strong ground motion. II. Applications of the model," *Bulletin of the Seismological Society of America*, Vol. 73, pp. 953-978.
- PARK, T. AND SILVER, M.L. (1975). "Dynamic soil properties required to predict the dynamic behavior of elevated transportation structures," *Report DOT-TST-75-44*, U.S. Department of Transportation, Washington, D. C.
- PATWARDHAN, A.S., KULKARNI, R.B., AND TOCHER, D. (1980). "A semi-Markov model for characterizing recurrence of great earthquakes," *Bulletin of the Seismological Society of America*, Vol. 70, No. 1, pp. 323-347.
- PAZ, M. (1950). *Structural Dynamics: Theory and Computation*, van Nostrand Reinhold, New York.
- PEREZ, V. (1974). "Time dependent spectral analysis of thirty-one strong motion earthquake records," *Open File Report 74-48*, U.S. Geological Survey, Reston, Virginia.
- PERLOFF, W.H. AND BARON, W. (1976). *Soil Mechanics*, Ronald Press, New York.
- PHILLIPS, C.J. AND DAVIES, T.R. (1991). "Determining rheological parameters of debris flow material," *Geomorphology*, Vol. 4, pp. 101-110.
- PILLAI, V.S. (1991). "Liquefaction analysis of sands: Some interpretation of Seed's $K\alpha$ (sloping ground) and $K\sigma$ (depth) correction factors using steady state concept," *Proceedings, 2nd International Conference on Recent Advances in Geotechnical Earthquake Engineering and Soil Dynamics*, St. Louis, Missouri, Vol. 1, pp. 579-587.
- POULOS, S.J. (1981). "The steady state of deformation," *Journal of the Geotechnical Engineering Division*, ASCE, Vol. 107, No. GT5, pp. 553-562.
- POULOS, S.J., CASTRO G., AND FRANCE, J.W. (1985). "Liquefaction evaluation procedure," *Journal of Geotechnical Engineering*, ASCE, Vol. 111, No. 6, pp. 772-792.

- POWER, M.S., COPPERSMITH, K.J., YOUNGS, R.R., SCHWARTZ, D.P., AND SWAN, R.H. (1981). *Seismic Exposure Analysis for the WNP-2 and WNP-1/4 Site: Appendix 2.5K to Amendment No. 18 Final Safety Analysis Report for WNP-2*, Woodward-Clyde Consultants, San Francisco, 63 pp.
- POWERS, J.P. (1992). *Construction Dewatering: New Methods and Applications*, Wiley, Inc., New York, 492 pp.
- PRANGE, B. (1981). "Stochastic excitation of rock masses," *Proceedings, 10th International Conference on Soil Mechanics and Foundation Engineering*, Stockholm, Vol. 4, pp. 89-880.
- PREVOST, J.H. (1977). "Mathematical modelling of monotonic and cyclic undrained clay behavior," *International Journal of Numerical and Analytical Methods in Geomechanics*, Vol. 1, No. 2, pp. 195-216.
- PREVOST, J.H. (1981). *DYNAFLOW: A Nonlinear Transient Finite Element Analysis Program*, Department of Civil Engineering, Princeton University, Princeton, New Jersey.
- PREVOST, J.H. (1989). DYNA1D: a computer program for nonlinear seismic site response analysis - Technical documentation, *Report NCEER-89-0025*, National Center for Earthquake Engineering Research, Buffalo, New York.
- PREVOST, J.H., ABDEL-GHAFFAR, A.M., AND LACY, S.J. (1985). "Nonlinear dynamic analysis of earth dams: a comparative study," *Journal of Geotechnical Engineering*, ASCE, Vol. 111, No. 2, pp. 882-897.
- PRIEBE, H.J. (1990). The prevention of liquefaction by vibro replacement, *Proceedings, International Conference on Earthquake Resistant Construction*, Berlin.
- PRIESTLEY, M.B. (1965). "Evolutionary spectra and non-stationary processes," *Journal of the Royal Statistical Society, Series B*, Vol. 27, pp. 204-237.
- PRIESTLEY, M.B. (1967). "Power spectral analysis of non-stationary random processes," *Journal of Sound and Vibration*, Vol. 6, No. 1, pp. 86-97.
- PYKE, R.M. (1973). "Settlement and liquefaction of sands under multi-directional loading," Ph.D. dissertation, University of California, Berkeley.
- PYKE, R.M. (1979). "Nonlinear soil models for irregular cyclic loadings," *Journal of the Geotechnical Engineering Division*, ASCE, Vol. 105, No. GT6, pp. 715-726.
- PYKE, R.M. (1985). *TESS1: A Computer Program for Nonlinear Ground Response Analysis. User's Manual*, TAGA Engineering Software Services, Lafayette, California.
- PYKE, R., SEED, H.B., AND CHAN, C.K. (1975). "Settlement of sands under multi-directional loading," *Journal of the Geotechnical Engineering Division*, ASCE, Vol. 101, No. GT4, pp. 379-398.
- RAJU, V.S. AND VENKATARAMANA, K. (1980). "Undrained triaxial tests to assess liquefaction potential of sands: Effect of membrane penetration," *Proceedings, International Symposium on Soils under Cyclic and Transient Loading*, Swansea, United Kingdom, pp. 483-494.
- RAMBERG, W. AND OSGOOD, W.R. (1943). "Description of stress-strain curves by three parameters," *Technical Note 902*, National Advisory Committee for Aeronautics, Washington, D.C.
- RAMIREZ, R.W. (1985). *The FFT: Fundamentals and Concepts*, Prentice Hall, Englewood Cliffs, New Jersey, 178 pp.
- RANKINE, W. (1857). "On the stability of loose earth," *Philosophical Transactions of the Royal Society of London*, Vol. 147.
- RAYLEIGH, LORD (1885). "On waves propagated along the plane surface of an elastic solid," *Proceedings of the London Mathematical Society*, Vol. 17, pp. 4-11.
- REAL, C.R. AND TENG, T. (1973). "Local Richter magnitude and total signal duration in southern California," *Bulletin of the Seismological Society of America*, Vol. 63, No. 5.

- REDPATH, B.B. (1973). "Seismic refraction exploration for engineering site investigations," *Technical Report E-73-4*, U.S. Army Corps of Engineers Waterways Experiment Station, Explosive Excavation Research Laboratory, Livermore, California, 55 pp.
- REDPATH, B.B. AND LEE, R.C. (1986). "In situ measurements of shear wave attenuation at a strong-motion recording site," *Report*, U.S. Geological Survey Contract 14-08-001-21823, URS/John A. Blume and Associates, San Francisco.
- REDPATH, B.B., EDWARDS, R.B., HALE, R.J., AND KINTZER, F.Z. (1982). "Development of field techniques to measure damping values for near-surface rocks and soils," *Report* URS/John A. Blume and Associates, San Francisco, 120 pp.
- REID, H.F. (1910). *The California Earthquake of April 18, 1906*, Publication 87, Vol. 21, Carnegie Institute of Washington, Washington, D.C.
- REID, H.F. (1911). "The elastic rebound theory of earthquakes," *Bulletin of the Department of Geology*, University of Berkeley, Vol. 6, pp. 413-444.
- REITER, L. (1990). *Earthquake Hazard Analysis - Issues and Insights*, Columbia University Press, New York, 254 pp.
- REYNA, F. AND CHAMEAU, J.-L. (1991). "Dilatometer based liquefaction potential of sites in the Imperial Valley," *Proceedings, 2nd International Conference on Recent Advances in Geotechnical Earthquake Engineering and Soil Dynamics*, St. Louis, Missouri, Vol. 1, pp. 385-392.
- RIAL, J.A., SALTZMAN, N.G., AND LING, H. (1992). "Earthquake-induced resonance in sedimentary basins," *American Scientist*, Vol. 80, No. 6, pp. 566-578.
- RICHARDS, R. AND ELMS, D. (1979). Seismic behavior of gravity retaining walls, *Journal of the Geotechnical Engineering Division*, ASCE, Vol. 105, No. GT4, pp. 449-464.
- RICHART, F.E., HALL, J.R., AND WOODS, R.D. (1970). *Vibrations of Soils and Foundations*, Prentice Hall, Englewood Cliffs, New Jersey, 401 pp.
- RICHTER, C.F. (1935). "An instrumental earthquake scale," *Bulletin of the Seismological Society of America*, Vol. 25, pp. 1-32.
- RICHTER, C.F. (1958). *Elementary Seismology*, W.H. Freeman, San Francisco.
- RIEMER, M.F. AND SEED, R.B. (1992). "Observed effects of testing conditions on the residual strength of loose, saturated sands at large strains," *Proceedings, 4th Japan-U.S. Workshop on Earthquake Resistant Design of Lifeline Facilities and Countermeasures for Soil Liquefaction*, in M. Hamada and T.D. O'Rourke, eds., Technical Report NCEER-92-0019, National Center for Earthquake Engineering Research, Buffalo, New York, Vol. 1, pp. 223-238.
- RIX, G.J. AND STOKOE, K.H. (1991). "Correlation of initial tangent modulus and cone penetration resistance," *Calibration Chamber Testing*, International Symposium on Calibration Chamber Testing, A.B. Huang, ed., Elsevier Publishing, New York, pp. 351-362.
- ROBERTSON, P.K. (1982). "Insitu testing of soil with emphasis on its application to liquefaction assessment," Ph.D. Thesis, University of British Columbia, Vancouver, British Columbia.
- ROBERTSON, P.K. AND CAMPANELLA, R.G. (1985). "Liquefaction potential of sands using the CPT," *Journal of Geotechnical Engineering*, ASCE, Vol. 111, No. 3, pp. 384-403.
- ROBERTSON, P.K. AND CAMPANELLA, R.G. (1986). "Estimating liquefaction potential of sands using the flat dilatometer," *Geotechnical Testing Journal*, ASTM, Vol. 9, No. 1, pp. 38-40.
- ROBERTSON, P.K., CAMPANELLA, R.G., GILLESPIE, D., AND RICE, A. (1985). "Seismic CPT to measure in-situ shear wave velocity," in *Measurement and Use of Shear Wave Velocity for Evaluating Dynamic Soil Properties*, ASCE, New York, pp. 18-34.
- ROBINSKY, E.I. AND MORRISON, D.E. (1964). "Sand displacement and compaction around model friction piles," *Canadian Geotechnical Journal*, Vol. 1, No. 2, pp. 81-

- ROESLER, S.K. (1977). "Correlation methods in soil dynamics," *Proceedings, DMSR 77*, Karlsruhe, Germany, Vol. 1, pp. 309-334.
- ROESLER, S.K. (1979). "Anisotropic stress modulus due to stress anisotropy," *Journal of the Geotechnical Engineering Division, ASCE*, Vol. 105, No. GT7, pp. 871-880.
- ROESSET, J.M. (1977). "Soil amplification of earthquakes," Chapter 19 in C.S. Desai and J.T. Christian, eds., *Numerical Methods in Geotechnical Engineering*, McGraw-Hill, New York, pp. 639-682.
- ROMO, M.P. AND SEED, H.B. (1986). "Analytical modelling of dynamic soil response in the Mexico earthquake of September 19, 1985," *Proceedings, ASCE International Conference on the Mexico Earthquakes - 1985*, Mexico City, pp. 148-162.
- ROSCOE, K.H. AND BURLAND, J.B. (1968). "On the generalized stress-strain behavior of 'wet' clay," in J. Heyman and F.A. Leckie, eds., *Engineering Plasticity*, University Press, Cambridge, pp. 535-609.
- ROSCOE, K.H. AND POOROSHAB, H.B. (1963). "A fundamental principle of similarity in model tests for earth pressure problems," *Proceedings, 2nd Asian Regional Conference on Soil Mechanics*, Tokyo, Vol. 1, pp. 134-140.
- ROSCOE, K.H. AND SCHOFIELD, A.N. (1963). "Mechanical behavior of an idealised 'wet' clay," *Proceedings, 2nd European Conference on Soil Mechanics*, Wiesbaden, Germany, Vol. 1, pp. 47-54.
- ROWE, P.W. (1952). "Anchored sheet pile walls," *Proceedings of the Institution of Civil Engineers*, Vol. 1, No. 1, pp. 27-70.
- RUFF, L. AND KANAMORI, H. (1980). "Seismicity and subduction processes," *Physics of the Earth and Planetary Interiors*, Vol. 23, pp. 240-252.
- RYAN, C.R. AND JASPERSE, B.H. (1989). "Deep soil mixing at the Jackson Lake Dam," in *Foundation Engineering: Current Principles and Practices*, Geotechnical Special Publication 22, ASCE, New York, Vol. 1, pp. 354-367.
- SALLEY, J.R., FOREMAN, B., BAKER, W.H., AND HENRY, J.F. (1987). "Compaction grouting test program Pinopolis West Dam," in *Soil Improvement: A Ten Year Update*, Geotechnical Special Publication 12, ASCE, New York, pp. 245-269.
- SANCHEZ-SESMA, F. (1990). "Elementary solutions for response of a wedge-shaped medium to incident SH- and SV-waves," *Bulletin of the Seismological Society of America*, Vol. 80, pp. 737-742.
- SANCHEZ-SESMA, F. AND CAMPILLO, M. (1993). "Topographic effects for incident P, SV, and Rayleigh waves," *Tectonophysics*, Vol. 218, No. 1-3, pp. 113-125.
- SANGREY, D.A., HENKEL, D.J., AND ESRIG, M.I. (1969). "The effective stress response of a saturated clay soil to repeated loading," *Canadian Geotechnical Journal*, Vol. 6, No.3.
- SARAGONI, G.R. AND HART, G.C. (1974). Simulation of artificial earthquakes, *Earthquake Engineering and Structural Dynamics*, Vol. 2, No. 2, pp. 249-267.
- SARMA, S.K. (1975). "Seismic stability of earth dams and embankments," *Geotechnique*, Vol. 25, pp. 743-761.
- SAVAREN SKY, Y.F. AND KIRNOS, D.P. (1955). *Elements of Seismology and Seismometry*, State Press of Technical-Theoretical Literature, Moscow, 543 pp.
- SAVY, H.B., SHAH, H.C., AND BOORE, D.M. (1980). "Nonstationary risk model with geophysical input," *Journal of the Structural Division, ASCE*, Vol. 106, No. ST1, pp. 145-164.
- SAYAO, A.S.F. AND VAID, Y.P. (1989). "Deformations due to principal stress rotation," *Proceedings, 12th International Conference on Soil Mechanics and Foundation Engineering*, Rio de Janeiro, Brazil, Vol. 1, pp. 107-110.
- SCHMERTMANN, J.H., SMITH, T.V., AND HO, R. (1978). "Example of an energy calibration report on a standard penetration test (ASTM Standard D1586-67) drill rig," *Geotechnical Testing Journal*, ASTM, Vol. 1, No. 1, pp. 57-61.

- SCHNABEL, P.B., LYSMER, J., AND SEED, H.B. (1972). "SHAKE: a computer program for earthquake response analysis of horizontally layered sites," *Report EERC 72-12*, Earthquake Engineering Research Center, University of California, Berkeley.
- SCHOFIELD, A.N. (1980). "Cambridge geotechnical centrifuge operations," *Geotechnique*, Vol. 30, No. 3, pp. 227-268.
- SCHOFIELD, A.N. AND WROTH, C.P. (1968). *Critical state soil mechanics*, McGraw-Hill, London.
- SCHWARTZ, D.P. (1988). "Geology and seismic hazards: Moving into the 1990s," *Proceedings, Earthquake Engineering and Soil Dynamics II: Recent Advances in Ground Motion Evaluation*, Geotechnical Special Publication 20, ASCE, New York, pp. 1-42.
- SCHWARTZ, D.P. AND COPPERSMITH, K.J. (1984). "Fault behavior and characteristic earthquakes: examples from the Wasatch and San Andreas fault zones," *Journal of Geophysical Research*, Vol. 89 No. B7, pp. 5681-5698.
- SCHWARTZ, D.P. AND COPPERSMITH, K.J. (1986). "Seismic hazards: New trends in analysis using geologic data," in R.E. Wallace, ed., *Active Tectonics*, Academic Press, Orlando, Florida, pp. 215-230.
- SCHWARZ, S.D. AND MUSSER, J.M., JR. (1972). "Various techniques for making in situ shear wave velocity measurements - a description and evaluation," *Proceedings, International Conference on Microzonation*, Seattle, Washington, Vol. 2, pp. 594-608.
- SCOTT, R.F. (1972). "The calculation of horizontal accelerations from seismoscope records," presented at Seismological Society of America Conference, Hawaii.
- SCOTT, R.F. (1986). "Solidification and consolidation of a liquefied sand column," *Soils and Foundations*, Vol. 26, No. 4, pp. 23-31.
- SEAOC (1990). *Recommended Lateral Force Requirements and Tentative Commentary*, Structural Engineers Association of California, San Francisco, 64 pp.
- SEED, H.B. (1976). "Some aspects of sand liquefaction under cyclic loading," *Proceedings, Conference on Behavior of Offshore Structures*, Norwegian Institute of Technology, Oslo.
- SEED, H.B. (1979). Considerations in the earthquake-resistant design of earth and rockfill dams, *Geotechnique*, Vol. 29, No. 3, pp. 215-263.
- SEED, H.B. (1979). Soil liquefaction and cyclic mobility evaluation for level ground during earthquakes, *Journal of the Geotechnical Engineering Division*, ASCE, Vol. 105, No. GT2, pp. 201-255.
- SEED, H.B. (1980). Closure to "Soil liquefaction and cyclic mobility evaluation for level ground during earthquakes," *Journal of the Geotechnical Engineering Division*, ASCE Vol. 106, No. GT6, p. 724.
- SEED, H.B. (1983). "Earthquake-resistant design of earth dams," in T.R. Howard, ed., *Proceedings, Symposium on Seismic Design of Earth Dams*, ASCE, New York, pp. 41-64.
- SEED, H.B. (1986). "Design problems in soil liquefaction," *Journal of Geotechnical Engineering*, ASCE, Vol. 113, No. 8, pp. 827-845.
- SEED, H.B. AND BOOKER, J.R. (1976). "Stabilization of potentially liquefiable sand deposits using gravel drain systems, *Report EERC-76-10*, Earthquake Engineering Research Center, University of California, Berkeley.
- SEED, H.B. AND BOOKER, J.R. (1977). "Stabilization of potentially liquefiable sand deposits using gravel drains, *Journal of the Geotechnical Engineering Division*, ASCE, Vol. 103, No. GT7, pp. 757-768.
- SEED, H.B. AND CHAN, C.K. (1966). "Clay strength under earthquake loading conditions," *Journal of the Soil Mechanics and Foundations Division*, ASCE, Vol. 92, No. SM2, pp. 53-78.
- SEED, H.B. AND DE ALBA, P. (1986). "Use of SPT and CPT tests for evaluating the liquefaction resistance of soils," *Proceedings, Insitu '86*, ASCE.
- SEED, H.B. AND IDRISI, I.M. (1969). "Rock motion accelerograms for high-magnitude earthquakes," *EERC Report 69-7*, Earthquake Engineering Research Center, University of California, Berkeley.

- SEED, H.B. AND IDRISI, I.M. (1970). "Soil moduli and damping factors for dynamic response analyses," *Report EERC 70-10*, Earthquake Engineering Research Center, University of California, Berkeley.
- SEED, H.B. AND IDRISI, I.M. (1971). "Simplified procedure for evaluating soil liquefaction potential," *Journal of the Soil Mechanics and Foundations Division*, ASCE, Vol. 107, No. SM9, pp. 1249-1274.
- SEED, H.B. AND IDRISI, I.M. (1982). *Ground Motions and Soil Liquefaction During Earthquakes*, Earthquake Engineering Research Institute, Berkeley, California, 134 pp.
- SEED, H.B. AND LEE, K.L. (1965). "Studies of liquefaction of sands under cyclic loading conditions," *Report TE-65-65*, Department of Civil Engineering, University of California, Berkeley.
- SEED, H.B. AND LEE, K.L. (1966). "Liquefaction of saturated sands during cyclic loading," *Journal of the Soil Mechanics and Foundations Division*, ASCE, Vol. 92, No. SM6, pp. 105-134.
- SEED, H.B. AND MARTIN, G.R. (1966). "The seismic coefficient in earth dam design," *Journal of the Soil Mechanics and Foundations Division*, ASCE, Vol. 92, No. SM3, pp. 25-58.
- SEED, H.B. AND PEACOCK, W.H. (1971). "Test procedures for measuring soil liquefaction characteristics," *Journal of the Soil Mechanics and Foundations Division*, ASCE, Vol. 97, No. SM8, pp. 1099-1119.
- SEED, H.B. AND SILVER, M.L. (1972). "Settlement of dry sands during earthquakes," *Journal of the Soil Mechanics and Foundations Division*, Vol. 98, No. SM4, pp. 381-397.
- SEED, H.B. AND WHITMAN, R.V. (1970). "Design of earth retaining structures for dynamic loads," *Proceedings, ASCE Specialty Conference on Lateral Stresses in the Ground and Design of Earth Retaining Structures*, pp. 103-147.
- SEED, H.B., IDRISI, I.M., AND KIEFER, F.W. (1969). "Characteristics of rock motions during earthquakes," *Journal of the Soil Mechanics and Foundations Division*, ASCE, Vol. 95, No. SM5, pp. 1199-1218.
- SEED, H.B., LEE, K.L., AND IDRISI, I.M. (1969). "Analysis of Sheffield Dam failure," *Journal of the Soil Mechanics and Foundations Division*, ASCE, Vol. 95, No. SM6, pp. 1453-1490.
- SEED, H.B., LEE, K.L., IDRISI, I.M., AND MAKDISI, R. (1973). "Analysis of the slides in the San Fernando dams during the earthquake of Feb. 9, 1971," *Report No. EERC 73-2*, Earthquake Engineering Research Center, University of California, Berkeley, 150 pp.
- SEED, H.B., MORI, K., AND CHAN, C.K. (1975). "Influence of seismic history on the liquefaction characteristics of sands," *Report EERC 75-25*, Earthquake Engineering Research Center, University of California, Berkeley, 21 pp.
- SEED, H.B., LEE, K.L., IDRISI, I.M., AND MAKDISI, F.I. (1975). "The slides in the San Fernando Dams during the earthquake of February 9, 1971," *Journal of the Geotechnical Engineering Division*, ASCE, Vol. 101, No. GT7, pp. 651-688.
- SEED, H. B., IDRISI, I. M., MAKDISI, F., AND BANERJEE, N. (1975) "Representation of irregular stress time histories by equivalent uniform stress series in liquefaction analyses," *EERC 75-29*, Earthquake Engineering Research Center, University of California, Berkeley.
- SEED, H.B., MURARKA, R., LYSMER, J., AND IDRISI, I.M. (1976). "Relationships of maximum acceleration, maximum velocity, distance from source and local site conditions for moderately strong earthquakes," *Bulletin of the Seismological Society of America*, Vol. 66, No. 4, pp. 1323-1342.
- SEED, H.B., UGAS, C., AND LYSMER, J. (1976). "Site-dependent spectra for earthquake-resistant design," *Bulletin of the Seismological Society of America*, Vol. 66, pp. 221-243.
- SEED, H.B., IDRISI, I.M., AND ARANGO, I. (1983). "Evaluation of liquefaction potential using field performance data," *Journal of Geotechnical Engineering*, ASCE, Vo. 109, No. 3, pp. 458-482.

- SEED, H.B., TOKIMATSU, K., AND HARDER, L. (1984). "The influence of SPT procedures in evaluating soil liquefaction resistance," *Report UCB/EERC-84-15*, Earthquake Engineering Research Center, University of California, Berkeley.
- SEED, H.B., WONG, R.T., IDRISI, I.M., AND TOKIMATSU, K. (1984). Moduli and damping factors for dynamic analyses of cohesionless soils," *Journal of Geotechnical Engineering*, ASCE, Vol. 112, No. 11, pp. 1016-1032.
- SEED, H.B., TOKIMATSU, K., HARDER, L.F., AND CHUNG, R.M. (1985). "Influence of SPT procedures in soil liquefaction resistance evaluations," *Journal of Geotechnical Engineering*, Vol. 111, No. 12, pp. 1425-1445.
- SEED, H.B., WONG, R.T., IDRISI, I.M., AND TOKIMATSU, K. (1986). Moduli and damping factors for dynamic analyses of cohesionless soils, *Journal of Geotechnical Engineering*, ASCE, Vol. 112, No. GT11, pp. 1016- 1032.
- SEED, R.B. AND ANWAR, H. (1986). "Development of a laboratory technique for correcting results of undrained triaxial shear tests on soils containing coarse particles for effects of membrane penetration," *Research Report SR/GT/86-02*, Department of Civil Engineering, Stanford University, Stanford, California.
- SEED, R.B. AND HARDER, L.F. (1990). "SPT-based analysis of cyclic pore pressure generation and undrained residual strength," in J.M. Duncan ed., *Proceedings, H. Bolton Seed Memorial Symposium*, University of California, Berkeley, Vol. 2, pp. 351-376.
- SEED, R.B., DICKENSON, S.E., REIMER, M.F., BRAY, J.D., SITAR, N., MITCHELL, J.K., IDRISI, I.M., KAYEN, R.E., KROPP, A., HARDER, L.F., AND POWER, M.S. (1990). "Preliminary report on the principal geotechnical aspects of the October 17, 1989 Loma Prieta earthquake," *Report UCB/EERC-90/05*, Earthquake Engineering Research Center, University of California, Berkeley, 137 pp.
- SEEKINS, L.C., BRADY, A.G., CARPENTER, C., AND BROWN, N. (1992). Digitized strong-motion accelerograms of North and Central American earthquakes 1933-1986, *Digital Data Series DDS-7* (CD-ROM), U.S. Geological Survey, Golden, Colorado.
- SEKO, T. AND TOBE, K. (1977). "An experimental investigation of sand sampling," *Proceedings of Specialty Session 2, 9th International Conference on Soil Mechanics and Foundation Engineering*, Tokyo, pp. 37-42.
- SENNESET, K. AND NESTVOLD, J. (1992). "Deep compaction by vibro wing technique and dynamic compaction," in *Grouting, Soil Improvement, and Geosynthetics*, Geotechnical Special Publication 30, ASCE, New York, Vol. 2, pp. 889-901.
- SERFF, N., SEED, H.B., MAKDISI, F.I., AND CHANG, C.-Y. (1976). "Earthquake-induced deformations of earth dams," *Report EERC 76-4*, Earthquake Engineering Research Center, University of California, Berkeley, 140 pp.
- SHAH, H. C., MORTGAT, C. P., KIREMIDJIAN, A. S., AND ZSUTTY, T. C. (1975). "A Study of Seismic Risk for Nicaragua, Part I," *Report 11*, The John A. Blume Earthquake Engineering Center, Stanford University, Stanford, California.
- SHAKAL, A.F. AND BERNREUTER, D.L. (1981). "Empirical analysis of near-source ground motion," Nuclear Regulatory Commission *Report NUREG/CR-2095*, Washington, D. C.
- SHAKAL, A.F., HUANG, M.-J., AND VENTURA, C.E. (1988). "The California Strong Motion Instrumentation Program: Objectives, status and recent data," *Proceedings, 9th World Conference on Earthquake Engineering*, Tokyo, Vol. 8, pp. 105-116.
- SHARMA, M.P. AND SHAH, H.C. (1986). "Time varying parameter domain modeling of strong ground motion," *Proceedings, 3rd Engineering Mechanics Specialty Conference on Dynamics of Structures*, ASCE, University of California, Los Angeles.

- SHERIF, M.A. AND FANG, Y.S. (1984a). "Dynamic earth pressures on wall rotating about the top," *Soils and Foundations*, Vol. 24, No. 4, pp. 109-117.
- SHERIF, M.A. AND FANG, Y.S. (1984b). "Dynamic earth pressures on wall rotating about the base," *Proceedings, 8th World Conference on Earthquake Engineering*, San Francisco, Vol. 6, pp. 993-1000.
- SHERIF, M.A., ISHBASHI, I., AND LEE, C.D. (1982). "Earth pressure against rigid retaining walls," *Journal of the Geotechnical Engineering Division, ASCE*, Vol. 108, No. GT5, pp. 679-695.
- SHINOZUKA, M. (1973). "Digital simulation of strong ground accelerations," *Proceedings, 5th World Conference on Earthquake Engineering*, Vol. 2, pp. 2829-2838.
- SHINOZUKA, M. AND DEODATIS, G. (1988). "Stochastic process models for earthquake ground motion," *Journal of Probabilistic Engineering Mechanics*, Vol. 3, No. 3, pp. 187-221.
- SHIRLEY, D.J. AND ANDERSON, A.L. (1975). "Acoustic and engineering properties of sediments, Report ARL-TR-75-58, Applied Research Laboratory, University of Texas, Austin.
- SHLIEN, S. AND TOKOSZ, M.N. (1970). "A clustering model for earthquake occurrences," *Bulletin of the Seismological Society of America*, Vol. 60, pp. 1765-1787.
- SIDDHARTHAN, R., ARA, S., AND NORRIS, G.M. (1992). "Simple rigid plastic model for seismic tilting of rigid walls," *Journal of Structural Engineering, ASCE*, Vol. 118, No. 2, pp. 469-487.
- SILLER, T.J. AND DOLLY, M.O. (1992). "Design of tied-back walls for seismic loading," *Journal of Geotechnical Engineering, ASCE*, Vol. 118, No. 11, pp. 1804-1821.
- SILLER, T.J. AND FRAWLEY, D.D. (1992). "Seismic response of multianchored retaining walls," *Journal of Geotechnical Engineering, ASCE*, Vol. 118, No. 11, pp. 1787-1803.
- SILVA, W.J. (1987). "WES RASCAL code for synthesizing earthquake ground motions," *Miscellaneous Paper S-73-1, Report 24*, U.S. Army Corps of Engineers, Waterways Experiment Station, Vicksburg, Mississippi, 73 pp.
- SILVA, W.J. (1988). "Soil response to earthquake ground motion," *EPRI Report NP-5747*, Electric Power Research Institute, Palo Alto, California.
- SILVA, W.J. (1988). "Soil response to earthquake ground motion," *EPRI Report NP-5747*, Electric Power Research Institute, Palo Alto, California.
- SILVER, N.L. AND SEED, H.B. (1971). "Volume changes in sands during cyclic loading," *Journal of the Soil Mechanics and Foundations Division, ASCE*, Vol 97, No. SM9, pp. 1171-
- SIMCOCK, K.J., DAVIS, R.O., BERRILL, J.B., AND MULLENGER, G. (1983). "Cyclic triaxial tests with continuous measurement of dissipated energy," *Geotechnical Testing Journal, ASTM*, Vol. 6, No. 1, pp. 35-39.
- SINGH, J.P. (1985). Earthquake ground motions: Implications for designing structures and reconciling structural damage, *Earthquake Spectra*, Vol. 1, No. 2, pp. 239-270.
- SINGH, S., SEED, H.B., AND CHAN, C.K. (1979). "Undisturbed sampling and cyclic load testing of sands," *Report UCB/EERC-79/33*, Earthquake Engineering Research Center, University of California, Berkeley, 131 pp.
- SLADEN, J.A. (1985). "Problems with interpretation of sand state from cone penetration test," *Geotechnique*, Vol. 39, No. 2, pp. 323-332.
- SLADEN, J.A., D'HOLLANDER, R.D., AND KRAHN, J. (1985). "The liquefaction of sands, a collapse surface approach," *Canadian Geotechnical Journal*, Vol. 22, No. 4, pp. 564-578.
- SLEMMONS, D.B. (1977). "Faults and earthquake magnitude," *Miscellaneous Paper S-73-1, Report 6*, U.S. Army Corps of Engineers Waterways Experiment Station, Vicksburg, Mississippi, 129 pp.
- SLEMMONS, D.B. (1982). "Determination of design earthquake magnitudes for microzonation," *Proceedings, 3rd International Earthquake Microzonation Conference*, Seattle, Washington, Vol. 1, pp. 119-130.

- SLEMMONS, D.B. AND MCKINNEY, R. (1977). "Definition of 'active fault,'" *Miscellaneous Paper S-77-8*, U.S. Army Corps of Engineers Waterways Experiment Station, Vicksburg, Mississippi.
- SMITH, S.W. (1976). "Determination of maximum earthquake magnitude," *Geophysical Research Letters*, Vol. 3, No. 6, pp. 351-354.
- SOLYMAR, Z.V. AND REED, D.J. (1986). "A comparison of foundation compaction techniques," *Canadian Geotechnical Journal*, Vol. 23, No. 3, pp. 271-280.
- SOSKE, J.L. (1959). "The blind zone problem in engineering geophysics," *Geophysics*, Vol. 24, pp. 359-365.
- SPAETH, M.G. AND BERKMAN, S.C. (1967). "The tsunami of March 28, 1964 as recorded at tide stations," *ESSA Technical Report C and GS 33*, U.S. Coast and Geodetic Survey, Rockville, Maryland.
- SPENCER, E. (1967). "A method of analysis of the stability of embankments assuming parallel interslice forces," *Geotechnique*, Vol 17, No. 1, pp. 11-26.
- STARAS-GAZETAS, E. (1986). "A method for inelastic response analysis of earth dams," Ph.D. dissertation, Renssalaer Polytechnic Institute, Troy, New York.
- STARAS-GAZETAS, E. AND DOBRY, R. (1991). "Inelastic seismic response of San Fernando and Santa Felicia dams," *Proceedings, 2nd International Conference on Recent Advances in Geotechnical Earthquake Engineering and Soil Dynamics*, St. Louis, Missouri, Vol. 2, pp. 1129-1135.
- STARK, T.D. AND MESRI, G. (1992). "Undrained shear strength of sands for stability analysis," *Journal of Geotechnical Engineering*, ASCE, Vol. 118, No. 11, pp. 1727-1747.
- STEEDMAN, R.S. (1991). "Centrifuge modelling for dynamic geotechnical studies," *Proceedings, 2nd International Conference on Recent Advances in Geotechnical Earthquake Engineering and Soil Dynamics*, St. Louis, Missouri, Vol. 3, pp. 2401-2417.
- STEEDMAN, R.S. AND ZENG, X. (1990). "The seismic response of waterfront retaining walls," *Proceedings, ASCE Specialty Conference on Design and Performance of Earth Retaining Structures, Special Technical Publication 25*, Cornell University, Ithaca, New York, pp. 872-886.
- STEINBRUGGE, K.V. AND CLOUD, W. (1962). "Epicentral intensities and damage in the Hebgen Lake, Montana earthquake of August 17, 1959," *Bulletin of the Seismological Society of America*, Vol. 52, No. 2, pp. 181-234.
- STEPP, J.C. (1972). "Analysis of completeness in the earthquake sample in the Puget Sound area and its effect on statistical estimates of earthquake hazard," *Proceedings, International Conference on Microzonation*, Seattle, Washington, Vol. 2, pp. 897-910.
- STEWART, W.P. AND CAMPANELLA, R.G. (1991). "Insitu measurement of damping in sands and silts," *Proceedings, 2nd International Conference on Recent Advances in Geotechnical Earthquake Engineering and Soil Dynamics*, St. Louis, Missouri, Vol. X, pp.
- STILLEY, A.N. (1982). "Compaction grouting for foundation stabilization," *Proceedings, ASCE Specialty Conference on Grouting in Geotechnical Engineering*, New Orleans, Louisiana, pp. 923-937.
- STOKOE, K.H. AND ABDUL-RAZZAK, K.G. (1975). "Shear moduli of two compacted fills," *Proceedings, In-Situ Measurement of Soil Properties Specialty Conference*, Raleigh, North Carolina, Vol. 1, pp. 422-449.
- STOKOE, K.H. AND HOAR, R.J. (1978). "Generation and measurement of shear waves in situ," *Dynamic Geotechnical Testing*, ASTM STP 654, ASTM, Philadelphia, pp. 3-29.
- STOKOE, K.H. AND LODDE, P.F. (1978). "Dynamic response of San Francisco Bay mud," *Proceedings, ASCE Specialty Conference on Earthquake Engineering and Soil Dynamics*, Pasadena, Vol. 2, pp. 940-959.

- STOKOE, K.H., LEE, S.H.H., AND KNOX, D.P. (1985). "Shear moduli measurements under true triaxial stresses," *Proceedings, Advances in the Art of Testing Soils under Cyclic Conditions*, ASCE, New York, pp. 166-185.
- STOKOE, K.H., NAZARIAN, S., RIX, G.J., SANCHEZ-SALINERO, R., SHEU, J.-C., AND MOK, Y.-J. (1988). "In situ seismic testing of hard-to-sample soils by surface wave method," *Proceedings, Earthquake Engineering and Soil Dynamics II: Recent Advances in Ground Motion Evaluation*, Geotechnical Special Publication 20, ASCE, New York, pp. 264-278.
- STOKOE, K.H., ROESSET, J.M., BIERSCHWALE, J.G., AND AOUAD, M. (1988). "Liquefaction potential of sands from shear wave velocity," *Proceedings, 9th World Conference on Earthquake Engineering*, Tokyo, Vol. 3, pp. 213-218.
- STOKOE, K.H., WRIGHT, S.G., BAY, J.A. AND ROESSET, J.M. (1994). Characterization of geotechnical sites by SASW method, *Geophysical Characterization of Sites*, R.D. Woods, ed., A.A. Balkema, Rotterdam, pp. 15-25.
- STONE, W.C., YOKEL, F.Y., CELEBI, M., HANKS, T., AND LEYENDECKER, E.V. (1987). "Engineering aspects of the September 19, 1985 Mexico earthquake," *NBS Building Science Series 165*, National Bureau of Standards, Washington, D.C., 207 pp.
- STREETER, V.L., WYLIE, E.B. AND RICHART, F.E. (1973). "Soil motion computations by characteristics methods," *Proceedings, ASCE National Structural Engineering Conference*, San Francisco.
- SUCCARIEH, M.F., YAN, L., AND ELGAMAL, A.M. (1991). "Modelling of observed deformation at La Villita dam," *Proceedings, 2nd International Conference on Recent Advances in Geotechnical Earthquake Engineering and Soil Dynamics*, St. Louis, Missouri, Vol. 2, pp. 1079-1086.
- SUMNER, J.S. (1969). *Geophysics, Geologic Structures, and Tectonics*, Wm. C. Brown, Dubuque, Iowa.
- SUN, J.I., GOLESORKHI, R., AND SEED, H.B. (1988). "Dynamic moduli and damping ratios for cohesive soils," Report No. EERC-88/15, Earthquake Engineering Research Center, University of California, Berkeley.
- SWAN, F.H. III, SCHWARTZ, D.P., AND CLUFF, L.S. (1980). Recurrence of moderate-to-large magnitude earthquakes produced by surface faulting on the Wasatch fault, *Bulletin of the Seismological Society of America*, Vol. 70, No. 5, pp. 1431-1462.
- SY, A. AND CAMPANELLA, R.G. (1994). Becker and standard penetration tests (BPT-SPT) correlations with consideration of casing friction, *Canadian Geotechnical Journal*, Vol. 31, No. 3, pp. 343-356.
- SYMES, M.J., GENN, A., AND HIGHT, D.W. (1988). "Drained principal stress rotation in saturated sand," *Geotechnique*, Vol. 38, No. 1, pp. 59-81.
- TAJIMI, H. (1960) "A statistical method of determining the maximum response of a building structure during an earthquake," *Proceedings of the 2nd World Conference on Earthquake Engineering*, Tokyo, Vol. 2, pp. 781-797.
- TAJIRIAN, R. (1981). "Impedance matrices and interpolation techniques for 3-D interaction analysis by the flexible volume method," Ph.D. dissertation, University of California, Berkeley.
- TAKI, D. AND YANG, D.S. (1991). "Soil-cement mixed wall technique," *Geotechnical Engineering Congress*, Geotechnical Special Publication 27, ASCE, New York, Vol. 1, pp. 298-309.
- TAN, K. AND VUCETIC, M. (1989). "Behavior of medium and low plasticity clays under cyclic simple shear conditions," *Proceedings, 4th International Conference on Soil Dynamics and Earthquake Engineering*, A.S. Cakmak and I. Herrera, eds., Mexico City, pp. 131-142.
- TANG, H.T. (1987). "Large scale soil-structure interaction," *Report EPRI NP-5513-SR*, Electric Power Research Institute, Palo Alto, California.

- TATSUOKA, F., SASAKI, T., AND YAMADA, S. (1984). "Settlement in saturated sand induced by cyclic undrained simple shear," *Proceedings, 8th World Conference on Earthquake Engineering*, San Francisco, Vol. 3, pp. 255-262.
- TATSUOKA, F., OCHI, K., FUJII, S., AND OKAMOTO, M. (1986). "Cyclic undrained triaxial and torsional shear strength of sands for different sample preparation methods," *Soils and Foundations*, Vol. 26, No. 3, pp. 23-41.
- TAWFIQ, K.S., AGGOUR, M.S., AND AL-SANAD, H.A. (1988). "Dynamic properties of cohesive soils from impulse testing," *Proceedings, 9th World Conference on Earthquake Engineering*, Tokyo, Vol. 3, pp. 11-16.
- TAYLOR, D.W. (1948). *Fundamentals of Soil Mechanics*, Wiley, New York, 700 pp.
- TAYLOR, F.B. (1910). "Bearing of the Tertiary mountain belt on the origin of the Earth's plan," *Bulletin of the Geological Society of America*, Vol. 21, pp. 179-226.
- TERZAGHI, K. (1943). *Theoretical Soil Mechanics*, Wiley, Inc., New York.
- TERZAGHI, K. (1950). Mechanisms of landslides, *Engineering Geology (Berkey) Volume*, Geological Society of America.
- THIERS, G.R. AND SEED, H.B. (1978). "Strength and stress-strain characteristics of clays subjected to seismic loading conditions," in *Vibration Effects of Earthquakes on Soils and Foundations*, Special Technical Publication 450, ASTM, Philadelphia, pp. 3-56.
- THOMANN, T.G. AND HRYCIW, R.D. (1991). "Seismic downhole, CPT, and DMT correlations in sand," *Proceedings, 2nd International Conference on Recent Advances in Geotechnical Earthquake Engineering and Soil Dynamics*, St. Louis, Vol. 1, pp. 97-101.
- THOMSON, W.T. (1950). "Transmission of elastic waves through a stratified solid," *Journal of Applied Physics*, Vol. 21, pp. 89-93.
- TIKA-VASSILIKOS, T.E., SARMA, S.K., AND AMBRASEYS, N. (1993). "Seismic displacements on shear surfaces in cohesive soils," *Earthquake Engineering and Structural Dynamics*, Vol. 22, pp. 709-721.
- TIMOSHENKO, S.P. AND GOODIER, J.N. (1951). *Theory of elasticity*, McGraw-Hill, New York, 506 pp.
- TING, J.M., CORKUM, B.T., KAUFFMAN, C.R. AND GRECO, C. (1989). "Discrete numerical model for soil mechanics," *Journal of Geotechnical Engineering*, ASCE, Vol. 115, No. 3, pp. 379-398.
- TOCHER, D. (1958). "Earthquake energy and ground breakage," *Bulletin of the Seismological Society of America*, Vol. 48, No. 2, pp. 147-153.
- TOKI, S., TATSUOKA, F., MIURA, S., YOSHIMI, Y., YASUDA, S., AND MAKIHARA, Y. (1986). "Cyclic undrained triaxial strength of sand by a cooperative test program," *Soils and Foundations*, Vol. 26, No. 3, pp. 117-128.
- TOKIMATSU, K. AND MIDORIKAWA, S. (1981). "Nonlinear soil properties estimated from strong motion accelerograms," *Proceedings, International Conference on Recent Advances in Geotechnical Earthquake Engineering and Soil Dynamics*, St. Louis, Missouri, Vol. 1, pp. 117-122.
- TOKIMATSU, K. AND NAKAMURA, K. (1986). "A liquefaction test without membrane penetration effects," *Soils and Foundations*, Vol. 26, No. 4, pp. 127-138.
- TOKIMATSU, K. AND SEED, H.B. (1987). "Evaluation of settlements in sand due to earthquake shaking," *Journal of Geotechnical Engineering*, ASCE, Vol. 113, No. 8, pp. 861-878.
- TOKIMATSU, K. AND YOSHIMI, Y. (1983). "Empirical correlation of soil liquefaction based on SPT N-value and fines content," *Soils and Foundations*, Vol. 23, No. 4, pp. 56-74.
- TOKIMATSU, K., KUWAYAMA, S., AND TAMURA, S. (1991). "Liquefaction potential evaluation based on Rayleigh wave investigation and its comparison with field behavior," *Proceedings, 2nd Interna-*

- tional Conference on Recent Advances in Geotechnical Earthquake Engineering and Soil Dynamics, St. Louis, Missouri, Vol. 1, pp. 357-364.
- TOKIMATSU, K., TAMURA, S., AND KOJIMA, H. (1992). "Effects of multiple modes on Rayleigh wave dispersion characteristics," *Journal of Geotechnical Engineering*, Vol. 118, No. 10, pp. 1529-1543.
- TORO, G.R., ABRAHAMSON, N.A., AND SCHNEIDER, J.F. (1995). "Engineering model of strong ground motions from earthquakes in the central and eastern United States," *Earthquake Spectra*, in press.
- TOWHATA, I. AND ISLAM, S. (1987). "Prediction of lateral movement of anchored bulkheads induced by seismic liquefaction," *Soils and Foundations*, Vol. 27, No. 4, pp. 137-147.
- TRIFUNAC, M.D. (1976). "Preliminary empirical model for scaling Fourier amplitude spectra of strong ground acceleration in terms of earthquake magnitude, source-to-station distance, and recording site conditions," *Bulletin of the Seismological Society of America*, Vol. 66, No. 4, pp. 1343-1373.
- TRIFUNAC, M.D. AND BRADY, A.G. (1975a). "On the correlation of seismic intensity with peaks of recorded strong ground motion," *Bulletin of the Seismological Society of America*, Vol. 65, pp. 139-162.
- TRIFUNAC, M. D. AND BRADY, A. G. (1975b) "A study of the duration of strong earthquake ground motion," *Bulletin of the Seismological Society of America*, Vol., 65, pp. 581-626.
- TRIFUNAC, M.D. AND HUDSON, D.E. (1971). "Analysis of the Pacoima Dam accelerograms - San Fernando earthquake of 1971," *Bulletin of the Seismological Society of America*, Vol. 61, No. 5, pp. 1393-1411.
- TRIFUNAC, M.D. AND LEE, V.W. (1987). "Frequency dependent attenuation of strong earthquake ground motion," in *Selection of Earthquake-Resistant Design Criteria for Nuclear Power Plants: Methodology and Technical Cases*, Report NUREG/CR-4903, Vol. 1, Nuclear Regulatory Commission, Washington, D. C.
- TRIFUNAC, M.D. AND WESTERMO, B. (1977). "A note on the correlation of frequency-dependent duration of strong earthquake ground motion with the MMI and geologic condition at the recording stations," *Bulletin of the Seismological Society of America*, Vol. 67, No. 3, pp. 917-927.
- TRIFUNAC, M.D., LEE, V.W., AND ANDERSON, J.G. (1987). "Methods for introduction of geologic data into characterization of active faults and seismicity and upgrading of the URS technique," *Report NUREG/CR*, Vol. 2, Nuclear Regulatory Commission, Washington, D. C.
- TSUCHIDA, H. (1970). "Prediction and countermeasure against the liquefaction in sand deposits," *Abstract of the Seminar in the Port and Harbor Research Institute*, pp. 3.1-3.33 (in Japanese).
- U. S. GEOLOGICAL SURVEY (1975). "A study of earthquake losses in the Puget Sound, Washington area," USGS Open File Report 75-375, 298 pp.
- U.S. GEOLOGICAL SURVEY (1975). *The Interior of the Earth*, U.S. Government Printing Office, Washington, D.C.
- U.S. DEPARTMENT OF THE NAVY (1982). Foundations and earth structures, *NAVFAC DM-7.2*, Naval Facilities Engineering Command, U.S. Government Printing Office, Washington, D.C., 244 pp.
- USCOLD (1985). Guidelines for selecting seismic parameters for dam projects, *Report of Committee on Earthquakes*, U.S. Committee on Large Dams.
- VAGLIENTE, V.H. (1973). "Forecasting risk inherent in earthquake-resistant design," *Technical Report 174*, Department of Civil Engineering, Stanford University, Stanford, California.
- VAID, Y.P. AND CHERN, J.C. (1983). "Effect of static shear on resistance of liquefaction," *Soils and Foundations*, Vol. 23, No. 1, pp. 47-60.
- VAID, Y.P. AND CHERN, J.C. (1985). "Cyclic and monotonic undrained response of saturated sands," in V. Khosla ed., *Advances in the Art of Testing Soils under Cyclic Conditions*, ASCE, New York, pp. 120-147.

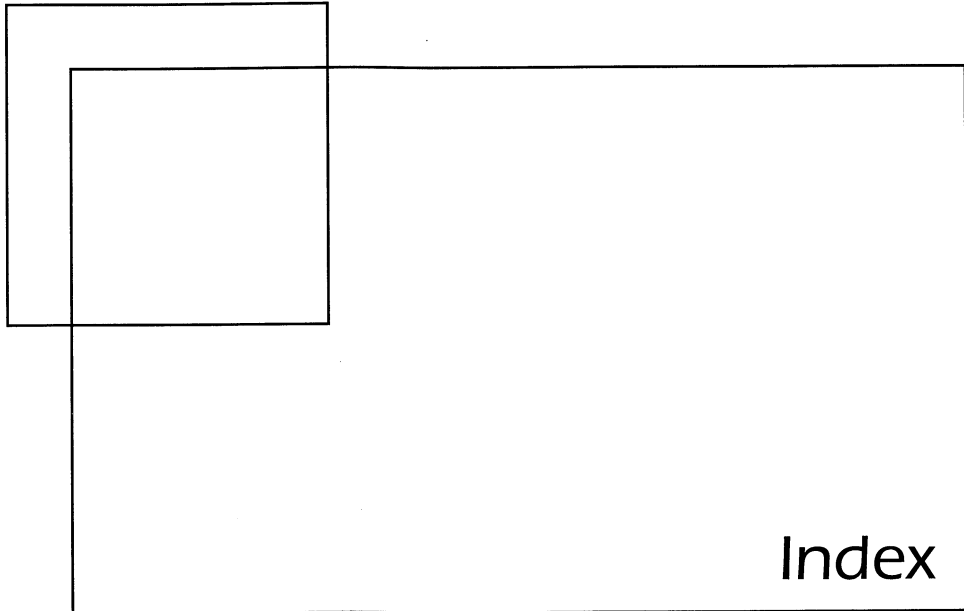
- VAID, Y.P. AND NEGUSSEY, D. (1984). "A critical assessment of membrane penetration in the triaxial test," *Geotechnical Testing Journal*, Vol. 7, No. 2, pp. 70-76.
- VAID, Y.P., CHUNG, E.K.F., AND KUERBIS, R.H. (1990). "Stress path and steady state," *Canadian Geotechnical Journal*, Vol. 27, No. 1, pp. 1-7.
- VAID, Y.P. AND THOMAS, J. (1995). Liquefaction and post-liquefaction behavior of sand, *Journal of Geotechnical Engineering*, ASCE, Vol. 121, No. 2, pp. 163-173.
- VAN IMPE, W.F. (1989). *Soil improvement techniques and their evolution*, A.A. Balkema, Rotterdam, The Netherlands, 125 pp.
- VANMARCKE, E.H. (1972). "Properties of spectral moments with application to random vibration," *Journal of the Engineering Mechanics Division*, ASCE, Vol. 98, No. 3, pp. 425-442.
- VANMARCKE, E.H. (1976). "Structural response to earthquakes," Chapter 8 in C. Lomnitz and E. Rosenblueth, eds., *Seismic Risk and Engineering Decisions*, Elsevier, Amsterdam, pp. 287-338.
- VANMARCKE, E.H. (1979). "State-of-the-art for assessing earthquake hazards in the United States: Representation of earthquake ground motion: scaled accelerograms and equivalent response spectra," *Miscellaneous Paper S-73-1, Report 14*, U.S. Army Corps of Engineers Waterways Experiment Station, Vicksburg, Mississippi.
- VANMARCKE, E.H. AND LAI, S.P. (1977). "Strong motion duration of earthquakes," *Report R77-16*, Massachusetts Institute of Technology, Cambridge, Massachusetts.
- VANMARCKE, E.H. AND LAI, S.P. (1980). Strong motion duration and rms amplitude of earthquake records, *Bulletin of the Seismological Society of America*, Vol. 70, pp. 1293-1307.
- VARNES, D.J. (1978). "Slope movement types and processes," in *Landslides: Analysis and Control*, Transportation Research Board Special Report 176, National Academy of Sciences, Washington, D.C., pp. 12-33.
- VASQUEZ-HERRERA, A. AND DOBRY, R. (1988). "The behavior of undrained contractive sand and its effect on seismic liquefaction flow failures of earth structures," *Report to U.S. Army Corps of Engineers*, Renssalaer Polytechnic Institute, Troy, New York, 510 pp.
- VASQUEZ-HERRERA, A., DOBRY, R., AND BAZIAR, M.H. (1990). "Re-evaluation of liquefaction triggering and flow sliding in the Lower San Fernando Dam during the 1971 earthquake," *Proceedings, 4th U.S. National Conference on Earthquake Engineering*, Palm Springs, California, pp. 783-792.
- VAUGHAN, D.K. (1983). *FLEX User's Guide*, Document UG8298, Weidlinger Associates, New York.
- VENEZIANO, D. AND CORNELL, C.A. (1974). Earthquake models with spatial and temporal memory for engineering seismic risk analysis, *Research Report R74-78*, Department of Civil Engineering, Massachusetts Institute of Technology, Cambridge, Massachusetts.
- VENEZIANO, D. AND LIAO, S. (1984). "Statistical analysis of liquefaction data," *Proceedings, 4th ASCE Specialty Conference on Probabilistic Mechanics and Structural Reliability*, pp. 206-209.
- VERDUGO, R. (1992). Discussion of "Correlation between liquefaction resistance and shear wave velocity," by K. Tokimatsu and A. Uchida, *Soils and Foundations*, Vol. 32, No. 2, pp. 144-145.
- VERE-JONES, D. AND OZAKI, T. (1982). "Some examples of statistical estimation applied to earthquake data. I. Cyclic Poisson and self-exciting models," *Annals of the Institute of Statistics and Mathematics*, Vol. 34, Part B, pp. 189-207.
- VERE-JONES, D.A. (1966). "A Markov model for aftershock occurrence," *Pure and Applied Geophysics*, Vol. 64, pp. 31-42.
- VERE-JONES, D.A. AND DAVIES, R.B. (1966). "Statistical survey of earthquakes in the main seismic region of New Zealand, Part 2: Time series analysis," *New Zealand Journal of Geology and Geophysics*, Vol. 9, pp. 251-284.

- VERHOODAN, J. (1960). "Temperatures inside the earth," *American Scientist*, Vol. 48, No. 2, pp. 134-159.
- VERNEY, P. (1979). *The Earthquake Handbook*, Paddington Press, New York.
- VIDALE, J.E. AND HELMBERGER, D.V. (1988). "Elastic finite difference of the 1971 San Fernando earthquake," *Bulletin of the Seismological Society of America*, Vol. 78, No. 1, pp. 122-141.
- VON THUN, J. L., ROCHIM, L. H., SCOTT, G. A., AND WILSON, J. A. (1988) "Earthquake ground motions for design and analysis of dams," in *Earthquake Engineering and Soil Dynamics II - Recent Advance in Ground-Motion Evaluation*, Geotechnical Special Publication 20, ASCE, New York, pp. 463-481.
- VUCETIC, M. (1990). "Normalized behavior of clay under irregular cyclic loading," *Canadian Geotechnical Journal*, Vol. 27, No. 1, pp. 29-46.
- VUCETIC, M. (1994). "Cyclic threshold shear strains in soils," *Journal of Geotechnical Engineering*, ASCE, Vol. 120, No. 12, pp. 2208-2228.
- VUCETIC, M. AND DOBRY, R. (1989). "Degradation of marine clays under cyclic loading," *Journal of Geotechnical Engineering*, ASCE, Vol. 114, No. 2, pp. 133-149.
- VUCETIC, M. AND DOBRY, R. (1991). "Effect of soil plasticity on cyclic response," *Journal of Geotechnical Engineering*, ASCE, Vol. 117, No. 1, pp. 89-107.
- WALLACE, R.E. (1981). "Active faults, paleoseismology, and earthquake hazards in the western United States," in D.W. Simpson and T.G. Richards, eds. *Earthquake Prediction: An International Review*, Maurice Ewing Series 4, American Geophysical Union, Washington, D. C., pp. 209-216.
- WANG, W. (1979). "Some findings in soil liquefaction," Water Conservancy and Hydroelectric Power Scientific Research Institute, Beijing, China.
- WARD, W.A. (1986). "Interpretation of CPT data for design of earth dams near Tehachapi, California," *Proceedings, In Situ '86*, Blacksburg, Virginia, Geotechnical Special Publication 6, ASCE, New York, pp. 1119-1133.
- WARNER, J. (1982). "Compaction grouting - the first thirty years," *Proceedings, ASCE Specialty Conference on Grouting in Geotechnical Engineering*, New Orleans, Louisiana, pp. 694-707.
- WEGENER, A. (1915). *Die Entstehung der Kontinente und Ozeane*, Vieweg, Braunschweig, Germany.
- WEICHERT, D. (1980). "Estimation of the earthquake recurrence parameters for unequal observation periods for different magnitudes," *Bulletin of the Seismological Society of America*, Vol. 70, No. 4, pp. 1337-1347.
- WEILER, W.A. (1988). "Small strain shear modulus of clay," *Proceedings, ASCE Conference on Earthquake Engineering and Soil Dynamics II: Recent Advances in Ground Motion Evaluation*, Geotechnical Special Publication 20, ASCE, New York, pp. 331-335.
- WELLS, D.L. AND COPPERSMITH, K.J. (1994). "New empirical relationships among magnitude, rupture length, rupture width, rupture area, and surface displacement," *Bulletin of the Seismological Society of America*, Vol. 84, No. 4, pp. 974-1002.
- WELSH, J.P. (1986). "In situ testing for ground modification techniques," *Proceedings, In Situ '86*, Geotechnical Special Publication 6, ASCE, New York, pp. 322-335.
- WELSH, J.P., ED. (1987). *Soil Improvement: A Ten Year Update*, Geotechnical Special Publication No. 12, ASCE, New York, 331 pp.
- WESNOUSKY, S.G. (1994). "The Gutenberg-Richter or characteristic earthquake distribution, which is it?" *Bulletin of the Seismological Society of America*, Vol. 84, No. 6, pp. 1940-1959.
- WESNOUSKY, S.G., SCHOLZ, C.H., SHIMAZAKI, K., AND MATSUDE, T. (1984). "Integration of geological and seismological data for the analysis of seismic hazard: A case study of Japan," *Bulletin of the Seismological Society of America*, Vol. 74, pp. 687-708.

- WESSON, R.L., HELLEY, E.J., LAJOIE, K.R., AND WENTWORTH, C.M. (1975). "Faults and future earthquakes," in R.D. Borcherdt, ed. *Studies for Seismic Zonation of the San Francisco Bay Region*, Professional Paper 941-A, U. S. Geological Survey, Reston, Virginia, pp. A5-A30.
- WESTERGAARD, H. (1931). "Water pressure on dams during earthquakes," *Transactions of ASCE*, Paper No. 1835, pp. 418-433.
- WHITMAN, R.V. (1971). "Resistance of soil to liquefaction and settlement," *Soils and Foundations*, Vol. 11, No. 4, pp. 59-68.
- WHITMAN, R.V. (1989). "Workshop on ground motion parameters for seismic hazard mapping," *Technical Report NCEER-89-0038*, National Center for Earthquake Engineering Research, State University of New York, Buffalo, 41 pp.
- WHITMAN, R.V. (1990). "Seismic design behavior of gravity retaining walls," *Proceedings, ASCE Specialty Conference on Design and Performance of Earth Retaining Structures*, Geotechnical Specialty Publication 25, ASCE, New York, pp. 817-842.
- WHITMAN, R.V. (1992). "Proceedings for the site effects workshop," *Technical Report NCEER-92-0006*, National Center for Earthquake Engineering Research, State University of New York, Buffalo, 35 pp.
- WHITMAN, R.V. AND LIAO, S. (1985), Seismic design of retaining walls, *Miscellaneous Paper GL-85-1*, U.S. Army Engineer Waterways Experiment Station, Vicksburg, Mississippi.
- WHITMAN, R.V., LAMBE, P.C., AND AKIYAMA, H. (1982). "Consolidation during dynamic tests on a centrifuge," *Preprint 82-063*, ASCE National Convention, Las Vegas, Nevada.
- WILSON, J.T. (1965). "A new class of faults and their bearing on continental drift," *Nature*, Vol. 207, pp. 343-347.
- WILSON, R.C. (1993). "Relation of Arias Intensity to magnitude and distance in California," *Open-File Report 93-556*, U.S. Geological Survey, Reston, Virginia, 42 pp.
- WILSON, R. C. AND KEEFER, D. K. (1985) "Predicting areal limits of earthquake-induced landsliding," in Evaluating Earthquake Hazards in the Los Angeles Region, Ziony, J. I., ed., U. S. Geological Survey, Reston, Virginia, Professional Paper 1360, 317-345.
- WOLF, J.P. (1985). *Dynamic Soil-Structure Interaction*, Prentice Hall, Englewood Cliffs, New Jersey, 466 pp.
- WOLF, J.P. (1991). "Consistent lumped-parameter models for unbounded soil: physical representation," *Earthquake Engineering and Structural Dynamics*, Vol. 20, No. 1, pp. 11-32.
- WONG, C.P. (1982). "Seismic analysis and an improved design procedure for gravity retaining walls," *S.M. Thesis*, Department of Civil Engineering, Massachusetts Institute of Technology, Cambridge, Massachusetts.
- WONG, R.K.S. AND ARTHUR, J.R.F. (1986). "Sand shear by stresses with cyclic variations in direction," *Geotechnique*, Vol. 36, No. 2, pp. 215-226.
- WONG, R.T., SEED, H.B., AND CHAN, C.K. (1975). "Liquefaction of gravelly soil under cyclic loading conditions," *Journal of the Geotechnical Engineering Division*, ASCE, Vol. 101 No. GT6, pp. 574-583.
- WONG, W. (1984). "Earthquake damages to earth dams and levees in relation to soil liquefaction and weakness in soft clays," *Proceedings, International Conference on Case Histories in Geotechnical Engineering*, Vol. 1, pp. 511-521.
- WOOD, D.M. (1991). Approaches to modelling the cyclic stress-strain response of soils," Chapter 2 in M.P. O'Reilly and S.F. Brown, eds, *Cyclic Loading of Soils*, Blackie, London, pp. 19-69.
- WOOD, H.O. (1908). "Distribution of apparent intensity in San Francisco, in the California earthquake of April 18, 1906," *Report of the State Earthquake Investigation Commission*, Carnegie Institute of Washington, Washington, D.C., Vol. 1, pp. 220-245.

- WOOD, J. (1973). "Earthquake-induced soil pressures on structures," *Report EERL 73-05*, California Institute of Technology, Pasadena, California, 311 pp.
- WOODS, R.D. (1978). "Measurement of dynamic soil properties," *Proceedings, Earthquake Engineering and Soil Dynamics Specialty Conference*, ASCE, Pasadena, California, Vol. 1, pp. 91-178.
- WOODS, R.D. (1991). "Field and laboratory determination of soil properties at low and high strains," *Proceedings, 2nd International Conference on Recent Advances in Geotechnical Earthquake Engineering and Soil Dynamics*, St. Louis, Missouri, Vol. 3, pp. 1727-1741.
- WOODWARD-CLYDE CONSULTANTS (1979). "Report of the evaluation of maximum earthquake and site ground motion parameters associated with the Offshore Zone of deformation, San Onofre Nuclear Generating Station," *Report to Southern California Edison Company*, Woodward-Clyde Consultants, San Francisco.
- WROTH, C.P. AND HOULSBY, G.T. (1985). "Soil mechanics - Property characterization and analysis procedures," *Proceedings, 11th International Conference on Soil Mechanics and Foundation Engineering*, San Francisco, Vol. 1, pp. 1-55.
- WU, S.-C., CORNELL, C.A., AND WINTERSTEIN, S.R. (1995). "A hybrid recurrence model and its implication on seismic hazard results," *Bulletin of the Seismological Society of America*, Vol. 85, No. 1, pp. 1-16.
- WYSS, M. (1979). "Estimating maximum expected magnitude of earthquakes from fault dimensions," *Geology*, Vol. 7, No. 7, pp. 336-340.
- YAN, L., AND BYRNE, P.M. (1990). "Simulation of downhole and crosshole seismic tests on sand using the hydraulic gradient similitude method," *Canadian Geotechnical Journal*, Vol. 27, No. 4.
- YAN, L. AND BYRNE, P.M. (1991). "Stress state and stress ratio effects in downhole and crosshole shear wave velocity tests on sands," *Proceedings, 2nd International Conference on Recent Advances in Geotechnical Earthquake Engineering and Soil Dynamics*, St. Louis, Missouri, Vol. 1, pp. 299-306.
- YANG, C.Y. (1986). *Random Vibration of Structures*, John Wiley and Sons, New York, 295 pp.
- YASUDA, N. AND MATSUMOTO, N. (1993). "Dynamic deformation characteristics of sands and rock-fill materials," *Canadian Geotechnical Journal*, Vol. 30, No. 5, pp. 747-757.
- YEGIAN, M.K. AND WHITMAN, R.V. (1978). "Risk analysis for ground failure by liquefaction," *Journal of the Geotechnical Engineering Division*, ASCE, Vol 104, NO. GT7, pp. 921-938.
- YEGIAN, M.K., GHARAMAN, V.G., AND HARUTIUNIAN, R.N. (1994). "Liquefaction and embankment failure case histories, 1988 Armenia earthquake," *Journal of Geotechnical Engineering*, ASCE, Vol. 120, No. 3, pp. 581-596.
- YEGIAN, M.K., MARCIANO, E.A., AND GHARAMAN, V.G. (1988). "Integrated seismic risk analysis for earth dams," *Report 88-15*, Northeastern University, Boston.
- YEGIAN, M.K., MARCIANO, E., AND GHARAMAN, V.G. (1991). "Earthquake-induced permanent deformations: probabilistic approach," *Journal of Geotechnical Engineering*, ASCE, Vol. 117, No. 1, pp. 35-50.
- YOSHIMI, Y., TOKIMATSU, K., AND HASAKA, Y. (1989). "Evaluation of liquefaction resistance of clean sands based on high-quality undisturbed samples," *Soils and Foundations*, Vol. 29, No. 1, pp. 93-104.
- YOUD, T.L. (1972). "Compaction of sands by repeated shear straining," *Journal of the Soil Mechanics and Foundations Division*, ASCE, Vol. 98, No. SM7, pp. 709-725.
- YOUD, T.L. (1978). "Major cause of earthquake damage is ground failure," *Civil Engineering*, ASCE, Vol. 48, No. 4, pp. 47-51.

- YOUSD, T.L. (1984a). "Recurrence of liquefaction at the same site," *Proceedings, 8th World Conference on Earthquake Engineering*, Vol. 3, pp. 231-238.
- YOUSD, T.L. (1984b). "Geologic effects - Liquefaction and associated ground failure," *Proceedings, Geologic and Hydrologic Hazards Training Program*, Open File Report 84-760, U.S. Geological Survey, Menlo Park, California, pp. 210-232.
- YOUSD, T.L. (1991). "Mapping of earthquake-induced liquefaction for seismic zonation," *Proceedings, 4th International Conference on Seismic Zonation*, Earthquake Engineering Research Institute, Stanford University, Vol. 1, pp. 111-147.
- YOUSD, T.L. (1993). "Liquefaction-induced lateral spread displacement," *Report TN-1862*, Naval Civil Engineering Laboratory, Port Hueneme, California, 44 pp.
- YOUSD, T.L. AND GARRIS, C.T. (1995). Liquefaction-induced ground surface disruption, *Journal of Geotechnical Engineering*, ASCE, Vol. 121, No. 11, in press.
- YOUSD, T.L. AND HOOSE, S.N. (1977). "Liquefaction susceptibility and geologic setting," *Proceedings, 6th World Conference on Earthquake Engineering*, New Delhi, Vol. 3, pp. 2189-2194.
- YOUSD, T.L. AND PERKINS, D.M. (1987). "Mapping of Liquefaction Severity Index," *Journal of Geotechnical Engineering*, ASCE, Vol. 113, No. 11, pp. 1374-1392.
- YOUSD, T.L., ET AL. (1985). "The Borah Peak, Idaho earthquake of October 28, 1983--liquefaction," *Earthquake Spectra*, Vol. 2, No. 1, pp. 71-89.
- YOUNGS, R. R. AND COPPERSMITH, K. J. (1985). "Implications of fault slip rates and earthquake recurrence models to probabilistic seismic hazard assessments," *Bulletin of the Seismological Society of America*, Vol. 75, No. 4, pp. 939-964.
- YOUNGS, R.R., DAY, S.M., AND STEVENS, J.L. (1988). "Near field ground motions on rock for large subduction earthquakes," *Proceedings, Earthquake Engineering and Soil Dynamics II: Recent Advances in Ground Motion Evaluation*, Geotechnical Special Publication 20, ASCE, New York, pp. 445-462.
- YU, H.S. (1994). "State parameter from self-boring pressuremeter tests in sand," *Journal of Geotechnical Engineering*, Vol. 120, No. 12, pp. 2118-2135.
- ZACHER, E.G. AND GRAF, E.D. (1979). "Chemical grouting of sand for earthquake resistance," *Civil Engineering*, ASCE, New York, Vol. 49, No. 1, pp. 67-69.
- ZARRABI-KASHANI, K. (1979). "Sliding of gravity retaining wall during earthquakes considering vertical accelerations and changing inclination of failure surface," S.M. thesis, Department of Civil Engineering, Massachusetts Institute of Technology, Cambridge, Massachusetts.
- ZELIKSON, A. (1969). "Geotechnical models using the hydraulic gradient similarity methods," *Geotechnique*, Vol. 19, pp. 495-508.
- ZEMELL, S. W. (1984) "Imposed upper limit for probabilistic seismic risk," *Proceedings, 8th World Conference on Earthquake Engineering*, San Francisco, pp. 239-245.
- ZEN, K., UMEHARA, Y., AND HAMADA, K. (1978). "Laboratory tests and in-situ seismic survey on vibratory shear modulus of clayey soils with different plasticities," *Proceedings, Fifth Japan Earthquake Engineering Symposium*, Tokyo, pp. 721-728.
- ZIENKIEWICZ, O.C. AND TAYLOR, R.L. (1989). *The Finite Element Method*, McGraw-Hill, London.
- ZOEPPRITZ, K. (1919). "Nach d. Konigl. Gessel d. Wissen, z. Gottingen," *Math-Phys.*, Berlin, pp. 66-94.



Index

A

Acceleration spectrum intensity, 83, 100
Accelerogram, 56
Accelerograph, 56
Accelerometer, 58
 force balance, 58
 piezoelectric, 59
Accretionary wedge, 31
Active earth pressure (see Retaining walls)
Active fault, 109-111
Aftershock (see Earthquake)
Amplification function, 310-312
Amplitude, 55, 529, 531, 533
Anchored bulkheads, 496-498
Apparent dip angle, 198-199
Argand diagram, 53
Arias intensity, 82, 99-100
Aseismic deformation, 25

Asperities, 38

Autocovariance, 101
Axioms of probability, 584-585

B

Backbone curve, 231-232, 240-243
Bandwidth, 76
Barriers, 38
Baseline error, 59, 62
Basin effects, 321-323
Becker hammer penetration test, 211-212
Bedrock motion (see Ground motion)
Bedrock outcropping motion (see Ground motion)
Benioff zone, 31
Blasting densification (see Soil improvement)
Blind zone, 197

- Body wave, 19-20, 144-156
 Body wave magnitude (see Magnitude)
 Borehole torsional shear test, 215
 Bracketed duration, 79-80, 95, 99
 Brune spectrum, 92-93
- C**
- Central frequency, 76-77
 Centrifuge test, 226-227
 Characteristic earthquake (see Recurrence law)
 Characteristic (frequency) equation, 577
 Characteristic intensity, 82
 Characteristic site period, 261
 Chiba array, 63
 Circular frequency, 529
 Coda, 48
 Coda magnitude (see Magnitude)
 Coefficient of variation (see Random variable)
 Coherency, 101-102
 Collapse surface, 363
 Compaction grouting (see Soil improvement)
 Compaction piles (see Soil improvement)
 Complex shear modulus, 177
 Complex stiffness, 570-571
 Complex wave number, 177, 260
 Conditional probability, 585-588
 Cone penetration (CPT) test, 212-213
 correlation to G_{\max} , 235
 correlation to liquefaction resistance, 383-385
 Constitutive models, 243-244
 Continental collision, 31
 Continental drift, 23-28
 Controlling earthquake, 114
 Convection, 28
 Core (see Earth), 22
 Corner frequency, 72
 Critical angle of incidence, 172, 196
 Critical damping coefficient, 551
 Critical distance, 196
 Critical level of repeated loading (CLRL), 245
 Critical void ratio, 355-357
 Cross-hole test, 205-207
- Crust (see Earth), 20
 Cumulative absolute velocity, 83
 Cumulative distribution function
 (see Probability)
 Cutoff frequency, 72
 Cyclic direct simple shear test, 223-224
 Cyclic mobility (see Liquefaction)
 Cyclic nonlinear models, 240-243
 Cyclic strength curves, 374-375
 Cyclic strength ratio, 245
 Cyclic stress ratio, 374-376
 Cyclic torsional shear test, 224-225
 Cyclic triaxial test, 220-223
- D**
- Damped natural frequency, 551
 Damping
 complex stiffness, 570-571
 effect on ground response, 260, 263
 from half-power bandwidth method, 568-569
 from hysteresis loop, 567-568
 from logarithmic decrement, 552
 material, 175-178
 quality factor, 92, 569
 radiation, 264
 viscous, 567-571
 Damping ratio
 definition, 551
 measurement of, 208, 217, 222
 of soils, 238-240
- Deaggregation (see Seismic hazard analysis)
 Deconvolution
 (see Ground response analysis)
 Degradation of shear modulus, 238-239
 Degrees of freedom, 544
 Dependent events, 122
 Design earthquakes
 and deterministic seismic hazard analysis, 114-117
 maximum credible earthquake, 324
 maximum probable earthquake, 324
 operating basis earthquake, 324
 safe shutdown earthquake, 324

- Design ground motion
code-based development, 328-339
from design earthquakes, 324
design response spectrum, 325-327, 334
site-specific development, 327-328
time history development, 340-345
uniform risk spectrum, 327
- Deterministic seismic hazard analysis, 114-117
- Dilatometer test, 213-214
correlation to G_{max} , 235
correlation to liquefaction resistance, 385-386
- Dip-slip movement (see Fault)
- Dirac function, 565
- Direct wave (see Seismic refraction test)
- Directivity effect, 39
- Dispersion, 164-165, 203-205
- Down-hole test, 207-208
- Drilled inclusions (see Soil improvement)
- Ductility
effect on design base shear, 330, 338
factor, 75
- Duhamel integral, 566
- Duration
and liquefaction, 369-370
definitions, 79-82
prediction of, 95
- Duration magnitude (see Magnitude)
- Dynamic compaction (see Soil improvement)
- E**
- Earth, 18-22
Benioff zone, 31
core, 22
crust, 20
mantle, 21
Mohorovicic discontinuity, 21
temperature, 21
wave velocities, 22
- Earth pressure (see Retaining walls)
- Earthquake
aftershock, 38, 122
energy, 50-51
- epicenter, 43
focus, 43
foreshock, 38, 122
historical, 1, 14-17
hypocenter, 43
intensity, 45-46
intraplate, 32
location, 44
magnitude, 46-50
multiple-event, 39
reservoir-induced, 42
- Earthquake-resistant design, 106
- Effective acceleration, 69
- Effective design acceleration, 70
- Effective peak acceleration, 83-84
- Effective peak velocity, 83-84
- Effective shear strain, 271-273
- Elastic rebound, 36-42
- Epicenter, 43
- Epicentral distance, 43
- Epicentral intensity (see Intensity), 45
- Equation of motion, 144, 152-154, 546, 575
- Equivalent lateral force, 580
- Equivalent linear model
advantages and limitations of, 279-280
and ground response analysis, 270-275, 284-286, 292
soil properties, 230-240
- Equivalent stress cycles, 369-371
- Evolutionary power spectrum, 73
- Expected value (see Random variable)
- Extended source effect, 101
- F**
- Fault
activity, 109-111
geometry, 33-34
movement, 34
types
dip-slip, 34-35
normal, 34-35
reverse, 34
strike-slip, 34, 36

- Fault (*cont.*)
 - thrust, 34
 Finite difference method, 275-279
 Finite element method, 281-286
 - boundary conditions, 283-284
 - discretization considerations, 283
 - elemental equations of motion, 281-283
 - global equations of motion, 283
 Fling, 39-40
 Flow failure (see Liquefaction)
 Flow liquefaction surface (see Liquefaction)
 Focal depth, 43
 Focus, 43
 Forced vibration, 548, 553-566
 Foreshock (see Earthquake)
 Fourier amplitude spectrum, 71-72, 92-93, 538
 Fourier phase spectrum, 71-72, 538
 Fourier series, 536-542; 562-563
 - discrete Fourier transform, 541
 - Fast Fourier transform, 541
 Free-field motion, 61, 255, 294, 300-302
 Free surface motion, 255-256
 Free vibration, 548-553
 Frequency
 - content, 55, 70
 - definition, 530
 - fundamental, 261, 577-578
 - equation, 577
 Fundamental mode of vibration, 578
- G**
- Gaussian distribution (see Normal distribution)
 Geophone, 59, 195
 Geotomography, 215
 Global Digital Seismographic Network, 62
 G_{\max} , 232-235
 Gravity walls, 489-492, 494-495
 Green's function
 - (see Time history development)
 Ground motion
 - bedrock motion, 255
 - bedrock outcropping motion, 255
 - coherency, 101-102
 free surface motion, 255
 measurement
 - accelerogram, 56
 - accelerograph, 56
 - accelerometer, 58
 - baseline error, 59, 62
 - instrument arrays, 62-64
 - seismogram, 56
 - seismograph, 56
 - seismometer, 58
 - seismoscope, 59
 parameters
 - acceleration spectrum intensity, 83, 100
 - Arias intensity, 82, 99-100
 - bandwidth, 76
 - bracketed duration, 79-80, 95, 99
 - central frequency, 76-77
 - characteristic intensity, 82
 - cumulative absolute velocity, 83
 - effective acceleration, 69
 - effective design acceleration, 70
 - effective peak acceleration, 83-84
 - effective peak velocity, 83-84
 - Kanai-Tajimi parameters, 78
 - peak acceleration, 67-68, 88-91
 - peak displacement, 68
 - peak velocity, 68, 90
 - predominant period, 76, 91-92
 - response spectrum intensity, 83
 - rms acceleration, 82, 98-99
 - shape factor, 77-78
 - sustained maximum acceleration, 69-70
 - sustained maximum velocity, 69-70
 - velocity spectrum intensity, 83, 100
 - v_{\max}/a_{\max} , 78-79, 94
 rock outcropping motion, 255
 Ground oscillation (see Liquefaction)
 Ground response analysis, 254-305
 - comparison of equivalent linear and nonlinear, 279-280, 291
 - deconvolution, 274-275
 - equivalent linear, 270-275, 284-286, 292
 - nonlinear, 275-279, 286, 292-293
 - one-dimensional, 255-280

Ground response analysis (*cont.*)
three-dimensional, 291-294
transfer functions, 256-275
two-dimensional, 280-291
Group velocity, 165
Grouting (see Soil improvement)
Gutenberg discontinuity, 22
Gutenberg-Richter recurrence law
(see Recurrence law)

H

Half-power bandwidth method, 568-569
Haskell-Thomson solution, 204
Head wave (see Seismic refraction test)
Historical seismicity, 113-114
Hydrodynamic pressure, 486
Hypocenter, 43
Hypocentral depth, 43
Hypocentral distance, 43
Hysteresis loop, 567-568

I

Impedance ratio
complex, 265
Impedance ratio, 167-169
Instrument arrays, 62-64
Chiba, 63
El Centro, 63, 64
GSDN, 62
Lotung, 63
WWSSN, 62
Instrumental seismicity, 114
Intensity
and peak horizontal acceleration, 67
epicentral, 45
isoseismal map, 45, 47
Japanese Meteorological Agency, 45
Medvedev-Spoonheuer-Kornik, 45
modified Mercalli, 45-46
Rossi-Forel, 45
Interface friction angle, 472-473
Intraplate earthquakes, 32

Intrusion grouting (see Soil improvement)
Isoseismal map (see Intensity)

J

Jet grouting (see Soil improvement)
JMA intensity (see Intensity)
JMA magnitude (see Magnitude)

K

Kanai-Tajimi power spectrum
(see Power spectrum)

L

Landslide (see Slope stability)
Lateral spreading, 5-8, 349-351, 367-368,
453-462
Lifelines, 11
Linear acceleration method, 574-575
Liquefaction, 348-422
cyclic mobility, 349-350, 367-368
effects, 5-8, 397-418
alteration of ground motion, 398-401
development of sand boils, 8, 400-402
ground oscillation, 399-400
instability, 5-8, 408-417, 451-462
residual shear strength, 410-413
settlement, 402-408
steady state shear strength, 409-410
flow liquefaction, 5-7, 349, 361-366, 413-
415
initiation, 361-398
cyclic strain approach, 390-394
cyclic stress approach, 369-390
effective stress-based response analysis,
395-396
energy dissipation approach, 394-395
factor of safety against liquefaction,
386-390
flow liquefaction surface, 361-369
initial liquefaction, 368-369
probabilistic approach, 396-397

- Liquefaction (*cont.*)
 resistance
 effect of fines, 378-380
 laboratory characterization of, 373-377
 insitu test characterization of, 377-387
 specimen preparation effects on, 377
 settlement dry sand, 402-404
 saturated sand, 404-408
 susceptibility, 351-360
 compositional criteria, 354-355
 geologic criteria, 353-354
 historical criteria, 352-353
 state criteria, 355-360
 Liquefaction Severity Index, 454-456
 Local magnitude (see Magnitude)
 Local site effects, 309-323
 Logarithmic decrement, 552
 Logic tree, 137-138
 Lognormal distribution, 594-595
 Loma Prieta earthquake, 316-317
 Lotung array, 63
 Love wave, 20, 162-164
- M**
- Magnification factor, 561
 Magnitude
 and fault rupture area, 111-113
 and maximum fault displacement, 111-113
 and surface rupture length, 111-113
 body wave, 48
 coda, 48
 duration, 48-49
 Japanese Meteorological Agency, 49
 moment, 49
 Richter local, 48
 saturation, 49
 surface wave, 48
 Makdisi-Seed analysis (see Slope stability)
 Mantle (see Earth), 21
 Markov model, 129
 Masing behavior, 241-242
 Material damping, 175-178
 Maximum credible earthquake, 115
 Maximum probable earthquake, 115
 Mean (see Random variable)
 Membrane penetration, 220
 Mexico City, 313-315
 Micromechanical modeling, 230
 Microplates, 23
 Microseismic activity, 54
 Mode of vibration
 of earth dam, 289-290
 of MDOF structure, 578
 of soil deposit, 261-262
 Mode shape, 261, 578
 Mode superposition method, 579-581
 Model tests, 225-228
 Modified Mercalli intensity (see Intensity)
 Modulus reduction curve (see Shear modulus)
 Mohorovicic discontinuity, 21
 Mohr circle of stress, 186
 Moment magnitude (see Magnitude)
 Mononobe-Okabe method
 (see Retaining walls)
 Multiple degree of freedom systems, 575-582
 equations of motion, 575-577
 response of linear MDOF systems, 577-582
 mode superposition method, 579-581
 response spectrum analysis, 581-582
 undamped free vibrations, 577-579
 Multiplication rule, 586
- N**
- Natural frequency, 548
 Natural hazards, 2
 Natural period of vibration, 548
 NEHRP Provisions
 effective peak acceleration coefficient
 335-336, 338
 effective peak velocity-related acceleration
 coefficient, 335, 337-338
 equivalent lateral force procedure, 338-340
 Newmark sliding block analysis
 (see Slope stability)
 Newmark-Hall design response spectrum,
 325-326

Nonlinear analysis
of SDOF systems, 572-575
of soil deposits, 275-280, 286, 290, 292-293
Nonperiodic motion, 527-528
Normal distribution, 591-593
cumulative distribution function values, 593
standard normal variable, 592
Normal fault (see Fault)
Normal stress, 150
Nyquist frequency, 73

O

Operating basis earthquake, 115

P

p-wave, 19, 154-156
Paleoseismology, 107
Pangaea, 23
Passive earth pressure (see Retaining walls)
Peak acceleration, 67-68, 88-91
Peak displacement, 68
Peak velocity, 68, 90
Period of vibration, 530
Periodic motion, 527-528
Permeation grouting (see Soil improvement)
Phase angle, 529, 531
Phase transformation, 357-358
Phase velocity, 165
Piezoelectric bender element test, 219-220
Plane wave, 156
Plates
boundary types
spreading ridge, 29
subduction zone, 30-31
transform fault, 32
major, 23, 26
microplates, 23
plate tectonics, 24-28
platelets, 23
Poisson model, 128-129, 134-135
Pore pressure ratio, 362, 376, 388
Power spectrum, 72, 542

Predictive relationships, 86-100, 126-127
acceleration spectrum intensity, 100
and probabilistic seismic hazard analysis,
126-127
Arias intensity, 99-100
bracketed duration, 95, 99
Fourier spectrum ordinates, 92-93
peak acceleration, 88-91
peak velocity, 90
predominant period, 91-92
response spectrum ordinates, 94-98
rms acceleration, 98-99
velocity spectrum intensity, 100
 v_{\max}/a_{\max} , 94

Predominant period, 76, 91-92

Pressuremeter test, 214-215, 235

Principal stresses, 187-188

rotation of, 189-190

Probabilistic seismic hazard analysis, 117-139

Probability, 585-595

axioms of, 584-585

cumulative distribution function, 589

multiplication rule, 586

of events, 585-588

probability density function, 588

total probability theorem, 587-588

Progressive failure, 432

Pseudo-spectral acceleration, 572

Pseudo-spectral velocity, 572

Pseudostatic analysis, 434-437, 478-481

Q

Quality factor, 92, 569

Quiet zone, 528

R

Radiation damping, 179-180, 266, 283-284,
298-299

Random variable, 588-589

coefficient of variation, 590

expected value, 589

mean, 589

- Random variable (*cont.*)
 - standard deviation, 590
 - variance, 590
 - Rate effects, 234
 - Ray path, 101, 170-171
 - Rayleigh damping, 580
 - Rayleigh wave, 20, 156-161
 - displacement, 160-161
 - use in subsurface exploration, 203-205
 - velocity, 159-160
 - Recurrence laws, 117, 120-126
 - Gutenberg-Richter, 121-124
 - characteristic earthquake, 124-125
 - Reflection, 165, 170, 193-195
 - Refraction, 171, 195-202
 - Reinforced soil walls
 - external stability, 501-502
 - internal stability, 502
 - Remnant magnetism, 29-30
 - Reservoir-induced seismicity, 42
 - Residual shear strength (see Liquefaction)
 - Resonance
 - of soil deposit, 257-260
 - of structure, 555
 - spurious, 279
 - Resonance, 555
 - Resonant column test, 216-219
 - Response spectrum, 73-75, 94-98, 571-572
 - Response spectrum analysis, 581-582
 - Response spectrum intensity, 83
 - Retaining walls, 11-12, 466-502
 - active earth pressure, 470-476
 - dynamic response, 477
 - failures, 11-12, 467-469
 - interface friction angles, 472-473
 - passive earth pressure, 470-476
 - seismic design considerations, 494-502
 - anchored bulkheads, 496-498
 - braced walls, 495-500
 - gravity walls, 494-495
 - reinforced soil walls, 500-502
 - tieback walls, 498-499
 - seismic displacements, 489-493
 - Richards-Elms method, 489-492
 - Whitman-Liao method, 492-493
 - seismic pressures, 477-489
 - effects of water, 486-489
 - Mononobe-Okabe method, 478-481
 - nonyielding walls, 484-486
 - Steedman-Zeng method, 482-484
 - static pressures, 469-477
 - types, 467
 - Reverse fault (see Fault)
 - Richards-Elms method (see Retaining walls)
 - Richter magnitude (see Magnitude)
 - Ridge push, 28
 - RMS acceleration, 82, 98-99
 - Rock outcropping motion, 255
 - Rossi-Forel intensity (see Intensity)
- S**
- s-wave, 19, 154-156
 - Safe shutdown earthquake, 115
 - Sample space, 583
 - Sampling, 215-216
 - Sand boil, 8, 401-403
 - Saturation (see Magnitude)
 - Scaling (see Time history development)
 - Scattering, 174
 - Seiche, 13
 - Seismic cone test, 208
 - Seismic gap, 40-41
 - Seismic hazard analysis, 106-139
 - deterministic, 114-117
 - probabilistic, 117-139
 - deaggregation, 135, 137
 - seismic hazard curve, 129-134
 - Seismic moment, 42
 - Seismic reflection test, 193-195
 - Seismic refraction test, 195-202
 - direct wave, 196
 - head wave, 196
 - Seismic safety evaluation^{*}earthquake, 115
 - Seismicity
 - characteristic earthquake, 125-125
 - Gutenberg-Richter recurrence law, 121-124
 - historical, 113-114

- Seismicity (*cont.*)
 instrumental, 114
- Seismogram, 56
- Seismograph, 56
- Seismology, 18
- Seismometer, 58
- Seismoscope, 59
- Settlement (see Liquefaction)
- SH-wave, 20, 170-174
- Shaking table test, 225-226
- Shape factor, 77-78
- Shear beam analysis
 linear inelastic shear beam, 290-291
 three-dimensional, 293
 two-dimensional, 286-291
- Shear modulus
 and s-wave velocity, 147, 155
 degradation of, 238-239
 maximum, 232-234
 modulus reduction curve, 232, 234-238
 variation with shear strain, 234-238
- Shear strain, 150
- Shear stress, 150
- Similitude, 227
- Simple harmonic motion, 527-533
- Single degree of freedom systems, 544-575
 equation of motion, 545-547
 response of linear SDOF systems, 547-575
 damped forced vibrations, 557-561
 damped free vibrations, 551-553
 undamped forced vibrations, 554-557
 undamped free vibrations, 548-550
- response of nonlinear SDOF systems, 572-575
- Slab pull, 28
- Slip-predictable model, 129
- Slope stability
 inertial instability, 433-450
 Makdisi-Seed analysis, 447-449
 Newmark sliding block analysis, 438-442
 pseudostatic analysis, 434-437
 stress-deformation analyses, 449-450
- landslides, 9-11, 424-428
- static, 430-433
- weakening instability, 450-462
 flow failure analysis, 451-453
 deformation failure analysis, 453-462
- Soil improvement, 506-522
 densification techniques
 blasting, 512-513
 compaction grouting, 513-514
 dynamic compaction, 510-512
 required extent of treatment, 514-515
 vibro rod, 509-510
 vibroflotation, 508-509
 drainage techniques, 521-522
 grouting and mixing techniques
 intrusion grouting, 519
 jet grouting, 520-521
 permeation grouting, 518-519
 soil mixing, 519-520
 reinforcement techniques
 compaction piles, 516
 drilled inclusions, 516-517
 stone columns, 515-516
 verification of effectiveness, 522-524
- Soil mixing (see Soil improvement)
- Soil-structure interaction, 294-303
 inertial interaction, 302-303
 kinematic interaction, 300-303
- Source spectrum (see Brune spectrum)
- Source zone, 114, 118-120
- Source-site distance, 86, 118-120
- Spatial variability (see Coherency)
- Specific impedance, 167
- Spectral analysis of surface waves (SASW)
 test, 203-205
- Spreading ridge (see Plates), 29
- Spurious resonance, 279
- Standard deviation (see Random variable)
- Standard normal variable, 592
- Standard penetration (SPT) test
 correlation to G_{\max} , 235
 correlation to liquefaction resistance, 378-382
 energy correction, 209
 overburden correction, 209-210
- State parameter, 360

Static liquefaction, 361-366
 Steady state of deformation, 357-360
 definition, 357-358
 state parameter, 360
 steady state line, 358-360
 steady state shear strength, 410-411
 Steady state vibration response, 558-559
 Steady state vibration test, 203
 Steedman-Zeng method (see Retaining walls)
 Stone columns (see Soil improvement)
 Strain energy, 36, 41-42
 Strain-displacement relationships, 145, 150
 Stress drop, 93
 Stress path, 188-190
 Stress reversal, 221-222
 Stress-strain relationships, 145, 151-152
 Strike-slip movement (see Fault)
 Strong ground motion (see Ground motions)
 Subduction zone (see Plates)
 Surface wave magnitude (see Magnitude)
 Surface wave, 19-20, 156-164
 Suspension logging test, 202
 Sustained maximum acceleration, 69-70
 Sustained maximum velocity, 69-70
 SV-wave, 19, 170-174
 System compliance, 220

T

Thrust fault, 34
 Tieback walls, 498-499
 Time-predictable model, 129
 Threshold strain
 volumetric, 230
 linear, 230, 236
 Time history development
 frequency domain generation, 343
 Green's function techniques, 343-345
 scaling of actual ground motions, 340-341
 time domain generation, 341-342
 Topographic effects, 319-321, 323
 Total probability theorem, 587-588
 Transfer function, 256-275, 285, 562-564
 argument, 563

modulus, 257, 563
 Transform fault (see Plates)
 Transient response, 558-559
 Trigger model, 129
 Tripartite plot, 533-534
 Tsunami, 13
 Tuning ratio, 57, 554

U

Ultrasonic pulse test, 219
 Uniform Building Code
 design base shear, 330-332
 design response spectrum, 334
 importance factor, 330, 332
 seismic zone factor, 330-331
 soil coefficient, 330, 334
 Uniform distribution, 590-591
 Uniform risk spectrum, 327
 Up-hole test, 207-208

V

Variance (see Random variable)
 Velocity
 group, 165
 Love wave, 163-164
 p-wave, 145, 155
 particle, 145
 phase, 165
 Rayleigh wave, 159-160
 reversal, 197
 s-wave, 147, 155
 Velocity spectrum intensity, 83, 100
 Venn diagram, 585
 Vibro rod (see Soil improvement)
 Vibroflotation (see Soil improvement)
 Viscous damping, 175-178, 567-570
 v_{\max}/a_{\max} , 78-79, 94

W

Wave number, 148
 Wave passage effect, 101

Wave propagation, 143-183
body waves, 19, 154-156
one-dimensional, 144-149, 165-170
three-dimensional, 149-165, 170-174
surface waves, 20, 156-164
Rayleigh waves, 156-161
Love waves, 162-164
Wavefront, 170-171

Wavelength, 148
Whitman-Liao method (see Retaining walls)
Wood-Anderson seismograph, 48, 57
Worldwide Standard Seismographic Network, 62

Y

Yield acceleration, 439, 442-445